Carrier Mobility Measurements in Vitreous Semiconductors

A Thesis presented by

Joseph M. Marshall

for the degree of

Doctor of Philosophy

of the

University of Edinburgh

1970

The author wishes to express his thanks to Dr. Alan E. Owen for his stimulating guidance and friendship during the period of this study.

The assistance and co-operation of many members of the academic and technical staffs of the University of Edinburgh, Department of Electrical Engineering, and of the University of Sheffield, Department of Glass Technology, is gratefully acknowledged.

A further debt of thanks is due to Mr. Charles Main and Mr. Feher M. Hayatee, colleagues during the period of study, whose friendship and assistance was one of the most pleasant aspects of the author's post-graduate experiences.

The assistance of Dr. W.E. Spear, now of the University of Dundee, in the design of the electron gun equipment, was extremely valuable.

The financial assistance provided by the Ministry of Technology, and the help given by the staff of Standard Telecommunications Laboratories in the printing of the thesis, are much appreciated.

Last, but by no means least, the tolerance and understanding shown by the author's wife, Jeanne, during the writing of this account, proved invaluable and is gratefully acknowledged.

CONTENTS

Abstract

Carrier Mobility Measurements in Vitreous Semiconductors

The construction and operation of experimental systems for the measurement of the drift and Hall mobilities in vitreous semiconductors is described. Such materials are characterised by very low values of mobility (less than 1 $cm^2V^{-1}sec^{-1}$), and usually by high values of resistivity. In consequence, the measurement of the transport parameters becomes more difficult than is the case for 'conventional' crystalline semiconductors.

After a review of the general properties of crystalline semiconductors, the properties of non-crystalline semiconductors are described. The modifications which must be made to the conventional band theory of solids in the consideration of such materials are then examined.

An account is given of the methods by which vitreous specimens, suitable for the measurement of Hall and drift mobilities, may be prepared. In particular, the production of thin film specimens, of a truly vitreous nature (rather than of the evaporated form which is frequently termed 'vitreous') is described.

The measurement of low values of drift mobility, by means of observations on the drift of a sheet of charge carriers through a thin film of material under the influence of an applied electric field, is examined. An account is given of the design and construction of an experimental system by which such measurements may be performed.

Observations of the drift of electron and hole carriers are reported in the systems; selenium, selenium + germanium, arsenic triselenide, and As_2Se_2Te, in terms of the variation of drift mobility with temperature and applied electric field. The results are

analysed in terms of theories of band and hopping conduction in such materials.

The design of Hall mobility measurement systems suitable for the examination of materials of low mobility and high resistivity is reviewed. The construction of such a system, which utilises an a.c. applied electric field in conjunction with periodic reversals of the specimen orientation in a steady magnetic field, is described.

Measurements obtained by using this system to study the vitreous compound $As_2Te_3Tl_2Se$ are reported, the frequency and temperature dependence of the Hall mobility being examined. An attempt to measure the Hall mobility in vitreous arsenic triselenide is also described.

Finally, an account is given of the observation of bistable switching in thin films of arsenic triselenide.

Chapter One

Introduction

1.1 The Study of Vitreous Semiconductors

The field of semiconductor physics covers a very wide range of materials. Within its bounds, there occur substances with conductivities from 10^{4} $ohm^{-1}cm^{-1}$ to less than 10^{-12} $ohm^{-1}cm^{-1}$, in which carrier mobilities may exceed 10^{5} $cm^{2}V^{-1}sec^{-1}$, or be below 10^{-2} $cm^{2}V^{-1}sec^{-1}$. Although the majority of semiconductors possess mobilities, μ, less than 100 $cm^{2}V^{-1}sec^{-1}$, examination has, until recently, been concentrated on materials of relatively high mobility. Theoretical analysis of conduction mechanisms has been based on the concept of a regular lattice with a high degree of periodicity; the lattice extending without structural interruption for many atomic distances. The result of this form of analysis has been the detailed development of the band theory of semiconductor physics. It has been found to be possible to apply the concepts of this theory to less perfect lattice conditions with surprisingly few modifications. However, as the consideration is extended to cover materials in which the mobility is very low, the concepts of the band theory become more questionable. It appears that, for all materials with $\mu < 100 cm^{2}V^{-1}sec^{-1}$, the mean free path of a carrier between trapping or scattering events is less than the quantum wavelength of the carrier, and that for $\mu < 5$ $cm^{2}V^{-1}sec^{-1}$, the interatomic distance actually exceeds the mean free path. When it is realised that no vitreous or amorphous semiconductor with a mobility greater than 0.5 $cm^{2}V^{-1}sec^{-1}$ has been reported to date, it becomes evident that the applicability of the band theory must be seriously examined. Even so, the band theory

seems to provide a reasonable description of many transport properties of such systems.

In the class of materials with very low mobilities, those exhibiting a disordered, non-crystalline structure are prominent. In discussing such materials, the terms 'amorphous' and 'vitreous' are frequently employed. 'Amorphous', in its usual context, implies the lack of a definite structure. However, the methods used in the preparation of what are usually referred to as amorphous solids (e.g. evaporation, chemical deposition, glass formation), generally result in the production of materials with some degree of ordering. Such ordering is limited to short spatial ranges, and would be expected to vary according to the method of preparation. In the following discussion, the term 'vitreous' will be used to describe solid materials prepared directly from a liquid by cooling sufficiently rapidly through the solidification range as to prevent crystallisation. The term 'amorphous' will be used to group other methods of preparation, such as evaporation.

The present examination is concerned with specifically vitreous materials. By their method of preparation, such materials retain the structure of the liquid at the temperature from which quenching occurred. It is possible to prepare a wide range of solids in the vitreous phase. The degree of disorder present in such materials is indicated by the results of X-ray diffraction examinations, which do not reveal the well defined line structure patterns characteristic of the periodic lattice. Rather, such an examination reveals a broad peak, indicating the preservation of short range order, which progresses into a continuous spectrum at greater atomic separations. Thus, no significant long range order

in the generally accepted sense is present. However, this does not necessarily infer that the structure is completely random. For example, long chains of atoms or other 'chemically regular' arrangements may exist in such a material. The indication is, therefore, that such structures, if present, occur in a somewhat irregular form. Slight variations of inter-atomic bond lengths and angles accumulate to give rise to the overall long range disorder.

In the majority of glasses, conductivities are extremely low, and conduction occurs by migration of ions through the bulk material. However, certain glasses can be prepared in which electronic conduction is the dominant mechanism of charge transfer. It is possible to perform experiments on a material in order to identify and separate the two forms of charge transport. For example, the concept of ionic conduction requires that the constituent elements of a glass migrate, and this can be detected in examinations of mass transfer, or by the use of radioactive tracer elements. Likewise, electronic conduction exhibits characteristic properties by which it may be recognised. By the application of such criteria, it is possible to ascertain that a number of glasses exhibit electronic conduction. Two major groups fall into this category; the chalcogenide and transition metal oxide glasses.

The chalcogenide classification, although somewhat loose in its application, generally relates to compounds between elements from group 5 and group 6 of the periodic table, and to mixtures of such compounds. Thus, in this class occur substances such as arsenic trisulphide, As_2S_3, and arsenic triselenide, As_2Se_3. Also, the glass formed by the element selenium is included in the group.

The chalcogenide materials generally form a vitreous phase quite readily.

The transition metal oxide glasses are formed from mixtures of the oxides of the elements in the first transition metal group of the periodic table with glass forming agents, such as P_2O_5 or B_2O_3. Of this group, the glasses containing the oxides of vanadium, iron, cobalt and copper have received the most attention.

The semiconducting glasses possess certain common characteristics. Their carrier mobilities are very low, no value of Hall or drift mobility higher than 0.5 $cm^2V^{-1}sec^{-1}$ having been reported. Room temperature conductivities are also generally low, although conductivities up to 10^{-2} $ohm^{-1}cm^{-1}$ have been measured in the glasses of more complex composition. The variation of conductivity with temperature is usually typical of intrinsic conduction in materials possessing a wide band gap; activation energies for the conductivity normally exceeding 1 eV. However, observations over extended temperature ranges have indicated that the measured activation energy often decreases markedly at low temperatures. This effect has been regarded as a manifestation of hopping conduction in the materials.

A further property of vitreous semiconductors and their amorphous counterparts has recently attracted considerable attention. The materials exhibit field-induced switching phenomena; both reversible and bistable (memory-type) switching having been observed. Such switching often involves a resistance change between the 'off' and 'on' states of eight or nine orders of magnitude, and the potential applications of devices utilising the characteristic are most attractive.

1.2 The Purpose of the Present Study

The aim of this study has been to develop systems for the study of drift and Hall mobilities of charge carriers in a range of vitreous semiconductors, and to use the completed systems in the examination of selected materials. If possible, it was hoped to make direct comparisons of Hall and drift mobilities in particular materials. In 'normal' crystalline semiconductors, the Hall mobility is always greater than the drift mobility, since the former is related uniquely to the velocity of carriers in motion, whilst the latter concerns the average carrier velocity, including the time spent in traps. However, in materials of very low mobility, the situation is by no means so clear. Transport by hopping is possible, and the occurrence and magnitude of the Hall mobility are not governed by conventional concepts. No widely accepted theory of the Hall mobility exists, but it has been indicated in the case of impurity hopping in crystalline semiconductors[1] that the Hall mobility may be anomalously low. Also, indications of a difference of sign between the Hall mobility and the thermoelectric power have been observed.

Academically, the present study was intended to be of value in extending the existing knowledge of the properties of vitreous semiconductors, by the examination of a fundamental parameter which had received little practical attention. No previous measurements of drift mobility in completely vitreous specimens had been reported, although some data was available on closely related evaporated films. Hall mobility measurements, by virtue of the exacting technical requirements of a suitable measurement system, had been rare, and limited mainly to the more conducting glass compositions. In view of the potential applications of vitreous semiconductors, it was felt

that a clearer understanding of their physical properties would prove to be necessary in order that they might be successfully exploited as electronic devices. In terms of device production, vitreous semiconductors have the advantage of possessing a process of conduction which is essentially bulk controlled, in contrast to the impurity controlled properties of most conventional semiconductor devices. Therefore, the problems associated with the controlled production of extremely pure material with a low density of lattice imperfections should be advantageously avoided.

In the examination itself, the intention was to restrict the choice of materials, as far as possible, to simple component systems, since it was felt that a basic understanding of such materials would be more useful than the examination of more complex systems.

In the following pages, an account is given of the measurement of Hall and drift mobilities, together with the results of subsidiary examinations of conductivity variations and switching phenomena.

In this account, it will be necessary to refer to a number of different forms of mobility. To avoid confusion, it will therefore be convenient to define these terms at this stage.

Microscopic mobility, μ_o: the true mobility of free carriers in the band states of a conventional, ordered, semiconductor.

Drift mobility, μ_d: the velocity of drift per unit field for a carrier moving in an electric field. (The drift mobility will be the same as the microscopic mobility only if no trapping processes are involved.)

Hall mobility, μ_H: the mobility as determined by a Hall effect technique.

Chapter Two

The Electronic Properties of Semiconductors

2.1 The Band Theory of Solids

Early developments in the field of solid state physics posed certain problems with regard to a number of materials which are now classed as semiconductors. The Rutherford-Bohr model of the atom showed that each atomic nucleus is surrounded by a number of electrons sufficient to neutralise the nuclear charge. However, many solids exhibited very low conductivities, whilst even in metals it could be shown that only about one electron per atom contributed to the conduction process. Furthermore, examination of the specific heats of materials showed that free electrons in a metal did not make the expected contribution to this property. A third problem arose concerning the sign of charge carriers when it was shown that Hall effect measurements indicated the presence of positively charged carriers in a large number of materials. These difficulties were essentially resolved in the early 1930's by the application of quantum mechanics to the analysis. The specific heat anomaly was solved by the application of the Fermi-Dirac statistics, by which it was possible to infer that only a small proportion of the electrons in a solid were free to contribute to the specific heat, or to any transport process. The other difficulties were resolved by the development of the band theory of solids. The electrons in a free atom arrange themselves as far as possible into closed groups or shells, which are generally inert. Only such electrons as are unable to become incorporated in these shells are able to take part in chemical reactions. The band theory of solids shows that an

analogous behaviour occurs in the solid state. The possible energy levels are arranged in bands of preferred energy, and these are separated by ranges containing no permitted levels of occupation. This situation is a consequence of the proximity of adjacent atoms, and of the positional uncertainty of their outermost electrons. The energy levels of the innermost atomic electrons are not greatly altered by the situation in a solid, being slightly modified to form narrow bands which are widely separated in energy. The discrete levels of the outer electrons are more significantly broadened, producing the relatively wide bands mentioned above. The processes of electronic transport are accomplished by the redistribution of electrons in these bands. It follows that the electrons in a band, in which all available energy levels are filled, are unable to contribute to these processes since redistribution in energy is not possible. This situation is changed only when the redistributing force is of sufficient magnitude as to transfer electrons to an unfilled band of higher energy, across the region of no preferred levels, or forbidden gap. The energies of electrons in an unfilled band may easily be increased by an exciting force, and it is these electrons which contribute to the conduction process. If, in a particular material, a band which is very nearly filled exists, the remaining vacant levels can behave in a manner equivalent to the presence of positively charged carriers ('holes') in a nearly empty band. The situation is indicated in the diagrams of figure 1. Figures 1a and 1b illustrate the general situation in the solid state, showing the arrangement of bands and the distribution of electrons in them. Generally, the situation in a metal is such that the lower (valence) band, and part

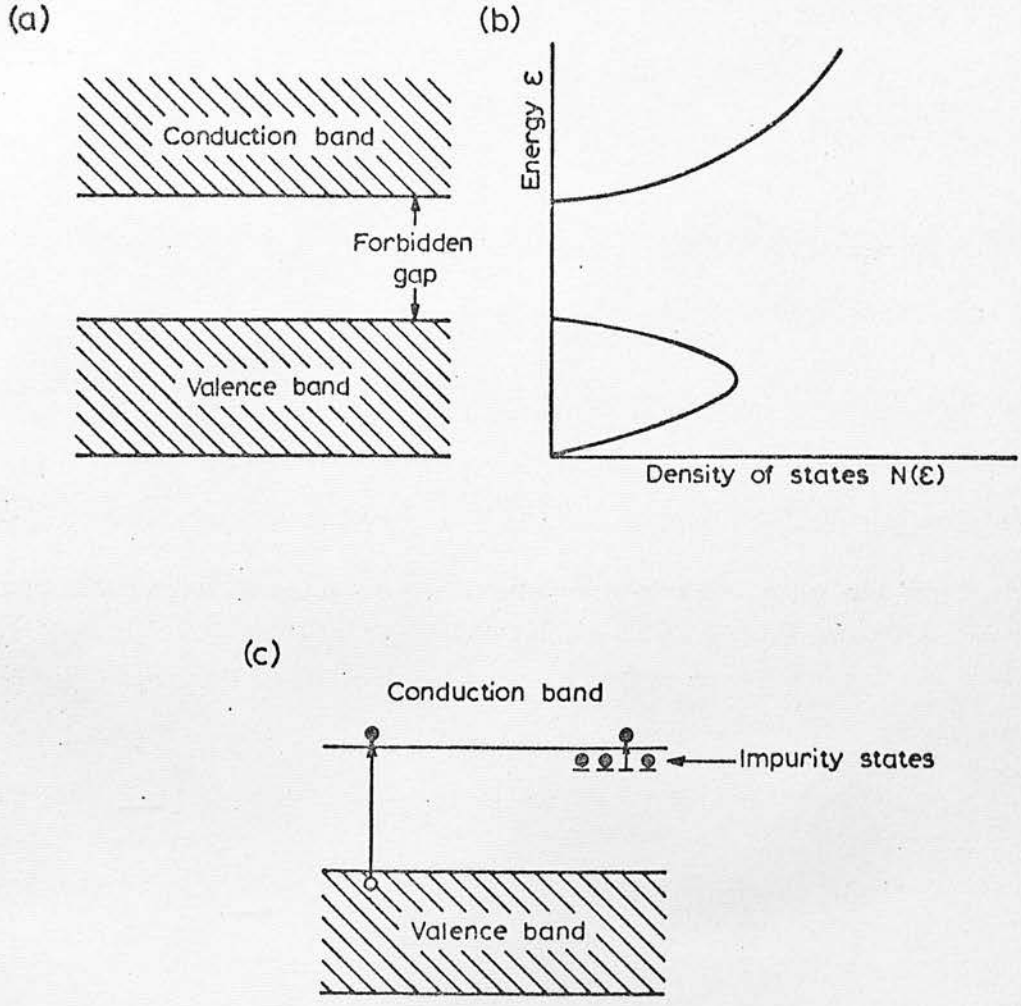

Fig. 1 The Band Structure of Crystalline Solids

of the upper (conduction) band are filled with electrons. The high conductivity is a consequence of the partially filled band, as described above. In an insulator, the valence band is still completely occupied, but the conduction band contains no electrons at zero temperature. At higher temperatures, there is a finite possibility of thermal excitation across the band gap, but this gap is sufficiently large so that only a small number of current carriers are produced in this manner. Hence, the electronic conductivity is extremely low, and conduction is usually of an ionic nature. Figure 1c illustrates the situation in a semiconducting material. Again, at zero temperature, the conduction band is empty and the valence band filled, but the width of the forbidden gap is sufficiently small that significant thermal excitation across it can occur at moderate temperatures. As already indicated, a positive 'hole' carrier is produced for every electron excited in this way, and both the electron and the hole may then contribute to the conduction process. This type of process is termed intrinsic, since it is a property of the fundamental lattice of the material. If, however, an extra atom is introduced into the lattice, it will distort the perfect periodicity of the structure. The energy levels associated with such an impurity atom can then be sufficiently displaced as to fall into the forbidden gap region. Such levels are termed impurity levels and are illustrated in figure 1c. It is evident that any electrons which may be excited from an impurity state will require much less energy for transfer into the conduction band than is necessary for intrinsic excitation. On the other hand, excitation of an impurity electron does not lead to the production of a mobile hole, but rather to a

fixed ionised centre. Thus, only one carrier, rather than two, is created by the excitation process. Impurities possessing more free electrons than are required for lattice formation tend to produce electron 'donor' levels lying below the conduction band as illustrated. Impurity atoms with less than the required number of electrons tend to produce 'acceptor' states above the valence band which may assimilate extra electrons, thus producing hole carriers in this band. The phenomena associated with the presence of impurities are termed extrinsic, since they are not characteristic of the fundamental lattice.

A familiar concept in the description of the distribution of carriers in energy states, is that of the Fermi level. According to the Fermi-Dirac statistics, the probability of occupation for a level of energy ε is

$$f(\varepsilon) = \frac{1}{e^{\alpha} e^{\varepsilon/kT} + 1} \qquad (2.1.1)$$

where T is the temperature, and α is a constant determined by the condition that the sum of the numbers of electrons in various levels should equal the total number of electrons in the band system of the material. An energy ε_f (termed the Fermi energy) is defined such that

$$\alpha = -\varepsilon_f/kT \qquad (2.1.2)$$

giving $$f(\varepsilon) = \frac{1}{e^{(\varepsilon-\varepsilon_f)/kT} + 1} \qquad (2.1.3)$$

At zero temperature, $f(\varepsilon) = 1$ for $\varepsilon<\varepsilon_f$, and $f(\varepsilon) = 0$ for $\varepsilon>\varepsilon_f$, giving the distribution shown in figure 2a. For non-zero temperatures, the Fermi energy is such that $f(\varepsilon) = \frac{1}{2}$ at $\varepsilon = \varepsilon_f$. For higher energies such that $\varepsilon - \varepsilon_f \gg kT$, then $f(\varepsilon) \simeq 0$, whilst for lower energies such that $\varepsilon_f - \varepsilon \gg kT$, then $f(\varepsilon) \simeq 1$. In the intermediate region, the

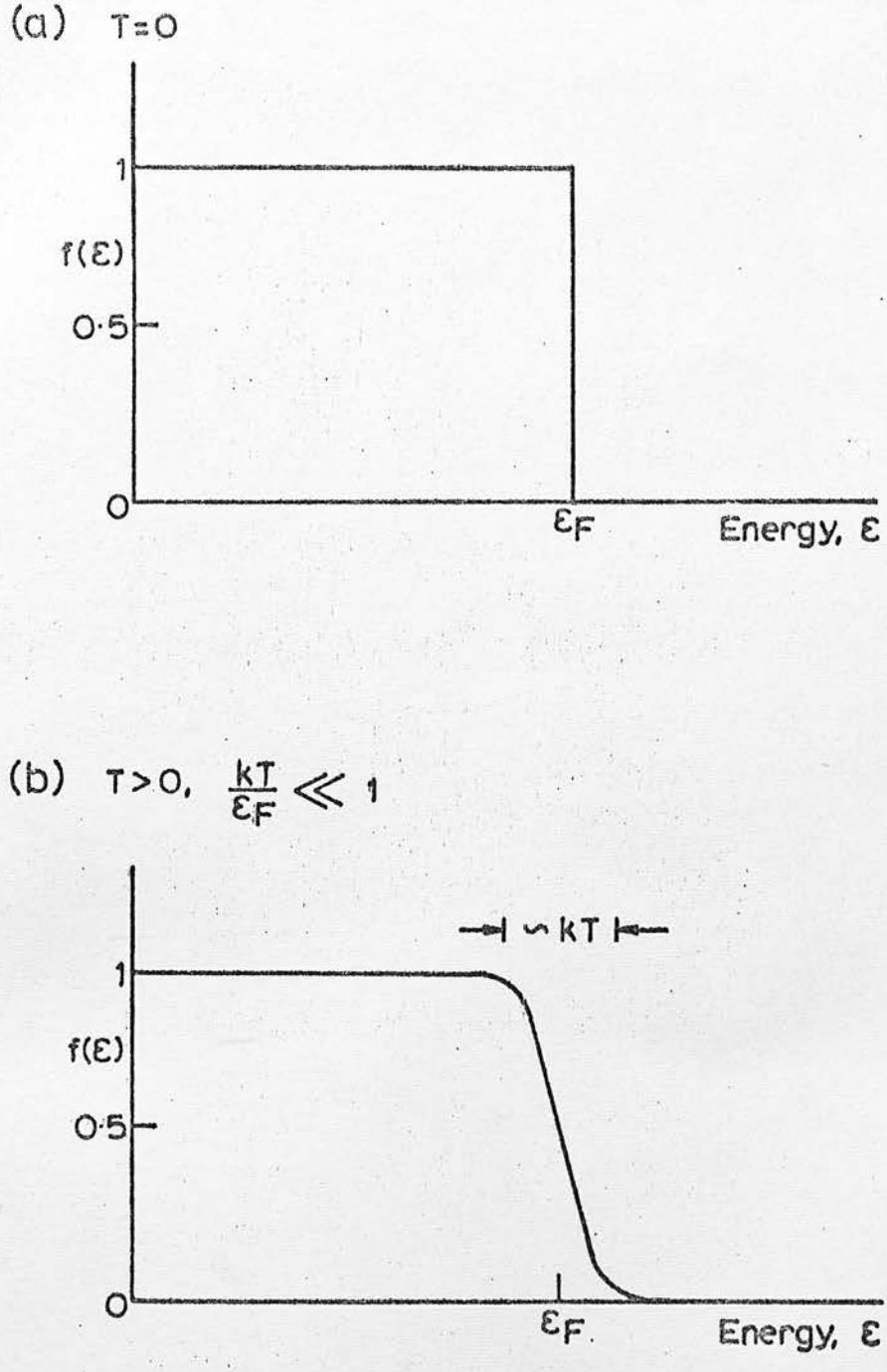

Fig. 2 Fermi-Dirac Distribution Function

distribution is rounded off as shown in figure 2b. The region over which the distribution is appreciably affected by temperature is of the order of kT in width.

In a semiconductor, the Fermi energy lies within the forbidden gap region so that, at zero temperature, the valence band states plus any additional impurity states below ε_f are completely filled, whilst the conduction band states and impurity levels lying above ε_f are completely empty. At higher temperatures, the occupancies of states within kT of the Fermi level will be modified as indicated, and, in cases where impurity states occur in the forbidden gap, the position of the Fermi level itself will generally change so as to remain consistent with equation 2.1.3.

One consequence of this description, of importance in the present study, is the situation with regard to trapping levels within the forbidden gap. A trapping site is able to interrupt the progress of a carrier moving in a band by spatial localisation. Once localised, the carrier may subsequently be re-excited into the band, or may be neutralised by the additional localisation of a carrier of the opposite sign on the same site. In the latter case, the 'trap' is more correctly described as a recombination centre. It follows from the above description that (electron) trapping levels which are situated at an energy ε, lying above the Fermi level such that $\varepsilon - \varepsilon_f > kT$, will have a low probability of occupation. Such levels are relatively close to the conduction band, and the probability of trap release will consequently be high. These states are normally referred to as 'shallow traps'. Similarly, levels situated well below the Fermi level such that $\varepsilon_f - \varepsilon > kT$, will have a high probability of occupation and a correspondingly low probability of

thermal carrier excitation into the conduction band. The description of such levels as traps or as recombination centres will depend on the relative probabilities of thermal excitation or of recombination in a particular case, the distinction being somewhat imprecise.[2] For convenience, such states will be collectively termed 'deep traps' in the subsequent text. It will be noted that the above description, in terms of electron traps and states, applies equally well to hole states, with the usual modifications to the terminology.

2.2 The Properties of Non-Crystalline Materials

In the preceding section, a fundamental description of the band theory, as applied to conventional materials, has been given. It is now necessary to consider whether the band model is applicable to materials which lack a regular crystalline structure, and if so, what modifications to the conventional model are necessary.

It is evident that the close proximity of the atoms in any solid will result in the distortion of individual energy levels, in accordance with the Pauli exclusion principle, by which no two electrons may have completely identical characteristics. Thus, the formation of a distributed electron energy spectrum is to be expected, and the occurrence of forbidden energy zones is not excluded. However, the quantum theories which are applied to the perfect lattice structure in order to derive the electron distributions of figure 1b can not be assumed, without examination, to be valid for a structure of greatly reduced periodicity. The necessary examination has been performed by Ioffe and Regel,[3] and others. It has been concluded that the band theory may be applied to such materials, subject to certain modifications. It appears that, provided a moving carrier experiences a reasonably periodic structure over its range of

motion (mean free path), then this is a sufficient condition for the band concepts to be valid in principle. Thus, the role of the long range order in a material is diminished, and attention is focussed on the nature of the short range order. The major consequence of the reduced periodicity appears to be that the sharply defined bands of the crystalline material become more diffuse, with tails of states extending into the forbidden gap as shown in figures 3a and 3b. The shaded states within the gap are of a localised nature, and are somewhat similar to the impurity levels previously mentioned. Mott[4] has further argued that there can, in fact, be no true gap if atomic centres in a solid are distributed at random, and that the models of figures 3c and 3d are applicable in such a case.

To complete the fundamental description, it is necessary to consider the actual differences which can be expected between the crystalline and vitreous states. Since a glass may be regarded as retaining the structure of the liquid phase at the temperature from which quenching occurred, it is instructive to examine the changes which take place when a crystalline material is liquified. A great deal of information on this subject has been brought together by Ioffe and Regel[3], and by Glazov et al[5]. It is evident that the details of the change depend strongly upon the structure of the material in question, and on the amount of order which is retained during the fusion process. For example, consider selenium, a substance of some interest in the present study. In the crystalline state, several allotropes can be obtained by different crystallisation procedures. The thermodynamically stable form at room temperature is grey selenium, which possesses a hexagonal structure consisting of helical chains parallel to the z-axis, as shown in figure 4.

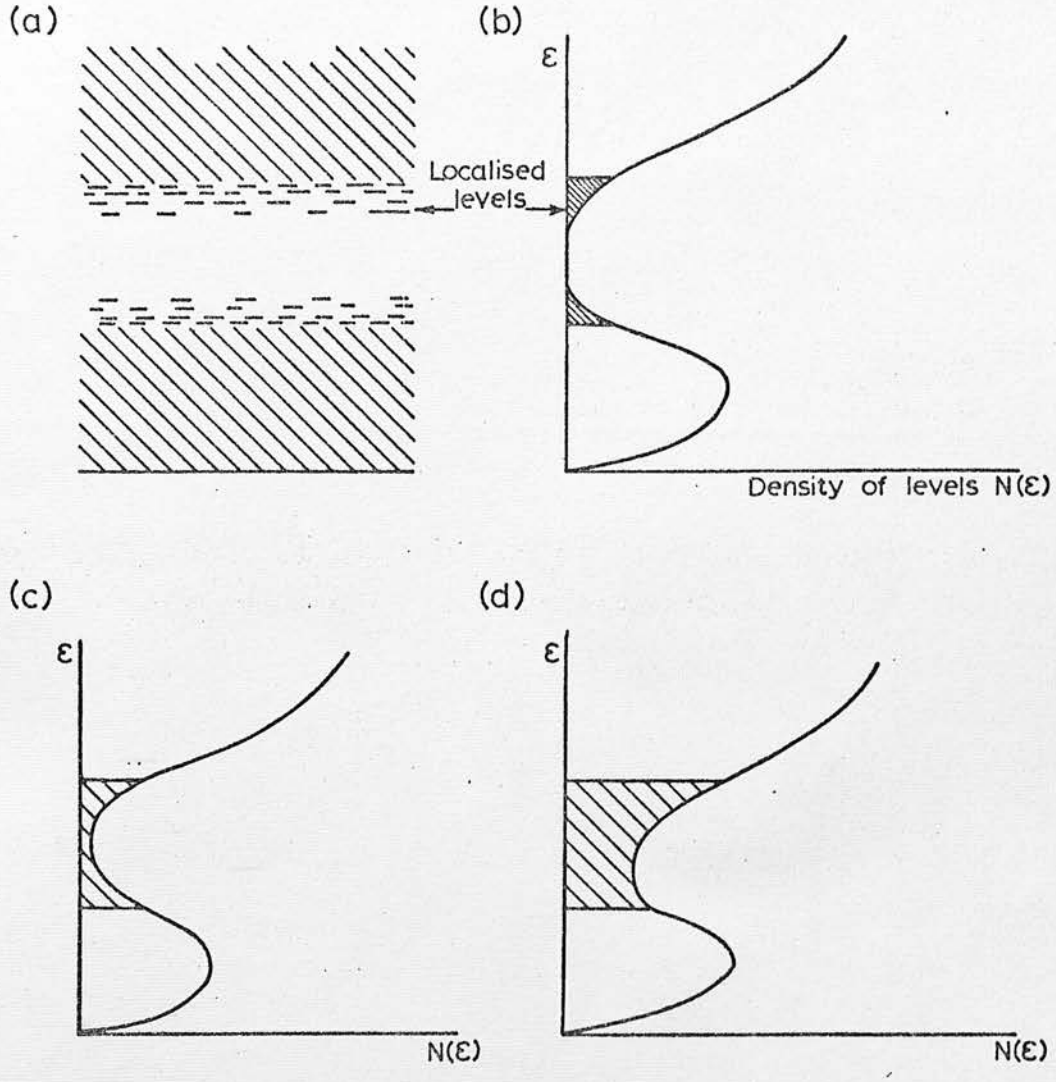

Fig. 3 Suggested Band Structures of Non-Crystalline Semiconductors

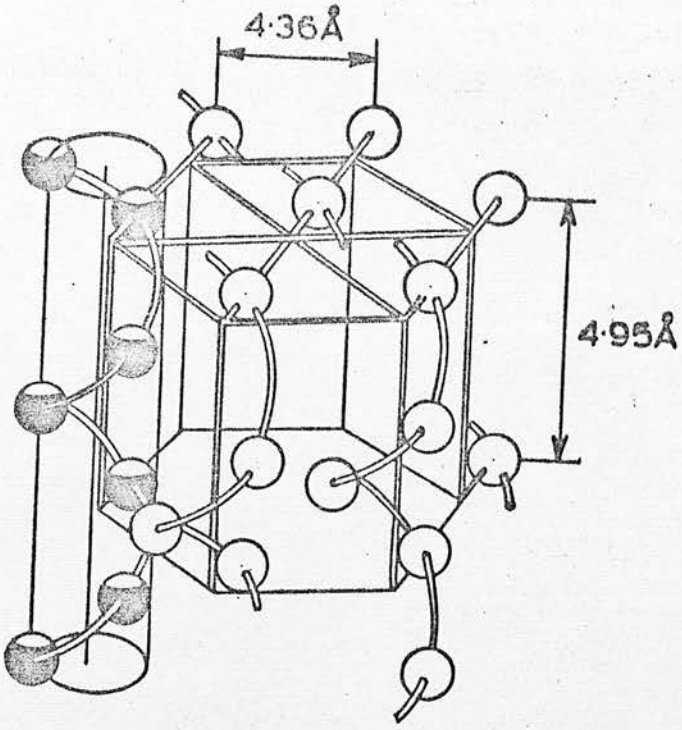

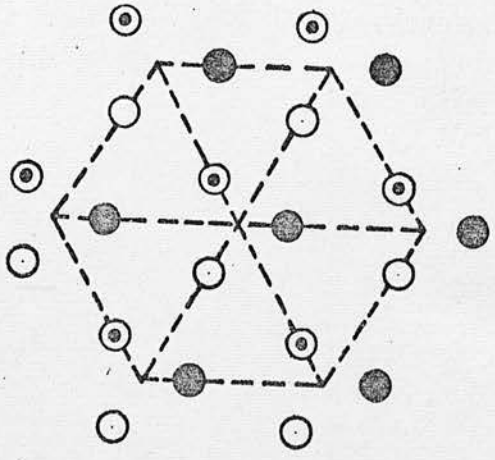

1 ● 2 ⊙ 3 ○

1, 2 and 3 represent the first, second and third atoms in a chain

Fig. 4 Structure of Hexagonal Selenium

According to Mooser and Pearson[6], the binding between chains is complex, involving electron d-orbitals. However, the majority of other authors suggest that the bonding is controlled by weak Van der Walls forces, as indicated by the low melting point and easy cleavage along planes parallel to the z-axis[5]. In the hexagonal form, the resistivity is very high, exceeding 10^{12} ohm.cm., and is somewhat anisotropic. The Hall coefficient and thermopower indicate p-type carriers, which have been associated with the presence of structural defects and, more specifically, with the finite length of the helical atomic chains whose unsatisfied valence bonds give rise to acceptor levels. The hole density decreases slowly with increasing temperature, whilst the mobility rises. The majority of investigators agree that the cause of such (for semiconductors) anomalous behaviour is the existence of potential barriers which the hole carriers surmount by thermal excitation. Henkels[7] and Kozyrev[8] have suggested that the presence of amorphous layers between crystal boundaries could give rise to such barriers. Stuke[9] has advanced the theory that the crystal structure itself might be responsible through the presence of an imhomogeneous distribution of defects, the suggestion being supported by the similarity of properties of single-crystal and polycrystalline specimens. Lange and Regel[10] have advanced a mechanism of hole generation which is consistent with this model. It is suggested that the structure becomes less imperfect with increasing temperature, causing the fall in carrier density and increase in mobility.

Upon melting, selenium is characterised as forming a molecular liquid. The existence of long chains, and of eight-membered rings, of atoms has been demonstrated in the fused material,

[11,12,13] and a theory of thermal equilibrium between chains and rings has been suggested[14]. Some of the physical properties which have been measured over the fusion range are recorded below.

a) Conductivity. Measurements by Abdullaev et al[15], and by Meilikhov[16], have stressed the importance of material purity and of measurement frequency upon the transport properties of crystalline selenium. Figure 5 shows some of the electrical measurements of these investigators. A decrease in the d.c. conductivity of specimens containing oxygen occurs upon melting (curves 1 to 3 of figure 5a, and figure 5b). This might be explained by the 13% density reduction which has been observed, with the conductivity change being primarily caused by the increase in atomic separation. However, the conductivity discontinuity disappears at very high measurement frequencies (figure 5c) and in oxygen-free material (curves 4 and 5 of figure 5a). It is also evident from these results that the activation energy of the conductivity is extremely sensitive to impurities and to measurement frequency, both in the solid and the liquid phases.

b) Thermopower. The sign of the thermopower in unpurified selenium is indicative of hole conduction in both the crystalline and liquid states, in most measurements. However, Meilikhov[16] has reported a transition from p to n-type characteristics on melting, as have Abdullaev et al[15] for deoxygenated material. It would therefore appear that impurity doping can have a considerable effect.

c) Viscosity. Measurements do not indicate that the chain structure of the crystal is seriously modified upon melting, and x-ray examination reinforces this opinion.

d) Susceptibility. Measurements of the diamagnetic susceptibility have shown an increase in this parameter on melting. The increase in

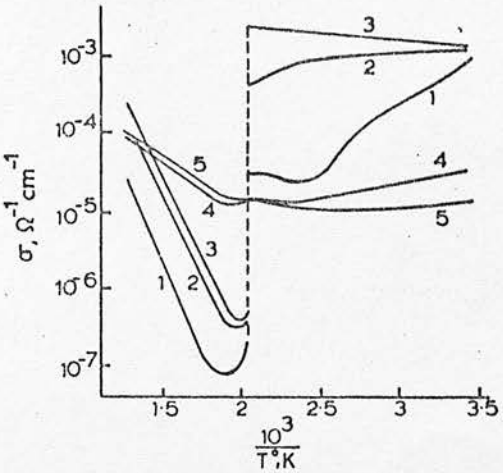

(a) D.C. measurements (Abdullaev et al.)
1, 2 and 3 : Material containing oxygen. 4 and 5 : Oxygen free material

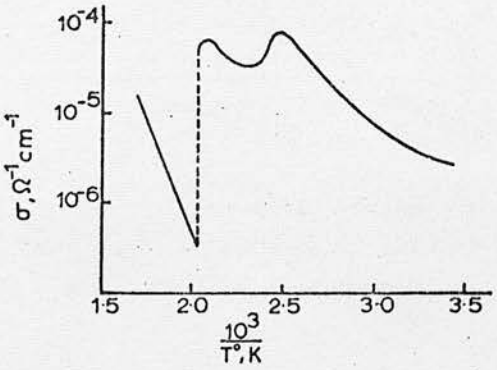

(b) D.C. measurement (Meilikhov)

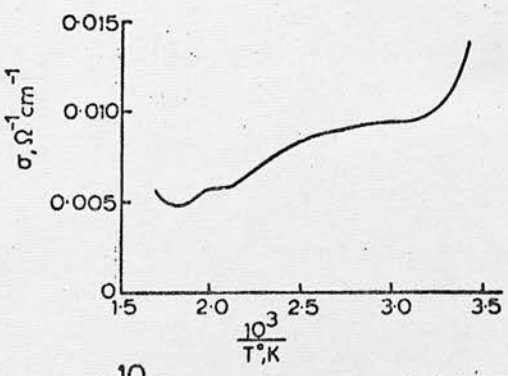

(c) 10^{10} Hz measurement (Meilikhov)

Fig. 5 Conductivity of Crystalline and Molten Selenium

total susceptibility may be due to a decrease in the paramagnetic component. Massen et al[17] have shown that the paramagnetic component is associated with the formation of hole carriers at the ends of selenium chains. This would infer that melting is accompanied by a closure of some chains into rings, resulting in a decrease in hole density.

When liquid selenium is cooled into the vitreous state, no abrupt variation of physical properties is observed on solidification. Thus, it is to be expected that no major structural differences occur between the liquid and vitreous phases, aside from the progressive change caused by the decrease in interatomic separation on cooling. In general, the results demonstrate that a high degree of order is retained in the transformation from the crystalline to the liquid state, and that this order persists on cooling to the vitreous state. An interesting study in this respect has been performed by Urazovskii and Lyuft[18]. Glasses were formed by rapidly quenching liquid selenium from various temperatures. The glasses were then crystallised by the action of special chemical agents. It was found that the ability to undergo such crystallisation decreased rapidly, and that the specific gravity increased, when the material was quenched from temperatures above 450°C. This would indicate that considerable dissociation occurs at such temperatures, and that the dissociation is preserved during the transition to the vitreous state.

The properties of other chalcogenide materials, such as antimony trisulphide and telluride, and bismuth triselenide and telluride, are discussed by Ioffe and Regel[3] and Glazov et al[5]. In general, it is again possible to conclude that no significant change in the short range order and co-ordination of the crystalline

structure occurs during liquefaction.

It is worth noting that the above descriptions apply specifically to the transitions between the crystalline and liquid, and the liquid and vitreous states. In considering the situation with respect to amorphous films, whether prepared by chemical means or by evaporation, it is not immediately evident that the order of the liquid phase will be preserved or duplicated in the amorphous structure. Even if a degree of short range ordering is present in amorphous films, and there is evidence to support the proposition, the identity of structure which is sometimes assumed between the vitreous and amorphous states must be critically examined. Conceivably, the amorphous structure might be close to that of a glass quenched from a very high temperature, and one would expect the degree of ordering in such a case to be less than that present in a glass prepared by conventional means.

Some of the properties of vitreous semiconductors have been indicated above. A more detailed description of these properties, in relation to materials of specific interest to the present study, will now be given. Since the study was, in practice, concerned primarily with the chalcogenide glasses, the following summary of properties is mainly concerned with such materials, although many of the characteristics are also applicable to the transition metal oxide glasses.

a) Conductivity. In the chalcogenide glasses of simple composition, the electrical conductivity is very low, typically being less than 10^{-10} $ohm^{-1}cm^{-1}$. With increasing complexity of composition, it is possible to prepare much more conducting glasses, with room temperature conductivities up to $10^{-2}ohm^{-1}cm^{-1}$. In the

room temperature region, the activation energy for conduction is high and generally well defined[19,20,21] (2.1 eV for As_2S_3, 1.8 eV for As_2Se_3). However, there is increasing evidence that the measured conductivity activation energy is temperature dependent, and the measured activation energy decreases with frequency, falling almost to zero at ultra-high frequencies. In examining the conductivities of thin films of highly resistive material, it has frequently been reported that a dependence upon the magnitude of the applied electric field is observed. This dependence has been associated with the field-assisted thermal excitation of charge carriers. In general, the modifications of conductivity produced by the addition of doping agents to vitreous semiconductors are much smaller than is the case for crystalline materials. Exceptions to this observation are usually indicative of the radical modification of the 'molecular' structure of the material.

b) Mobility. Hall mobility measurements on vitreous and evaporated specimens[22-26] have revealed mobilities generally of the order of $10^{-1} cm^2 V^{-1} sec^{-1}$. Drift mobility measurements on evaporated films[27-35] have indicated mobilities ranging from 10^{-1} to 10^{-5} $cm^2 V^{-1} sec^{-1}$. The activation energy of the Hall mobility has been found to be very low in the more conductive materials studied to date, and the Hall coefficient is apparently negative, indicating charge transfer by electrons to be dominant. However, drift mobility measurements have indicated that the mobility of holes is much higher that the electron mobility. Activation energies for the drift mobility in the range 0.1 to 0.5 ev have been reported.

c) Thermoelectric Power. Measurements[36] have shown a positive coefficient, indicating hole transport to be dominant. In

magnitude, the thermoelectric power is comparable with that observed in crystalline materials, being of the order of $10^3 \mu V/^oC$. There would appear to be a general disagreement between the signs of the Hall and thermoelectric effects, although the dependence of the latter on purity in the liquid state[15,16] indicates that such an assertion must be made with some reservations.

d) Optical Properties. Many of the simpler compositions (Se, As_2S_3, As_2Se_3, etc.) are transparent, either in the visible or infra-red regions of the spectrum. The more conducting 'alloy' compositions often have a metallic appearance. Measurements of optical absorption indicate a diffuse, exponentially varying absorption edge with little fine structure. In As_2Se_3, the 'edge' occurs over the range 1.4 to 1.9 eV[21]. Edmond[19,20] has measured an optical activation energy of 1.85 eV for As_2Se_3, and 2.0 eV for As_2S_3. However, in view of the uncertainty of position of the absorption edge, Owen[37] has pointed out that the activation energies may be as high as 2.0 and 2.5 eV respectively.

3) Switching Behaviour. Mention of the property of field-induced switching has already been made. A wide range of materials have shown this characteristic, which is potentially of great value. However, the mechanisms governing such behaviour are incompletely understood. The phenomenon is often described in terms of structural reorientation, which may include local crystallisation.[38,39,40,41]

The above review of the properties of vitreous semiconductors necessarily contains data on a wide range of materials. However, even allowing for this fact, it is seen that the fundamental characteristics of such materials are extremely complex, and to date

no single theory has been advanced which successfully covers the whole spectrum of properties. Certain models have, from time to time, been suggested to account for the major characteristics of electrical conduction. One such suggestion, which is frequently encountered, postulates the existence of conducting islands or zones within an insulating medium, with individual models differing in the supposed nature of the zones.[9,42,43]. In this context, crystalline, vitreous phase separated, and macromolecular zones have been suggested. In figure 6a, such a postulated structure is shown. It is suggested that the conduction type in the zone might be of the opposite sign to that outside, and that the conductivity would be higher in the zone. Thus, measurements of an essentially d.c. nature, such as the d.c. conductivity, thermopower, and drift mobility would reveal the properties of the relatively insulating bulk; the zones being isolated by virtue of the p-n junctions present at their perimeters. At higher frequencies, the conducting zones would make a progressively greater contribution to the observed effects, so that the conductivity would increase with frequency. It has been shown[44,45] that examinations of the d.c. Hall effect in materials of an inhomogeneous nature can lead to obscure results, even in the absence of p-n junction barriers. The conclusions of the analysis depend on the parameters of the model under consideration, but it is indicated that the measured mobility may be more characteristic of the conducting zones than of the insulating medium. In such a case, the measured mobility would be smaller than that in the zones by a factor of the order of the ratio of the zone resistivity to the measured (i.e. average) d.c. resistivity. This could account for the low values of Hall mobility which have been measured, and it might be possible

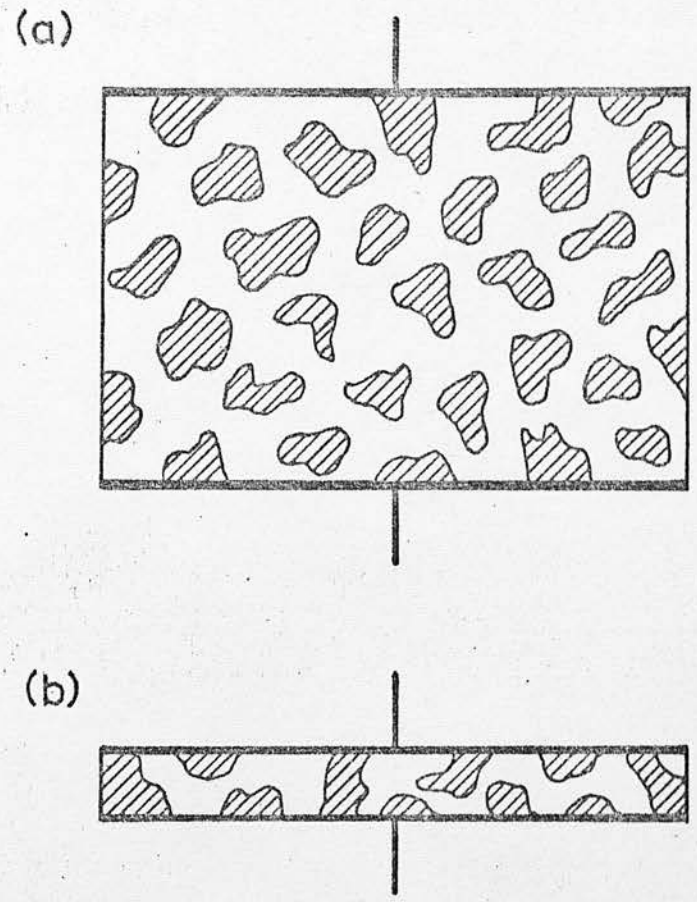

Fig. 6 A Possible Structural Model for Vitreous Semiconductors

to extend such an examination to explain the sign difference between the Hall and thermoelectric data. Such an extension would require an estimate of the effects of p-n junctions, present if the zones and insulating matrix were characterised by carriers of opposite sign. A consequence of the 'zone' model would be that the magnitude of the measured Hall mobility would be expected to increase with increasing frequency, in proportion to the decrease in measured resistivity. At high frequencies, the mobility would approach a value equal to that in the conducting zones, which, for band conduction, would not be expected to be less than 10 $cm^2V^{-1}sec^{-1}$. It might even be possible to regard the observed field dependence of the conductivity as resulting from excitation of carriers across the junction barriers around the zones. Objections to this type of model have, however, been raised by certain measurements. The presence of a large number of semiconductor junctions in a material should be revealed by an examination of the noise spectrum, whereas this has not been the case in practice; a very low noise level being measured[46]. Furthermore, physical considerations of junction width suggest that a minimum zone diameter of a few microns could be expected. One would therefore expect that, in specimens of decreasing thickness, a point would be reached at which single zones would span the specimen, as shown in figure 6b. Consequently, a much higher conductivity should be observed at such a width. Measurements upon thin film specimens, of thickness down to one micron, have shown no such effect. By a similar argument, it would be expected that the relatively high drift mobility proposed for the zones would be observed in thin films, whereas such is not the case in practice. It is, however, possible to further develop this type of structural

model, particularly in terms of a polymerised large molecule zone which would not necessarily be subject to the above objections, and to explain by it many of the properties of vitreous materials[85]. Thus, the possibility of such a structure cannot be discounted at present.

An alternative approach to the problem is to accept the observed low conductivity and mobility values as being representative of the overall situation in the bulk material, and to examine possible conduction mechanisms by which such low values might be expected. In the situation shown in figures 3a and 3b, where disorder in a material has caused the band structure to be distorted so as to create 'tails' of localised levels at the extremities of the conduction and valence bands, there are two major processes by which transport phenomena may take place. For simplicity, it will be convenient to consider the situation with respect to electron transport, as shown in figure 7. The analysis will apply equally to the hole transport properties.

An electron possessing an energy sufficiently above the critical value, ε_c, will move in the region of non-localised states in a manner similar to the motion of an electron in the conduction band of a conventional semiconductor. The motion will be limited by the usual trapping and scattering events, and a carrier may also experience extra scattering due to the reduced periodicity of its surroundings. For the situation to have any physical validity, it is necessary that the mean free path, L, of the carrier (between scattering events) be at least as great as its quantum wavelength. By applying the Maxwell-Boltzmann statistics to the free electron

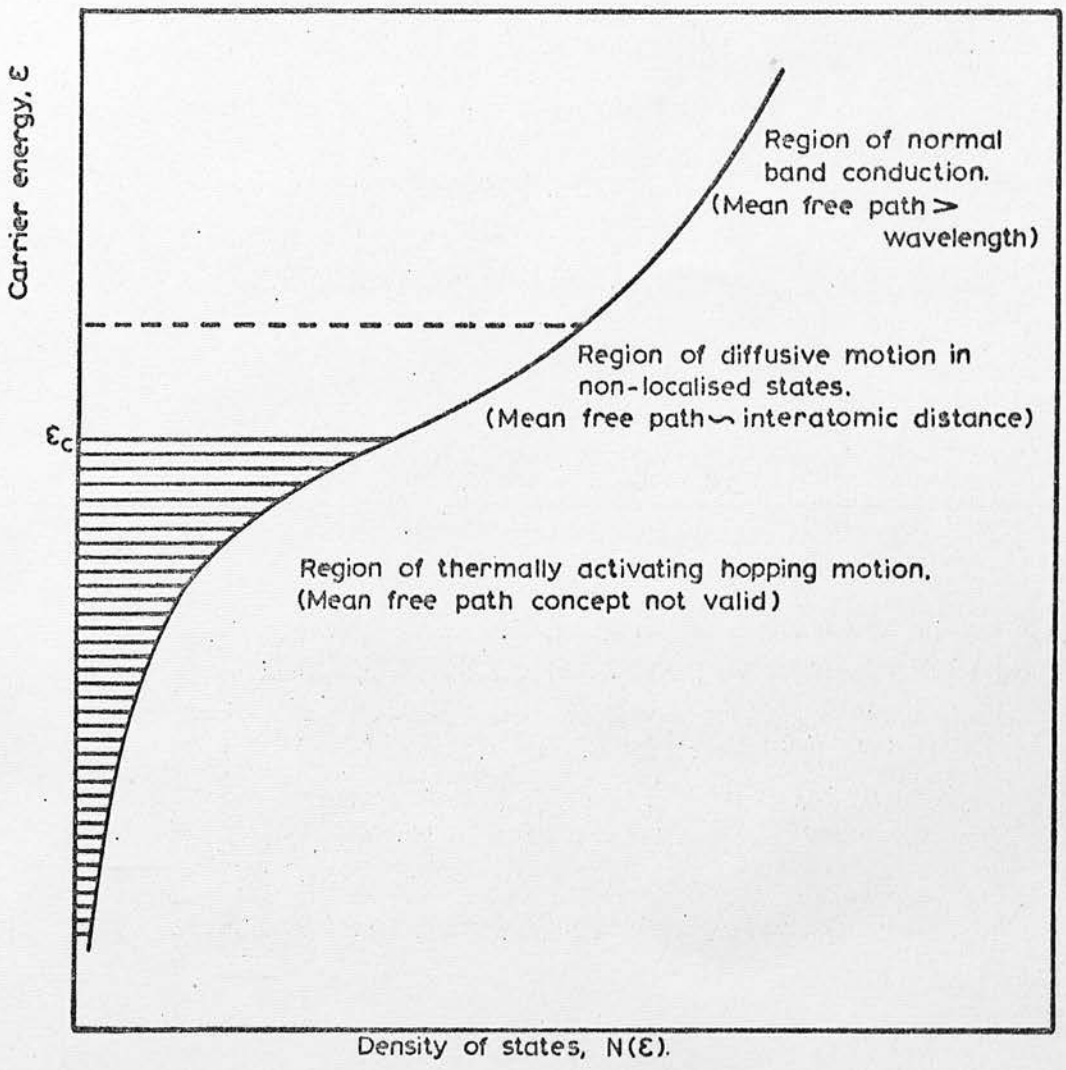

Fig. 7 Density of States in a Disordered Semiconductor, Showing Various Regions of Electron Transport.

cloud in the conduction band, the thermal velocity, v, of the carrier at room temperature can be estimated as 10^7cm/sec, giving a carrier wavelength of approximately 50 Å. The conventional formula for the microscopic mobility of a semiconductor[47] is

$$\mu_o = eL/mv \qquad (2.2.1)$$

where e and m are the electronic charge and mass.

Thus, $$\mu_o \gtrsim 100 \text{ cm}^2\text{V}^{-1}\text{sec}^{-1} \qquad (2.2.2)$$

It should be noted that the drift mobility, μ_d, may be significantly less than this value due to the reduction of the <u>average</u> velocity by trapping events, but the lowest value of the microscopic mobility which is physically meaningful is still of the order of 100 $\text{cm}^2\text{V}^{-1}\text{sec}^{-1}$.

An alternative mode of transport, which must be considered in view of the postulated high density of localised levels, may occur if the electron hops from one localised state to another without activation to energies greater than ε_c. Under these conditions, the mobility may be written as

$$\mu_{hop} = (e\nu_p a^2 \phi/kT)\exp(-W/kT) \qquad (2.2.3)$$

where a is the average interatomic distance

ν_p is a phonon frequency $\sim 10^{12}$ to 10^{13}sec^{-1}

ϕ is a factor dependent upon the overlap between wave functions of the localised states.

W is the hopping energy.

Mott[4] has noted that the phonon frequency, ν_p, (appropriate here since thermal vibrations of the lattice provide the excitation energy for the hopping process) is valid only if $W > k\theta_{Debye}$ and is not valid for impurity conduction at very low temperatures. The factor ϕ

contains terms for the probability of carrier tunnelling, $\exp(-2\alpha a)$, and for the overlap of the wave functions. Here, α is the rate at which the atomic wave function falls off with distance. If the overlap is small, ϕ behaves approximately as $\exp(-2\alpha a)$, and approaches unity as the overlap increases. Mott has further pointed out that, for energies approaching ε_c, each localised state will overlap with a large number of others, so that ϕ will become much larger than unity. Ignoring, for the moment, the possibility of such multiple overlap, it is possible to estimate the upper limit of magnitude for the hopping mobility. As ε approaches ε_c, it is expected that the hopping energy will tend to zero. Setting the overlap factor, ϕ, equal to one, the mobility becomes

$$\mu_{hop} = \frac{e\,\nu_{ph}\,a^2}{kT} \qquad (2.2.4)$$

$$\leq 0.5\ cm^2V^{-1}sec^{-1} \text{ at room temperature.}$$

Mott[4], and Cohen[48] have also considered the situation for electrons in the non-localised region for ε just greater than ε_c, and both have predicted a mobility of the form

$$\mu_{diff} = \frac{e\,\nu_{el}\,a^2}{kT} \qquad (2.2.5)$$

where ν_{el} is an electron frequency of the order of 10^{15} sec^{-1}. The carrier motion can be regarded as a diffusive process, differing from the hopping motion described above in that no hopping energy or tunnelling factor is concerned in the process. The mobility is of the order of 100 $cm^2V^{-1}sec^{-1}$ at room temperature, i.e. about 100 times greater than in the hopping case. It will further be noted that the diffusive mobility is of the same magnitude as that calculated for the lower limit of the band mobility. Mott[4] is of the opinion that values of the mobility less than this figure should not be expected in

the non-hopping range unless the density of states is low. It can be seen that, as the electron energy crosses the critical value ε_c, a large change in mobility should occur. A similar situation occurs for hole conduction in the region of the top of the valence band, and the overall picture can be illustrated as shown in figure 8, introducing the concept of a 'mobility gap' between the limits of non-localised states. Over the region of the abrupt mobility change, Mott[4] points out that the factor ϕ in the hopping analysis may be large, so that no actual discontinuity in the conductivity (and thus mobility) is to be expected for non-zero temperatures. Cohen[48] also suggests that no discontinuity will occur, and introduces a 'correlation factor', f, in the expression for the diffusive mobility (equation 2.2.5) such that $0 \leqslant f \leqslant 1$. Owen[37] has pointed out that, if a carrier traverses only a few atomic distances between trapping events, the diffusive mobility rather than the microscopic mobility should be employed in expressions for the trap-limited drift mobility. Furthermore, the simplified picture of the energy band structure presented here and in the distributions shown in figure 3 will be complicated by the particular properties of individual semiconducting glasses. Structural peculiarities may give rise to high densities of localised levels at particular energy values, and the localised 'tails' may actually overlap in the more complex materials, producing charged states in the overlap region. The conductivity energy gap, calculated from considerations of the gap between states making maximum contributions to the conductivity (figure 9), will not necessarily be equal to the mobility gap. Differences in the contributions to conductivity from electron and hole states, as indicated by the areas

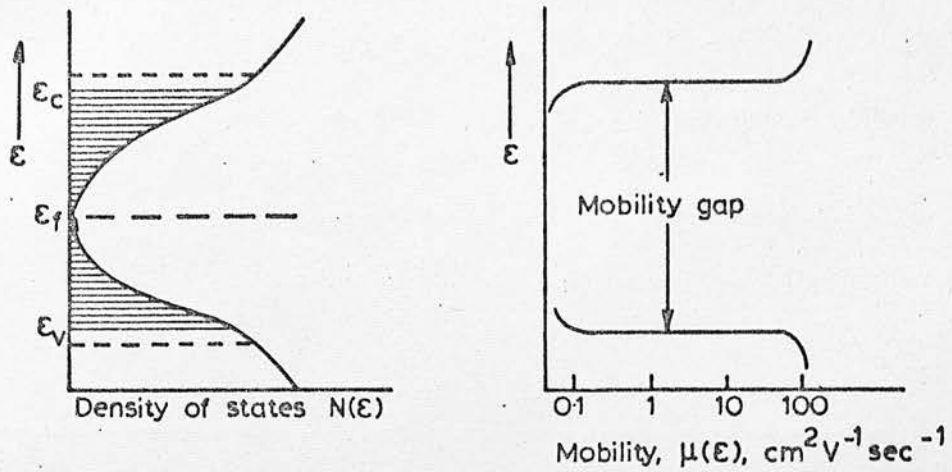

Fig. 8 Density of States Function and Mobility Gap in a Disordered Semiconductor

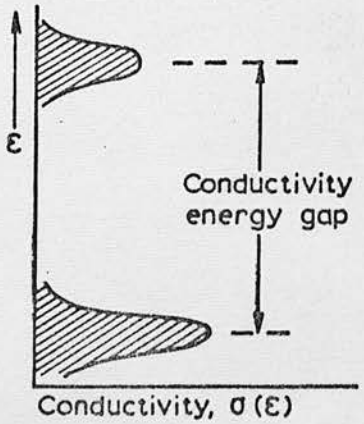

Fig. 9 Contributions to Conductivity from States of Different Energies

of the shaded regions in figure 9, will also depend on the material under consideration.

The theories outlined above have been developed from considerations appropriate to wide-band semiconductors, and only states near the bottom of the conduction band and top of the valence band have been considered in discussing the transport properties. In such conditions, the carriers will have low values of effective mass, m*. Owen[37] has suggested that a relatively small overlap of atomic or molecular wave functions would result in the production of narrow energy bands separated by wide gaps. The carriers of high effective mass nearer the centres of the bands would then play an important role in the transport properties. Increasing the effective mass of a carrier decreases its quantum wavelength, and an effective mass m* > 100m will lead to a wavelength of less than an atomic spacing. Carrier localisation, and a hopping form of transport, will then occur. Owen indicates that this situation may well apply to vitreous semiconductors, so that localisation may not primarily be due to the structural disorder.

In a material in which carrier transport may occur either by hopping or by excitation into (and motion in) a band, the variation of the carrier transport properties with temperature may be regarded in terms of the two processes acting 'in parallel'. In the case of thermally activated hopping in conjunction with trap-controlled band motion, the drift mobility will be represented as the sum of two components, each exponentially dependent upon temperature. The situation bears a strong similarity to the case of impurity conduction observed in conventional crystalline semiconductors; that is, in materials containing a large number of

donor states in addition to a smaller number of acceptor states. Electrons are transferred from the donor to the acceptor states leaving empty donor states which are utilised in the electron hopping process. For convenience, the discussion is here limited to the case of n-type material. The impurity conduction process has been examined by (among others) Miller and Abrahams[49], and Mott and Twose[1]. Following the discussion above, the trap controlled drift mobility may be expected to exhibit a high temperature value of over 100 $cm^2V^{-1}sec^{-1}$ and to decrease with decreasing temperature with a (relatively large) activation energy determined by the depth of the controlling traps. The hopping mobility, on the other hand will be expected to have a maximum (high temperature) value of less than 10^{-1} $cm^2V^{-1}sec^{-1}$. This value will also decrease with temperature, but with a substantially smaller activation energy. Thus, the hopping component of the transport process becomes dominant at low temperatures. In the examinations mentioned above, the donor hopping centres are regarded as forming a random lattice in the dielectric medium of the bulk of the crystal. Because of the nature of the hopping process, the transport properties are extremely sensitive to the separation of the hopping centres, and hence to the impurity concentration. For very high concentrations, the individual states overlap sufficiently as to cause the formation of an 'impurity band', and metallic conduction is observed. However, it is the situation at lower impurity concentrations, where hopping can occur, which is of interest here. Mott and Twose reach some interesting conclusions on the nature of the Hall mobility in the hopping region. In particular, it is suggested that the Hall mobility may be much smaller than would conventionally be expected,

or that this mobility may be zero at low impurity concentrations (and low temperature). Also, considering the motion of electrons between the positively charged donor vacancies, it is indicated that the sign of the Hall effect will be negative, so that the positive vacancies can not be regarded as equivalent to hole carriers in the normal manner. If the impurity model is qualitatively applicable to the situation in vitreous semiconductors, these conclusions could be used to explain the low measured values of the Hall mobility, and the sign anomaly between the Hall and thermoelectric measurements.

A large proportion of the study of hopping conduction in amorphous materials has been concerned with the properties of the polaron[50-53]. Essentially, the introduction of an electron (or hole) into a polar lattice can produce distortion of the lattice resulting in a polarisation charge with which the carrier can interact. Under conditions of sufficiently strong interaction, the carrier and its polarisation charge may move together as a single entity, which is termed a polaron. Considerations of the coupling energy, determining the 'size' of the polaron, show that the 'small polaron' concept is particularly applicable to materials of interest here. In such an entity, the radius of the polarisation potential well is less than the interatomic distance; hence the terminology. In non-crystalline materials, possessing no regular lattice, the application of the polaron concept is not of obvious validity. However, consideration has shown that the concept may be applied to polar glasses[4,47], and small polaron conduction has even been postulated in non-polar materials such as sulphur[54,55], although it is difficult to envisage how a high degree of local polarisation could occur in such materials.

In considering the variation of conductivity (and mobility) with temperature under hopping conditions, Mott[4,47] has shown that the increase of hopping distance with decreasing temperature will lead to a relationship of the form

$$\log_e \sigma = A - BT^{-\frac{1}{4}} \qquad (2.2.6)$$

where σ is the conductivity, T the temperature, and A and B are constants. The derivation of this equation is independent of the formation of polarons. Killias[56], considering the hopping of small polarons, has also predicted a non-linear temperature dependence of the conductivity, of the form

$$\log_e \sigma = A - \frac{B(1 - \theta_R/T)}{T} \qquad (2.2.7)$$

where A and B are again constants, and θ_R is a characteristic temperature.

An exponential dependence of conductivity on the square root of the applied electric field has been observed in a variety of dielectric materials. This phenomenon is normally ascribed to two related phenomena; the Poole-Frenkel and Schottky effects. The Poole-Frenkel effect concerns the field assisted thermal emission of carriers from charged trapping centres. Figure 10a depicts a charged coulombic trap. The potential energy in the field of such a centre is given by the usual coulombic expression $-e^2/4\pi K\varepsilon_o x$, where e is the electronic charge, K is the relative high-frequency dielectric constant, ε_o is the permittivity of free space, and x is the distance from the trap centre. In the absence of an applied electric field, a trapped carrier must surmount a barrier of energy ϕ to enter the conduction band. If an electric field, E, is now applied, the situation is modified as shown in figure 10b. The coulombic

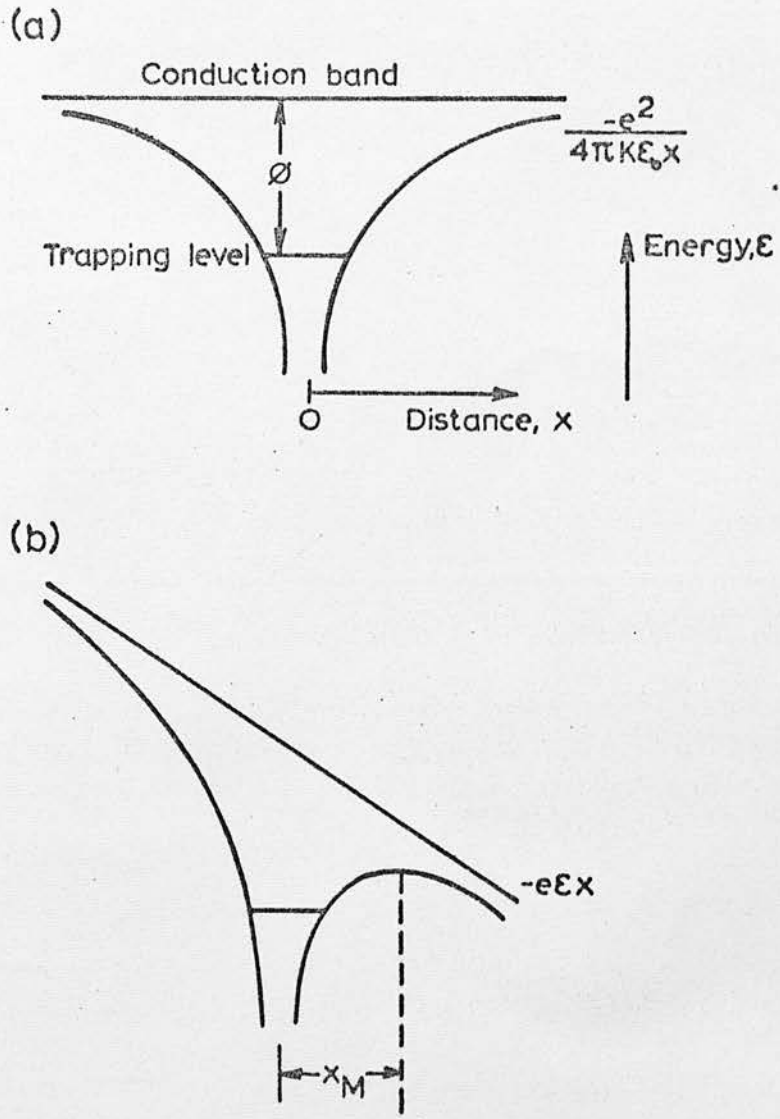

Fig. 10 Effect of Applied Electric Field on a Charged Trapping Centre

potential in the field direction is reduced by a factor -eEx, and the potential barrier for electron excitation is correspondingly smaller. The potential energy now has a maximum at a position x_M, where $x_M = (e/4\pi K\varepsilon_o E)^{\frac{1}{2}}$, and the maximum of potential is

$$\phi_M = -(Ee^3/\pi K\varepsilon_o)^{\frac{1}{2}} \qquad (2.2.8)$$

The barrier lowering is then $\phi - |\phi_M|$

The resultant conductivity is given by

$$\log_e \sigma = A - \frac{\phi}{2kT} + \frac{(Ee^3/\pi K\varepsilon_o)^{\frac{1}{2}}}{kT} \qquad (2.2.9)$$

where k is the Boltzmann constant.

Thus, at constant temperature,

$$\log_e \sigma = A' + \frac{\beta E^{\frac{1}{2}}}{kT} \qquad (2.2.10)$$

where $\beta = (e^3/\pi K\varepsilon_o)^{\frac{1}{2}}$

Expression (2.2.9) is somewhat modified if one allows for the three-dimensional nature of the trapping centres, and for traps of a non-coulombic form. Hartke[57] has examined this problem, and has concluded that the general effect is a reduction of β by a factor of up to 50%. Simmons[58] has pointed out that a further lowering of the constant will occur if shallow neutral traps are present in the material together with the deep-lying charged traps under consideration. However, a more fundamental objection has been expressed by Jonscher[59], who points out that the postulation of a coulombic centre implies that a trapped carrier is capable of orbiting around the centre and can sample the coulombic potential over relatively large distances. He estimates that, in an applied field of $10^5 V.cm.^{-1}$, the value of x_M is of the order of 50 Å, or 10 interatomic distances. In view of the low periodicity and mean free path in the materials under consideration,

the validity of the Poole-Frenkel analysis is thus questionable. A concept of field-assisted hopping would be more valid, and Klinger[51] has indicated that the occurrence of non-Ohmic effects at high applied fields can be expected for small polaron hopping transport. Such effects will be discussed at greater length in subsequent chapters.

The Schottky mechanism, similar in its manifestation but not in its origin, results from the field stimulated thermal injection of carriers into a material over electrode potential barriers. Again, the effect of an applied electric field is to reduce the barrier height, and a field dependence which is similar to that of the Poole-Frenkel mechanism is produced. However, in the Poole-Frenkel theory, an immobile charge is associated with the trapping centre, which is not the case in the Schottky mechanism. Consequently, the theoretical barrier lowering in the latter case is one half of that in the former. In view of the uncertainty associated with the practical value of the Poole-Frenkel constant, it is not generally possible to distinguish between these two mechanisms by an examination of the magnitude of β. However, in a material with a trap-limited drift mobility it can be shown that the Poole-Frenkel effect will produce a field dependence of the mobility which would not be expected from the Schottky mechanism, so that it should be possible to make an identification by means of a study of the mobility. Also, since the Schottky effect is essentially a surface phenomenon, whilst the Poole-Frenkel effect is a bulk property, a comparison of observations in specimens of different thicknesses can allow the effects to be differentiated.

In addition to the Poole-Frenkel and Schottky effects, other non-Ohmic phenomena may occur in dielectric materials. In particular, significant information can be obtained from a study of space-charge

limited currents in suitably prepared specimens. A description of this topic is beyond the scope of this account, but may be found in the literature (e.g. Lamb[60]).

Chapter Three

Preparative Techniques

3.1 Bulk Material Preparation

The glasses examined in this study were prepared by melting their constituents in evacuated, sealed tubes of fused silica. Batch weights of approximately 20 gms. were used, and the general arrangement employed is illustrated in figure 11. The constituents, either in elemental or compound form, were weighed to an accuracy of better than ± 1 mgm., inside the silica tube. As far as possible, large lumps of material were used in preference to powder, so that surface adsorption of gases might be minimised. Constituents were normally of 5N purity. On completion of the weighing, a loosely fitting plug of silica rod was inserted into the pre-shaped neck of the tube. The assembly was then connected to a rotary/diffusion vacuum pump, and the internal pressure was slowly reduced to approximately 15 microns of mercury. Care was necessary at this stage, to ensure that no loss of material from the tube occurred due to too rapid a change of internal pressure. Controlled heating was then applied to the bottom section of the tube, and considerable outgassing of the constituents took place. When such outgassing was judged to be complete, the system was allowed to cool under continuous evacuation at a pressure of 5 to 10 microns. Since such a pressure implied the presence of less than 10^{-8} gms. of gas in the tube, further evacuation was judged to be unnecessary. Sealing was then accomplished by directing a finely focussed flame, from an oxy-hydrogen torch, on to the neck of the tube. By this means, the tube and internal silica plug were fused together to form a seal; the process being aided by the tendency of the neck to collapse inwards under the force of the external air pressure.

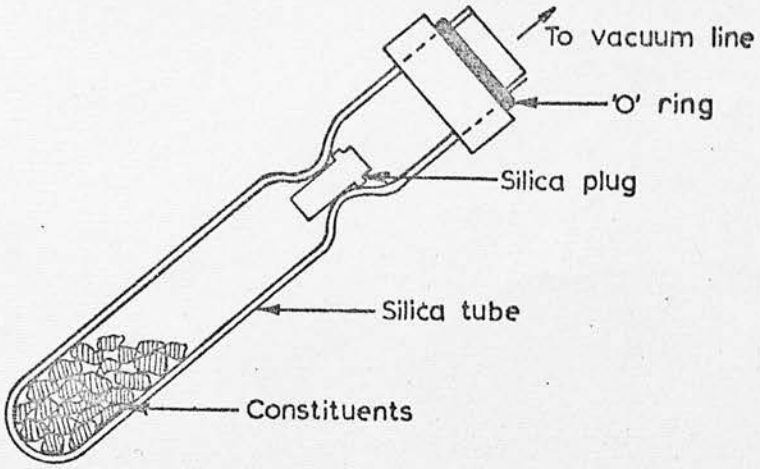

Fig. 11 Silica Tube Arrangement for Material Preparation

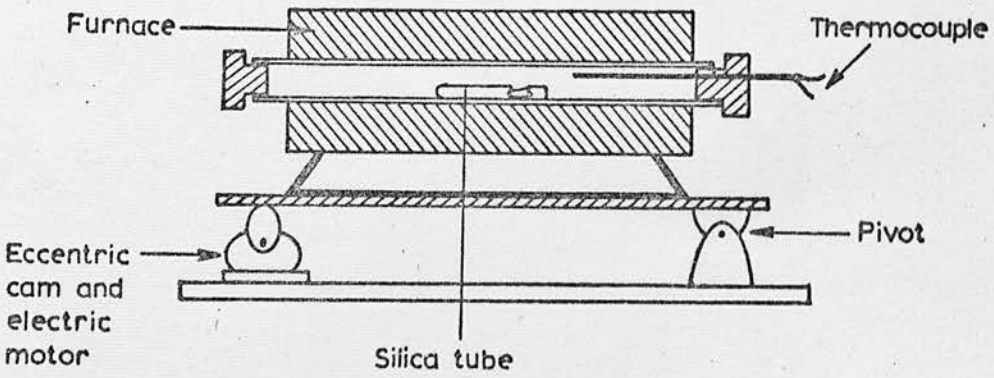

Fig. 12 Specimen Preparation Furnace

The quality of the seal was checked by using a Tesla coil to monitor the internal gas pressure after removal of the tube assembly from the vacuum line. A further check was provided by weighing the assembly both before and after the melting process, to ensure that no loss of material had occurred.

The furnace arrangement shown in figure 12 was used to fuse the constituents, and to ensure adequate mixing. The furnace temperature naturally varied according to the glass being prepared, but was generally in the region of 800°C. An offset cam arrangement allowed the melt to be continuously agitated, the whole furnace being rocked back and forth. The period of melting was generally greater than four hours, allowing sufficient time for mixing of the constituents. After this time, the tube was removed and set vertically in a large container, packed with glass fibre. Cooling then proceeded at a rate suitable for the formation of the vitreous solid, whilst excessive thermal shock was avoided. Occasionally, in cases where more rapid cooling was necessary to avoid devitrification, cooling in air or by quenching in a strong aqueous salt solution could be employed. Normally, no separate annealing cycle was performed on the materials, since they were to receive further heat treatment in drift mobility specimen preparation, and since a detailed study of the effect of annealing on the Hall mobility was not possible in the time available.

The plug of vitreous material was removed from its tube by slicing off the ends using a rotary saw with a diamond-impregnated blade. Generally, differential contraction was such that the plug of material could then be easily extracted. Typically, samples of 1 cm. diameter and 4 cm. length were produced in this manner. The

treatment of these ingots to produce specimens suitable for the measurement of the drift and Hall mobilities will be described in the following sections.

3.2 Preparation of Drift Mobility Specimens

From published data on the magnitudes to be expected for carrier mobilities in vitreous materials, it was indicated that films of thickness in the range 1 to 50 microns would be required. After some experimentation, two separate techniques were developed for the production of such films. The first, involving the preparation of thin bubbles, was suitable for the production of films from 1 to 5 microns in thickness. The second, a compression technique, was suitable for the 20 to 50 micron range. With some difficulty, it was possible to extend the above ranges sufficiently so that no problems were presented by the 5 to 20 micron 'gap'.

The bubble films were fabricated in a glove box under a nitrogen atmosphere. A small crucible of material was heated to a temperature sufficiently above the melting point so that the liquid flowed in a viscous manner. Excessive heating was carefully avoided, and the melt was normally covered to minimise evaporation. A section of fine bore glass tubing was dipped into the melt and withdrawn, so that a globule of molten material adhered to the end of the tube. A bellows arrangement was then used to force nitrogen gas down the tube, and a bubble of glass was formed from the molten material. With practice, it was possible to prepare bubbles of approximately 10 cm. length and 5 cm. diameter, of a fairly constant thickness. The thickness of such bubbles could be varied by altering the bellows pressure. The handling of films prepared in this manner presented a problem. For practical purposes, relatively flat sections

of film at least 5mm. square, were required. Since electrodes were to be deposited by evaporation, it was necessary to manipulate the sections with a fair degree of safety. In an initial attempt to solve this problem, it was found that floating the films on water increased the handling capabilities. Pieces of mica, 5 mm. square, with a central hole of 2 mm. diameter, were used to lift sections of the film from the water. On drying, the sections were generally found to adhere strongly to the mica. Approximately 50% of such specimens presented a tolerably flat, crack-free appearance on inspection. Aluminium or gold electrodes of 3 mm. diameter were evaporated on to each side of the film/mica assembly, covering the glass and part of the mica. It was then necessary to make contact to the electrodes without destroying the film. This was attempted using a liquid indium-gallium alloy, producing the arrangement shown in figure 13. Electrical and thermal contact to the underside of the film was provided by mounting it on a brass sheet using the liquid alloy. On the upper surface, a further drop of alloy provided the contact. This technique was found in practice to have two defects. Firstly, a large percentage of films broke up on assembly, and secondly, a chemical reaction between water vapour in the air and aluminium, if used as an electrode material, was strongly catalysed by the indium-gallium, so that the electrodes were quickly destroyed. In an attempt to eliminate these problems, silver'Dag' suspension and a silver-epoxy compound were used in place of the liquid metal. Samples thus prepared showed a much lower failure rate and avoided the electrode destruction effect, but were found to possess anomalously high conductivities. It was concluded that rapid silver migration into the specimens was the cause of this

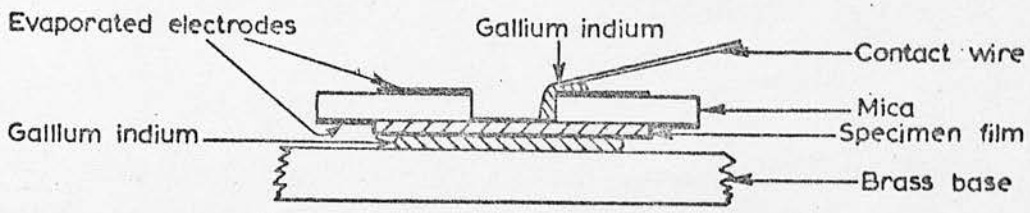

Fig. 13 Thin Film Specimen Assembly : Early Technique

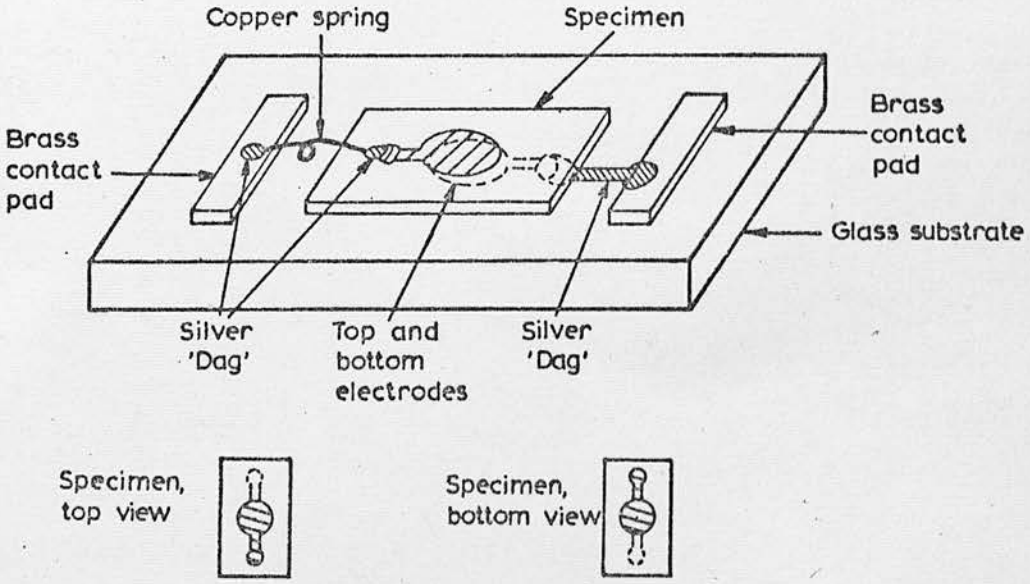

Fig. 14 Thin Film Specimen Assembly : Final Technique

phenomenon. A recent electron microscope study of the diffusion rates of a number of metals into amorphous layers of arsenic triselenide[61], gives support to this conclusion. In this examination, it was found that silver and copper diffused rapidly into the films, producing regions of polycrystalline Ag_2Se and Cu_2Se respectively. Aluminium was found to be the least mobile or reactive material, and was concluded to be the most suitable metal for electrode production. To avoid the effects of silver diffusion in the present study, a system using an offset electrode contacting arrangement was finally adopted, as shown in Figure 14. Selected flat sections of film were clamped in a double sided mask for the evaporation process, producing electrode areas of the shape shown. The loss of mica as a supporting medium increased the failure rate substantially during the preparation procedure, but this was tolerated since the final specimens were reasonably robust and easy to handle. The films, with evaporated electrodes, were mounted on to strips of glass microscope slide, approximately 20 x 4 mm. in area. A thin line of silver 'Dag' suspension was painted in from one end of the slide for about 5 mm., and the sample was quickly set in place so that the suspension wetted the lower contact pad and effectively attached the sample to the slide substrate. In the early preparations, further contact and rigidity were provided by applying liquid Araldite around the edges of the specimen. However, it was found that samples formed in this way tended to break up on cooling below $-30^{\circ}C$ due to differential contraction effects. For this reason, the use of Araldite was discontinued, and contact was made to the top pad by a spring of fine copper wire and silver 'Dag', as shown in the diagram.

For the production of thicker specimens, in the 20-50 micron range, a different technique was adopted. Thin mica plates, approximately 5 cm. square, were pre-heated to around 350°C under a nitrogen atmosphere. A small pellet of the material to be examined was sandwiched between the hot plates and pressure immediately applied. The material became molten and quickly flowed into a wide thin layer between the mica sheets. Being of very low thermal capacity, the structure cooled to room temperature in a few seconds, causing the material to solidify in a vitreous phase. It was found to be relatively simple to peel away the mica leaving a large sample of glass, with high quality surfaces and with thickness variations of less than 20% in a 2 cm. diameter specimen. Microscopic examination showed no signs of crystallisation in such films. From these layers, specimens of 10 x 3 mm. area were produced by dicing the films using a diamond scriber. These specimens were selected for uniformity of thickness, a maximum tolerance of ± 2% being acceptable. The procedure for electrode evaporation and specimen mounting was identical with that finally adopted in the case of the thinner films.

The measurement of film thickness, for both thick and thin specimens, presented a further problem. Several techniques, described below, were investigated.

a) Weighing. A relatively large (> 5 cm^2) area of film could be weighed directly, and its thickness calculated from the area, weight, and density. However, the errors involved in the measurement of the first two of these variables, and in the non-uniformity of the film thickness itself, made the method highly inaccurate.

b) Resistance and/or Capacitance A measurement of these parameters for a specimen would yield the thickness if the resistivity or dielectric constant, and electrode area were known. Thickness estimates made in this way also proved to be unreliable, although the capacitance method should have been fairly accurate. The failure of thickness determinations by resistance measurements is ascribed to the non-Ohmic nature of the films.

c) Electron Bombardment Induced Conductivity Observation of the current through a specimen, as a function of the energy of a bombarding electron beam, can be used to derive the thickness. A sharp rise in current at a certain electron beam energy is observed, which can be related to film thickness if certain bulk properties are known[62,63,64]. Such a determination, however, constitutes a lengthy experiment in itself, and the derived thickness is a function of a semi-empirical constant.

d) Optical Absorption A small test assembly, to investigate the use of absorption measurements in thickness assessment, was constructed as shown in figure 15. A gallium arsenide lamp, driven by a 1 khz square wave, provided light pulses in the near infra-red. Since most of the materials of interest in the present study are somewhat transparent in the infra-red, specimens placed as shown allowed some of the incident radiation to be transmitted to a phototransistor detector. The output of the detector was amplified and displayed on an oscilloscope. It was hoped that the thickness of specimens could be measured prior to electrode evaporation, by using a simple Beer's law equation after calibration of the system by means of a few specimens of known thickness. In practice, it was found that

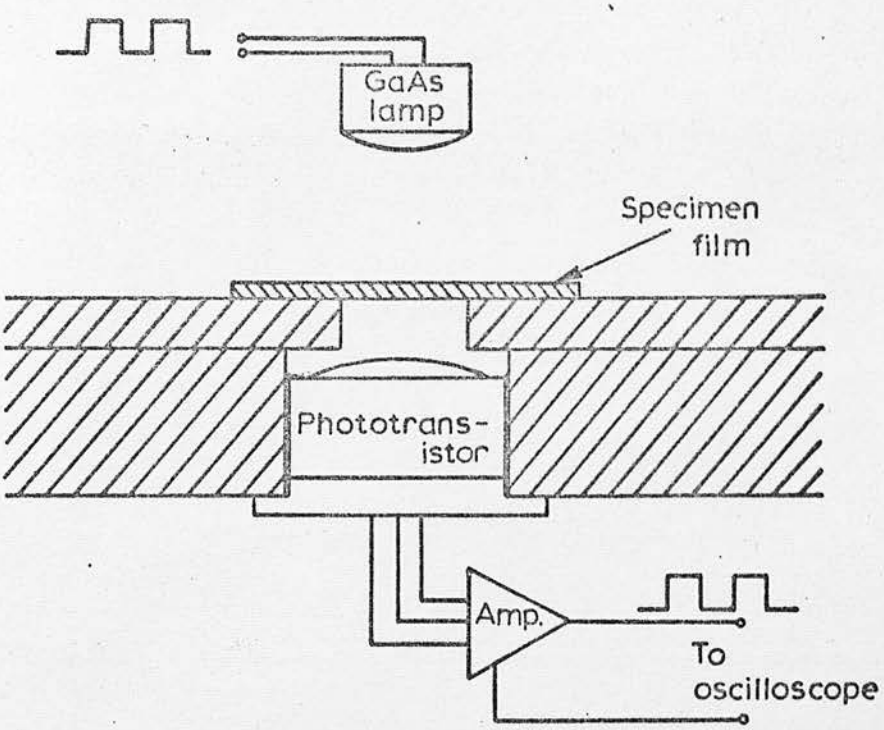

Fig. 15 Arrangement for Thickness Measurement by Optical Absorption

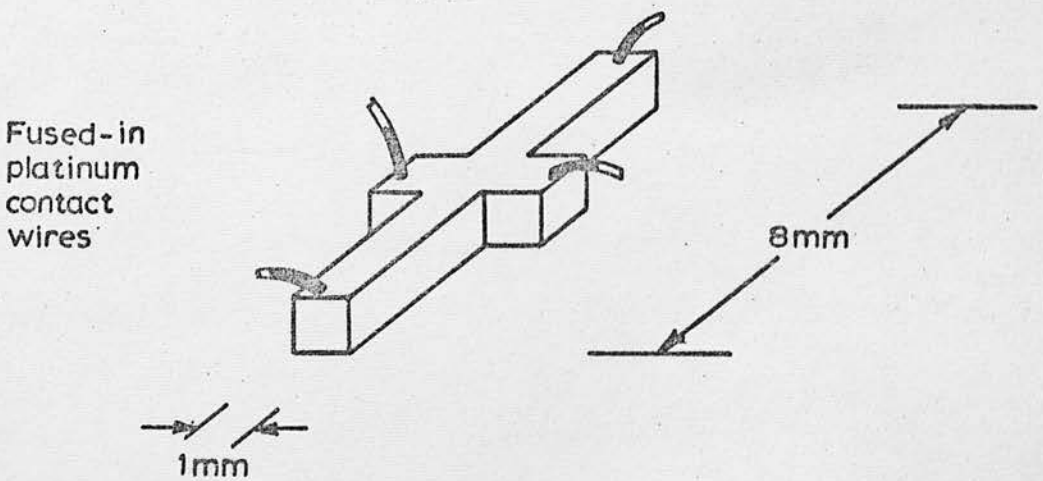

Fig. 16 Hall Sample Configuration

reflection from the upper specimen surface accounted for almost all the measured reduction in light intensity, so that the technique was not feasible. It is possible that a similar technique operating at a higher light frequency would have been more successful, but the error potential was considered to be so great that the investigation was not pursued further. It is understood that a related system using ultrasonic vibrations is possible, but this was not investigated in the present study.

e) Direct Measurement The technique of direct measurement of thickness, although perfectly acceptable for thick specimens, was approached with some misgivings for the thin films of interest here. A Talysurf Model 4 (Taylor Hobson), capable of measuring extremely small thickness changes, was available. The operation of this instrument depends upon the amplification of vertical deflections of a stylus, in contact with the upper surface of a specimen, as the stylus is drawn horizontally across the surface. However, the thinner films were so fragile that it was obvious that they would be destroyed during such a measurement. Also, since the instrument was only capable of measuring thickness changes, it would be necessary to make very good physical contact between the specimen and a flat substrate. On investigation, however, the latter problem did not prove to be too severe. Small areas of film, applied to a damp microscope slide, were found to adhere very strongly on drying, although larger areas were either fractured in the process or showed insufficient adhesion. After some study, the following system of thickness measurement was therefore adopted. For the 'thick' films produced by the pressure technique, it was possible to make the thickness determination prior to electrode evaporation by the

'Talysurf' technique. The specimens were fixed to microscope slides as described, and the thickness measured at a number of points around their diameter. The specimens were removed from the slides by immersion in water, and re-cleaned in trichloroethylene. Electrode evaporation then proceeded. For the 'thin' specimens prepared by the bubble process, thickness measurement was deferred until mobility measurements were complete. The specimens were then removed from their substrates and broken into small sections which were fixed on to microscope slides as before. Talysurf measurements were then carried out on the individual sections to obtain an average value for the specimen thickness. In spite of the drawbacks mentioned above, this technique was found to provide a consistent, accurate measurement of thickness, and was adopted for all the specimens examined in the present study.

Evaporated layers of aluminium or gold were used as electrode materials. Mobility values were found to be consistent using either material, and in using 'mixed' electrodes (one aluminium, one gold). However, the observed pulse heights were much increased by the use of aluminium, which forms a hole blocking contact, for both electrodes.

3.3 Preparation of Hall Mobility Specimens

Hall specimens were fabricated in the conventional 'Maltese cross' shape, as shown in figure 16. Initially, ingots of bulk material were sliced into sections of 1 mm. thickness, using the diamond impregnated saw mentioned previously. The Hall samples were prepared from such slices by an air abrasion technique. Specimen areas were defined by means of suitably shaped copper pre-forms, prepared from thin copper sheet by photo-etching; these pre-forms being fixed to the surface of the slices using wax. During the

air-abrasion, the areas beneath the copper were protected, so that the specimens remained when the surrounding material had been abraded away. The procedure, although lengthy, was found to produce fairly well defined Hall samples.

Electrode contact to the input and Hall arms of the specimens was achieved using fused-in platinum wires. In the adopted process, a current was passed through a fine platinum wire, causing ohmic heating, and the specimen was brought into contact with the hot wire, allowing local fusion of the wire into the material. Tests indicated that satisfactory ohmic contacts were produced in this manner; no evidence of a time-dependent resistance, or of rectifying effects, being observed.

Chapter Four

Drift Mobility - Theory and Measurement

4.1 Introduction

In considering electronic conduction in semiconductors of high mobility, it is often assumed that the carriers are scattered only by thermal lattice vibrations (phonons) and by lattice impurities, without ever being trapped by the imperfections in the lattice. In this ideal situation, a mobility for the carriers, which is often termed the microscopic mobility, μ_o, may be calculated. This quantity is usually defined by the vector relationship

$$\bar{v}_o = \mu_o \bar{E} \qquad (4.1.1)$$

where $\bar{v}_o$ is the average drift velocity of the carrier under the influence of the applied electric field $\bar{E}$. The above relation defines the mobility as a tensor of the second rank in the most general case, but in common usage, it is reduced to a scalar quantity.

In non-ideal materials, where the trapping of carriers is not negligible, it is convenient to introduce a quantity which reflects the long-range motion of the carrier by including the effects of periodic trapping events. Such a quantity is termed the drift mobility, μ_d, and is defined in a manner similar to the microscopic mobility, except that the carrier drift velocity is now averaged over a time including a number of trapping events. Thus, consider a material containing a single level of shallow traps, in which the carrier trapping and release times, T_t and T_r, are defined as follows: if a carrier is in the conduction band (electrons) or valence band (holes), then its probability per unit time of being trapped is $1/T_t$, whilst if the carrier is in a trap, its probability per unit time of

being released is $1/T_r$.

In the presence of an applied field $\bar{E}$, the velocity of a mobile carrier is given by equation 4.1.1, and the distance travelled between trapping events is thus

$$\bar{s} = T_t \mu_o \bar{E} \qquad (4.1.2)$$

However, the average time taken to travel this distance is $T_t + T_r$, since it must include one complete trapping event, and so the average carrier velocity is

$$\bar{v} = \frac{T_t \mu_o \bar{E}}{T_t + T_r} \qquad (4.1.3)$$

but the drift mobility is defined by

$$\bar{v} = \mu_d \bar{E} \qquad (4.1.4)$$

and so

$$\mu_d = \frac{\mu_o T_t}{T_t + T_r} \qquad (4.1.5)$$

The variation of drift mobility with temperature is thus a compound of the individual variations of the trapping and release times, and of the microscopic mobility. However, the release time is often the dominant factor in low mobility semiconductors, and the drift mobility frequently exhibits an activation energy characteristic of the thermal release of carriers from trapping centres.

Practical measurements of drift mobility involve the determination of the time taken for carriers to travel a known distance under a known applied field, or of the distance travelled in a known time. Thus, an early examination[65] used the arrangement shown in figure 17a. Minority carriers, injected at the emitter electrode A of a filament of germanium, drift towards the collector electrode B

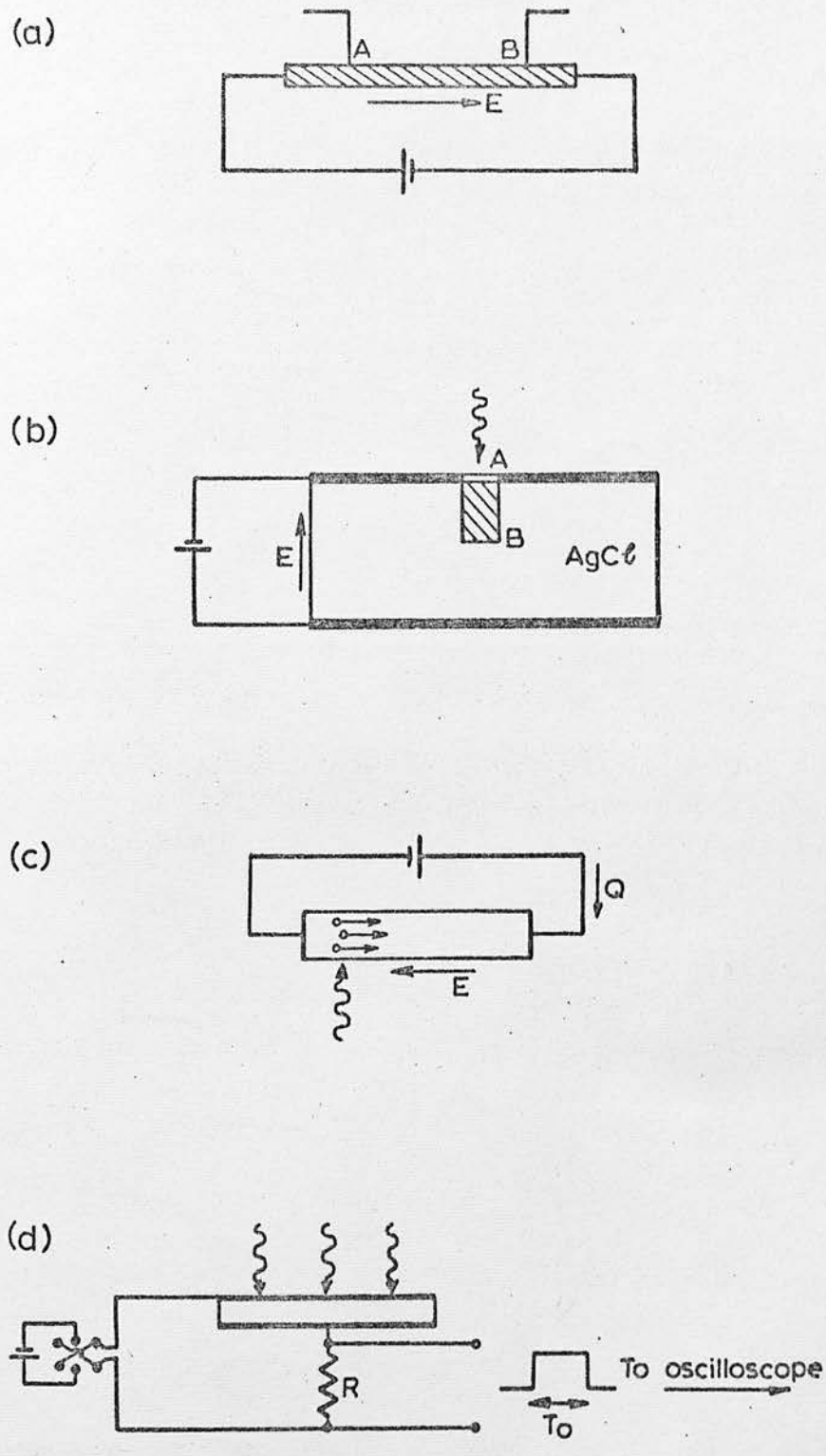

Fig. 17 Arrangements for Measuring the Carrier Drift Mobility

under the influence of the applied field E. It is possible to measure the times of injection of the holes at A, and of their arrival at B, by the electric impulses induced in the collector circuit, and thus to deduce the hole mobility. Similarly, it is possible to observe the motion of electrons in silver chloride[66] by the method shown in figure 17b. Photoelectrons are produced at the face A of a crystal of silver chloride by a short light pulse. The application of an electric field E for a known period causes the electrons to drift to the point B. The distance AB is determined by the blackening of the crystal which is observed after repeating the experiment a number of times, and thus the mobility may be calculated.

The two techniques described above are of limited applicability. The first, because of the physically large distance which the carriers must travel, is suitable only for materials of high mobility. The second relies upon the 'photographic' blackening property of silver chloride, and very few materials possess this characteristic. The first steps towards the development of a system of wider applicability were made by Pohl[67], who described a system for the measurement of the trapping time of photoelectrons in low mobility materials by the observation of the electric pulse induced by the spatial displacement of photoelectrons in the arrangement shown in figure 17c. The duration of the pulse gives a measure of the trapping time, and it is possible to derive a relationship between the distance travelled in this time and the total induced charge, Q, so that the mobility may be calculated. Again, however, the method relies upon the known processes of photoconductivity in the solid under examination. In recent years, this form of measurement has been refined by the use of sufficiently thin specimens

so that the induced carriers are able to traverse the whole width of the material without becoming 'permanently' trapped in deep-lying centres. This form of measurement, the development of which owes much to Spear[27,28,64,68,84], is performed with the system shown in figure 17d. A number of carriers of both signs are produced in a thin layer close to the top electrode of the sample, by means of a short exciting pulse, which may be provided by a light flash, a high energy electron beam, or by the use of sub-atomic particles. Charge carriers of one sign are then caused to drift through the bulk of the specimen by the applied field, and their motion is detected by the voltage developed across the resistor R (R being much smaller in value than the specimen resistance). The form of this voltage is as indicated, and from it the time of transit of the charge carriers, T_o, may be determined. The drift velocity, v, of the carriers is then given by

$$v = x/T \qquad (4.1.6)$$

where x is the specimen thickness.

The drift mobility is

$$\mu_d = x/ET_o = x^2/VT_o \qquad (4.1.7)$$

where V(= Ex) is the applied voltage.

It will be noted that carriers of either sign may be examined in this manner by selecting the polarity of the applied voltage. Since this form of measurement was adopted in the present study, it will receive further consideration in a subsequent section.

4.2 Drift Mobility in Low Mobility Materials

The general characteristics of currently accepted models of conduction in low mobility materials have been described in Chapter Two. It will be recalled that, for carrier energies well above a critical

value, ε_c, it is expected that carrier transport will occur by a conventional band mechanism, with a microscopic mobility in excess of 100 $cm^2V^{-1}sec^{-1}$. For energies <u>just</u> greater than ε_c, band transport of a form is still predicted, but the process is envisaged as diffusive, the diffusive mobility being of the order of 100 $cm^2V^{-1}sec^{-1}$. Thus, in the absence of significant carrier trapping, the mobility is not expected to be less than 10 $cm^2V^{-1}sec^{-1}$. For energies below ε_c, transport occurs predominantly by a hopping process, with mobility values of less than 10^{-1} $cm^2V^{-1}sec^{-1}$. In the former (band) case, measured drift mobility values may be significantly less than the value given above, if the drift of carriers is controlled and limited by trapping events. The drift mobility measurement averages out the time which the carrier spends in motion and in traps. Therefore, it is possible to consider the occurrence of drift mobilities below $10^{-1}cm^2V^{-1}sec^{-1}$ either in terms of trap-controlled band motion or in terms of carrier hopping. In the following discussion, the characteristics to be expected from these alternative transport mechanisms will be examined in greater detail.

a) <u>Trap-Controlled Band Motion</u>

If the conventional analysis is applied to low mobility materials, the calculated mean free path between trapping events is very small. Transport of charge carriers is then considered as involving a large number of trapping events, with very short trapping times and comparatively long trap release times. The drift mobility may then be expressed in terms of equation 4.1.5. In addition to the shallow trapping levels considered in this manner, it can generally be expected that much deeper levels with long carrier release times will

occur in practice. The lengths of the trapping and release times for these levels will have a major effect on the transfer of charge over relatively long distances. It is this type of 'permanent' capture which must be avoided if transit time measurements are to be attempted. Assuming that it is physically possible to arrange that transit times are short compared to the deep trapping time, the limiting factors on the measured drift mobility are the microscopic (or the diffusive) mobility, and the shallow trapping and release times.

Microscopic Mobility.

In the discussion so far, the only limitation on the mean free path of a carrier has been that set by the occurrence of trapping events. It is also possible for the motion of a carrier to be interrupted by scattering phenomena, so that a more general analysis should include such effects. For simplicity, it will be convenient to use the term 'mean scattering path' to describe the average distance travelled by a carrier between scattering events, in the absence of trapping (or whilst travelling between traps). It is then this mean scattering path which is the controlling factor in determining the microscopic mobility, and the variation of the mobility with temperature will depend on the form of scattering which is dominant in a particular material. First, consider the situation in a regular crystalline lattice. If the scattering is elastic, the energy lost in a collision is small, and the interaction with the lattice will be restricted to the lowest energy modes of vibration. These are the longitudinal or acoustic modes, and scattering by them is expected to lead to a mean scattering path which is inversely

proportional to the temperature, T. For semiconductors,[69], this leads to a temperature dependence of the microscopic mobility of the form

$$\mu_o \alpha T^{-3/2} \qquad (4.2.1)$$

Measurements of temperature variations of mobility over suitable ranges of temperature have indicated a behaviour close to this in a number of materials. However, a number of assumptions are involved in the derivation of the relationship, and it is not, perhaps, surprising that many materials exhibit significantly different temperature dependencies. To account for such experimental observations, it is necessary to consider other factors, such as scattering by optical mode vibrations, by charged and uncharged impurities, and by other carriers[70]. Thus, even in high mobility semiconductors, it is difficult to predict the behaviour of the microscopic mobility.

For carrier energies in the diffusive range, the concept of scattering becomes obscure, so that the temperature dependence of $\mu_{diff.}$ is probably restricted to that expressed in equation 2.2.5; i.e.

$$\mu_{diff} = \frac{e \nu_{el} a^2}{kT}$$

Shallow Trap Release Time.

The fundamental properties of a shallow charged trap in a semiconductor are well established[2,65]. The probability of escape from a trap of depth ϕ and capture cross section S_c is given by

$$P = N_{eff} \, v \, S_c \exp(-\phi/kT) \qquad (4.2.2)$$

where N_{eff} is the effective density of states in the conduction band (for electron carriers) or valence band (for holes), and v is the thermal velocity of the carriers.[2] The first term of equation

4.2.2 gives, according to the band model, a temperature dependence of the form

$$N_{eff} \propto T^{3/2} \tag{4.2.3}$$

$$\text{or} \quad N_{eff} = N_c T^{3/2} \tag{4.2.4}$$

where N_c is constant.

Similarly, the thermal velocity, v, has a dependence

$$v \propto T^{\frac{1}{2}} \tag{4.2.5}$$

However, for reasons which will become apparent, it is sufficient to express the relationship as $v = v(T)$. The variation of the capture cross section, S_c, with temperature is more difficult to analyse. Experiments on crystalline semiconductors indicate that it is often reasonable to assume temperature independence, but that there are also certain types of centre for which a temperature dependence is observed. For instance, the cross section for coulomb attraction would be expected to vary as T^{-2}. It should also be mentioned that the capture cross section of a trap may be significantly modified by the application of a high electric field. Considering such a possibility, Karpushin[71] has calculated that a field of 10^5 V/cm can reduce the cross section of a shallow'hydrogenic' surface state to zero. Again, it is sufficient here to express the cross section as $S_c = S_c(T)$.

In view of the above comments, one might expect a temperature variation of the trap release time, of the form

$$1/T_r = P = N_c T^{3/2} S_c(T)\, v(T) \exp(-\phi/kT) \tag{4.2.6}$$

Another phenomenon which may influence the trap release time has been mentioned in Chapter Two. This is the field stimulated

emission, or Poole-Frenkel effect. In view of the barrier lowering expressed in equations 2.2.9 and 2.2.10, we may expect that equation 4.2.6 will become

$$1/T_r = N_c\, T^{3/2}\, S_c(T)\, v(T) \exp(-\phi/kT) \exp(\beta E^{\frac{1}{2}}/kT) \qquad (4.2.7)$$

Shallow Trapping Time.

The simplest equation for the trapping time is of the form

$$1/T_t = (N_t - n_t)\, S_c(T)\, v(T) \qquad (4.2.8)$$

where N_t is the density of traps, and n_t is the number of traps which are occupied. By the predictions of band theory;

$$n_t = \frac{N_t}{1 + g^{-1} \exp(\Delta\varepsilon/kT)} \qquad (4.2.9)$$

where g is the degeneracy factor of the traps, and $\Delta\varepsilon$ is the energy difference between the trap and Fermi energy levels; i.e.

$\Delta\varepsilon = \varepsilon_t - \varepsilon_f$ for electrons, and $\varepsilon_f - \varepsilon_t$ for holes.

If the traps are shallow, then $\Delta\varepsilon/kT$ is large (>1), and

$$n_t \approx N_t\, g \exp(-\Delta\varepsilon/kT) \qquad (4.2.10)$$

Alternatively, if the traps are deep-lying, $\Delta\varepsilon/kT < -1$, and

$$n_t \approx N_t \qquad (4.2.11)$$

Since we are primarily concerned with shallow traps in the present context, we may substitute (4.2.10) into (4.2.8) giving

$$1/T_t = N_t\{1 - g \exp(-\Delta\varepsilon/kT)\}\, S_c(T)\, v(T) \qquad (4.2.12)$$

The degeneracy factor, g, is 2 in the simplest case, and we have already stated that $\Delta\varepsilon/kT > 1$, so that

$$1/T_t \approx N_t\, S_c(T)\, v(T) \qquad (4.2.13)$$

We note in passing, that the situation for deep traps must be analysed by a substitution of (4.2.9) into (4.2.8), followed by simplification,

giving

$$1/T_t \approx N_t\, g^{-1}\, S_c(T)\, v(T)\, \exp(\Delta\varepsilon/kT) \qquad (4.2.14)$$

where $\Delta E/kT$ is <u>negative</u> (<-1), as indicated above.

Having thus made a brief analysis of the factors which are likely to influence the drift mobility in a shallow-trap controlled case, it is possible to examine the overall position reflected in equation (4.1.5). Restating this equation,

$$\mu_d = \frac{\mu_o T_t}{T_t + T_r}$$

In the present case, the examination is focussed on materials of low mobility, and it is reasonable to assume that $\mu_d \ll \mu_o$. It then follows from (4.1.5) that $T_t \ll T_r$, so that

$$\mu_d \approx \mu_o \frac{T_t}{T_r} \qquad (4.2.15)$$

Thus, from equations (4.2.7) and 4.2.13)

$$\mu_d = \mu_o \frac{N_c\, T^{3/2}\, S_c(T)\, v(T)\, \exp(-\phi/kT)\, \exp(\beta E^{\frac{1}{2}}/kT)}{N_t\, g^{-1}\, S_c(T)\, v(T)}$$

$$= \mu_o\, A\, T^{3/2}\, \exp(-\phi/kT)\, \exp(\beta E^{\frac{1}{2}}/kT) \qquad (4.2.16)$$

Where the constant $A = g \frac{N_c}{N_t}$.

It has already been mentioned that the microscopic mobility itself may vary with temperature, due to the existence of scattering mechanisms. Thus, a variation of the form given in equation (4.2.1) would lead to a disappearance of the pre-exponential temperature term in (4.2.16), and other mechanisms would lead to a modification of this term. In the diffusive region, replacing μ_o by μ_{diff} as defined in equation (2.2.5)

would lead to a pre-exponential temperature dependence on $T^{\frac{1}{2}}$. Generally, the strong temperature variation caused by the exponential dependence tends to dominate observed results, and it is difficult to identify any pre-exponential term unless a high power of T is involved.

Having examined the temperature dependence predicted by the conventional concepts of band theory, certain reservations must be expressed when the model is applied to materials of very low mobility. Firstly, in view of the extremely short mean free path between trapping events, the scattering of carriers is quite likely to be a minor effect. Fundamentally, the scattering concept is only relevant if the mean free path is much greater than the atomic spacing. In addition, the disordered structure of many of the materials of interest in the present study makes the prediction of scattering phenomena extremely complex.

b) Hopping Motion

In considering carrier transport by a hopping process, the concepts of scattering, microscopic mobility, and shallow trapping are inapplicable. The motion of the carrier is envisaged as a 'percolation' process, with the carrier making virtually instantaneous transitions between localised sites. The hopping distance is of the order of an atomic spacing, and the mean free path concept is no longer valid. It is, however, still possible to consider the deep trapping of carriers, and to regard the deep states responsible for such trapping as possessing characteristic trapping and release times. The theoretical predictions of the mobility properties of carriers with energies less than the critical value, ε_c, have previously been

described in some detail. The hopping is regarded as an activated process

$$\mu_{hop} = f(T) \exp(-W/kT) \qquad (4.2.17)$$

where W is the hopping activation energy, and f(T) is proportional to T^{-1} and is $\leq 10^{-1}$ $cm^2V^{-1}sec^{-1}$ at room temperature. Mott[4,47], Pollack[72], and Killias[56] have predicted a decrease in activation energy at low temperatures. By the nature of the hopping process, the modification of the drift mobility by the applied electric field cannot be considered in terms of the Poole-Frenkel effect, but it is still possible for the applied field to modify the hopping activation energy. Thus, Austin and Mott[52] have shown that the hopping probability will be proportional to sinh(e.a.E/kT) where a is the hopping distance and E the applied field. Klinger[51] has also indicated that (small polaron) hopping may show field effects for values of field for which $E \geq kT/a$, and Drake, Scanlan, and Engel[73], in a hopping model based on dipole formation, have predicted a field dependence analogous to that of the Poole-Frenkel effect.

4.3 Considerations in the Measurement of the Drift Mobility

The fundamental technique for the measurement of the drift mobility by the transit time method has been described in section 1 of this chapter. It has been indicated that, using the system shown in figure 17d, a square pulse with a length equal to the carrier transit time may be observed. In practical measurements, it is often convenient to place a capacitor across the sampling resistor R, so as to integrate the observed transit trace, as shown in figure 18a. Under conditions of negligible carrier trapping, or of multiple trapping and release by shallow traps, a pulse with a well defined

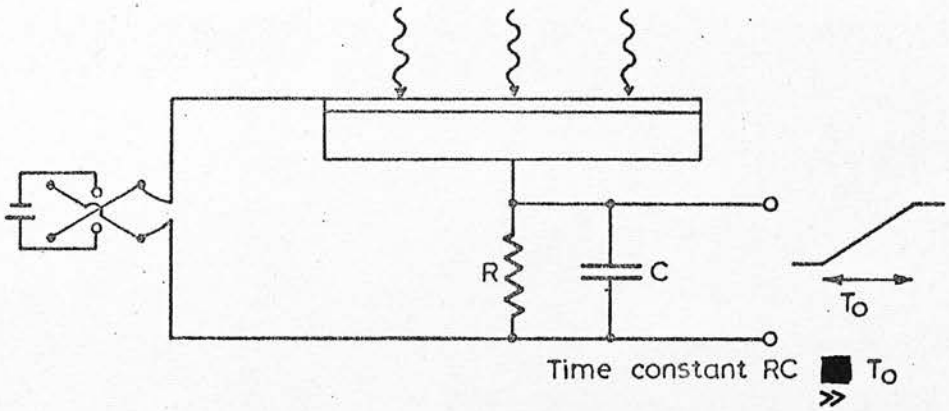

Fig. 18a Arrangement for Transit Time Measurements, Showing Positioning of the Capacitor, C, used for Pulse Integration

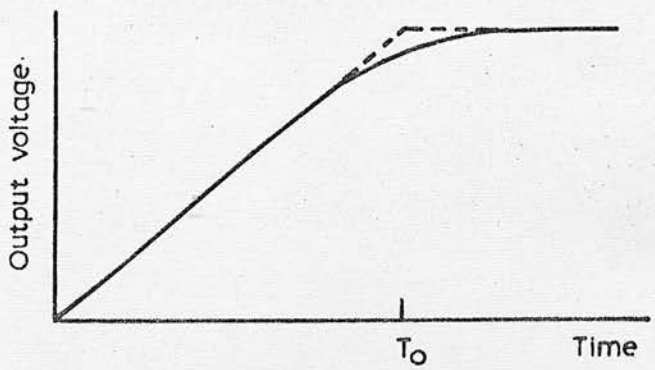

Fig. 18b Carrier Transit Pulse, Showing Pulse Rounding due to Diffusion and Finite Width of Charge Sheet

discontinuity of slope, indicative of the end of the transit, will be observed in the ideal case. However, in a practical examination, a number of factors may modify the pulse shape. Firstly, the layer of carriers produced by excitation close to the top electrode will have a finite width, so that a spread of arrival times at the bottom electrode will occur. Secondly, there will be a tendency for the width of the drifting layer to increase due to the statistical distribution of individual carrier velocities, again giving rise to a spread of arrival times at the lower electrode. These effects produce a 'rounding off' of the discontinuity region of the transit pulse, as shown in figure 18b. A more important factor arises when the presence of deep-lying trapping levels is considered. An examination of the effect of such traps has been provided by Tefft[74], who considers the situation when the traps are confined to a single level. In view of its relevance to the present study, this paper will be described below in some detail.

Tefft first derives the probability, $P(x,t)dx$ that a carrier, initially at the upper specimen electrode, will be at a distance between x and x+dx from this electrode at time t. For an untrapped carrier travelling in a band, the drift velocity is μE_o, where E_o is the external applied field. The probability that such a carrier has not been trapped by time t is $\exp(-t/T_t)$. Thus,

$$P(x,t)dx = \exp(-t/T_t)\ \delta(x - \mu E_o\ t)\ dx \qquad (4.3.1)$$

where $\delta(z)$ is the Dirac delta function:

$$\delta(z) = 1 \quad \text{for } z = 0$$

$$\delta(z) = 0 \quad \text{for } z \neq 0$$

Tefft continues by evaluating the positional probabilities for a carrier which experiences a number of trapping events before time t;

the cases in which the carrier is finally trapped and finally untrapped being considered. Summing the probabilities for these cases and that given in equation (4.3.1), he obtains

$$P(x,t)dx = \exp(t/T_t)\ \delta(x-\mu E_o t)\ dx$$

$$+ \exp\left[-(t/T_r)+y(T_r^{-1}-T_t^{-1})\right] \sum_{m=0}^{\infty} \frac{(s/2)^{2m}}{m!}\left[1+\frac{y}{(m+1)T_r}\right] S(t-y)\frac{dx}{\mu E_o T_t} \qquad (4.3.2)$$

where $y = x/\mu E_o$ is the time required for an untrapped carrier to reach x.

$$s = 2\left[y(t-y)/T_r T_t\right]^{\frac{1}{2}}$$

$S(r) = \int_{-\infty}^{r} \delta(x)\,dx$ is the unit step function

The step function S(r) is inserted because the average velocity of a carrier must be less than μE_o if any time is spent in traps. Performing the summations in equation (4.3.2), Tefft obtains

$$P(x,t)dx = \exp(-t/T_t)\delta(x-\mu E_o t)dx$$

$$+ \exp\left[-t/T_r+y(T_r^{-1}-T_t^{-1})\right]\left[I_0(s)+(2y/T_r s)I_1(s)\right]S(t-y)dx/\mu E_o T_t \qquad (4.3.3)$$

where I_0 and I_1 are modified Bessel functions of the first kind, of orders zero and one respectively.

Having derived this equation, Tefft considers the carrier transit trace for the case of hole transport. The field, E(x,t) in the specimen is regarded as consisting of three components;

E_o; the external applied field.

$(-en_o/\varepsilon)$; the field due to the ~~immobile~~ induced electron carrier sheet.

$(+en_o/\varepsilon)\int_o^x P(x,t)\,dx$; the field due to the moving hole sheet.

where n_o is the number of carriers of each sign produced by the initial excitation, and ε is the dielectric constant of the specimen.

Thus, $$E(x,t) = E_o - (en_o/\varepsilon) + (en_o/\varepsilon)\int_o^x P(x,t)dx \qquad (4.3.4)$$

The potential across the specimen is obtained by integration,

$$V(t) = \int_o^{\ell} E(x,t)\, dx$$

$$= V_o - (en_o\ell/\varepsilon) + (en_o/\varepsilon)\int_o^{\ell} (\ell-x)P(x,t)dx \qquad (4.3.5)$$

where V_o is the external applied voltage, and ℓ is the specimen thickness. Substituting for $P(x,t)$, and performing the integration over the delta function, Tefft obtains an equation for $V(t)$ which cannot be evaluated in a closed form, but he is able to apply approximations to obtain a solution for certain time regions. In particular, when $t \lesssim T_o$ or $|t-T_o| \ll T_t$, where T_o is the transit time for untrapped carriers ($= \ell/\mu E_o$),

$$V(t) \approx V_o - \frac{en_o\mu E_o}{\varepsilon(T_t^{-1}+T_r^{-1})}\left\{\frac{t}{T_r} + \frac{1 - \exp\left[-t(T_t^{-1}+T_r^{-1})\right]}{1 + T_t/T_r}\right\}$$

$$+ \frac{en_o\mu E_o}{\varepsilon} \exp(-t/T_t)\,(t-T_o)\left[1 + \frac{(t-T_o)}{2T_t}\left(1+\frac{t}{T_r}\right)\right] S(t-T_o)$$

(4.3.6)

Differentiating equation (4.3.6) with respect to time gives

$$\frac{dV}{dt} \approx \frac{-en_o\mu E_o}{\varepsilon(1+T_t/T_r)}\left\{\frac{T_t}{T_r} + \exp\left[-t(T_t^{-1}+T_r^{-1})\right]\right\}$$

$$+ \frac{en_o\mu E_o}{\varepsilon} \exp(-t/T_t)\left[1+\frac{t(t-T_o)}{T_tT_r}\right] S(t-T_o) \qquad (4.3.7)$$

It is evident from this equation that there is a discontinuity of slope at $t = T_o$ unless $T_o \gg T_t$, so that the transit time may be directly determined. Tefft considers the situations in which;

(a) the trapping time is very long compared to the transit time, or no traps are present.

(b) the trap release time is very much longer than the transit time, and the trapping time is equal to the transit time.

(c) as (b), but the transit time is five times the trapping time.

(d) trapping time, release time, and transit time are all equal.

The form of the transit pulse, as predicted by equation (4.3.6), is shown in figure 19a,b,c,d, for the above situations. As noted above, a measurement of the transit time is possible unless a large number of carriers are trapped in a 'permanent' manner during the experiment. If such permanent capture does occur, the observed pulse is of an exponential form, with a time constant equal to the trapping time, (case (c)). In practice, it might also be difficult to measure a transit time in case (d), since diffusion and other effects would tend to round off the pulse, obscuring the discontinuity. However, in principle, a measurement is possible in such conditions, and could be performed by extrapolation of the 'linear' regions adjoining the discontinuity, so as to determine the point of their intersection.

It is worth noting that Tefft continues his analysis and demonstrates that, if the traps are very shallow, so that thermal equilibrium is established between the free and trapped carriers in a time much shorter than the measurement time, the effect of the traps is simply to reduce the mobility to the value

$$\mu_d = \mu_o T_t/(T_t + T_r) \qquad (4.3.8)$$

This relationship is generally assumed in such a case, and has previously been expressed (equation 4.1.5).

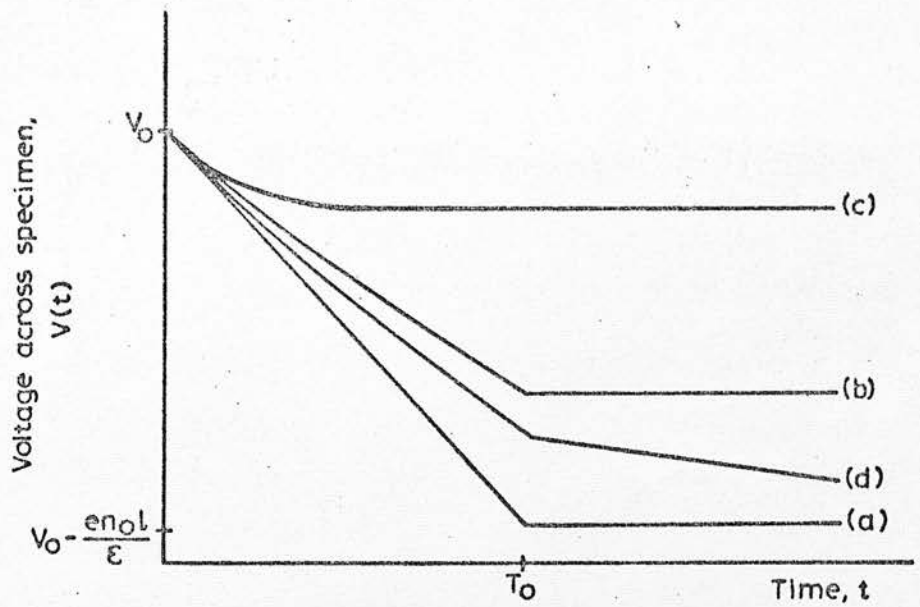

Fig. 19 Form of the Carrier Transit Pulse for Various Conditions of Carrier Capture and Release

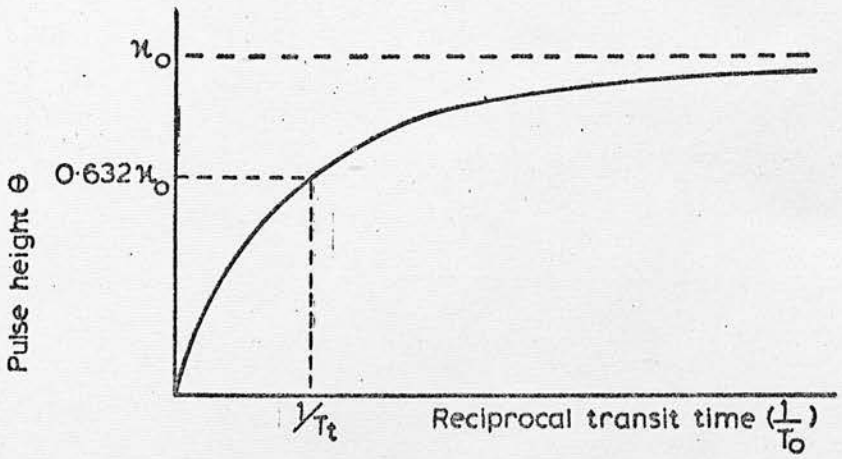

Fig. 20 'Hecht Curve' of Observed Pulse Height as a Function of Reciprocal Transit Time in the Presence of Trapping Centres .

The limitations of the Tefft analysis are as follows;

(a) the model has been restricted to the consideration of a single level of traps.

(b) no quantitative assessment of diffusive effects within the charge sheet has been made.

(c) the model is limited to the case where magnitude of the induced charge is small, so that no perturbation of the applied field is produced by the carrier sheet.

(d) the effects of dielectric relaxation, and of recombination have not been examined.

Various other theoretical examinations of the charge-transit method of mobility measurement have been made, being of varying degrees of complexity. For instance, Keating and Papadakis[75] have considered the perturbation of the applied field by the induced carriers, predicting certain modifications to the shape of the transit pulse. Papadakis[76] has further considered this situation, and his predictions are consistent with the results obtained by Gibbons and Papadakis[77] on orthorhombic sulphur. A similar analysis, in which the existence of a carrier reservoir close to the upper electrode is assumed, has been performed by Many and Rakavy[78]. However, such considerations are not fundamentally relevant to the present study, in which excited carrier concentrations were sufficiently low as to produce no significant perturbation on the applied specimen field. There does not appear to be any existing analysis of the (more relevant) modifications to the transit pulse which would be expected in the presence of multiple trapping levels.

It is evident that, when the trapping effects described above occur in conjunction with the other sources of pulse rounding,

the interpretation of an observed transit pulse can be difficult. A survey of the literature shows that, in materials with drift mobilities greater than 10^{-2} $cm^2V^{-1}sec^{-1}$, it is generally possible to observe a transit pulse in which the rounding is relatively slight. In such cases, the position of the discontinuity is inferred by extrapolation of the linear regions before and after T_o. However, in materials of very low mobility, it is often found that the observed pulse becomes more rounded. It is then necessary to ascertain that a true transit pulse, rather than an indication of the deep trapping time, is being observed. In such a case, there are certain criteria which may be applied, and these are itemised below.

a) Pulse Height.

It will be recalled that the increase of trapping effects gives rise to a progressive decrease in the height of the observed pulse. The determining factor for this effect is the ratio of the trapping and transit times. Since, in the absence of field effects, the transit time is inversely proportional to the applied field, it is possible to vary this ratio and examine the observed pulse height. In ideal conditions, it is possible to obtain the deep trapping time by plotting the pulse height as a function of the reciprocal of the observed transit time. A curve of the form shown in figure 20 is then obtained. This type of plot, commonly known as a Hecht curve[79,80], has the theoretical form

$$\theta = (n_o T_o/T_t)(1 - e^{-Tt/To}) \qquad (4.3.9)$$

where θ is the pulse height in units of electronic charge. For very short transit times, such that $T_o/T_t \gg 1$, then $\theta = n_o$, whilst when $T_o = T_t$, $\theta = 0.632n_o$. It is therefore possible, in

principle, to determine T_t in a relatively simple manner. A complicating factor in such a determination is the possible dependence of the carrier generation efficiency, and thus of n_o, on the magnitude of the applied electric field. In an examination of the transport properties of selenium, Tabak and Warter[31] have shown such an effect to be present. As a consequence, they estimate that the calculations of carrier ranges using data determined from a 'Hecht' curve, as reported in earlier examinations, are 20 to 100 times too small. It would thus appear that data from the Hecht analysis can only be regarded as providing a lower limit for the trapping time, unless further evidence can be provided of the validity of the analysis in a particular case.

b) The Scaling Laws.

Examination of a number of specimens, of different thicknesses, can provide a fairly conclusive identification of the transit pulse. If two specimens of different thickness are subjected to the same applied field, different transit times will be observed. However, the samples will possess identical trapping times if their structures are similar. Therefore, a comparison of the observed response times in the two cases will allow an identification of the nature of the pulse.

c) Effect of Impurities.

It appears that the major effect of impurities in many low mobility materials lies in the production of deep trapping centres. Thus, in principle, the deep trapping time can be reduced by the controlled addition of suitable impurities. In this manner, it might be possible to draw conclusions as to the nature of the observed pulse.

d) Temperature and Field Dependence.

The materials of interest in the present study normally possess a sufficiently high activation energy to cause a large change in drift mobility over a moderate range of temperature. The deep trapping time would be expected to be characterised by a weaker temperature dependence; either having a low activation exponential dependence, or varying as some low power of T. The situation in this respect has received some consideration in Chapter Four, section 2, and is expressed in equation (4.2.14). Thus, if the temperature is reduced so that the transit time approaches the trapping time in a particular material, a sharp decrease in the observed activation energy, accompanied by a rapid reduction in the observed pulse height, would be expected. Conversely, if a pulse of large amplitude is observed over a wide temperature range, then there is some justification for the consideration of the pulse as representing a true carrier transit, even if the pulse is of an extremely rounded form.

It has already been mentioned that the conductivity (and drift mobility) of many dielectric materials exhibits a dependence on the magnitude of the applied electric field. A strong dependence of the deep trapping time on the applied field is not, however, commonly expected. Some modification might occur through a change in the capture cross section, and shallow states might even become delocalised in a strong field, but it is not expected that deep trapping time could show a dependence of the form and magnitude which is experimentally observed. Again therefore, the observation of a strong field modification of the mobility, especially if a similar modification of the conductivity is observed, indicates that a true transit time can be associated with measurements obtained from the drift pulse.

4.4 Relevant Previous Measurements

a) Selenium

Because of its commercial applications, the properties of selenium have been examined in more depth than is the case for any other vitreous semiconductor. In the crystalline state, measurements of the carrier mobility (α - monoclinic Se) have been reported by Spear[81], and Caywood and Mead[82]. Amorphous evaporated films have been studied by Spear[27,28], Hartke[33], Kolomiets and Lebedev[34], Grunwald and Blakney[29], and members of the Xerox research team [30-32]. Their measured values of the room temperature drift mobilities and activation energies for hole and electron carriers are summarised in the following table.

	Mobility, $cm^2V^{-1}sec^{-1}$		Activation energy, eV.	
	holes	electrons	holes	electrons
Spear	0.14	$5x10^{-3}$	0.14	0.25
Hartke	0.165	$8x10^{-3}$	0.14	0.285
Kolomiets & Lebedev	0.12	$5x10^{-3}$	0.13	0.285
Grunwald & Blakney	0.34	$7x10^{-3}$	0.21	0.31
Xerox Group	0.14	$6x10^{-3}$	0.16	0.33

A certain amount of averaging has been performed in compiling these data, since most authors reported a spread of values, especially in the results for the electron mobility and activation energy.

Hartke also examined electron and hole lifetimes (for deep trapping), and ranges. For holes, a room temperature free drift time of approximately 10^{-7}sec, increasing with decreasing temperature with an 'activation energy' of -0.14 eV was reported.

This gave a hole range of about 3×10^{-8} cm^2V^{-1}, which was approximately independent of temperature. For electrons, the reported room temperature free drift time was 10^{-5} sec, and the 'activation energy' was -0.2 eV for commercial grade selenium and -0.13 eV for distilled material. The electron range at room temperature was approximately 10^{-7} cm^2V^{-1}, and decreased in both cases with decreasing temperature. Lifetime measurements were also reported by Kolomiets and Lebedev, whose results were in reasonable agreement with those of Hartke, and by the Xerox group, who realised the problem of field controlled photo-generation in the excitation process, and the inapplicability of the Hecht analysis. As mentioned previously, allowing for such a process, the Xerox researchers calculated that carrier lifetimes should be much longer than those previously reported. They estimated a hole lifetime of between 10 and 50 μsec, and an electron lifetime of 50 μsec at room temperature. Surprisingly, although the hole lifetime is much longer than earlier values, the electron lifetime is not; being slightly smaller than Hartke's estimate.

In several of the studies mentioned above, the effect of impurity addition was examined. A summary of the results obtained is shown in figure 21. Hartke's investigation was confined to the addition of arsenic, which he found to have little or no effect on the magnitude or activation energy of the hole mobility. The activation energy of the electron mobility was likewise unchanged, but the magnitude of the mobility was progressively reduced as the arsenic concentration increased. Kolomiets and Lebedev examined the effect of a range of impurities, in concentrations of up to 10% in some cases. In general, the hole mobility was found to be insensitive to impurity

Figure 21. Results of Previous Examinations of the Effects of Doping Additives on the Transport Properties of Amorphous Selenium.

Examination	Material	Holes		Electrons	
		Mobility $cm^2V^{-1}sec^{-1}$	Lifetime μsec	Mobility $cm^2V^{-1}sec^{-1}$	Lifetime μsec
Xerox[30]	Se (5N)	0.14	10-50	6×10^{-3}	50
"	Se+2.1%S	0.12	0.5	6×10^{-3}	60
"	Se+12%S	0.042	0.42	1.8×10^{-3}	150
"	Se+1%Te	0.009	20	1.2×10^{-3}	30
"	Se+5.4%Te	0.006	25	-	-
"	Se+2%As	-	<0.3	7.8×10^{-4}	200
"	Se+9%As	-	-	1×10^{-5}	3000
Hartke[33]	Se (5N)	0.165	0.15	8×10^{-3}	25
"	Se+2%As	0.14	-	7×10^{-4}	-
Kolomiets & Lebedev[34]	Se (7N)	0.12	0.13	6.5×10^{-3}	10
"	Se+3%S	0.10	0.1	4×10^{-3}	15
"	Se+10%S	-	-	2.6×10^{-3}	3
"	Se+0.65%Te	0.12	0.1	2.5×10^{-3}	15
"	Se+3%Te	0.10	0.1	5.4×10^{-4}	40
"	Se+1%P	0.10	0.08	-	-
"	Se+3%P	0.08	0.08	-	-
"	Se+2%As	-	-	5×10^{-4}	35
"	Se+6%As	-	-	5×10^{-5}	-

addition, but it was found to be impossible to observe any hole trace in selenium containing relatively high concentrations of arsenic or sulphur. The magnitude of the electron mobility was generally reduced by the addition of impurities, and no electron pulse was detectable in specimens doped with phosphorus. The examination of the Xerox team was possibly more valuable, and was combined with information from measurements of other properties to successfully clarify the situation with regard to carrier transport and doping effects in selenium. It will thus be useful to describe their measurements in some detail. The relevant information is contained in the papers by Schottmiller et al[30], Tabak and Warter[31], and Tabak[32]. Of these examinations, the first was primarily concerned with the effects of doping additives in general, the second with the study of carrier photogeneration, and the third with the addition of arsenic up to the composition As_2Se_3. There is, however, some degree of duplication in the reports, and it will be convenient to combine the three in the following survey, rather than to provide separate descriptions. In terms of the properties of undoped material, information from the studies of viscosity, differential thermal analysis, radiation distribution analysis, Raman and infra-red spectroscopy, and transport properties, was described and reviewed, showing the presence of Se 8-membered rings and chains in both vitreous and evaporated material. A convincing identification of the dependence of the electron transport on the presence of the Se_8 rings was made. A correlation was less rigorously suggested between the hole transport properties and the occurrence of deep traps at the branch points of Se chains. Two possible mechanisms

for the electron transport were advanced. The first of these postulated a shallow trap controlled mobility; the addition of impurities reducing the Se_8 ring population and thus increasing the trap density and lowering the mobility. The second model considered the possibility of a thermally activated tunnelling (hopping) process between Se_8 rings. Addition of impurities was again envisaged as reducing the Se_8 ring population, with the resulting increased ring separation causing a reduced hopping probability and mobility. Impurity additions were classified according to the structural modifications produced by the impurity. In this respect, univalent (Cl,Tl), isoelectronic (S,Te), and branching (As,Ge,Bi) additives were identified. Univalent additives were described as producing deep electron traps of coulombic form. Isoelectronic elements produced mixed rings which reduced the Se_8 ring population and thus the electron mobility. Branching additives again reduced the ring population by inducing the presence of branched chains. At the branch points of such chains, deep hole traps were produced, reducing the hole lifetime.

The addition of germanium and arsenic is of particular relevance to the present study, and the observations and conclusions with regard to these materials will be reviewed in greater detail below.

Germanium. This was classed as a branching element. Addition of small amounts of germanium was found to cause a reduction in electron mobility, with 1% Ge producing a decrease from 6×10^{-3} to 3.8×10^{-3} $cm^2V^{-1}sec^{-1}$. No significant change in the activation energy of the electron mobility was found to accompany this reduction.

The addition of 1% Ge caused a reduction of the hole lifetime from over 10^{-5} sec to less than 3×10^{-7} sec, and the addition of a few percent of germanium caused a significant decrease in the magnitude of the hole mobility, coupled with the appearance of marked rounding of the transit trace. Such rounding was also observed as a consequence of arsenic addition, as described below, and was ascribed to a similar source in both cases.

Arsenic. This, again, was classed as a branching additive, with each arsenic atom bonding to three selenium atoms to produce an extended network structure at high arsenic concentrations. The electron mobility was found to decrease approximately exponentially with increasing arsenic concentration up to 9% As. Above this level, the rate of mobility reduction decreased. Measurements of electron mobility activation energy at concentrations of 0.5 and 2% As gave a value identical to that measured in pure Se. These effects were associated with a reduction of Se_8 ring concentration up to 9% As, and with the production of an As-Se network at higher concentrations. Spectroscopic studies were cited, showing a falling ring concentration, extrapolated to zero at 20% As. In hole transport measurements, the addition of As was observed to produce a complex transit pulse shape. At low As concentrations, the pulse showed a fast initial region giving a mobility equal to that for pure Se, and a much slower 'exponential tail' region indicating a mobility of about $10^{-5} cm^2 V^{-1} sec^{-1}$. Measurements on specimens of different thickness were correlated, showing that this region was due to a complete transit rather than to deep trapping effects. With increasing As concentration, the magnitude of the slow portion of the curve increased at the expense

of the fast portion, until the latter became invisible at a concentration of 18% As. The exponential pulse was associated with the presence of the As-Se network, and it was suggested that the compositional disorder could cause a whole range of capture and release times giving a poorly defined transit time.

In the study of the photoelectric properties[31], it was shown that the efficiency of carrier photogeneration in selenium is strongly field dependent as has already been mentioned. The variation of the photocurrent with temperature was found to be strongly dependent upon applied field; the activation energy decreasing from 0.12 eV at a field of 2×10^3 V/cm, to 0.034 eV at 2.5×10^4 V/cm. This effect was explained as a manifestation of the Poole-Frenkel lowering of Coulombic potential barriers by the applied field, causing a dependence of photogeneration efficiency upon field.

In the above examinations on evaporated films, no significant dependence of mobility on electric field was reported, although Spear and Hartke described a minor dependence by which a plot of reciprocal transit time against applied voltage gave a non-zero intercept on the voltage axis. This effect was considered by them to be due to the build up of a surface charge layer close to the upper electrode.

b) Arsenic Selenide

In addition to the inferences which can be drawn on the properties of arsenic selenide from the arsenic-doped selenium studies above, carrier transport in evaporated films of arsenic selenide has been studied by Kolomiets & Lebedev[35] and by Tabak[32].

The examination of Kolomiets and Lebedev[35] was somewhat superficial. A rounded hole pulse indicating a mobility of 4×10^{-4} $cm^2V^{-1}sec^{-1}$ at room temperature was observed at an applied electric field of about 5.5×10^5 $V\ cm^{-1}$. The mobility was found to be smaller by a factor of 1.5 to 2 at -10^oC. It was not possible to observe any electron transit trace during the investigation. No field dependent mobility effects were reported, but the shape of the hole transit pulse was found to be somewhat dependent upon the magnitude of the applied voltage.

Tabak's study formed part of his examination of arsenic doping in selenium, and was again superficial. A room temperature hole mobility of about 10^{-5} $cm^2V^{-1}sec^{-1}$ was measured; no electron transit pulse being visible. As mentioned previously, comparison of results in specimens of various thicknesses at identical values of applied field was used to identify the observed 'exponential' pulse as representing a transit, rather than a trapping phenomenon.

c) Other Materials

Hirsch[83] has attempted to measure drift mobilities in arsenic trisulphide. It was found that very low carrier mobilities, coupled with strong deep trapping effects, precluded the observation of transit pulses, both for electrons and for holes. However, by examining the induced conductivity produced by electron bombardment of thin arsenic trisulphide films, a carrier mobility of about 5×10^{-7} $cm^2V^{-1}sec^{-1}$ was inferred for one type of carrier (believed to be the electron), whilst the mobility of the other carrier was estimated as 10^{-8} $cm^2V^{-1}sec^{-1}$. Further examination of the electron bombardment induced conductivity has been made by, among others, Ansbacher and Ehrenberg[62].

In addition to the studies described above, the technique of drift mobility measurement by observation of carrier transit pulses has been applied to a wide range of low mobility materials, of crystalline, amorphous, liquid, and organic nature. Such reports are too numerous to allow for their description here.

Chapter Five

Drift Mobility - The Present Examination

5.1 Experimental Technique and Equipment

The practical requirements for the determination of drift mobilities by the transit time method have been discussed in Chapter Four. Essentially, a sheet of carriers is produced by some means of excitation, in a suitable thin film specimen. The drift of these carriers through the bulk of the material under the influence of an applied electric field is then observed. Thus, having decided to attempt such a measurement, it is necessary to select the form of the excitation source, and to examine what is required in terms of a 'suitable thin film specimen'.

Carriers may be excited by pulsed beams of light, electrons, or radioactive ions. Since the production of short pulses of ions is relatively difficult, and since the technique seems to offer no significant advantages over its alternatives, the third technique was quickly rejected in the present study. The use of light pulses offers the advantage that no complex vacuum system is necessary, and presents the possibility of the examination of spectral response effects by means of a controlled variation of the source frequency. The present 'state of the art' makes possible the production of sufficiently short light pulses (down to a few nanoseconds in length). Further, it would appear that beam intensities sufficient for the present application are now relatively easy to attain. The only major problem arises in the requirement that carriers be produced in a very thin layer at the surface of the specimen. Thus, whilst the system is admirably suitable for materials of high optical absorption, more transparent

substances would be difficult to examine. By using a focussed electron beam as an excitation source, it should be possible to overcome this problem. By varying the energy of the beam, its absorption in a thin layer may be ensured. The use of such a beam also allows the electron beam induced photoconductivity to be examined. The major disadvantage of the technique lies in its relative complexity, since the use of a specialised electron gun and its associated equipment is required. Even so, excitation by electron beam was adopted as most suitable for the present study. A further examination of the relative merits of various excitation techniques is provided in a review article by Spear[84].

The selection of a suitable film preparation technique was also examined in some detail. The possible distinction between evaporated and bulk vitreous specimens has previously been discussed, as has the difficulty of evaporating materials of non-stoichiometric composition. The techniques which were finally adopted in an attempt to preserve the vitreous nature and the composition of the specimen films have been described in Chapter Three.

Drift Mobility Measurement Equipment

The drift mobility measurement assembly is shown in figure 23a, and the fundamental units of the equipment are indicated in schematic form in figure 22a. Film specimens were mounted in a specimen holder, by which the specimen temperature could be varied over a wide range. The holder was situated inside an electron gun, the pulsed operation of which was controlled by the H.T. electronics section. Overall control of the experiment was effected by the L.T. electronics section, which provided triggering for the H.T. equipment, controlled the specimen environment and applied field, and

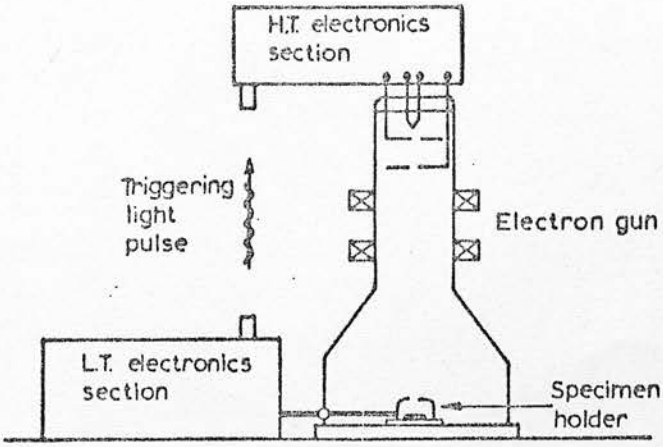

Fig. 22a Schematic Diagram of Drift Mobility Measurement Equipment

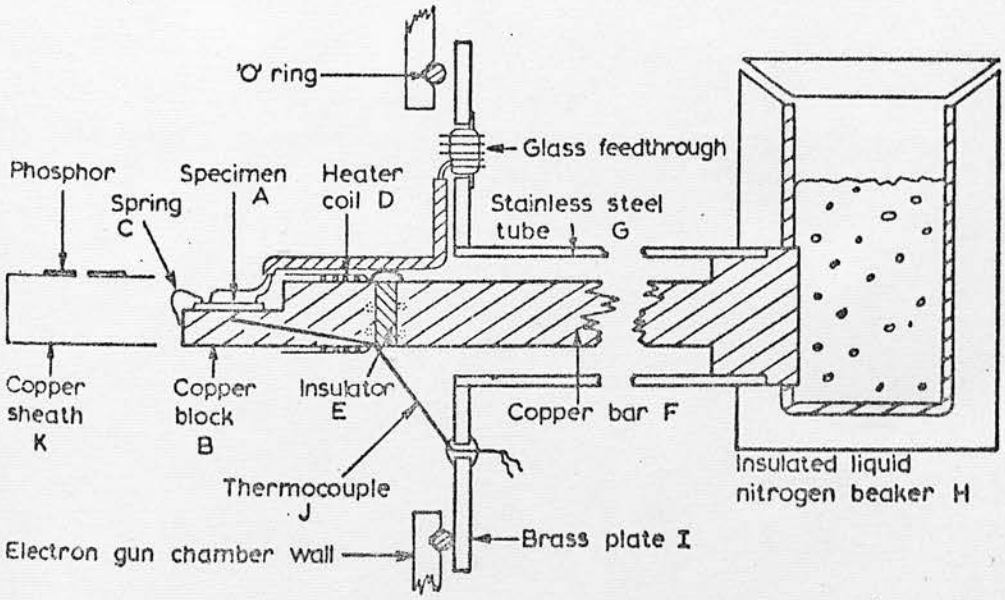

Fig. 22b Specimen Holder for Drift Mobility Measurement System

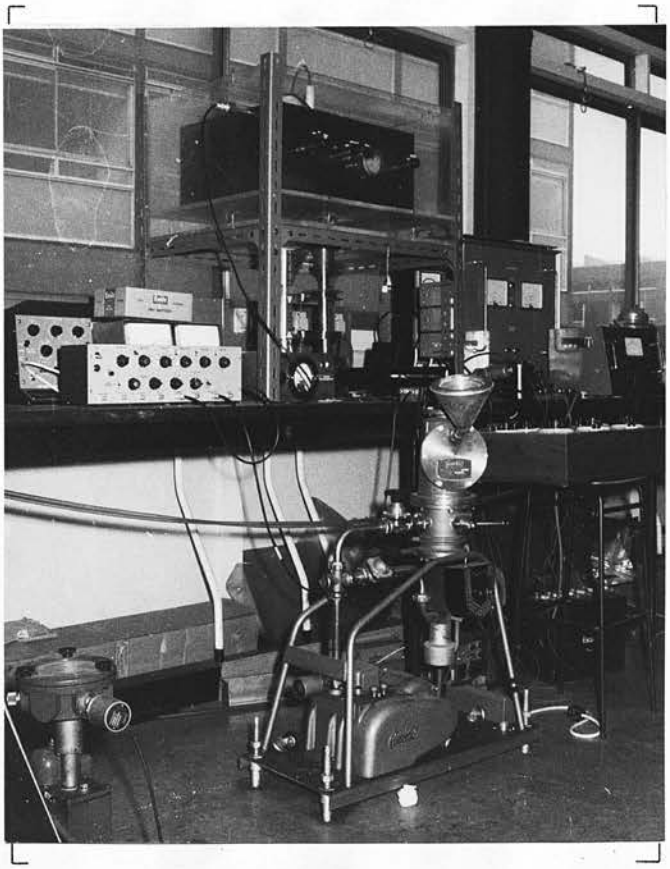

(a) Drift Mobility Measurement Assembly

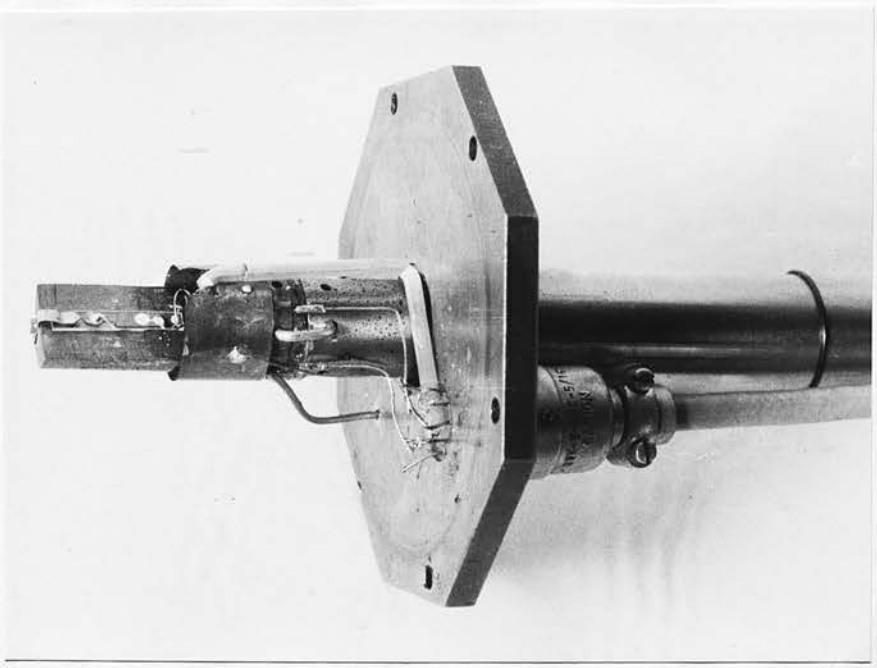

(b) Drift Mobility Specimen Holder

Fig.23

dealt with the detection of transit pulses. The four sections will be described in more detail below.

a) Specimen Holder.

During the development of the equipment, several designs of specimen holder were tried. The final arrangement, employed in all the measurements reported in the drift mobility study, is shown on figures 22b and 23b. This system permitted the specimen temperature to be continuously varied within the range 100 to 450^{o}K. The specimen, A, on its glass substrate, was held in position on a shaped copper block, B, by a spring clip, C. A heating coil of nichrome wire, D, was non-inductively wound around the block, which was cemented to a ceramic insulator disc, E, followed by a copper bar, F. The bar F was supported inside a stainless steel tube, G. By means of a thermally insulated copper beaker, H, filled with liquid nitrogen, the temperature of the block B could be reduced, whilst the low thermal conductivity of the tube G minimised the cooling of the outer electron gun chamber. A set of copper heat shunt rods could be used to bridge the insulator E, and thereby control the rate of cooling of B. The use of this arrangement in conjunction with the heating coil allowed the specimen temperature to be varied over a wide range, and to be stabilised at any particular value by balancing the heating and cooling systems against each other. A plate, I, soldered on to the outside of the tube, G, permitted the system to be connected to the specimen chamber of the electron gun. A multiple glass/metal feedthrough in the plate,I, was used to provide current for the heating coil, and to make contact to the specimen. The specimen leads were directed from the feedthrough to the specimen

via a double bore silica tube, and the wires were attached to the specimen by silver 'Dag' suspension. In this way, a very high leakage resistance between the leads was ensured. The specimen temperature was monitored using a chromel/alumel thermocouple, J, set into the block B in a position directly beneath the specimen. Thermal and electrical shielding of the specimen was provided by a copper sheath, K, which also served to define the path of the electron beam. The beam passed to the specimen through a 1½mm diameter hole in the shield. The exterior of the shield was coated with a layer of phosphorescent material, to allow visual focussing and positioning of the electron beam.

b) Electron Gun

Two electron gun systems were used in this study. One of these was a triode arrangement prepared by the General Electric Company, and the other, a tetrode system was made in this Department. For a great deal of help in the design of this latter gun, we are indebted to Dr. W.E. Spear, now of the University of Dundee.

The triode gun, used as an interim device during the preparation of the tetrode system, was found to be subject to three rather severe limitations. The beam current was strongly dependent upon the accelerating voltage, and the grid pulse necessary to drive the gun from its normal 'off' state to the 'on' state, was very large, being well over 100V. Furthermore, the necessary pulse height was itself dependent upon the accelerating voltage. Hence, the complexity of the equipment producing the switching pulse was unnecessarily great. Finally, the gun was not demountable, so that electrode adjustment, or filament replacement, was extremely difficult. However, preliminary

experiments performed using this system did serve as useful guides in the development of later equipment, and allowed the development of the specimen preparation technique to continue in the absence of the tetrode system.

The second electron gun was a completely demountable structure which adequately overcame the limitations of its predecessor. Its construction is shown in figure 24, and the electrical system is included in figure 25. The cathode was a directly heated tungsten wire, powered from a six volt accumulator and regulated by a variable series resistor. The lateral and vertical positions of the filament with respect to the modulating grid were easily adjustable, allowing the filament to be correctly positioned in the immersion field of the grid system. The cathode was held in the off state by an adjustable positive bias, normally between 20 and 30V, relative to the casing of the H.T. section of the gun. The modulation grid, situated below the cathode, was driven via a feedthrough in the side of the gun. A selected sub-miniature, non-inductive, 75 ohm resistor was connected between the grid lead and the case to provide correct termination of the drive pulses. Due to this resistor, the grid was normally at the casing potential, so that its negative bias with respect to the cathode held the gun in the off state. A sufficiently large positive pulse on the grid served to switch the beam on. The anode grid, situated below the modulation grid, was held at a potential of about +330V with respect to the cathode, and served to stabilise the operation of the gun. With this arrangement, the beam current was found to be virtually independent of the accelerating voltage over the range 0 to 30 kV. In addition, the

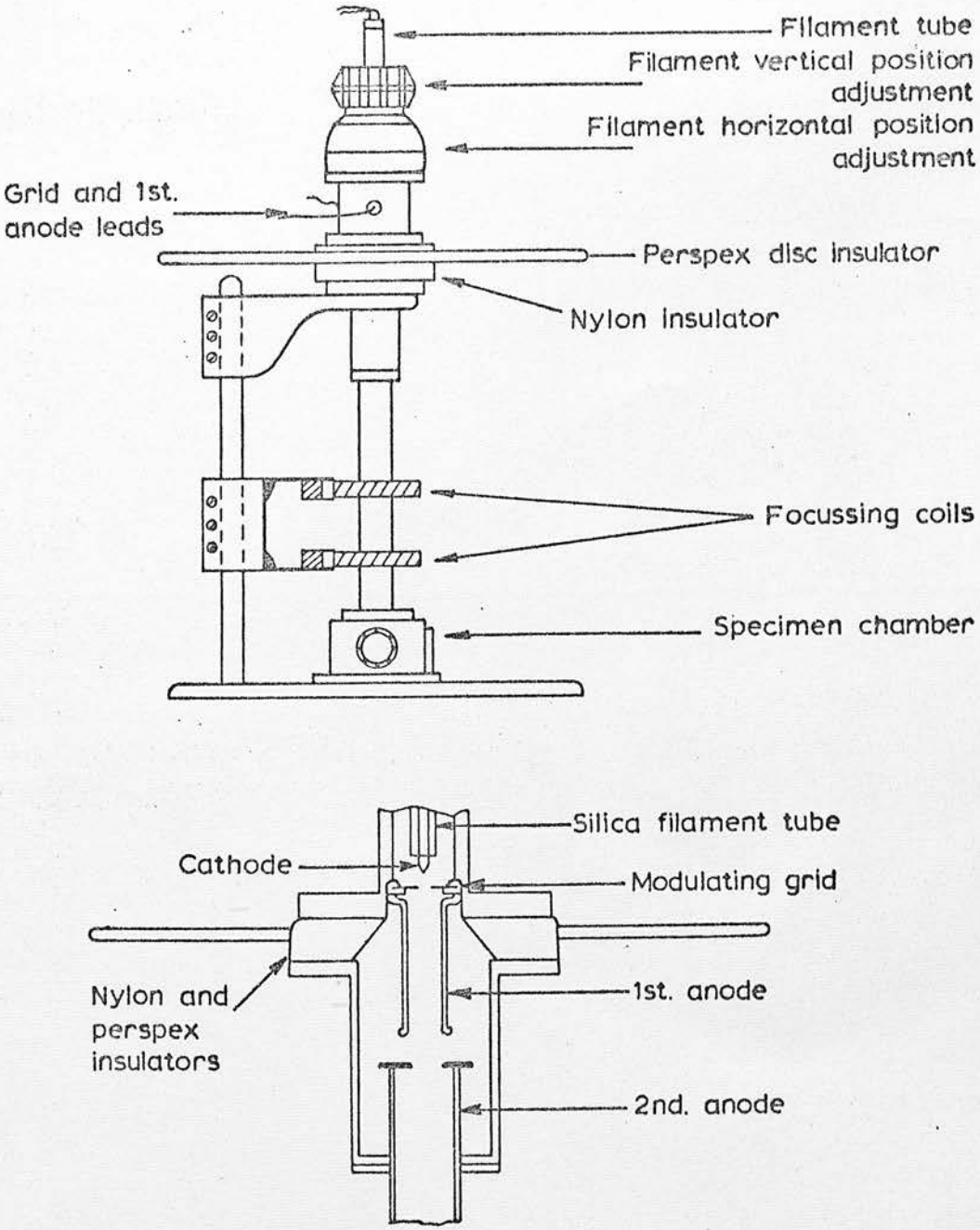

Fig. 24 Drift Mobility Equipment; Tetrode Electron Gun

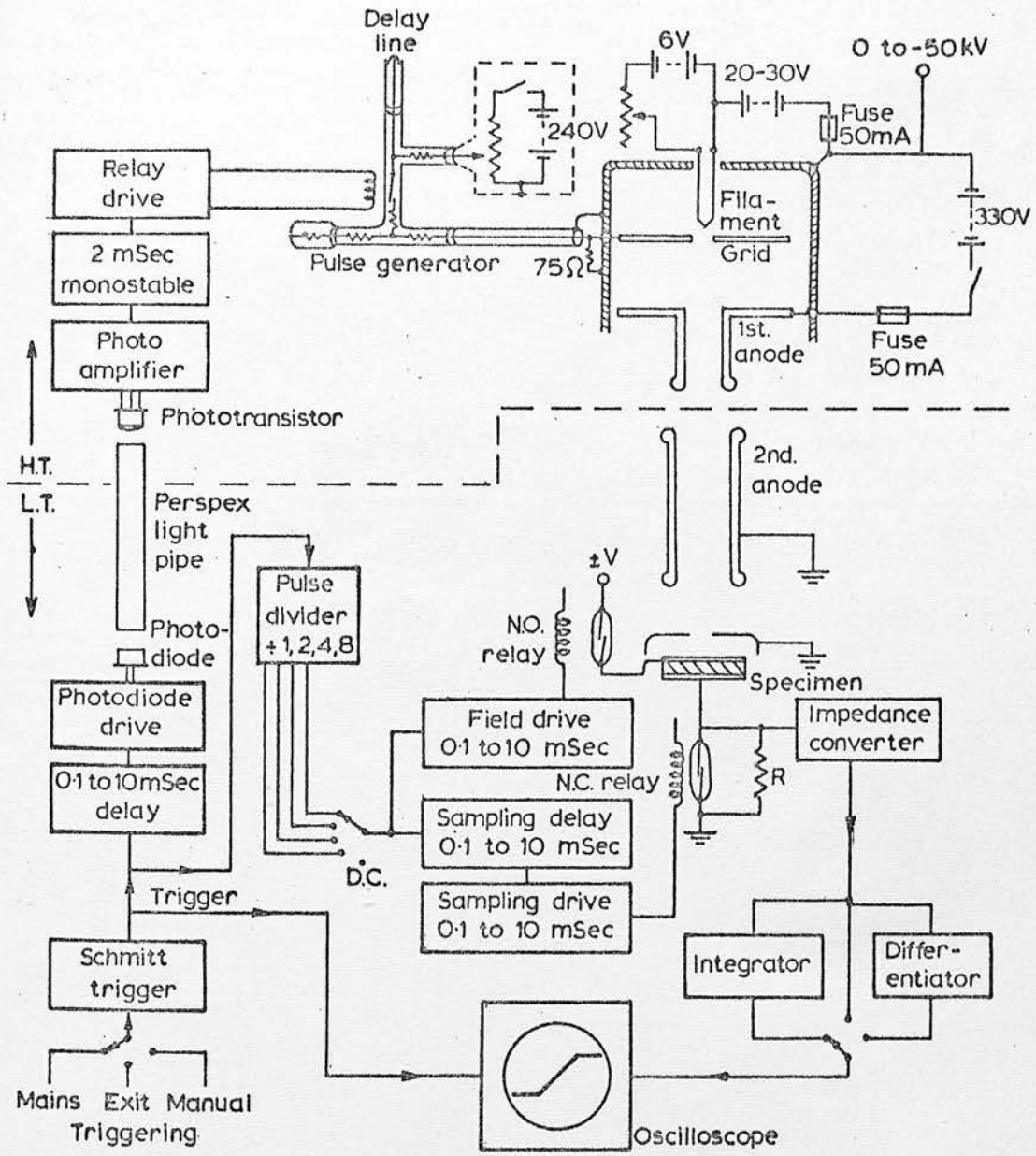

Fig. 25 Drift Mobility Equipment: Electrical System

modulator switching voltage was reduced to around 30V., easing the problems of the driving pulse equipment. The electron beam was focussed by means of two adjustable magnetic coils, which allowed control of the beam position relative to the specimen.

H.T. Electronic Equipment

The electron gun accelerating potential was supplied by a Brandenberg MR 50/R generator. A diagram of the equipment situated in the H.T. section of the equipment is shown in figure 25. A triggering pulse, provided by a gallium arsenide lamp at earth potential, was transmitted to the H.T. equipment through a perspex light pipe, and was detected by a phototransistor amplifier. The output of this unit served to trigger a 2 msec. monostable multivibrator which controlled a power transistor driven relay coil. This coil formed part of a high voltage fast pulse generator built on the lines described by Spear et al[68]. The essence of this unit, shown in figure 26, was a T shaped brass tube fitted with 75 ohm BNC sockets on the end of each arm. The vertical section of the tube housed a mercury wetted contact relay (Elliot 226D) driven by an externally wound coil. At the output of this arm was connected a length of open ended co-axial cable acting as a delay line. This line was charged through a high-value resistor from a 0 to 240V source. The remaining arms of the T section contained selected 25 ohm non-inductive resistors. One of these arms was connected to the grid of the electron gun through the 75 ohm termination and the other arm, available for monitoring performance, was normally terminated by a 75 ohm resistance element. By careful impedance matching throughout, it was possible to minimise the

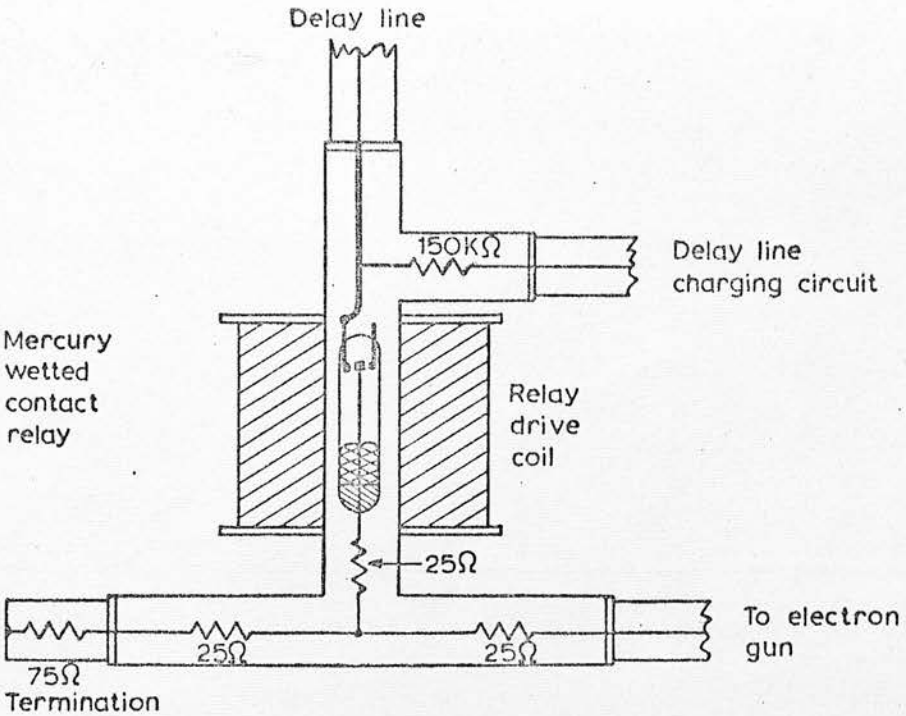

Fig. 26 Drift Mobility Equipment, Fast Pulse Generator

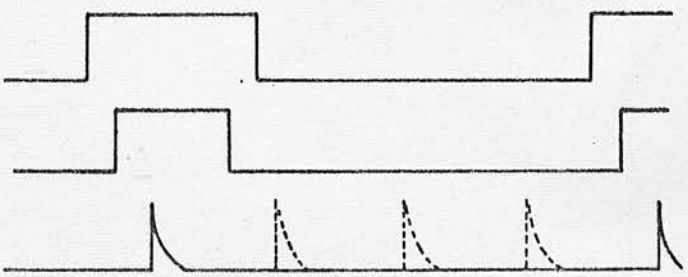

Fig. 27 Timing Relationship between Field, Sampling and Excitation Pulses

distortion and reflection of fast pulses in the system. The pulses were supplied by the discharge of the delay line upon the closing of the mercury relay. The relay had a rise time of 3×10^{-10} sec, allowing the production of 'square' pulses of under 10 nsec length; the length being controlled by the dimensions of the delay line, being approximately 10 nsec/metre of line. For the purposes of this study, a pulse length of 60 nsec proved suitable. During the development of the equipment, several other methods for the generation of short duration high voltage pulses were examined, including circuits based upon the avalanche transistor, step recovery diode, and thyristor. In evaluation, it was found to be difficult to attain a sufficiently large amplitude of pulse, especially for use with the triode electron gun. Thus, the delay line technique using the mercury relay proved most suitable. The limitations of this type of generator lay in fundamental properties of the relay. The pulse repetition rate was necessarily less than 200 Hz, but this did not pose a serious problem in the present application. More seriously, a small jitter in the relay turn-on time produced a fluctuation in the arrival time of the excitation pulse at the specimen, which tended to make observations difficult when very fast carrier transits were being examined. It is considered that this defect could be remedied by extracting a triggering pulse from the auxiliary termination of the pulse generator, and transmitting this to the L.T. section by means of a GaAs lamp system. In this manner, synchronised oscilloscope triggering could be ensured. Alternatively, replacement of the mercury relay pulse generator by an avalanche transistor circuit should be feasible.

L.T. Electronic Equipment.

The control equipment was constructed making extensive use of logic microcircuits, and is shown in schematic form in figure 25. The initiating pulse for the circuitry was provided by a Schmitt trigger, which could be driven internally at 50 Hz, or by an external input. Single shot manual operation was also possible. The internal 'mains' triggering was found to be advisable since it stabilised the position of the observed transit pulse with respect to any mains pick-up. The output from the Schmitt trigger was differentiated and rectified to produce short positive pulses with a (normally) 50 Hz repetition rate. These pulses performed the functions of

1. Oscilloscope triggering.
2. H.T. section triggering via a delay unit and GaAs lamp.
3. Specimen field control.

For the purpose of specimen field control, the Schmitt output was directed to a pulse dividing section, capable of giving an output pulse for every 1, 2, 4, or 8 input pulses. The output of this unit was used to trigger a 0.1 to 10 msec monostable multivibrator which controlled a relay to apply a voltage across the specimen. In this manner, a pulsed field could be applied to the specimen for every 1, 2, 4, or 8 excitation pulses from the electron gun. The purpose of this arrangement was to allow some degree of specimen stabilisation with respect to the excitation pulses between transit time measurements, and to allow any space charge to leak away between transit time measurements. Since sudden application of the specimen field resulted in the production of transient oscillations in the output detection circuitry, it was necessary to protect the output

by the means described by Spear[84]. In this system, the detection resistor R is temporarily short circuited during the application of the field pulse, by means of a sampling relay as shown in the diagram. A delay unit and variable monostable multivibrator allow the correct adjustment of the output sampling system. The time relationship between the applied field and the bombarding and sampling pulses is shown in figure 27. In addition to these pulsed arrangements, it was arranged that a continuous applied field could be used. In the practical investigation, it was found to be expedient to use such a 'd.c.' field for nearly all the measurements for the following reasons. Firstly, the purpose of the pulsed field was to counter the effect of space charge accumulation in the sample. It was hoped that by bombardment of the specimen only a few milliseconds after application of the field, space charge accumulation would be minimised, and that any charge which built up during the application of one field pulse would have decayed by the time the next pulse was applied. However, this did not prove to be the case due to the long time constants for decay which were encountered. Fortunately, space charge effects proved, in practice, to be small, and transit measurements were not seriously affected by such effects. Therefore, no improvement in observed pulse height was obtained by the use of the pulsed technique. Secondly, the phenomenon of switching to a conducting state was exhibited by certain of the materials under study. With a specimen in such a state, the pulsing circuitry presented the applied field with a virtual short circuit at certain periods of the pulsing cycle. Furthermore, the specimen switching was positively assisted by the large transient voltages set up by the pulsed field application.

Thus, the drawbacks of the pulsed arrangement were judged to outweigh its advantages, so that the d.c. system was generally employed. For detection of the transit pulse, the use of an impedance transforming amplifier and of output integration and differentiation was investigated. The purpose of the amplifier was to reduce the spurious output pick-up by a reduction of the high impedance presented by the resistor R to a low value; the resistor and amplifier being as physically close to the specimen as possible. The integration and differentiation, electronically controlled using a linear microcircuit, allowed observation of the current or voltage waveform produced by the charge transit. In practice, such systems were again frequently discarded since the high impedance amplifier tended to be destroyed by the large voltage caused by occasional specimen switching, and since a combination of the specimen capacitance and the resistance of R provided a time constant which was generally sufficient for adequate integration of the transit pulse. Since such integrated pulses provided the most effective means of observation of the transit, the position in this respect was satisfactory. Spurious pick-up was reduced to an insignificant level by careful shielding of the output circuitry. In practice, a value of R of less than 10^6 ohms was suitable, and the use of a Tektronix 545B oscilloscope with a Type 1A6 plug in unit provided sufficient pulse amplification coupled with an input impedance of 10^6 ohms. It is, however, accepted that the use of an impedance transforming amplifier, allowing subsequent pulse integration and differentiation, and the employment of a sampling oscilloscope, would prove extremely useful in the examination of a wide variety of materials, and that such a system is thus generally advisable.

Measurement Technique

The use of the equipment has been described in principle in preceding sections. Basically a measured voltage was applied to the specimen at a known temperature. Excitation pulses were then directed through the upper specimen electrode, and the transit of the resultant charge sheet was displayed on an oscilloscope. In practice, a number of transit traces were photographed at each temperature and applied field, and an average transit time was determined. Figure 28 shows typical transit pulses, as observed for hole transit in selenium and in arsenic selenide. As can be seen, the analysis of the selenium traces presented no problem, since the end of the transit was well defined by the discontinuity of the slope. The analysis for arsenic selenide was not so straightforward, since no discontinuity of slope occurred. By applying the criteria described in section 4.3, it was experimentally possible to determine that the observed trace was a manifestation of a complete charge transit, rather than a partial transit limited by trapping. It will be recalled that Tabak[32] formed a similar conclusion during his examination. However, since no unique transit time occurred, it was necessary to develop a reasonably simple means for characterising the observed response time. The extrapolation of linear portions of the transit curve, as employed in cases where only slight rounding was evident, was obviously not applicable since no linear portions existed. Any attempt to 'force' the curves, by drawing straight lines through them, could only lead to inaccurate and inconsistent results. In an attempt to provide a technique which would yield a consistent value proportional to the 'average transit time', the

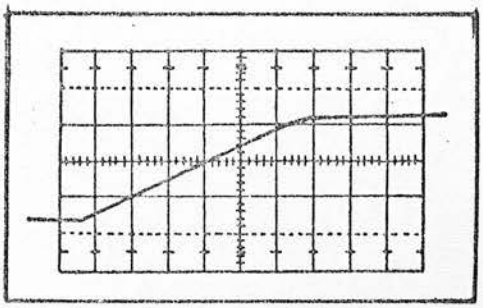

(a) Hole transit trace : Selenium
Scale 0·2 μsec per major horizontal division
2mV per major vertical division
Applied field = 2·3 x 10^4 V/cm.
Specimen thickness = 44 microns

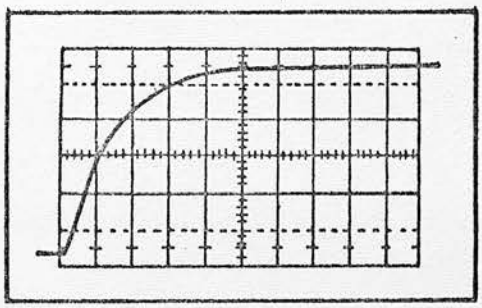

(b) Hole transit trace : Arsenic Selenide
Scale 1μsec per major horizontal division
5mV per major vertical division
Applied field ≈ 3 x 10^5 V/cm.
Specimen thickness ≈ 3 microns

Fig. 28 Typical Transit Pulses as Observed in Selenium and in Arsenic Selenide

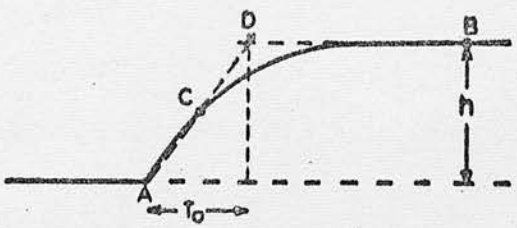

Fig. 29 Method for Evaluation of the Transit Time from Rounded Pulses

process illustrated in figure 29 was adopted in this investigation. The pulse height, h, at a point B at which the pulse showed no significant slope, was measured. The point C, and which the pulse height was equal to h/2, was then identified. A line drawn through the pulse origin, A, and C was extrapolated to give an intersection with a horizontal line drawn through B. The time interval between this point, D, and the origin, A, was then taken as the 'transit time' T_o. In the limiting case for which the transit curve is exponential, the method will give a value of T_o equal to approximately 1.4 times the exponential time constant. The adopted method was selected in preference to one in which the 'time constant' was calculated, since the latter gives an incorrect estimate in the ideal case of a linearly rising pulse, whilst the former gives the correct result.

The measurement of specimen current in the investigation of conductivity was performed by monitoring the voltage developed across the known resistor, R. In cases where the current was sufficiently large as to cause a significant potential to develop across R, a correction for this effect was applied in the calculation of the specimen field.

5.2 Measurement Errors

The major sources of error in this study occurred in the measurement of film thickness and of transit time. Since the criteria for these measurements differed with the material under examination, it will be convenient to discuss the two major materials (selenium and arsenic selenide) separately.

a) Selenium

To measure the film thickness using Talysurf equipment, a series of about ten thickness readings was taken for each specimen,

and the average value was then determined from these figures. Statistical analysis of the readings taken on a number of specimens allowed the calculation of an r.m.s. error of 4% for the film thickness. It should be noted that the thickness occurs as a squared term in the expression for the mobility (equation 4.1.7), so that the r.m.s. error in the calculated mobility due to thickness variations was 8%. The accuracy of the Talysurf equipment was checked using calibrated standards, and errors were found to be negligibly small in comparison with the above figure. In the measurement of T_o, about five transit time readings were taken at each value of temperature and field, and an average value calculated. From the analysis of such data, an r.m.s. error of 2% was calculated for the measured transit time. In addition, the error inherent in the measurement system was estimated. It will be recalled that rounding of the last 10% of the response pulse occurred for hole transits in selenium at room temperature, as indicated in figure 28a. This rounding was due to a number of parameters, such as charge diffusion during the transit, finite specimen penetration by the excitation beam, material inhomogeneity, and the finite length of the excitation pulse. Of these, it is likely that the last effect was dominant in hole transit pulses at higher temperatures, since the excitation pulse was 60 nsec. long, whilst the transit times were of the order of 1 μsec. Thus, a rounding of the last 6% of the pulse could be expected from this source. Since the extrapolation procedure used in transit time estimations 'averages out' the rounding, allowance for the finite excitation time should strictly have been made by subtracting 30 nsec from the measured time. A value would then be obtained for the time taken for carriers, produced at the

start of the excitation pulse, to reach the lower electrode. Since this procedure was not adopted in the study, an error of 3% could be expected in the faster transit measurements; this error decreasing for the slower pulses produced at lower (values of) temperature and field. The error due to penetration of the specimen by the excitation beam was small, since the 10keV electrons used in the examination were calculated to have a range of less than 0.5% of the specimen thickness[64]. The rounding of the pulse by carrier velocity variations during transit must be considered as a property of the material, rather than as a source of error, and the extrapolation technique produces an average transit time, as is desirable under these conditions. Allowing for an error of ± 2% in the calibration of the oscilloscope time base, and 1% in the measurement of the specimen voltage, the total estimate for the accuracy of the mobility measurement was ± 15%.

b) Arsenic Selenide

The reservations with regard to the technique adopted for the extraction of transit time values from the curved response pulses obtained in this material have already been expressed. It has been mentioned that the technique is expected to give a value proportional to, and of the order of, the average transit time, in so far as this term is applicable to the situation. It is impossible to make any quantitative estimates of errors in this respect, and the following discussion will therefore be limited to system errors and the self-consistency of the measurements. Following the procedure described for selenium, the accuracy of thickness measurements was estimated as ± 10%, the figure being larger than that for selenium due to the

thinner nature of the specimens, and to the necessity to destroy the films during the thickness measurement. Similarly, comparison of a series of measured transit times was made, giving a measurement accuracy of ± 6%. Since transit times were much longer than in the case of selenium, the finite length of the 60 nsec excitation pulse produced a negligible error. However, the 8 keV beam energy caused a 5% penetration of the specimens (∿5 μm thick). Including the oscilloscope time base and specimen voltage errors, an accuracy of ± 30% is calculated for the mobility, although this figure must be considered in the context of the unknown accuracy of the technique for transit time extraction.

5.3 Experimental Results

a) Pure Selenium

A number of specimens, prepared by the compression technique, were examined at room temperature. The measured hole mobility is shown in the following table.

specimen	electrodes top	electrodes bottom	thickness (microns)	field (V/cm)	hole mobility ($cm^2V^{-1}sec^{-1}$)
A	Au	Au	32.0	3.12×10^4	1.14×10^{-1}
M	Al	Al	37.5	2.67×10^4	1.37×10^{-1}
M	Al	Al	37.5	8.01×10^4	1.32×10^{-1}
R	Al	Al	44.0	2.27×10^4	1.60×10^{-1}
S	Au	Au	37.5	4.00×10^4	1.12×10^{-1}
V	Au	Al	41.0	2.44×10^4	1.46×10^{-1}
W	Au	Al	37.0	2.70×10^4	1.25×10^{-1}
Y	Al	Al	37.0	2.78×10^4	1.37×10^{-1}
Y	Al	Al	37.0	5.56×10^4	1.33×10^{-1}

These figures give an average room temperature hole drift mobility of

$$1.33 \times 10^{-1} \text{ cm}^2\text{V}^{-1}\text{sec}^{-1} \pm 10\% \text{ r.m.s.}$$

In early measurements of the dependence of mobility upon temperature, the effect of the electric field on the mobility at low temperatures had not been realised. The results obtained were therefore mainly contradictory and meaningless. At a later stage in the investigation, the dependence of hole mobility on temperature and applied field was examined for specimen M. The results are shown in figure 30. (A full table of the readings related to this and other results is given in Appendix I.) As the mobility decreased, the hole transit traces tended to become slightly rounded in form. However, well defined linear sections of the curves were still evident, so that the transit times could be determined by extrapolation, as previously described.

On examining the transit of electrons in selenium, the pulse heights were found to be much smaller than was the case for holes, and a degree of pulse rounding was evident even at room temperature. This rounding was found to increase with decreasing temperature, whilst the pulse height progressively decreased. For this reason, electron mobility measurements over an extended temperature range were impractical. The results of a brief examination of the electron mobility in specimen M are shown in figure 31.

b) Germanium-Doped Selenium.

The examination of the properties of selenium doped with 1% germanium (atomic percentage) was very similar to the study made on pure selenium. The room temperature hole mobility was measured in several specimens, and the results are contained in the table below.

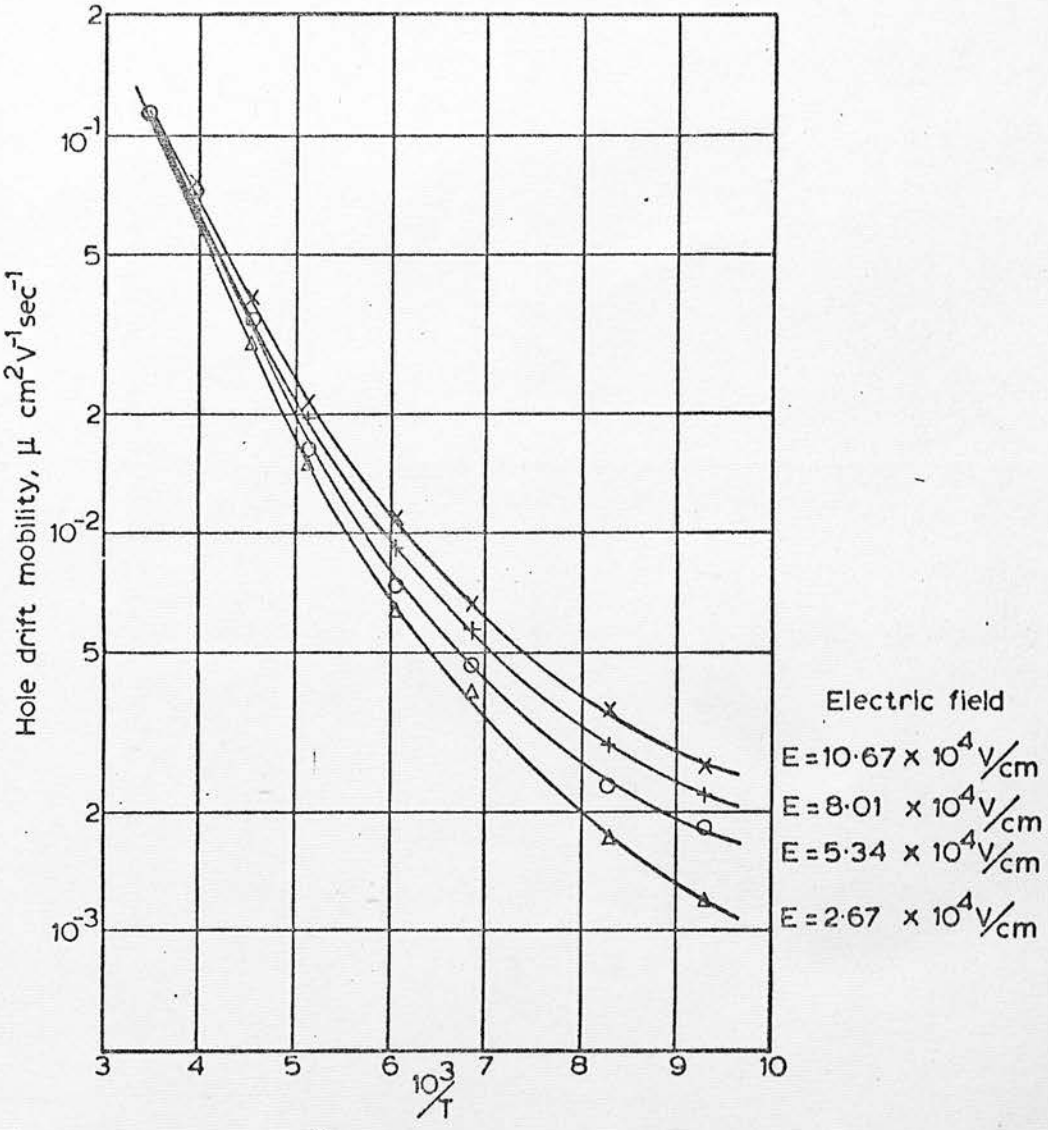

Fig. 30 Dependence of Hole Drift Mobility on Reciprocal Temperature and Applied Field; Selenium

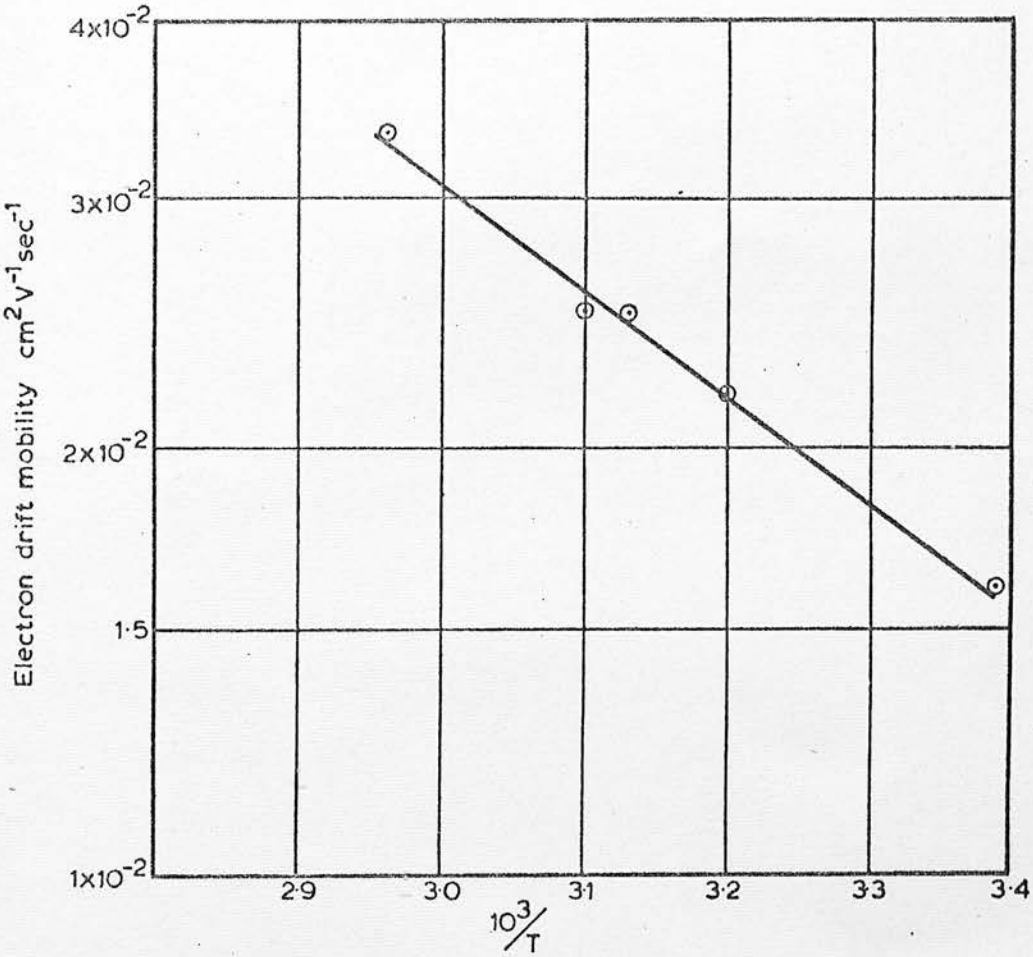

Fig. 31 Dependence of Electron Drift Mobility on Reciprocal Temperature; Selenium

(Field, $E = 9{\cdot}34 \times 10^4$ V/cm)

specimen	electrodes top	bottom	thickness (microns)	field (V/cm)	hole mobility ($cm^2V^{-1}sec^{-1}$)
C	Al	Al	42.5	2.35×10^4	1.40×10^{-1}
F	Al	Au	48.5	2.06×10^4	1.44×10^{-1}
H	Al	Al	36.0	2.78×10^4	1.39×10^{-1}
X	Al	Al	42.5	2.36×10^4	1.65×10^{-1}

The above results give an average room temperature hole drift mobility of 1.47×10^{-1} $cm^2V^{-1}sec^{-1}$. ± 7% r.m.s.

Again early measurements of the temperature dependence of the mobility were confused by the unexpected dependence of mobility upon field. Later, the dependence of the hole mobility on temperature and field was examined for specimen H, when the results shown in figure 32 were obtained.

The electron mobility was found to be much reduced by the addition of 1% Ge, and a meaningful examination was impractical. A room temperature value of between 5 and 10 x 10^{-4} $cm^2V^{-1}sec^{-1}$ was estimated, but deep trapping effects caused a rapid disappearance of the transit pulse.

Upon examination of the effects of larger doping concentrations of germanium, the situation was found to be complex. In specimens containing 3, 5, and 7% Ge, it was impossible to observe any hole transit pulse, even when using a pulsed specimen field. However, the addition of 3% Ge produced an electron transit pulse which was of much greater magnitude than the pulses observed in pure selenium. The decrease in pulse height with time was also much less than was the case for pure selenium, although the pulse shape was found to be modified by the accumulation of space charge with a time constant of about 15 sec. By making transit time measurements in the first

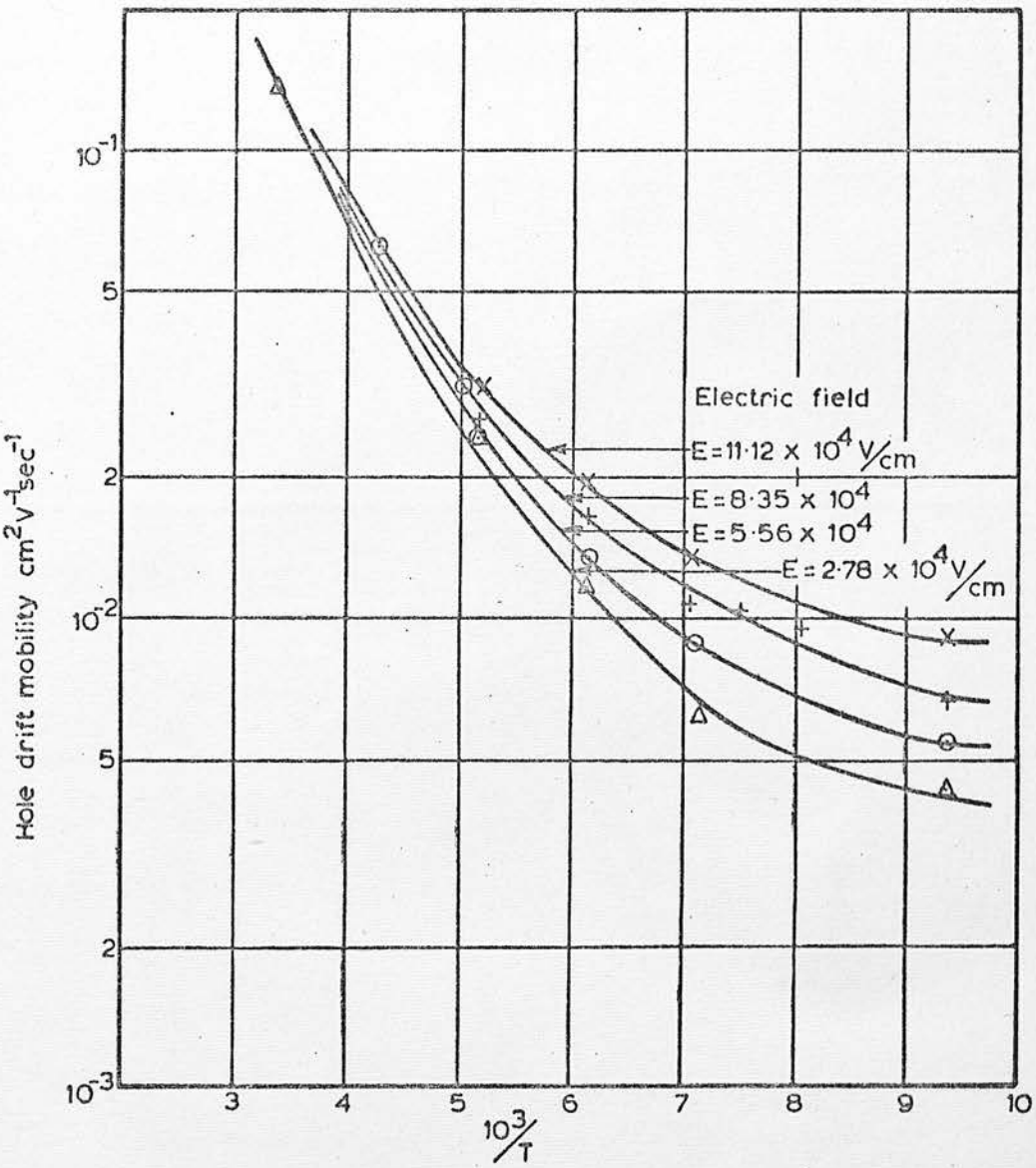

Fig. 32 Dependence of Hole Drift Mobility on Reciprocal Temperature and Applied Field. Selenium + 1% Germanium

five seconds after the field application, such effects were minimised, and an examination of the dependence of electron mobility upon temperature and (to some extent) upon applied field was made. The results of this examination are shown in figure 33.

In specimens containing 5% Ge, it was impossible to observe either hole or electron transit pulses, with applied fields up to 10^5V/cm.

With a germanium concentration of 7%, the situation was somewhat similar to that observed at a 3% concentration, although electron transit pulses were somewhat smaller in the former case than in the latter. At room temperature, an electron drift mobility of between 2 and 3 x 10^{-4} $cm^2V^{-1}sec^{-1}$ was estimated. Decay of observed pulse height due to space charge accumulation was again pronounced.

c) Arsenic Triselenide.

Specimens for this study were prepared from bubbles blown from the melt, as previously described, and were from 1 to 5 microns in thickness. All specimens possessed evaporated aluminium electrodes. Hole drift mobilities were found to be extremely low, and transit traces were of the non-linear form discussed previously. After the examination of a number of specimens in an exploratory manner, the hole drift mobility was found to be strongly field dependent at room temperature and above. At this stage, characterisation of the observed transit trace as being representative of charge transfer rather than trapping was made by the application of the criteria described in section 4.3. Five specimens were subsequently studied, but two of these were inadvertently destroyed prior to thickness measurement. However, since it was possible to extract information

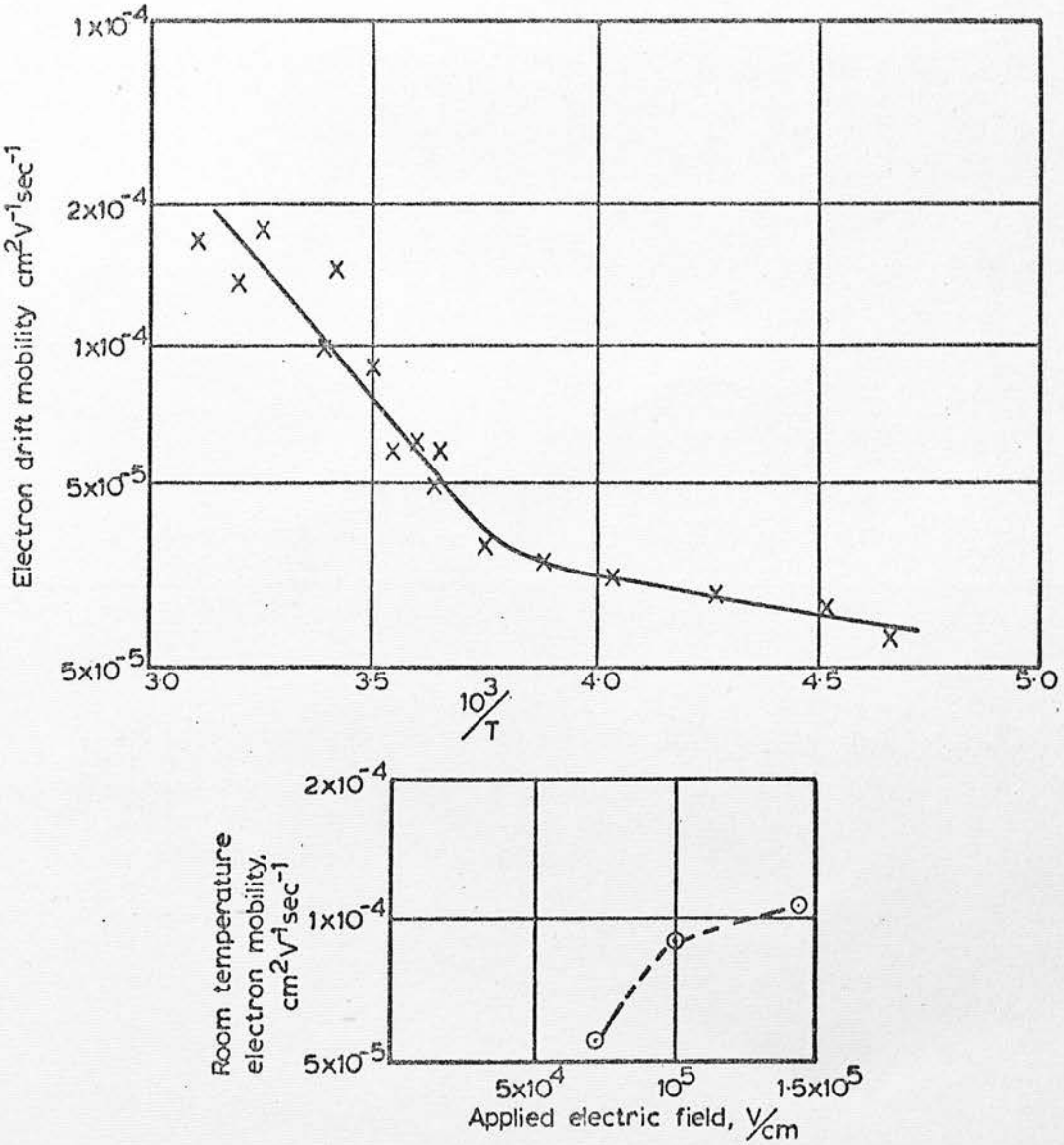

Fig. 33 Dependence of Electron Drift Mobility on Reciprocal Temperature; Se + 3% Ge (Field, $E = 14·3 \times 10^4$ V/cm)

from all five specimens, the measurements made on all of them are included below. The following table shows the specimen thicknesses and the symbols used to represent them in the figures.

specimen	thickness (microns)	symbol
1	1.275	⊙
2	2.90	x
3	unknown	+
4	unknown	*
5	0.95	Δ

Figure 34 shows the room temperature dependence of drift mobility upon applied electric field. An investigation of the variation of conductivity with applied field was also performed for specimen 2. Initial examination revealed a non-reversible current/voltage dependence, presumably due to electrode forming effects. After voltage cycling the specimen several times, the relationship became reproducible, and the current/voltage variation was then accurately measured, and converted into a dependence of conductivity upon applied field. The results are shown in figure 35. The dependence of hole drift mobility upon temperature at various values of applied field was examined in specimen 1. A subsidiary examination of the temperature dependence of the hole mobility at a single value of applied field was performed for specimen 5. The results are shown in figure 36. Figures 34 and 36 also include the exploratory results of Kolomiets and Lebedev[35], for comparison purposes. The dependence of conductivity upon temperature at constant applied field was studied in specimen 3. Since it was not possible to measure the thickness of this sample, conductivity and field values could not be computed,

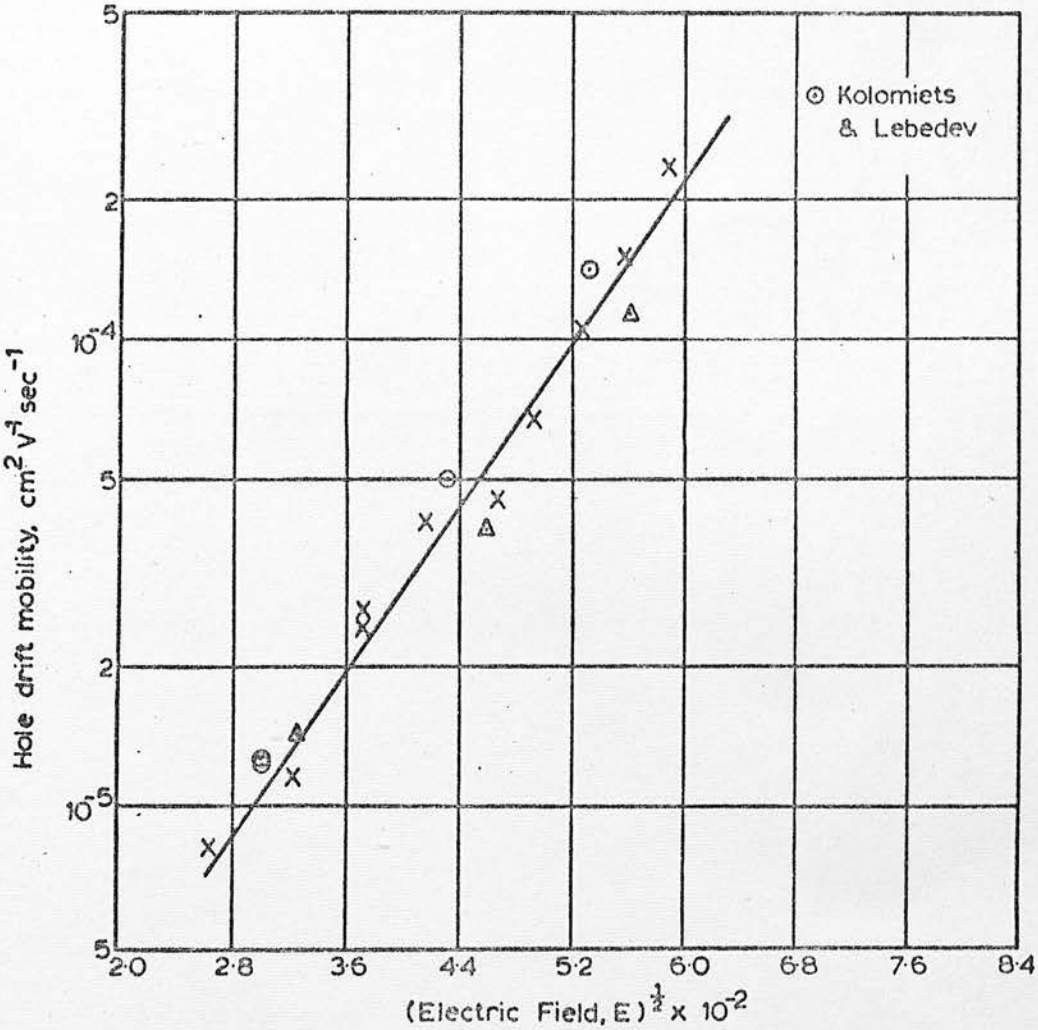

Fig. 34 Dependence of Hole Drift Mobility on Electric Field at Room Temperature; Arsenic Selenide

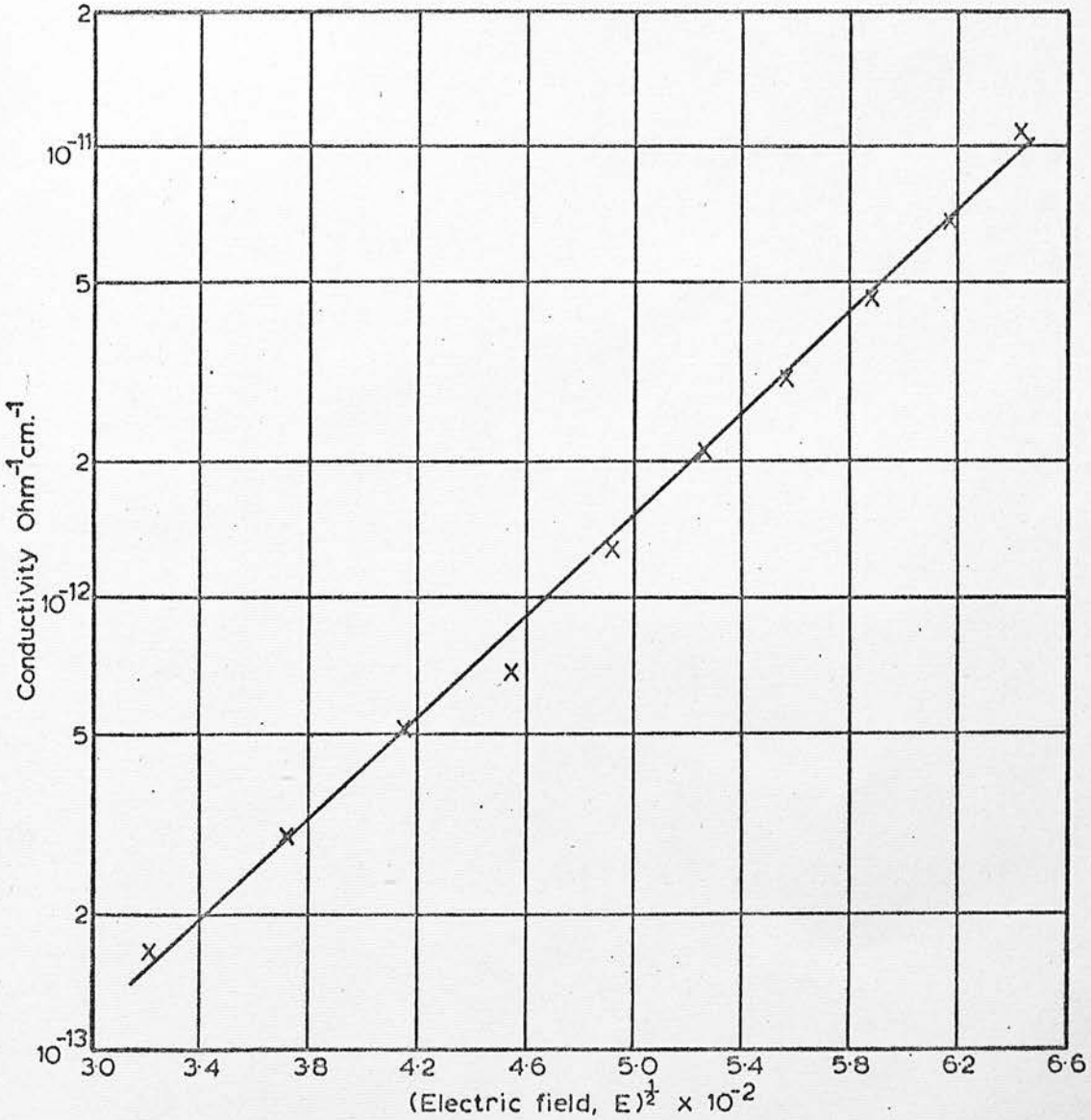

Fig. 35 Dependence of Conductivity on Electric Field at Room Temperature; Arsenic Selenide

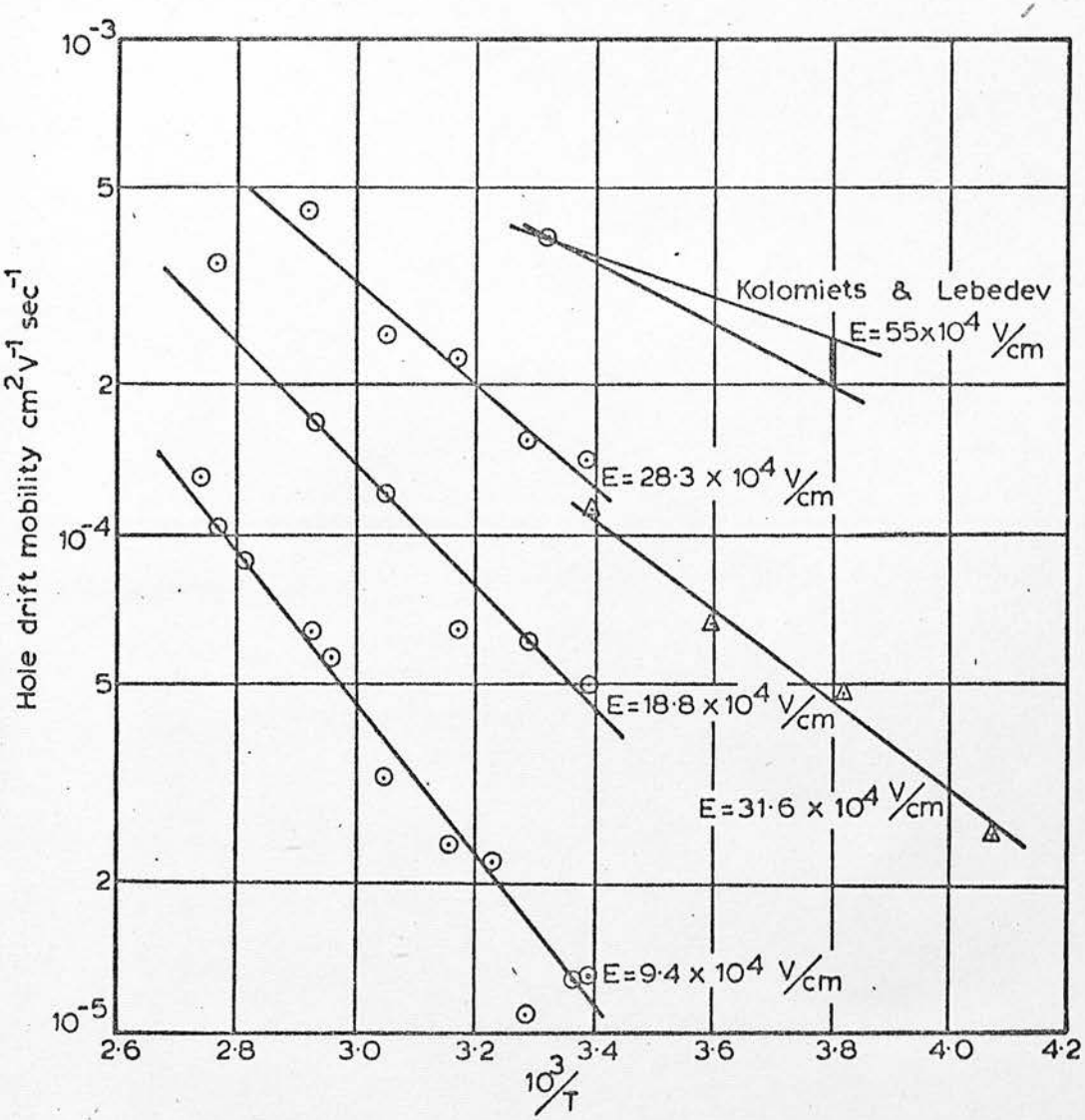

Fig. 36 Dependence of Hole Drift Mobility on Reciprocal Temperature at Various Values of Applied Field; Arsenic Selenide

but figure 37 shows the specimen current as a function of temperature. Figure 38 shows an examination of pulse height as a function of transit time in specimen 4. This is not a true 'Hecht curve' since both temperature and applied field changes were used to vary the transit time, but a strong similarity is to be expected. This curve was used in the identification of the observed trace as representing charge transit.

It will be noted that the examination of mobility as a function of temperature, as shown in figure 36, was not extended to temperatures above 100°C. The limit was set by the onset of appreciable diffusion of aluminium from the electrodes into the bulk. This effect was detected by time dependent and irreversible changes in the measured mobility, as indicated in figure 39. The very low magnitude of measured mobility set a lower practical limit on the examination.

An attempted study of electron transport in the above films, and in others possessing gold electrodes, indicated that mobility measurements were impractical, even at relatively high values of temperature and field. Although it was possible to observe a pulse due to electron motion, the pulse height was extremely small, and was almost certainly limited by strong trapping effects. From the observed traces, it was inferred that the electron drift mobility was less than 10^{-6} $cm^2V^{-1}sec^{-1}$ at 100°C, and with applied fields of up to 3×10^5 V/cm.

d) Arsenide Trisulphide, and (e) Vanadium Pentoxide/Phosphorus Pentoxide.

Specimens, approximately one micron in thickness, were

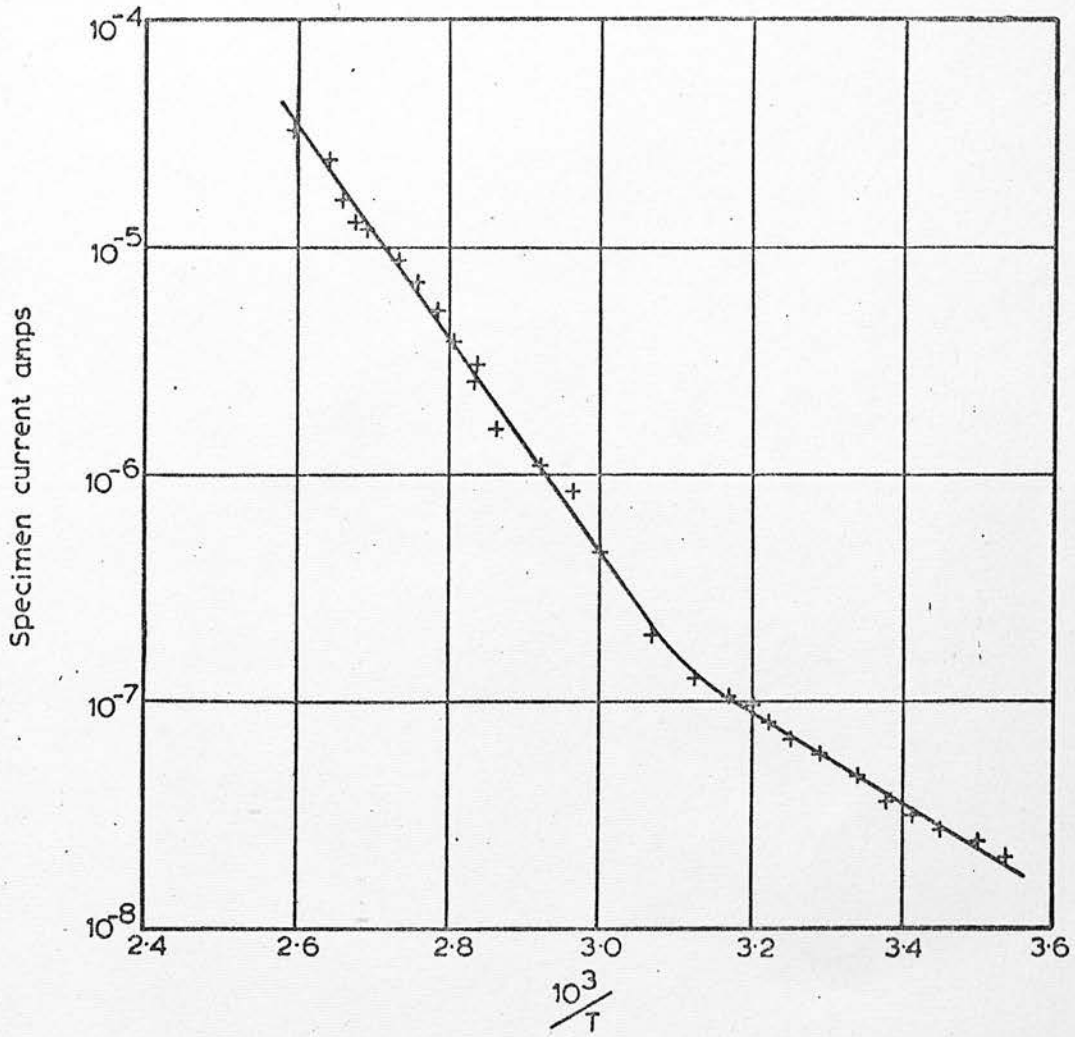

Fig. 37 Dependence of Specimen Current on Reciprocal Temperature; Arsenic Selenide

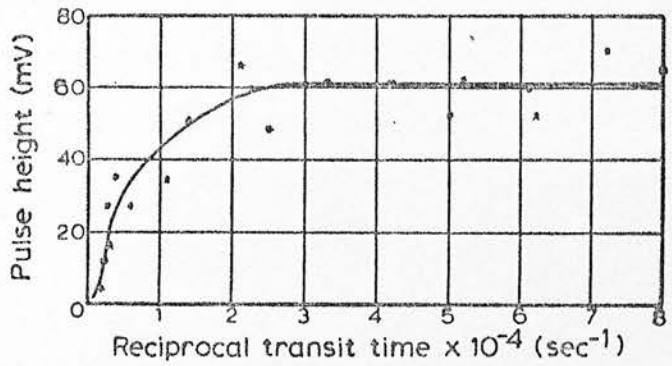

Fig. 38 Dependence of Pulse Height upon Reciprocal Transit Time; Arsenic Selenide

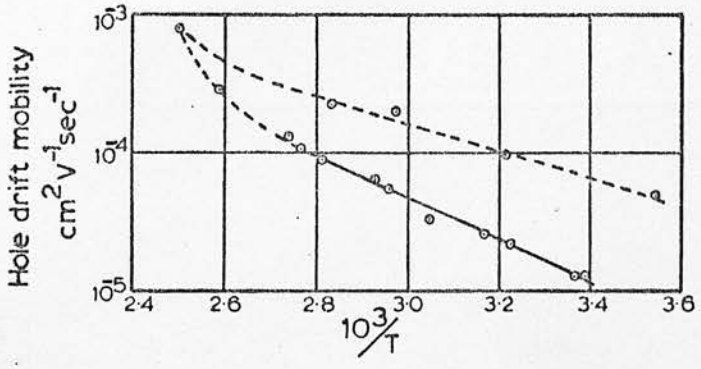

Fig. 39 Mobility/Temperature Curve illustrating Irreversible Section (Dotted). Arsenic Selenide

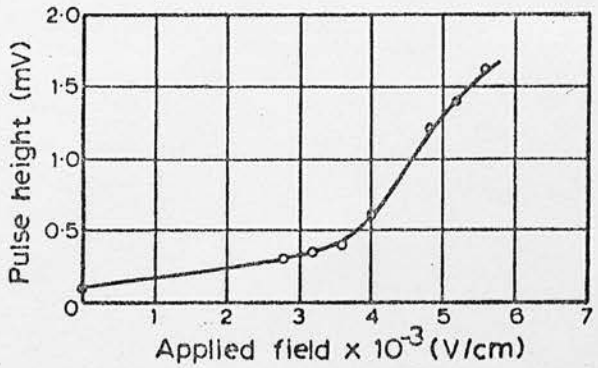

Fig. 40 Dependence of Pulse Height upon Applied Field; As_2Se_2Te

prepared of arsenic sulphide and of 90% V_2O_5/10% P_2O_5. Gold and aluminium were employed as electrode materials. It was found to be impossible to observe hole or electron transit traces in either material, indicating very low values of drift mobility in each case. In view of the positive results being obtained for the other materials previously described, the examination was concentrated upon the selenium and arsenic selenide systems, and no detailed study was performed for arsenic sulphide or V_2O_5/P_2O_5.

f) As_2Se_2Te

An attempt to study this material was made in view of the fact that the Hall mobility had previously been measured[22]. A specimen of 76 microns thickness was prepared by the compression technique, and aluminium electrodes were evaporated. The relatively conducting nature of the material made the application of high fields at room temperature impractical. An examination in fields of up to 2.5×10^3 V/cm produced hole drift pulses with a response time which was independent of the magnitude of the applied field. Thus, it was concluded that a trapping time rather than a transit time was being measured. A value of approximately 20 μsec was indicated for the hole trapping time at 20°C. The situation at -20°C was very similar, with a somewhat longer trapping time being indicated. From the results obtained in the -20 to -30°C temperature range, it was possible to infer that the hole mobility was less than 10^{-2} $cm^2V^{-1}sec^{-1}$. In an attempt to make a closer examination, a thinner specimen, 25microns in thickness was prepared. However, trapping effects again prevented mobility measurements. A room temperature study of the observed pulse height as a function of applied field was made, with the

results shown in figure 40.

5.4 Discussion and Analysis

a) Pure Selenium

The measured value of the room temperature hole mobility, 1.33×10^{-1} $cm^2V^{-1}sec^{-1}$ is in good agreement with the results previously published for evaporated films, as documented in Chapter Four. The measured room temperature electron mobility, 3×10^{-2} $cm^2V^{-1}sec^{-1}$, is marginally lower than the published results. It is not possible to decide whether the lowering is due to a low concentration of impurities, or to a structural difference between the present vitreous and the previous evaporated films.

A striking departure from previously reported characteristics is exhibited by the measurements of the temperature dependence of the hole mobility, as shown in figure 30. In the temperature range 200 to 300°K, which has previously been studied, the present results indicate a mobility activation energy of between 0.09 and 0.1 eV, depending on the value of the applied electric field. In equivalent measurements on evaporated specimens, activation energies in the range 0.13 to 0.21 eV have been reported, and no major field effects have been indicated. Measurements at temperatures of less than 200°K do not appear to have been previously made, but in the present study, the activation energy is found to decrease markedly at low temperatures, whilst the applied field exerts an increasing influence on the mobility. Examination of figure 30 shows that it is, in fact, impossible to define any unique value(s) of activation energy. The analysis of the results has been undertaken in two sections. Firstly, the effect of applied electric field on the mobility has been examined,

and attempts have been made to calculate the 'zero field' mobility in the absence of electric field perturbations. Secondly, the dependence of this 'zero field' mobility on temperature has been examined in the light of the transport properties which have been predicted for low mobility materials.

Field Effects.

By examination of the data in figure 30, it has been found that the mobility may be represented as

$$\mu_d = A(T) \exp \{B(T).E^n\} \qquad (5.4.1)$$

where A(T) and B(T) are independent of the magnitude of the applied electric field. However, it has not been possible to positively determine the value of n, since graphs showing μ_d (logarithmic scale) as a function of (say) $E^{\frac{1}{2}}$ and E both show approximately linear relationships, as shown in figures 41a and 41b respectively. Nor is there any conclusive agreement with particular theoretical predictions. For instance, the data in figure 41a could be considered as a manifestation of the Poole-Frenkel effect, but calculations of the field dependence constant, β, yield values which are much smaller than would be expected. Figure 42 shows the magnitude and temperature dependence of β, as compared to the value of 2.83×10^{-4} $eV/V^{\frac{1}{2}}cm^{-\frac{1}{2}}$ which is predicted by the basic theory of the effect, taking K = 7.2 as indicated by Kolomiets[36]. This figure for β is not expected to vary with temperature. As has been mentioned previously, a reduction of the above theoretical value results from modifications to the simple (one dimensional) theory, but this reduction is not of sufficient magnitude to allow the data in figure 42 to be considered in terms of the Poole-Frenkel model. A dependence of the form shown

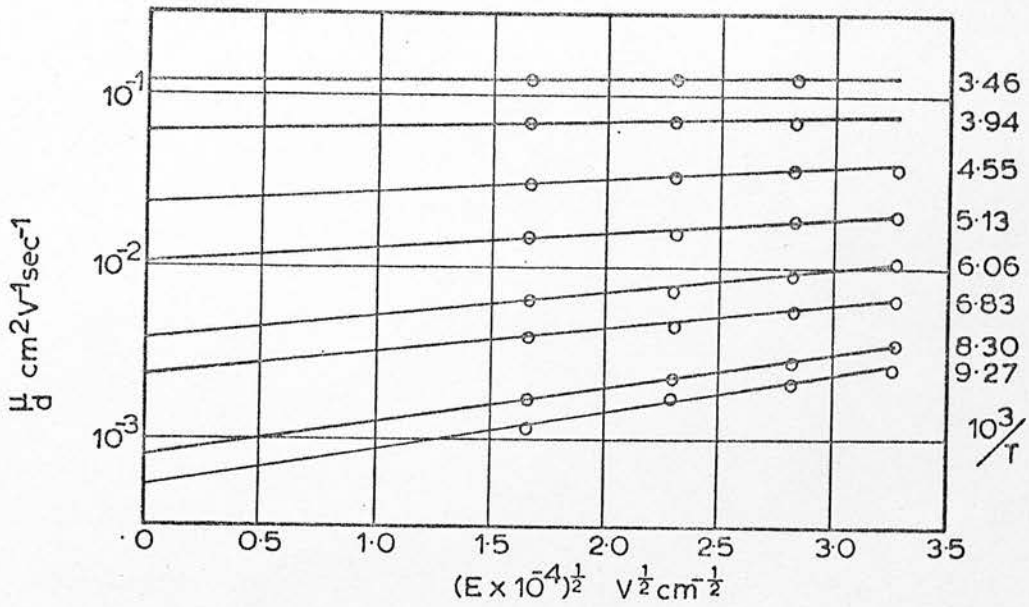

(a) μ_d as a function of $E^{\frac{1}{2}}$

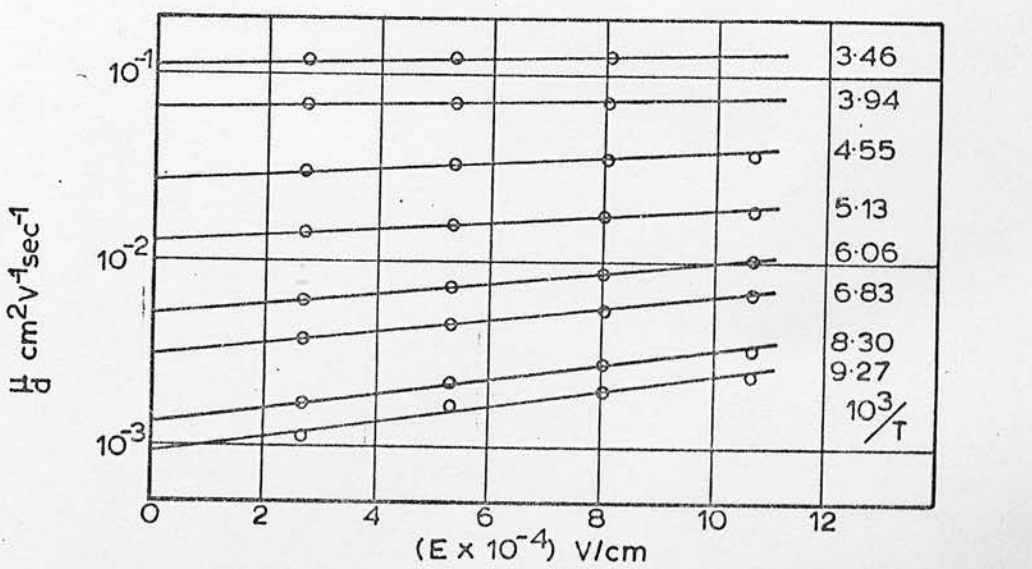

(b) μ_d as a function of E

Fig. 41 Dependence of Hole Drift Mobility upon Applied Field at Various Temperatures; Selenium

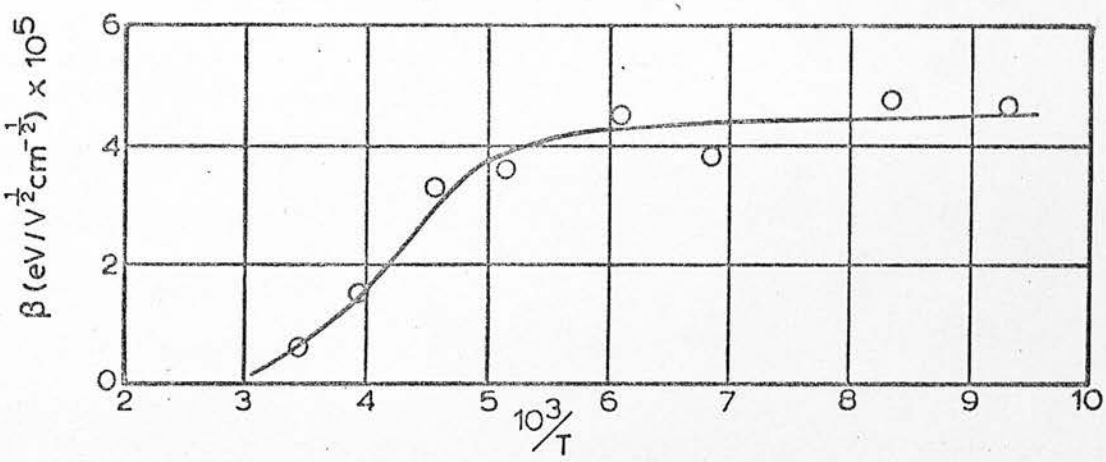

Fig. 42 Dependence of Field Proportionality Constant, β, upon Reciprocal Temperature; Selenium

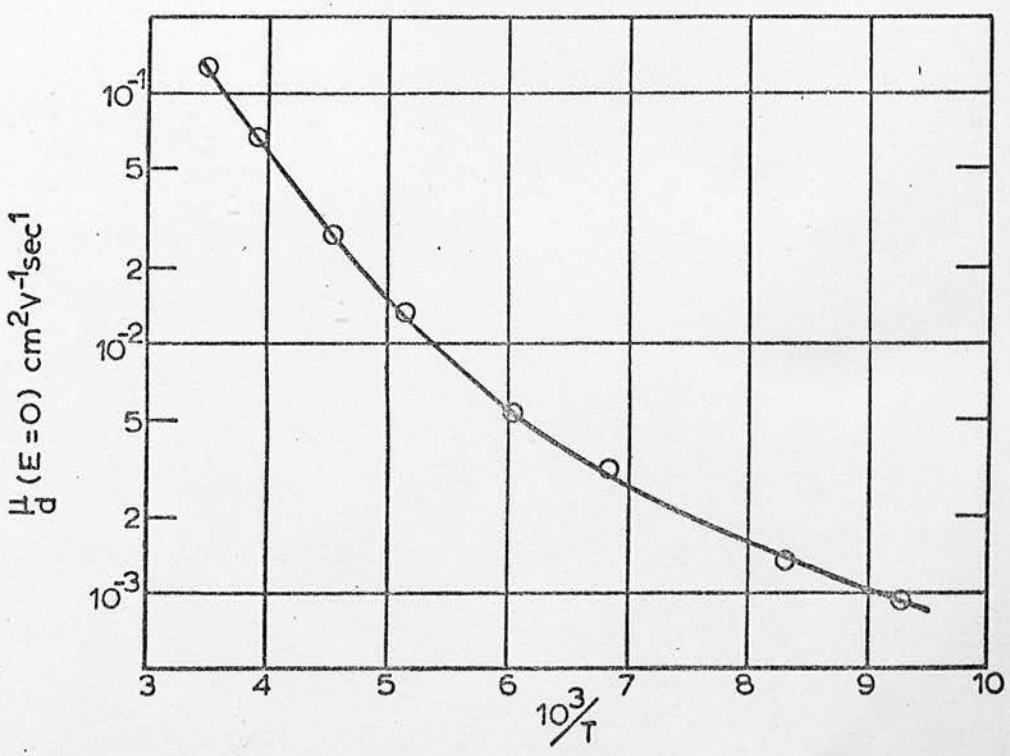

Fig. 43 Dependence of 'Zero Field' Hole Drift Mobility on Reciprocal Temperature; Selenium

in figure 41b could be associated with the predictions of hopping transport theory. As indicated in Chapter Four, a hopping probability of the form

$$P = 2C \exp(-W/kT) \sinh(eaE/kT) \qquad (5.4.2)$$

has been calculated by Austin and Mott[52] and others. Here, C is a constant proportional to the 'attempt to escape' frequency of the trapped carrier (i.e., the phonon frequency ν_p in the present context). The hopping mobility is proportional to the hopping probability per unit applied field, and to the hopping distance, a, so that

$$\mu_{hop} \alpha \frac{2Ca}{E} \exp(-W/kT) \sinh(eaE/kT) \qquad (5.4.3)$$

In the limit of low applied fields ($eaE<kT$), the hyperbolic term may be replaced by its argument, and the expression reduces to that given in equation 2.2.3. At high fields, the hyperbolic term becomes approximately exponential, and

$$\mu_{hop} \alpha \frac{2Ca}{E} \exp(-W/kT) \exp(eaE/kT) \qquad (5.4.4)$$

For sufficiently high field values, the exponential field term will dominate the pre-exponential term, and the expression is of the form shown in equation 5.4.1, with n = 1. Once again, however, the agreement between the theoretical and experimental results is not conclusive. Substitution of the results obtained at $10^3/T = 9.27$ into equation 5.4.4 indicates a hopping distance of 25 Å, whilst a lower figure would be expected. It will, in fact, be shown that the pre-exponential term in equation 5.4.4 indicates a hopping distance of between 1 and 5 Å, which is considered to be a more reasonable estimate. Thus, it appears that the field values used in the experiment were at least a factor of 5 lower than the values which would be expected to produce the observed mobility changes.

In spite of these reservations, it has been necessary to assume a dependence (i.e. a value of n) in order to allow an analysis to be made of the effect of temperature on the 'zero field' mobility. In the following analysis, the cases n = 1 and n = $\frac{1}{2}$ have both been considered, but it is felt that the former is more likely to be valid, since the low temperature values of the 'zero field' mobility will be explained in terms of hopping transport, so that the Poole-Frenkel model would not be expected to be applicable. In general, it is felt that the objections to the validity of the Poole-Frenkel mechanism are more fundamental than those indicated for the 'hopping' field dependence model. Even so, as will be shown, the conclusions of the following analysis are not radically changed if the 'zero field' mobilities estimated from figure 41b are replaced by those estimated from figure 41a.

Temperature Dependence of the Zero Field Mobility.

From the data in figure 41b, the temperature dependence of the 'zero field' mobility is found to be as shown in figure 43. This curve has been interpreted in terms of a combination of trap-controlled band transport and of hopping transport. The curve has also been compared with the predictions of the Mott (equation 2.2.6) and Killias (equation 2.2.7) theories of hopping transport.

The possibility of trap controlled band transport and hopping transport, operating 'in parallel', has been indicated in the case of impurity conduction by Mott and Twose[1]. From general considerations, it would be expected that trap controlled band transport, characterised by relatively high values of pre-exponential mobility ($\mu_o \geq 100$ $cm^2V^{-1}sec^{-1}$) and of activation energy, would predominate at

high temperatures. Hopping motion, with low values of mobility ($\mu_{hop} < 0.1$ cm^{2}V^{-1}sec^{-1}) and of activation energy, would be observed at lower temperatures. The total drift mobility (of holes) should be of the form

$$\mu_d = \frac{N_v}{N_t}\mu_o \exp(-\varepsilon/kT) + \frac{e\,\nu_p\,a^2}{kT}\exp(-W/kT) \qquad (5.4.5)$$

It should be mentioned that, in the application of this form of analysis to crystalline germanium (see [1]), it has been found to be necessary to include a third exponential term, the physical significance of which is not clear. The inclusion of such a term in the present analysis is not considered to be justified.

The data in figure 43 may be fitted to equation 5.4.5, giving the following values of the constants.

$$\frac{N_v}{N_t}\mu_o = 25.3 \text{ cm}^2\text{V}^{-1}\text{sec}^{-1}$$

$$\varepsilon = 0.135 \text{ eV}$$

$$W = 0.050 \text{ eV}$$

$$\frac{e\,\nu_p a^2}{k} = 20 \text{ cm}^2\text{V}^{-1}\text{sec}^{-1}\,{}^{o}\text{K}$$

For ν_p between 10^{12} and 10^{13}sec^{-1}, the hopping distance, a, is calculated as between 1.3 and 4.2 Å. The calculation of the microscopic mobility, μ_o, is less straightforward, since values of N_v and N_t must be assumed. Spear[28] has taken

$$N_v = 2.5 \times 10^{19} (T/300)^{3/2}(m^*/m)^{3/2} \text{ cm}^{-3}$$

$$N_t \simeq 10^{20} \text{ cm}^{-3} \text{ (estimated from x-ray data)}$$

$$m^* = 2.5\, m \quad \text{(from Faraday effect data)}$$

and estimates $\mu_o \simeq 60$ cm^{2}V^{-1} sec^{-1} for amorphous selenium films.

Applying his data to the present results, and taking T = 300°K, the value $\mu_o \simeq 25\ cm^2V^{-1}sec^{-1}$ is obtained.

Alternatively, the pre-exponential constant in the band transport term may be calculated from consideration of the 'tail of localised states' model due to Mott[4]. The derivation given below has been suggested by Owen[85].

(a) The density of states is assumed to be a linear function of energy in both the localised and non-localised regions of energy, as shown in figure 44.

Thus,
$$\frac{N(\varepsilon)}{N_c} = \frac{(\varepsilon - \varepsilon_o)}{(\varepsilon_c - \varepsilon_o)} = \frac{(\varepsilon - \varepsilon_o)}{\Delta\varepsilon} \qquad (5.4.6)$$

(b) The number of occupied states is given by
$$n = \int N(\varepsilon)\, f(\varepsilon)\, d\varepsilon \qquad (5.4.7)$$

and the probability of occupation, $f(\varepsilon)$, is (by the Boltzmann approximation)
$$f(\varepsilon) = \exp\{-(\varepsilon - \varepsilon_f)/kT\} \qquad (5.4.8)$$

Substituting equations 5.4.6 and 5.4.8 in equation 5.4.7, the total number of localised (trapping) states is

$$n_t = \int_{\varepsilon_o}^{\varepsilon_c} \frac{\varepsilon - \varepsilon_o}{\Delta\varepsilon} N_c \exp\{-(\varepsilon - \varepsilon_f)/kT\}\, d\varepsilon$$

$$= \frac{N_c kT}{\Delta\varepsilon} \exp\{-(\varepsilon_c - \varepsilon_f)/kT\} \left\{kT\{\exp(\Delta\varepsilon/kT) - 1\} - \Delta\varepsilon\right\}$$

Similarly, the total number of unlocalised states is

$$n_o = \int_{\varepsilon_c}^{\infty} \frac{(\varepsilon - \varepsilon_o)}{\Delta\varepsilon} N_c \exp\{-(\varepsilon - \varepsilon_f)/kT\}\, d\varepsilon$$

$$= \frac{N_c kT}{\Delta\varepsilon} \exp\{-(\varepsilon_c - \varepsilon_f)/kT\}\ (kT + \Delta\varepsilon)$$

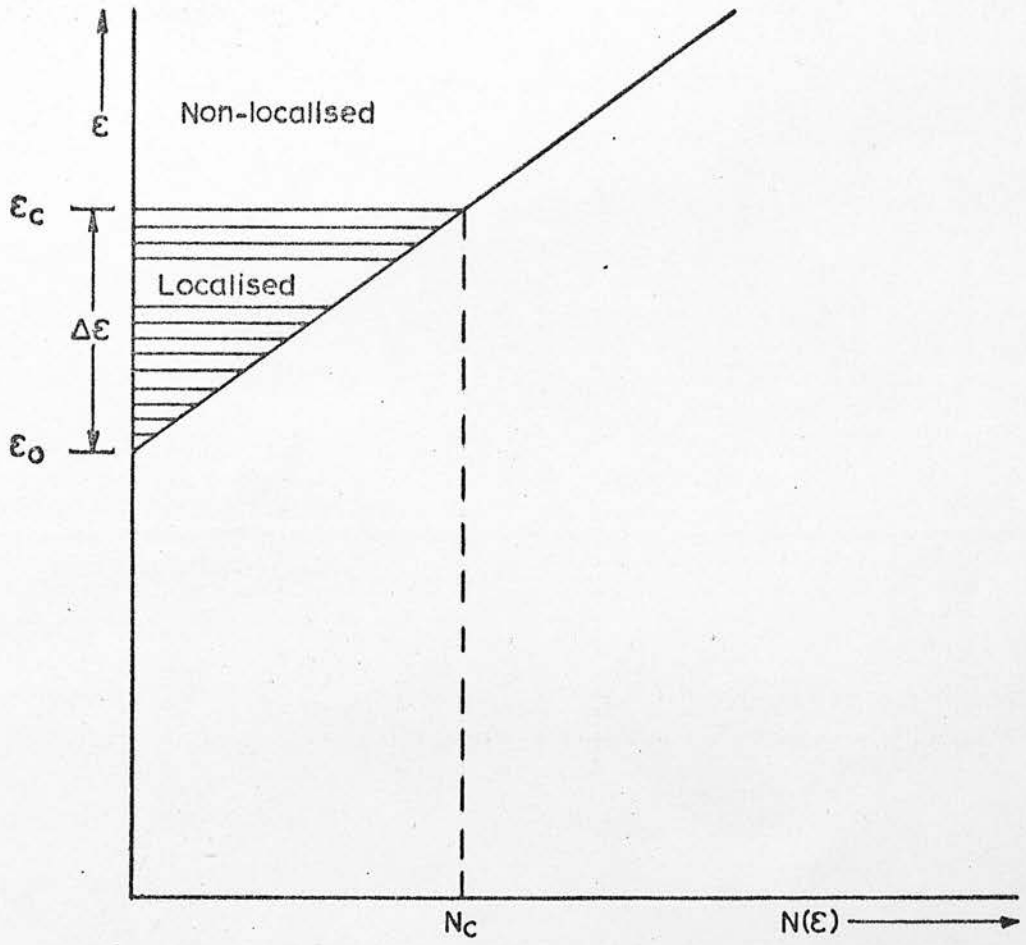

Fig. 44 Density of States Distribution, as used in Estimating Pre-Exponential Mobility for Trap-Controlled Band Transport

(c) The drift mobility is given by

$$\mu_d = \mu_o \frac{n_o}{n_o + n_t} \approx \mu_o \frac{n_o}{n_t} \qquad (5.4.9)$$

for $\mu_o \ll \mu_o$.

Thus, using the above expressions, and taking $\Delta\varepsilon \gg kT$,

$$\mu_d = \mu_o (kT + \Delta\varepsilon) / \left\{ kT\{\exp(\Delta\varepsilon/kT) - 1\} - \Delta\varepsilon \right\}$$

$$\approx \mu_o \frac{\Delta\varepsilon}{kT} \exp(-\Delta\varepsilon/kT) \qquad (5.4.10)$$

Applying this analysis to the present results, with $\Delta\varepsilon$ = 0.135 eV and kT = 0.025 eV, the value $\mu_o \approx 5$ $cm^2V^{-1}sec^{-1}$ is obtained.* In both forms of the analysis, the values obtained for the microscopic mobility are seen to be low, since a mobility in excess of 100 $cm^2V^{-1}sec^{-1}$ is to be expected for conventional band transport. It is likely, therefore, that the high temperature mobility should more correctly be regarded as involving diffusive motion within the band states. In this case, the pre-exponential term $\mu_o N_v/N_t$ in equation 5.4.5 should be replaced by $e\nu_{el}a^2/kT$. Taking ν_{el} to be 10^{15} sec^{-1}, and T = 300°K, then a = 2.5 Å, a figure which is consistent with the value previously calculated for the hopping distance (1.3 to 4.2 Å).

If the data in figure 41a, rather than that in figure 41b, is used to estimate the 'zero field' mobility, the following values of the constants in equation 5.4.5 are obtained.

$$\frac{N_v}{N_t}\mu_o = 73 \text{ cm}^2\text{V}^{-1}\text{sec}^{-1}$$

$$\varepsilon = 0.159 \text{ eV}$$

$$W = 0.0655 \text{ eV}$$

$$\frac{e\nu_p a^2}{k} = 54 \text{ cm}^2\text{V}^{-1}\text{sec}^{-1}\,{}^{o}\text{K}$$

* This value of μ_o is calculated from eqn. 5.4.10. using a value of $\Delta\varepsilon$ derived from eqn. 5.4.5. Strictly, this is incorrect in view of the pre-exponential temperature dependence of eqn 5.4.10. A direct application of eqn. 5.4.10. to the experimental data leads to a slightly higher value of $\Delta\varepsilon$, and approximately doubles the magnitude of μ_o. This, however, does not affect the conclusion that μ_o is anomalously small.

The hopping distance, a, is calculated as between 2.2 and 6.8 Å. The microscopic mobility is approximately 70 $cm^2V^{-1}sec^{-1}$ (Spear's data) or 10 $cm^2V^{-1}sec^{-1}$ ('tail of states' model).* It is again considered that an interpretation in terms of diffusive motion is more valid, and this leads to a value of a = 4.25 Å, which is consistent with the value obtained for the hopping distance.

To summarise the results of the analysis, the experimental readings have been considered in terms of a combination of band and hopping transport, with the appearance of a field dependence of the mobility at low temperatures. The analysis has given values of the microscopic mobility which are considered to be too low for conventional band motion, and the situation at high temperatures has been re-analysed in terms of diffusive motion within the band states. The diffusive mean free path obtained in this way is in good agreement with the value obtained for the hopping distance, and is of the correct magnitude, being of the order of the interatomic spacing. The high temperature activation energy is in good agreement with the values reported for evaporated specimens, and the hopping activation energy is of the expected order. The field dependence of the mobility, as observed at low temperatures, has been considered in terms of two models, but neither provides a completely satisfactory explanation of the results. A field perturbation of the hopping activation energy is considered to be most consistent with the situation.

As previously mentioned, the results have also been compared with the predictions of non-linear temperature dependence for hopping conduction, as advanced by Mott and Killias. Mott's analysis leads to a linear relationship between log μ (or log σ) and $T^{\frac{1}{4}}$, as indicated

* See footnote to p. 98.

in equation 2.2.6. However, an attempt to interpret the present 'zero field' results in this form leads to a distinctly non-linear dependence, indicating the model to be inappropriate. It is possible to fit the Killias Formula,

$$\log_e \mu_d = A - \frac{B(1 - \theta_R T^{-1})}{kT} \qquad (5.4.11)$$

to the results, giving the following constants;

constant	value assuming $\log \mu \propto E$	value assuming $\log \mu \propto E^{\frac{1}{2}}$
A ($cm^2 V^{-1} sec^{-1}$)	50.3	96
B (eV)	0.181	0.201
θ_R (^oK)	47.7	47.7

In spite of the fact that a relatively good 'fit' to the experimental results is obtained using these values, the Killias equation is of doubtful applicability. The equation is specifically concerned with small polaron hopping, and it is by no means established that small polaron formation is to be expected in an essentially non-polar material such as selenium. The application by Killias of Schnakenberg's equation for the Hall mobility[86] is therefore probably incorrect in terms of the present analysis. Moreover, the values obtained for the pre-exponential mobility, A, are not considered to be consistent with hopping transport. Finally, the Killias formula, as fitted to the present results, indicates that the mobility would be expected to rise with decreasing temperature for $10^3/T > 10$, and this is not considered to be physically likely.

For comparison purposes, figure 45 shows the curves obtained by fitting equation 5.4.5 and equation 5.4.11 to the data in figure 43.

The examination of electron transport in pure selenium was

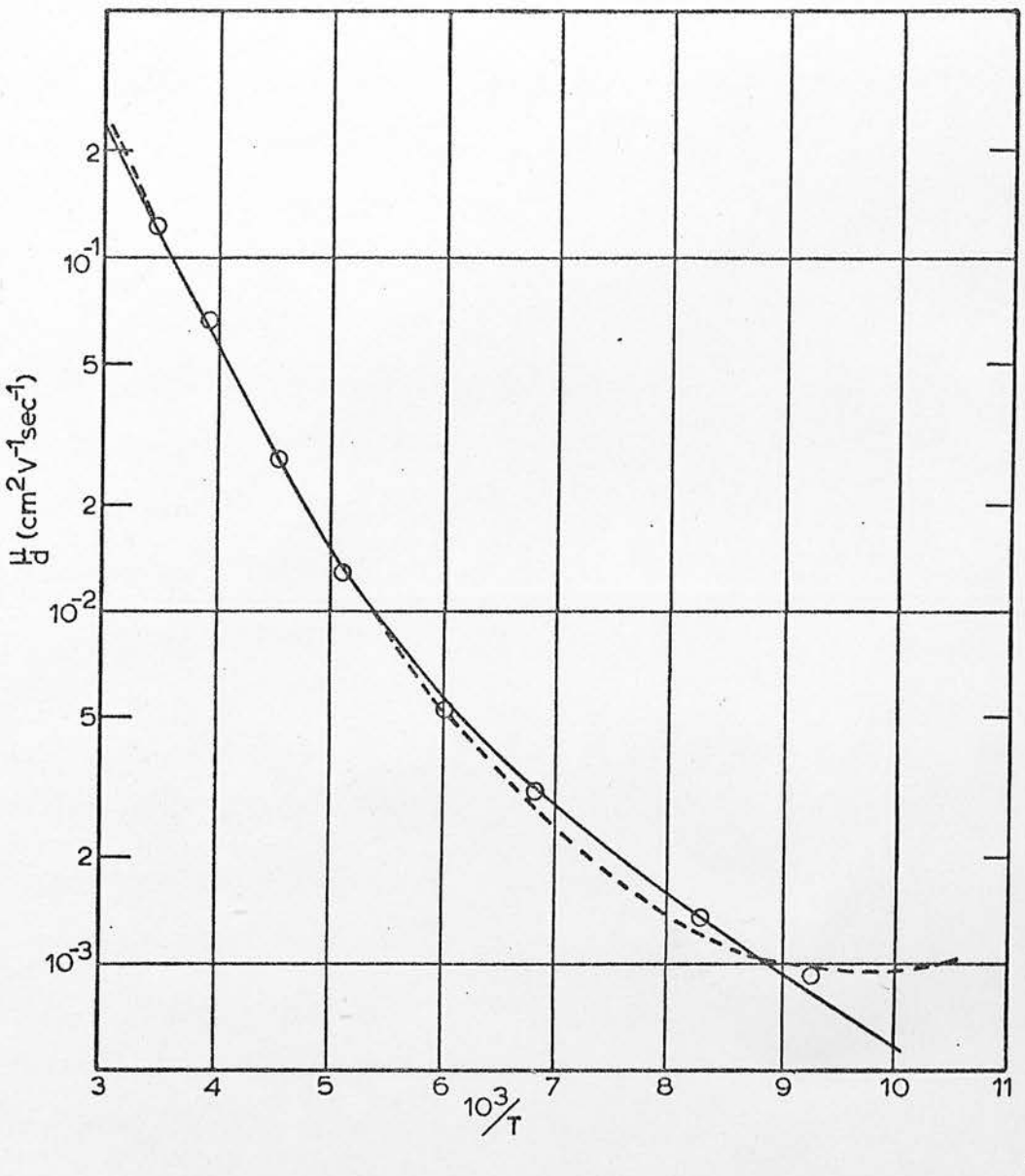

—— $\mu = 25.3\exp(-0.135/kT) + \frac{20}{T}\exp(-0{\cdot}05/kT)$

– – – $\mu = 50.3\exp\left[-0.181(1-47.7T^{-1})/kT\right]$

o Experimental results

Fig. 45 Fitted Theoretical Predictions of the Variation of Hole Drift Mobility with Temperature; Selenium

of a superficial nature, since the specimens prepared for studying the hole properties were too thick to allow a comprehensive study of the (relatively low) electron mobility. The results shown in figure 31 indicate an activation energy of 0.15 eV, at an applied field of 9.34×10^4 V/cm. This figure is low in comparison with the values reported for amorphous films, which range from 0.25 to 0.33 eV. The high value of the transit time prevented the use of lower values of applied field, so that it was not possible to examine the field dependence of the mobility, or of its activation energy. Similarly, it was not possible to extend the measurements to low temperatures, so that the possibility of a temperature dependent activation energy could not be examined.

b) Germanium-Doped Selenium

The similarity between the measured values of the room temperature hole mobility for pure Se and Se + 1% Ge indicates that the hole transport process is not significantly modified by germanium addition at this level of concentration. The inability to observe hole transit pulses at higher germanium concentrations has been reported in amorphous films, as well as in the present study. The association of this effect with a marked increase in the concentration of deep hole trapping centres (Schottmiller et al[30]) would appear to be consistent with the present observations. The progressive reduction of the room temperature electron mobility with increasing germanium concentration has also been observed in studies of amorphous films[30]. From the varying difficulty of observation of the electron transit pulse, it would appear that a complex relationship exists between the addition of germanium and the presence of deep electron traps.

One of the purposes of examining the effect of germanium addition was to further investigate the anomalous results described by Frank[87], who found that a number of specimens of the composition Se + 5% Ge exhibited a relatively high conductivity. In the present study, a number of specimens of this composition were examined, without any indications of such an anomaly. It would appear that the 5% composition is characterised by particularly high concentrations of electron and hole traps, since both hole and electron transit pulses could not be observed. It would thus be expected that, in examinations of the d.c. conductivity, strong space charge effects would occur, tending to increase the measured value of specimen resistance. It is therefore not possible to advance any convincing explanation of Frank's results on the basis of the present measurements. The only suggestion which can be offered is that the specimens in question might have been in the 'on' switching state. In Chapter Eight of this report, the observation of switching effects in arsenic triselenide films will be described, and it is worth mentioning here that several of these films were found to be in the 'on' state prior to the application of any large voltage. It is thus possible to postulate that Frank's specimens were similarly switched. Switching effects were not observed in pure or doped selenium films in the present examination, possibly because the applied fields were not of sufficient magnitude, so that no quantitative data can be applied to the suggestion. It is, in fact, somewhat puzzling that, if such effects occur, they should apparently be confined to the 5% composition, unless the high trap density is of assistance to the switching process.

The measured temperature and electric field dependence of the hole mobility in a Se + 1% Ge specimen has been shown in figure 32.

This data is similar to that obtained in the examination of pure selenium, although the reductions of activation energy at low temperature are even more pronounced. The analysis of figure 32 will proceed on similar lines to that given to the pure material, and the conclusions reached will be seen to be similar. Thus, to some extent, the following discussion will be limited to comments on the differences between, and the similarities of, the properties of the doped and pure material. Figures 46a and 46b show the dependence of the hole mobility on applied field ($E^{\frac{1}{2}}$ and E respectively) at various temperatures, and figure 47 shows the temperature variation of the field dependence constant, β, as calculated from figure 46a by assuming the occurrence of the Poole-Frenkel effect. As before, it is felt that Poole-Frenkel analysis is invalid, and that an interpretation in terms of figure 46b is more likely to be correct, although the hopping distance is again considered to be too high if the results are interpreted in terms of equation 5.4.4. Using the 'zero field' mobilities extrapolated from figure 46b, plus a number of mobility measurements taken at high temperatures where the field dependence was a very small effect, the dependence of the 'zero field' mobility on temperature is as shown in figure 48. The data has again been fitted to equation 5.4.5, giving the values of the constants as

$$\frac{N_v}{N_t}\mu_o = 11 \text{ cm}^2\text{V}^{-1}\text{sec}^{-1}$$

$$\varepsilon = 0.111 \text{ eV}$$

$$W = 0.0305 \text{ eV}$$

$$\frac{e\nu_p a^2}{k} = 7.2 \text{ cm}^2\text{V}^{-1}\text{sec}^{-1}{}^{o}\text{K}$$

For ν_p between 10^{12} and 10^{13} sec^{-1}, the hopping distance, a, is between

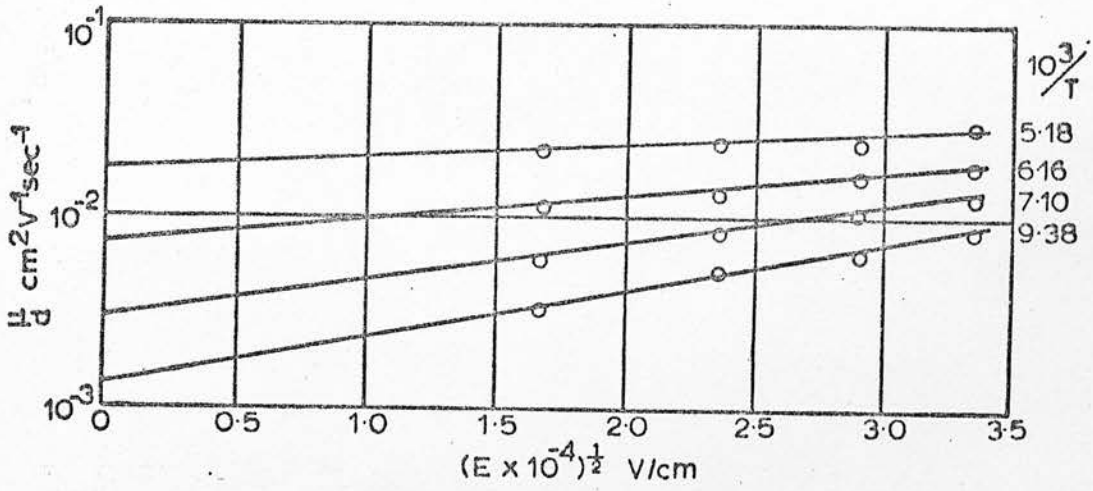

(a) μ_d as a Function of $E^{\frac{1}{2}}$

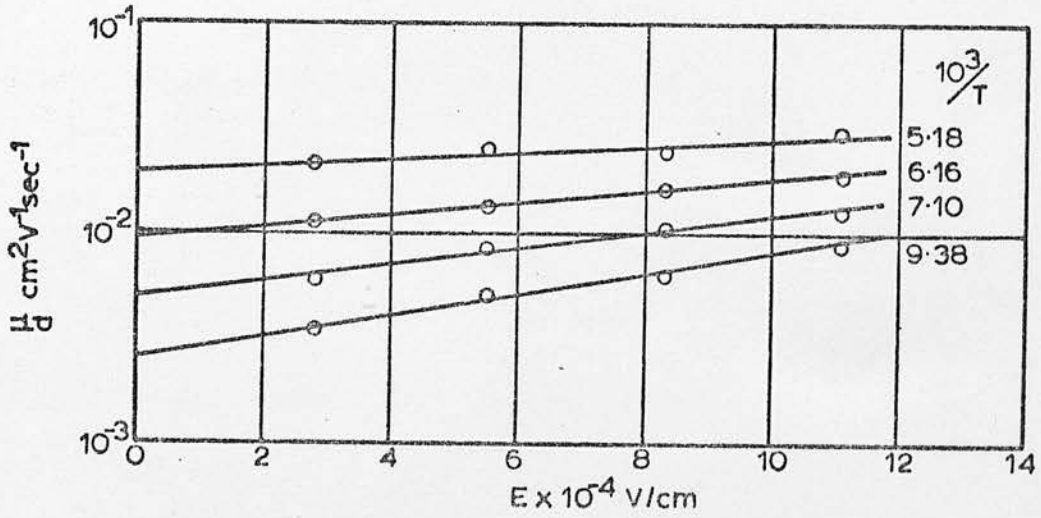

(b) μ_d as a function of E

Fig. 46 Dependence of Hole Drift Mobility upon Applied Field at Various Temperatures; Selenium + 1% Germanium

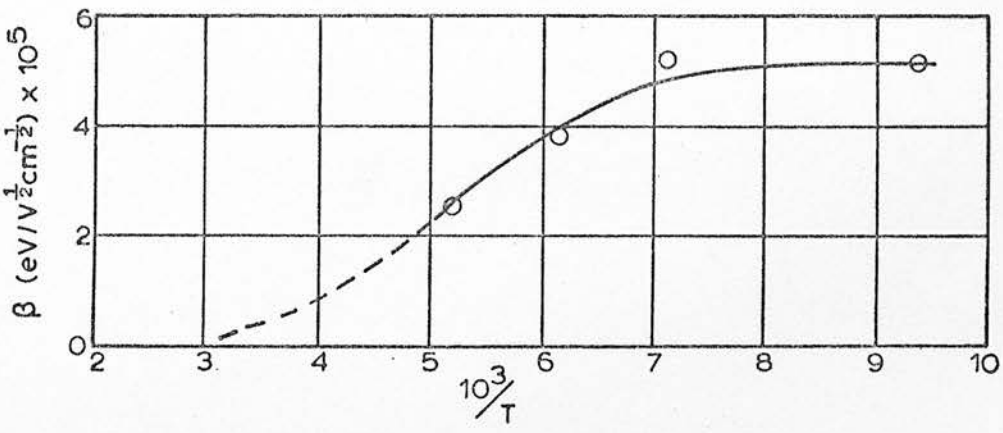

Fig. 47 Dependence of Field Proportionality Constant, β, upon Reciprocal Temperature; Selenium + 1% Germanium

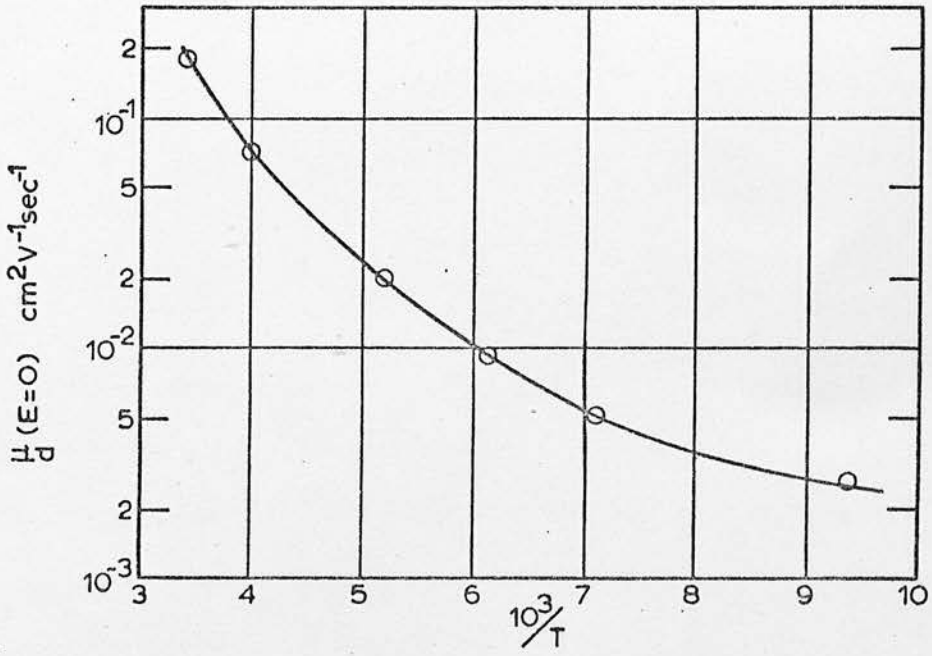

Fig. 48 Dependence of 'Zero Field' Hole Drift Mobility upon Reciprocal Temperature; Selenium + 1% Germanium

0.8 and 2.5 Å. The calculation of the microscopic mobility gain requires an estimate of the values of N_v and N_t, and the necessary data is not available as it was for pure selenium. It might be possible to assume that the conditions are not radically different in the two cases, since the values of the room temperature hole mobility and of ε are comparable, so that $\mu_o \sim 10$ $cm^2V^{-1}sec^{-1}$ taking Spear's data. The 'tail of states' model may still be applied, giving $\mu_o \sim 3$ $cm^2V^{-1}sec^{-1}$.* Once again, the values are too low to be compatible with conventional band motion, and a re-interpretation in terms of diffusive motion within the band states is preferable. Performing this as before, it is found that a = 1.7 Å, which is in agreement with the value obtained for the hopping distance.

The analysis has been repeated using the data in figure 46a rather than that in figure 46b to estimate the zero field mobilities. The constants in equation 5.4.5 then become

$$\frac{N_v}{N_t}\mu_o = 8.6 \text{ cm}^2\text{V}^{-1}\text{sec}^{-1}$$

$$\varepsilon = 0.106 \text{ eV}$$

$$W = 0.052 \text{ eV}$$

$$\frac{e\nu_p a^2}{k} = 17 \text{ cm}^2\text{V}^{-1}\text{sec}^{-1}\,{}^{o}\text{K}$$

The hopping distance is estimated as 1.2 to 3.8 Å, and the microscopic mobility is again too low to be acceptable (9 $cm^2V^{-1}sec^{-1}$ from Spear's data and 2 $cm^2V^{-1}sec^{-1}$ from the 'tail of states' model*). Assuming diffusive band motion, it is found that a = 1.5 Å.

Once again, the results have been examined in terms of the Mott and Killias equations, and it has been found that Mott's analysis is inapplicable. The Killias equation has been fitted to the experimental 'zero field' results, giving the constants

* See footnote to p.98.

constant	value assuming $\log \mu \propto E$	value assuming $\log \mu \propto E^{\frac{1}{2}}$
A ($cm^2V^{-1}sec^{-1}$)	34.2	129
B (eV)	0.168	0.198
θ_R (^oK)	51.3	49.7

The reservations previously expressed, with regard to the applicability of the Killias analysis to the results for pure selenium, are equally strong in the present case.

Figure 49 shows a comparison of the predictions of the above analyses (for the case in which figure 46b is used to calculate the 'zero field' mobilities) with the experimental results from figure 48.

It should be mentioned that it is possible that the differences between the calculated constants for doped and pure selenium are due, at least in part, to inaccuracies in the measurements. A comparison of figures 30 and 32 indicates that the mobility measurements for the doped material were less accurate than those for pure selenium, so that the 'zero field' hole mobility curve for Se + 1% Ge (figure 48) would also be expected to be less reliable, particularly at low temperatures. The analysis of figures 43 and 48 in terms of equation 5.4.5 is strongly dependent on the accuracy of the curves. For instance, it has been estimated that a 10% error in the 'fitted' values of activation energy could lead to an error in the pre-exponential constants of a factor of 2.

To complete the discussion of germanium doped selenium, it is necessary to consider the data obtained at higher germanium doping levels. Figure 33 shows the temperature dependence of the electron mobility for a specimen containing 3% germanium. For values of $10^3/T$ greater than 3.75, the results indicate an activation energy

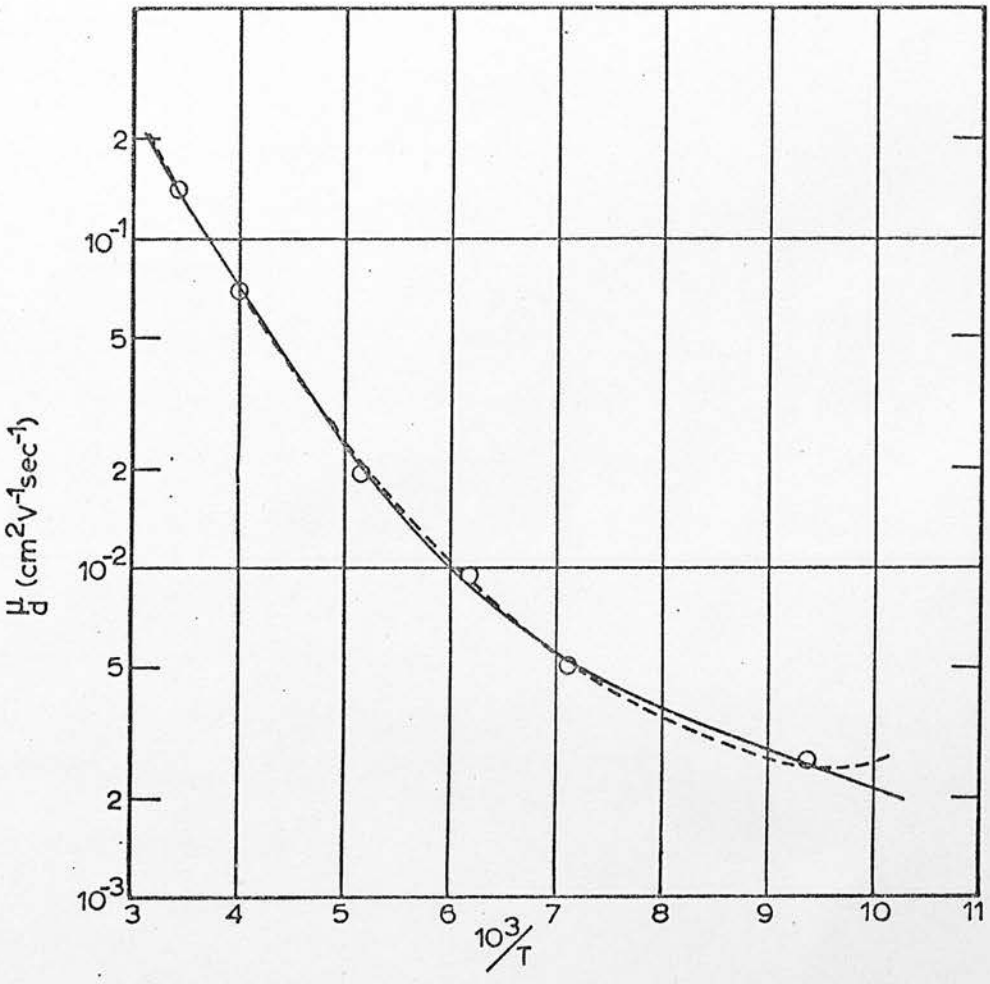

—— $\mu = 11\exp(-0.111/kT) + \frac{7.2}{T}\exp(-0.035/kT)$

- - - $\mu = 34.2\exp\left[-0.168(1 - 51.3T^{-1})/kT\right]$

o Experimental results

Fig. 49 Fitted Theoretical Predictions of the Variation of Hole Drift Mobility with Temperature; Selenium + 1% Germanium

of 0.22 ± 0.02 eV. The sharp discontinuity of slope observed at $10^3/T = 3.8$ was accompanied by a rapidly decreasing transit pulse height at lower temperatures, indicating the controlling presence of deep trapping levels. It is thus likely that a trapping time, rather than a transit time, was being measured for $10^3/T > 3.8$. The electric field dependence of the room temperature electron mobility, as also shown in figure 33, again indicates that a field stimulated process was present, but the examination was not of sufficient accuracy to allow a quantitative analysis of the process.

c) Arsenic Triselenide.

In this material, a strong field dependence of the hole drift mobility is observed over the whole range of measurement ($2.8 < 10^3/T < 4.0$). Once again, this property has been considered in terms of the Poole-Frenkel effect, and of a field assisted hopping process. From a preliminary examination, it is concluded that the latter process is unlikely, since a hopping distance of the order of 50 Å is calculated, and since the pre-exponential term in the drift mobility equation is found to be of the order of 30 $cm^2V^{-1}sec^{-1}$. Both of these values are considered to be unacceptable for hopping transport. It is thus argued that the results should be considered in terms of trap-controlled band transport, and the following analysis will proceed along these lines.

Figure 34, which shows the dependence of the hole drift mobility upon $(\text{applied field})^{\frac{1}{2}}$, has been analysed in terms of the Poole-Frenkel effect. The field dependence constant, β, is calculated as 2.6×10^{-4} $eV/V^{\frac{1}{2}}cm^{-\frac{1}{2}}$, as compared with the value of 2.17×10^{-4} $eV/V^{\frac{1}{2}}cm^{-\frac{1}{2}}$ predicted by the simple, one dimensional, Poole-Frenkel theory (taking Kolomiets[36] figure of K = 12.25). The dependence

of conductivity on applied field, as shown in figure 35, gives a value of β of 3.3×10^{-4} $eV/V^{\frac{1}{2}}cm^{-\frac{1}{2}}$. The correspondence of the mobility and conductivity field constants indicates that the applied field only serves to stimulate the emission of carriers from shallow (mobility controlling) traps, and that the thermal equilibrium of the carriers with respect to deep traps is not seriously disturbed. The analysis of the Poole-Frenkel effect in three dimensions, as performed by Hartke[57], leads to a lowering of the theoretical value of β, so that the above experimental values would appear to be somewhat high. However, this is not considered to be a serious objection, since the theoretical analysis is critically dependent on the assumed nature of the trapping centres.

It will be noted from figure 34 that the exploratory result of Kolomiets and Lebedev[35], on an evaporated specimen, is in good agreement with the data from the present study. Figure 36 shows the temperature dependence of the mobility at various values of the applied field (2 specimens). The correspondence of results is fairly good, and the measurements of Kolomiets and Lebedev are again consistent with the data. This may well indicate that the transport properties are structure, rather than impurity, dependent. If so, it would appear that there is a close structural similarity between evaporated and vitreous specimens.

From the three sets of data obtained for specimen 1 in figure 36, it is possible to estimate the magnitude of the mobility activation energy at zero applied field. For this specimen, the calculated activation energies at various fields are;

E (V/cm)	$E^{\frac{1}{2}}$	ε (eV)
9.42×10^4	3.07×10^2	0.303
18.8×10^4	4.33×10^2	0.242
28.3×10^4	5.32×10^2	0.205

If the measured activation energy, ε, is related to the zero field activation energy, ε_o, and the field, E, by the equation

$$\varepsilon = \varepsilon_o - \beta E^{\frac{1}{2}} \qquad (5.4.12)$$

then the values in the above table may be substituted, giving

$$\varepsilon_o = 0.43 \text{ eV}$$

$$\beta = 4.3 \times 10^{-4} \text{ eV/V}^{\frac{1}{2}}\text{cm}^{-\frac{1}{2}}$$

Alternatively, mobility values taken from figure 36 may be plotted as a function of $E^{\frac{1}{2}}$, as shown in figure 50, and the 'zero field' mobilities estimated by extrapolation. Figure 51 shows such values plotted against 1/T, and indicates an activation energy of 0.43 eV. If figure 50 is used to calculate β, the value obtained is found to be slightly temperature dependent, as shown in figure 52. Figure 51 indicates a value of pre-exponential mobility which is too low to be explained in terms of conventional band motion, but the situation is consistent with diffusive motion within the band states. Fitting the date to equation 2.2.5, and assuming that the mobility is still controlled by shallow traps, then

$$\mu_{diff} = \frac{e\nu_{e\ell}a^2}{kT} \exp(-\varepsilon/kT) \qquad (5.4.13)$$

with $$\frac{e\nu_{e\ell}a^2}{k} = 1.05 \times 10^4 \text{ cm}^2\text{V}^{-1}\text{sec}^{-1}\,{}^{o}\text{K}$$

and $$\varepsilon = 0.46 \text{ eV}$$

Taking $\nu_{e\ell} = 10^{15}$ sec^{-1}, then a = 3 Å, which appears to be a reasonable figure.

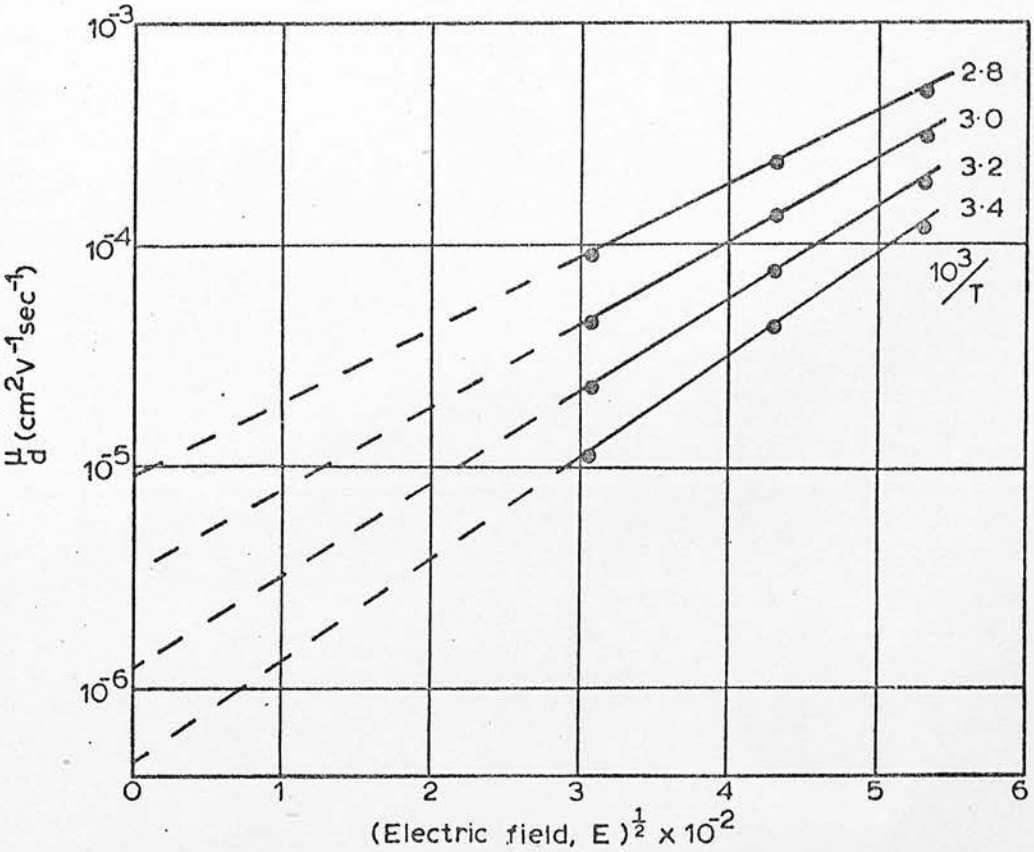

Fig. 50 Dependence of Hole Drift Mobility upon Applied Field at Various Temperatures; Arsenic Triselenide

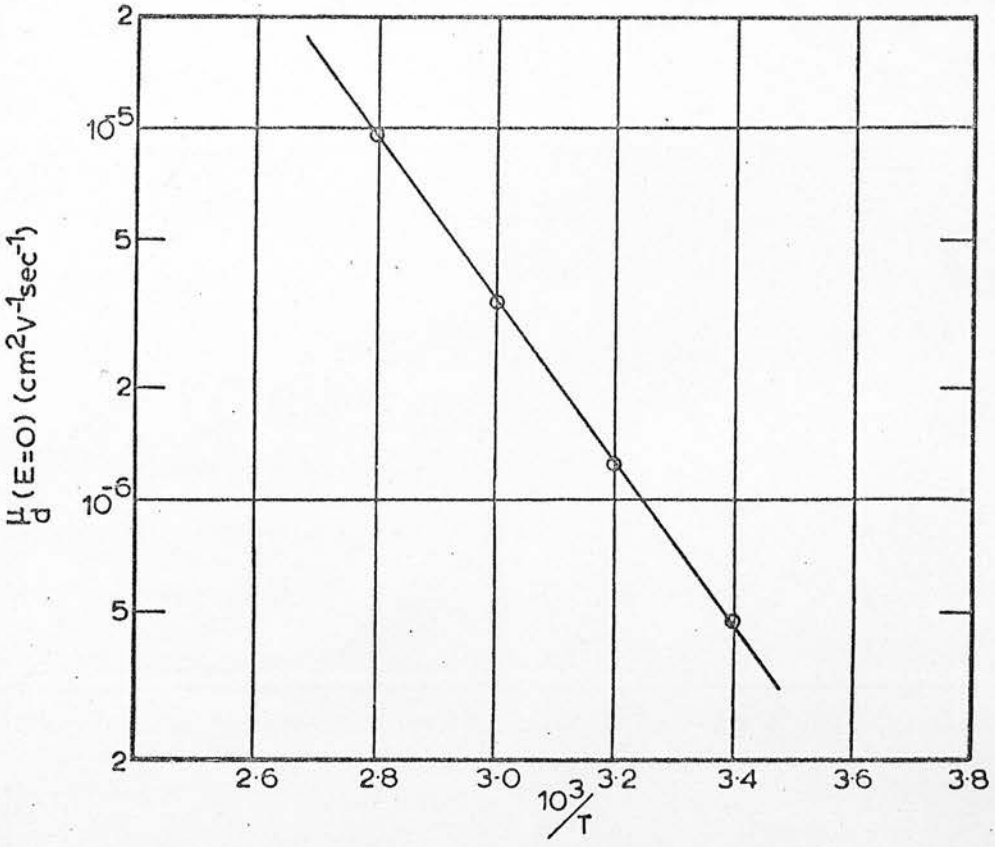

Fig. 51 Dependence of 'Zero Field' Hole Drift Mobility upon Reciprocal Temperature; Arsenic Triselenide

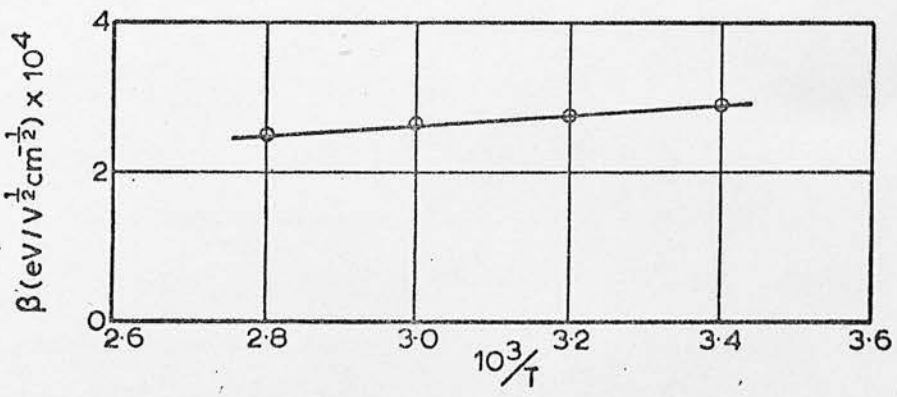

Fig. 52 Depence of Field Proportionality Constant, β, upon Reciprocal Temperature; Arsenic Triselenide

The variation of specimen current with temperature at a fixed applied field is shown in figure 37, and it will be noted that a sharp discontinuity of slope occurs at $10^3/T = 3.1$ ($T = 320^oK$). For temperatures greater than this value, the conductivity activation energy is estimated as 0.93 eV, as compared to the values of 1.06 eV calculated from the data of Edmond[20] for liquid material, and 1.08 eV from the data of Owen[88] for solid material. It should be noted that these activation energies have been calculated using the equation $\sigma = \sigma_o \exp(-\varepsilon/kT)$, rather than from $\sigma = \sigma_o \exp(-\varepsilon/2kT)$. The latter equation is the more frequently used, and strictly the more correct expression, but the former has been adopted here to allow a direct comparison with the mobility activation energy. The value of the conductivity activation energy obtained in the present study will be reduced due to the high value of the applied field, and a correction for this effect should be applied. Since the specimen thickness was not accurately known, it is not possible to make an accurate correction, but assuming a thickness of 2 microns (typical value), the field would be of the order of 3×10^5 V/cm. The correction to the activation energy, $\beta E^{\frac{1}{2}}$, would then be 0.19 eV taking β as 3.3×10^{-4} eV/V$^{\frac{1}{2}}$ cm$^{-\frac{1}{2}}$ as calculated previously. The zero field activation energy would then be approximately 1.1 eV; a figure which is in agreement with the published measurements.

At lower temperatures, figure 37 indicates an activation energy of 0.4 eV. As far as is known, no previous conductivity measurements have been reported at the temperatures obtaining in the present study; the very low value of the conductivity preventing measurements on the thick specimens which have been examined. Such a sharp discontinuity of slope is not consistent with the predictions

of Mott[4] or Killias[56], but has been predicted by Owen[85]. This prediction is founded on an 'island' type structural model for As_2S_3 and As_2Se_3 glasses, in which it is suggested that both localised and non-localised states may be present in the forbidden gap. Owen has stressed that the model is extremely tentative, and requires a critical examination of the validity of its foundations. Even so, it is possible to make a qualitative explanation of many of the major physical properties of As_2S_3 and As_2Se_3 glasses, including some of the anomalous characteristics, in terms of the model. A particular prediction is that the d.c. conductivity should exhibit a relatively abrupt change of activation energy at 'low' temperatures (i.e. conceivably below room temperature), and that the 'low temperature' activation energy should be approximately equal to the drift mobility activation energy. In the present study, a hole drift mobility activation energy of 0.2 eV was measured at a field of 2.8×10^5 V/cm, so that the model is somewhat (but not totally) supported by the measurements. It is possible that a closer agreement would be observed if the applied field in the conductivity experiment was more accurately known.

The 'Hecht' curve of figure 38 was used in the identification of the observed drift pulses with a true transit phenomenon. The Hecht analysis[79] shows that, when the transit and deep trapping times are equal, the observed pulse height is reduced to 63% of its full value, as indicated by equation 4.3.9. Thus, in these terms, figure 38 indicates a deep trapping time of approximately 125 μsec. The inclusion of field-controlled carrier generation effects in the analysis, as considered by Tabak and Warter[31] would be expected to increase this figure, so that 125 μsec may be considered as a lower

limit for the trapping time. Tefft[74] indicates that a representative transit time is measured if the deep trapping time is not less than the transit time (see figure 19). Thus, the present results are considered to be valid, since no response time of more than 100 μsec occurred in the mobility measurements. As previously stated, this conclusion is supported by the report of Tabak[32], by the self-consistency of the results, and by the agreement with the results of Kolomiets and Lebedev[35].

d) Arsenic Trisulphide, and (e) Vanadium Pentoxide/Phosphorus Pentoxide

From the present brief examination, it is only possible to conclude that the electron and hole drift mobilities in these materials are extremely low, and that deep trapping times are sufficiently short as to completely prevent the observation of any transit pulses. In the case of arsenic trisulphide, the findings are consistent with those of Hirsch[83] on evaporated films.

f) As_2Se_2Te

As previously stated, it was impossible to perform transit time measurements in this material, due to the effects of deep trapping. In figure 40, the results of an examination of the pulse height as a function of the applied field are shown. Comparison of this curve and the predictions of equation 4.3.9 shows that the situation is indeed dominated by deep trapping, and that a complete charge transit does not occur. By inference therefore, the transit time is more than three times greater than the trapping time. Equally however, the rapid rise in pulse height for applied fields greater than 4×10^3 V/cm. indicates that the transit time is not

more than an order of magnitude greater than the trapping time. Thus, for an applied field of 5×10^3 V/cm, and a room temperature pulse response time (i.e. trapping time) of 15 μsec, it may be assumed that the transit time is between 45 and 150 μsec, giving a hole drift mobility

$$3 \times 10^{-3} < \mu_d < 10^{-2} \text{ cm}^2\text{V}^{-1}\text{sec}^{-1}$$

It is realised that the above discussion is somewhat speculative, and ignores the possibilities of field dependent mobility and carrier generation efficiency. Even so, it is felt that there is some liklihood that the mobility is of the order indicated. One of the aims of the examination was to attempt to compare the Hall and drift mobilities where possible. The Hall mobility in As_2Se_2Te has been found by Male[22] to be about $10^{-1}\text{cm}^2\text{ V}^{-1}\text{sec}^{-1}$. Since the drift mobility was not positively measured in the present study, direct comparison of the mobilities is not possible. It is worth noting, however, that if the drift mobility is assumed to be band-controlled, as expressed in the equation

$$\mu_d = \mu_o \frac{N_v}{N_t} \exp(-\varepsilon/kT)$$

and if $N_v/N_t \sim 1$, then μ_o will be greater than 1 $\text{cm}^2\text{V}^{-1}\text{sec}^{-1}$ provided that the mobility activation energy is greater than 0.1 eV. Thus, under these conditions, the Hall mobility would certainly be anomalously low. However, whilst it is felt to be quite possible that μ_o will be of this order, a quantitative evaluation is impossible, so that further discussion would be fruitless.

Chapter Six

Hall Mobility - Theory and Measurement

6.1 Introduction

Since its discovery in 1879 by E.H. Hall, the Hall effect has become a tool of increasing importance in the field of solid state physics. The effect provides a fundamental measure of the velocity of charge carriers by subjecting a specimen to crossed electric and magnetic fields. Thus, in figure 53, a specimen in the form of a bar is situated in an electric field E_x in the x-direction, and a magnetic field B_z in the z-direction. In general terms, an electron moving with velocity $\bar{v}$ in a magnetic field $\bar{B}$ will experience a Lorentz force

$$\bar{F} = (\bar{B} \times \bar{v})e \qquad (6.1.1)$$

where e is the electronic charge.

Thus, with the geometric arrangement of figure 53,

$$F_y = B_z v_x e \qquad (6.1.2)$$

The electrons deflected by this force will create a charge imbalance across the specimen and will produce an applied field in opposition to the deflection. In an equilibrium situation, this field E_y will exert a force

$$F'_y = e E_y \qquad (6.1.3)$$

which exactly balances the force F_y. Thus,

$$E_y = B_z v_x \qquad (6.1.4)$$

If, now, the Hall mobility μ_H of the electron is defined as the average drift velocity which it acquires whilst in motion in a unit electric field, then

$$v_x = \mu_H E_x \qquad (6.1.5)$$

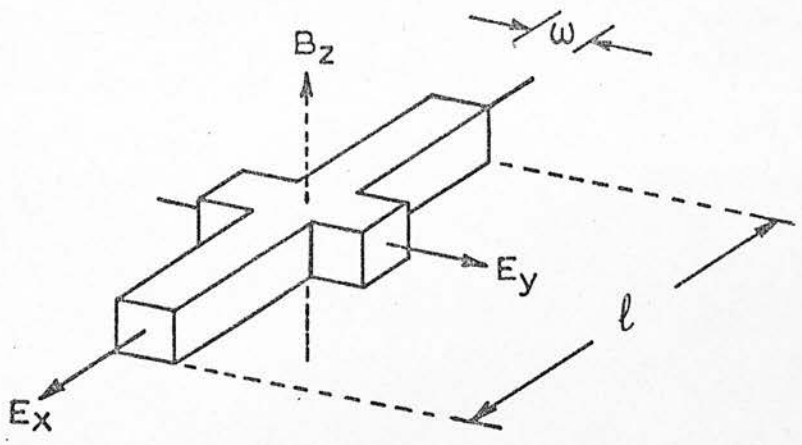

Fig. 53 Illustration of the Hall Effect

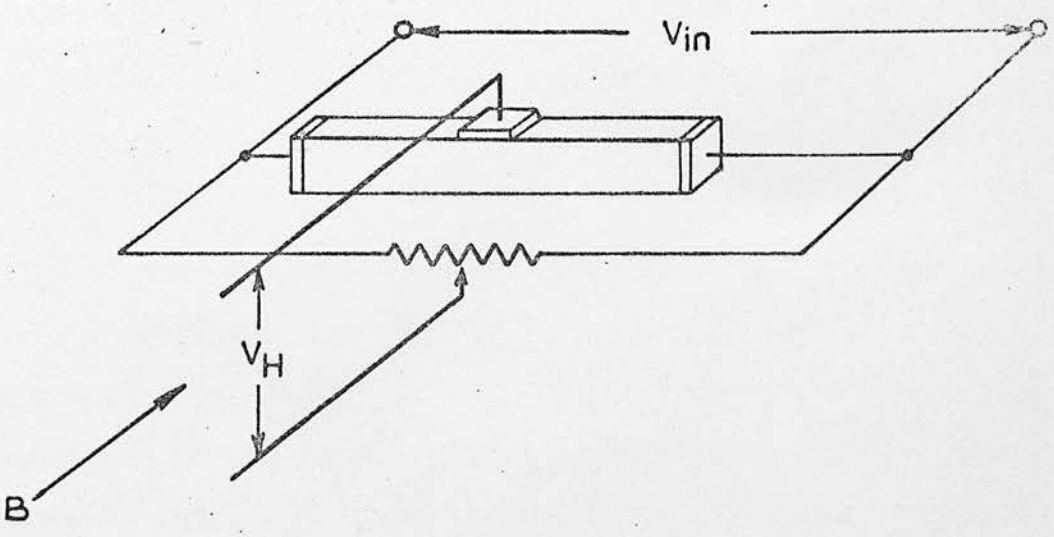

Fig. 54 Three Electrode Hall Specimen

Thus, from equation 6.1.4,

$$E_y = B_z E_x \mu_H \qquad (6.1.6)$$

Consequently, since $E_x = V_x/\ell$ and $E_y = V_y/w$, where V_x and V_y are the applied voltage and the measured Hall voltage, and ℓ and w are the specimen length and width, then

$$\mu_H = \frac{V_y}{V_x} \cdot \frac{\ell}{w} \cdot \frac{1}{B_z} \qquad (6.1.7)$$

In the commonly employed units, μ_H is expressed in $cm^2V^{-1}sec^{-1}$, and B is measured in Gauss ($B_{Gauss} = B_{e.m.u.} \times 10^{-8}$), so that equation 6.1.7 becomes

$$\mu_H = \frac{V_y}{V_x} \cdot \frac{\ell}{w} \cdot \frac{10^8}{B_z} \ cm^2V^{-1}sec^{-1}. \qquad (6.1.8)$$

If the current carriers in a material are holes, instead of the electrons considered above, the combination of their opposite direction of motion and positive charge will cause a deflection in the same direction as for electrons. The resulting Hall voltage across the specimen will thus be of the opposite sign to that produced by electron deflection. In the case of mixed conduction, when both electrons and holes are mobile in a material, the measured Hall voltage will be the difference of the individual voltages due to the two types of carrier.

As already mentioned, the Hall mobility is uniquely related to the velocity of mobile carriers, rather than to the average velocity including any time spent in trapping centres. In the conventional case of band motion in a regular crystalline lattice, the Hall mobility is thus determined by the occurrence of carrier scattering events in any particular situation. There is therefore a

close correspondence between the Hall and microscopic mobilities. In fact, in an isotropic solid, the application of classical statistics leads to the relationship

$$\mu_H = \frac{3\pi}{8} \mu_o \qquad (6.1.9)$$

The numerical factor in equation 6.1.9 arises from the difference of the statistical averaging processes employed in calculating the two mobilities[89]. It is possible to derive theoretical relationships for the temperature dependence of the Hall mobility under various scattering conditions (acoustic lattice, optical lattice, ionised impurity, neutral impurity, etc.) and for various degeneracies of impurity states (classical, degenerate statistics, arbitrary degeneracy, etc.). Accounts of such analyses are contained in the literature[2,89] but will not be reproduced here, since their predictions are not expected to be particularly applicable to the non-crystalline materials of interest in the present study. It is sufficient to note that, under conditions where lattice scattering is dominant, the mobility increases with decreasing temperature, since thermal perturbations of the lattice decrease. Impurity scattering often leads to a power law dependence of the mobility on temperature.

6.2 The Hall Mobility in Low Mobility Materials

The discussion above has been concerned with the conventional motion of carriers within the band states of an ordered semiconductor. In such materials, as has previously been noted, the microscopic mobility is not expected to be less than 100 $cm^2V^{-1}sec^{-1}$, and the Hall mobility should be comparably high. However, no value of Hall mobility greater than 1 $cm^2V^{-1}sec^{-1}$ has been measured to date in any semiconducting glass. It is therefore apparent either that the measured

Hall mobility is anomalously low, so that the carrier motion may not be of the conventional type. The former situation could occur in an inhomogeneous structure, such as that postulated for some vitreous semiconductors and shown in figure 6. Volger[44], and Bube[45], have analysed this type of model, and have shown that the magnitude of the mobility is dependent upon the parameters of mobility and resistivity inside and outside the conducting zones, and on the ratio of the zone diameter to the inter-zone separation. Thus, for zones of mobility μ_1, diameter ℓ_1, and resistivity ρ_1, separated by distances ℓ_2 in a material of mobility μ_2 and resistivity ρ_2,

$$\bar{\mu}_H = \frac{\alpha}{\alpha + \beta} \mu_1 + \frac{\beta^2}{\alpha + \beta} \mu_2 \qquad (6.1.10)$$

where $\bar{\mu}_H$ is the measured Hall mobility, $\alpha = \rho_1/\rho_2$, and $\beta = \ell_1/\ell_2$. An interesting situation occurs when the signs of the carriers dominating conduction inside and outside the zones are different. The terms on the right hand side of equation 6.1.10 are then subtracted rather than added, and the measured Hall mobility may be of either sign, depending on the values of the parameters in the equation. Since the thermoelectric power will not, in general, be determined by a dependence exactly analogous to that shown in equation 6.1.10, the possibility of a sign difference between the thermoelectric power and the Hall mobility may occur. However, it must be pointed out that the possibility of a sign difference between the carriers inside and outside the zones implies the presence of p-n junction barriers around the zone perimeters. Such barriers have not been considered in the derivation of equation 6.1.10. Even so, it is apparent that the magnitude of the Hall mobility is extremely difficllt to predict in an inhomogeneous

material.

The possibility that the low value of the measured Hall mobility may reflect an unconventional transport mechanism has also received some consideration in the literature, particularly in terms of a hopping form of transport. To date, various analyses of the Hall mobility in the hopping region have shown no conclusive agreement with each other. The case of non-adiabatic hopping of small polarons has been examined by Friedman and Holstein[90], Kurosawa[91], Firsov[92], Klinger[51,93,94], Schnakenberg[86,95], and Holstein and Friedman[96]. Although many of these analyses are based on the same assumptions (application of the Kubo[97,98] formalism, etc.), the predictions with regard to the nature of the Hall mobility differ appreciably.

The argument in its simplest form[43,52] is as follows. At any particular time, the magnetic field can exert an influence only on carriers which are in the process of hopping. These carriers will form a fraction $\exp(-W_1/kT)$ of the total carrier concentration, where W_1 is the energy needed to bring two hopping sites into a coincidence of energy. In addition, only carriers which have a choice of hopping sites may be magnetically deflected, so that it is necessary to introduce a second exponential factor, $\exp(-W_2/kT)$, where W_2 is the activation energy for a <u>triple</u> site coincidence. The Hall mobility is of the form

$$\mu_H \alpha \exp\{-(W_2 - W_1)/kT\} \qquad (6.1.11)$$

The point where the analyses differ is in the relative magnitudes of W_1 and W_2. It will be noted that this is an important difference, since it may affect both the magnitude and the temperature dependence

of the mobility quite drastically. Thus, Friedman and Holstein[90,96] predict $W_2 = 4W_1/3$, so that

$$\mu_H = A\exp(-W_1/3kT), \text{ where } A \sim 0.5 \text{ cm}^2\text{V}^{-1}\text{sec}^{-1}. \quad (6.1.12)$$

However, Firsov[92] has indicated that W_2 may be less than W_1, so that, at high temperatures

$$\mu_H \propto \exp(+\Delta W/kT) \quad (6.1.13)$$

Schnakenberg[95] has calculated the two energies to be of the same order, giving an essentially unactivated Hall mobility, and other authors have obtained results which are different again.

Emin and Holstein[99] have considered the hopping of small polarons under adiabatic conditions, and have again concluded that the activation energy may be very small.

In view of the lack of agreement between the above analyses, it is impossible to apply them quantitatively to the results obtained for the Hall mobility in amorphous materials, especially since it has not been established that charge transport occurs by the motion of samll polarons. Thus, the low values of the measured Hall mobility, and of its activation energy, must be regarded as being unexplained.

The possibility that the sign of the Hall effect in the hopping region may be 'anomalous', has also been suggested[1,4,52,100]. It appears that, for many of the envisaged hopping mechanisms, the Hall effect will indicate n-type conduction, irrespective of whether the carriers involved have a positive or negative charge. Again, however, it has not been positively established that the anomaly which is observed in non-crystalline materials may be explained in this manner.

In conclusion, it appears that the form of the Hall mobility

either in terms of a structural (island) model, or in terms of transport by hopping. It is considered that the former approach is unlikely to be correct, especially since a very low value of Hall mobility is observed even in the most conducting types of vitreous semiconductors, and since the presence of p-n junction barriers within specimens is not substantiated by noise measurements[46]. Analysis of the experimental data in terms of hopping conduction is more likely to yield fruitful results, but it is evident that a substantial development of the present theory will be necessary if a conclusive identification of the experimental data is to be made.

6.3 Considerations in the Measurement of the Hall Mobility

In principle, a measurement of the Hall mobility may be made by placing a specimen in crossed electric and magnetic fields, and by measuring the resulting transverse voltage. In practice, it is extremely unlikely that such an attempt would succeed, since the Hall voltage would almost certainly be masked by other, spurious, signals. The techniques by which the Hall voltage may be identified in such a situation will now be outlined.

The most fundamental problem in the study of the Hall effect concerns the positioning of the probes used to measure the Hall voltage. It is highly unlikely that these probes will lie on an equipotential of the applied electric field, so that an extraneous misalignment voltage will be developed between them, in addition to the Hall voltage. However, the latter may easily be identified by reversing the polarity of the applied magnetic field. Such a reversal will cause a change of sign of the Hall voltage, but will not affect the misalignment voltage. Therefore, a nett change in the total output voltage, equal to twice the Hall voltage, will occur.

Further problems arise when the existence of other galvanomagnetic effects is considered. Any situation which causes a non-uniform velocity distribution of the current carriers in a specimen may give rise to a transverse voltage when the specimen is suitably positioned in a magnetic field. For instance, if a temperature gradient exists along the length of the sample, faster 'hot' electrons will tend to diffuse down the temperature gradient and be deflected by the magnetic field so as to produce a transverse electric field. As in the Hall effect, the sign of this field will depend upon the polarity of the magnetic field, so that a reversal of the latter will not assist in the identification of the Hall voltage. There are, in fact, four major galvanomagnetic phenomena; the Hall effect, the Nernst effect which is described above, the Ettinghausen effect in which a transverse temperature gradient is caused by the application of crossed electric and magnetic fields, and the Righi-Leduc effect in which a longitudinal temperature gradient causes a transverse temperature gradient in the presence of a magnetic field. Undesirable effects of these types may be eliminated in Hall measurements by replacing the d.c. applied electric field by an alternating field. It has been shown[101] that the galvanomagnetic coefficients in a homogeneous crystalline semiconductor are apparently the same whether measured by a.c. or d.c. techniques. The substitution of the a.c. electric field will allow the Hall voltage, now of an alternating form, to be identified from the 'd.c.' thermal effects. It should be mentioned that the error introduced by the presence of spurious galvanomagnetic effects is usually small. For instance, the error due to the Ettinghausen effect is normally less than 1%. However,

the use of an a.c. applied field offers other advantages, so that an a.c. technique is often employed in practice. Before the development of instruments capable of the stable amplification of d.c. signals from sources of high impedance, it was much easier to examine materials of low conductivity by an a.c. technique. Even with the present state of the art in this respect, there are often significant advantages in the a.c. form of measurement. Furthermore, in view of the low Hall voltage signal levels which are to be expected in low mobility materials, the use of tuned filter networks, the relative ease of amplification, and the possibility of phase-sensitive detection are extremely attractive. Also, there exists the possibility of using an alternating magnetic field in conjunction with the a.c. electric field. In such a situation, the Hall voltage is generated at the beat frequencies of the two applied fields, thus enabling pick-up from either of the individual fields to be eliminated by suitable filtering and choice of the applied field frequencies. Finally, it may be of interest in certain materials to measure the frequency dependence of the Hall mobility itself. Normally, as mentioned above, the Hall effect is frequency independent for frequencies up to the microwave range, but in certain situations this would not be so. For instance, in the 'island' model suggested for some semiconducting glasses, the mobility and carrier concentration in the conducting zones are envisaged as being appreciably higher than that in the surrounding insulating matrix. The use of high measurement frequencies, at which an increasing proportion of the applied electric field would be developed across the zones, would be expected to produce a marked increase in the Hall voltage over that measured under d.c. conditions. In the case of hopping transport

a complex frequency dependence of the Hall mobility has been predicted by Holstein[100]. The relationship is difficult to apply in a quantitative manner, since both the activation energy and the hopping distance are calculated to change with frequency, and since it is not possible to estimate meaningful values of the constants involved from the existing data on non-crystalline materials. However, since there are indications, both in the case of the 'island' and of the hopping model, that a frequency dependence may occur, the use of an a.c. measurement technique would seem to be desirable. A review of the possible forms of such a measurement, coupled with an attempt to evaluate some of the advantages and disadvantages which may occur, will now be provided. In the nomenclature, the terms 'd.c.' and 'steady' will be used with the proviso that periodic reversals of a non-oscillatory field will generally be required to distinguish the Hall voltage from any misalignment and pick-up voltages present in the detector system.

1. A.C. Electric Field; Steady Magnetic Field

The fundamental advantages of this arrangement have already been mentioned. In addition to the elimination of the spurious effects described previously, the method is valuable in the study of materials of low conductivity by virtue of the effective elimination of electrode contact potential effects, and of the polarisation which often results from the continued application of a d.c. electric field to a highly resistive specimen. Examination of figure 53 shows that only one of the four electrodes applied to the specimen may be at earth potential if a correct measurement of the Hall voltage is to be made. Thus, there are two alternatives for the choice of the ground

point. Firstly, one of the primary electrodes of the applied electric field may be earthed. It is then necessary to examine the Hall output using an amplifier with a floating input. A push-pull type double input amplifier is frequently used to satisfy this requirement. Secondly, one of the Hall electrodes may be grounded, allowing the detection amplifier to be operated in the conventional manner. A non-grounded input voltage is usually provided by coupling the specimen and its driving source through a transformer. In the case of highly resistive specimens, the presence of small stray capacitances to ground from both sides of this transformer must be carefully controlled in order to avoid the production of troublesome phase shifts between the specimen electrodes.

In materials of very low mobility, the spurious voltages due to misalignment and pick-up will usually be several orders of magnitude greater than the Hall signal. Amplification of the latter signal will be essential for detection purposes, and the spurious signals must be removed prior to such amplification if saturation of the amplifier system is to be avoided. Several systems may be used to provide this elimination. The specimen output may be applied to one input of a differential amplifier, whilst a 'balancing' signal of suitable amplitude and phase is applied to the second input. Alternatively, the balancing signal may be added to the specimen output via a transformer, one winding of which is introduced into the specimen output line. A third possibility involves the use of the 'three electrode' technique, as illustrated in figure 54. Here, only one output electrode is applied to the specimen, and the other electrode is replaced by a potentiometer. By suitable adjustment

of the earthed sliding contact on the potentiometer, it is possible to adjust the simulated position of the missing electrode so as to eliminate misalignment effects. This advantage is countered by the fact that the Hall output is halved.

In Hall measurements on materials of very low conductivity, the impedance between the Hall probes will be high. To avoid 'shorting' the Hall voltage, an even higher impedance will be required at the input of the detection circuitry. Under these conditions, the problem of pick-up from stray electric and magnetic fields can be very serious. Such interference may be limited by situating an impedance reducing pre-amplifier as close to the specimen as is possible. Even so, in view of the finite input capacitance of such an amplifier it is evident that the input impedance will decrease with increasing frequency, and this may limit the use of an a.c. system to relatively low frequencies. Furthermore, in spite of the extremely low leakage currents which can be achieved using existing amplifiers, it must be considered that even a very low current through the specimen can cause polarisation, reducing the advantage gained by the use of the a.c. technique. In spite of such objections, the a.c. system still offers outstanding practical advantages, and has found great favour among modern investigators.

2. D.C. Electric Field; Alternating Magnetic Field.

In principle, this technique possesses many of the advantages and disadvantages inherent in the system described above. The major additional problem lies in the production of a powerful a.c. magnet, which can provide considerable practical difficulties. Furthermore, such a system would probably be limited to operation at a fixed frequency, and would certainly be restricted to low frequency operation,

so that no effective examination of the variation of Hall mobility with frequency could be undertaken. Having surmounted the practical problems of provision of the alternating magnetic field, the system offers relatively easy control in that the applied electric field may be reversed more quickly and easily than could the steady magnetic field in system (1). However, in highly resistive specimens, the problem of polarisation may again arise. Also, the presence of a very strong alternating magnetic field requires a searching examination of the possibility of eddy current effects, and of the thermal variations which eddy current heating of the apparatus could produce in the specimen.

3. Alternating Electric and Magnetic Fields

As already stated, the Hall signal in such a situation is produced at the beat frequencies f_1+f_2 and f_1-f_2 of the applied fields (frequencies f_1 and f_2). At either of the two beat frequencies, the Hall voltage is one half of that which would be produced in the d.c. case, the total voltage being given by

$$E_y = \tfrac{1}{2}\mu_H E_o B_o \left[\cos\{2\pi(f_1+f_2)t + \phi\} + \cos\{2\pi(f_1-f_2)t-\phi\}\right] \qquad (6.3.1)$$

where $E_x = E_o \sin(2\pi f_1 t)$, and $B_z = B_o \sin(2\pi f_2 t + \phi)$

In principle, the use of this agreement in conjunction with a frequency selective amplifier tuned to one of the beat frequencies can eliminate the misalignment and pick-up voltages present, with the exception of any component produced by a mixing of the individual applied fields. In fact, the main technical difficulty involved in this type of measurement is to avoid such mixing in any part of the electrical circuit or in the specimen[104,105]. Practically, this requires

the balancing out of the f_1 and f_2 signals at the Hall electrodes, and of the f_2 signal in the primary circuit. However, it is not necessary to perform such balancing with the precision required in the methods previously described. The disadvantages of the system are similar to those applicable to method (2), with the production of a powerful electromagnet and the effective limitation of the investigation to low frequencies presenting problems.

Having examined the various field configurations, it will now be useful to mention the possibilities of non-standard specimen and electrode configurations. The basic four electrode examination is frequently performed with a 'Maltese Cross' specimen configuration, as shown in figure 53. It may be shown[89] that shorting of the Hall voltage by the primary field electrodes is negligible provided the length/width ratio of the specimen is greater than 5. The use of the 'cross' arrangement minimises any distortion of the primary field by the Hall electrodes, but serves to increase the output impedance of the specimen. The configuration also serves to minimise the effect of the noise in the current carrying contacts. The three electrode system of figure 54 has previously been mentioned, but it is worth noting here that the artificial positioning of the fourth electrode results in an increased instability of the output voltage with respect to any drift caused by thermal or other variations. A configuration employing six electrodes is shown in figure 55. In this system, both the primary electrodes are split, producing a bridge network which may be balanced to minimise spurious output signals. However, the stability and balance of the applied electric field networks may again be problematic. A variation of the three electrode system, in which one of the two output electrodes is split, is shown in figure 56.

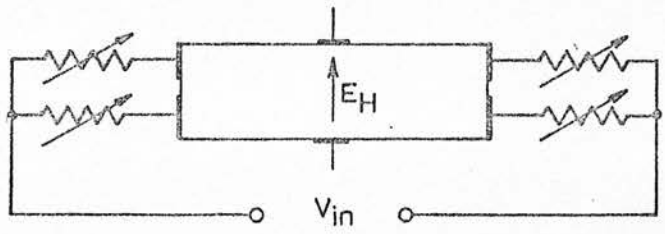

Fig. 55 Six-Electrode Hall Specimen

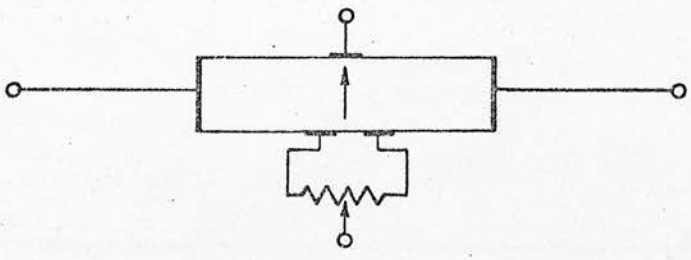

Fig. 56 Five-Electrode Hall Specimen

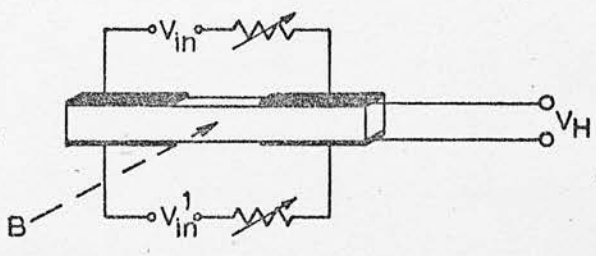

Fig. 57 Unconventional Four-Electrode Hall Specimen

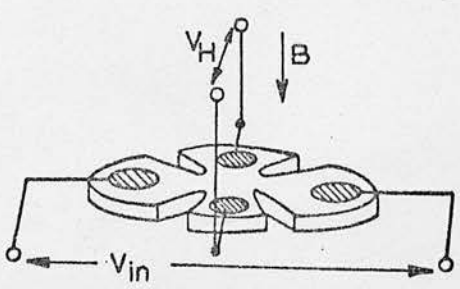

Fig. 58 Van Der Pauw Hall Specimen

The principle of operation is similar to that described for the three electrode system, but the balancing may be more finely controlled, and the system is less susceptible to drift problems. However, the noise level of the Hall output is increased, since the split electrode must now be regarded as carrying current. Figure 57 shows a configuration in which both the Hall electrodes, as such, are eliminated. The specimen current is provided via two balanced networks, as in figure 55, but the electrodes may be of much larger area, extending over an appreciable fraction of the specimen length. The Hall voltage is developed as an imbalance between the two input networks in the presence of a magnetic field. The relatively large area of the electrodes results in a comparatively low value of impedance between the output leads, making the system valuable for the examination of highly resistive specimens. The disadvantages lie in the necessity for stability in the input networks, and in the increase in output noise level due to the current carrying nature of the electrodes. This form of specimen has been successfully employed by Austin et al[102]. A further departure from the classical arrangement occurs in the Van der Pauw measurement system, which has been developed from a consideration of Hall measurements in specimens of arbitrary shape[103]. It has been calculated that the use of a specimen in the form of a 'clover leaf', as shown in figure 58, will minimise the effect of contacts upon the measurement. Thus, relatively large contact areas may be used with such specimens without seriously jeopardising the accuracy of the results.

Having described the possible specimen and applied field configurations, it is necessary to examine the factors relevent to the

detection of the Hall signal in materials of very low mobility and high resistivity. Considering the conventional 'Maltese cross' form of specimen, and taking typical parameters

$$V_x = 1 \text{ volt}, \quad \ell = 1\text{cm}, \quad w = 0.1 \text{ cm}, \quad B = 10^4 \text{ Gauss}$$

then equation 6.1.8 shows that the detection sensitivity must be of the order of 10^{-7}V if the equipment is to be capable of measuring a mobility of 10^{-2} $cm^2V^{-1}sec^{-1}$. The spurious signal on the output due to probe misalignment and pick-up in the detection circuitry may be expected to be of the order of $V_x/10$, or 10^{-1}V, so that the signal to noise ratio will be of the order of 10^{-6}. Even if extremely accurate elimination of spurious signals is achieved, the problem of thermal noise will arise in specimens of high resistance. The r.m.s. value of the thermal noise voltage, N, in a specimen is given by

$$N^2 = 4kTRF \qquad (6.3.2)$$

where R is the specimen resistance (ohms), and F is the detection bandwidth. At room temperature, for a detector possessing a 1 sec response time,

$$N = 0.46 \times 10^{-10} R^{\frac{1}{2}} \text{ volts r.m.s}$$

$$\equiv 3.9 \times 10^{-10} R^{\frac{1}{2}} \text{ volts peak-peak.}$$

For material of 10^8 ohm cm resistivity, R would normally be of the order of 10^9 ohms, so that N would be about 12 μV peak-peak; giving a signal to noise ratio of 10^{-2}. Increasing the effective detector time constant by electronic or mathematical averaging provides an obvious means of increasing the signal:noise ratio, but this is often prevented by drift of spurious output voltages due to causes such as slow temperature changes in the specimen, resulting in saturation of the high gain amplifier system in a relatively short time. Pick up from the magnetic field can also be a troublesome factor. Although

this is essentially a very low frequency phenomenon in systems utilising a non-oscillatory magnetic field, it should be noted that the motion of a 10 cm diameter loop in the earth's magnetic field can induce signals of several tenths of a microvolt in magnitude. Thus, in magnetic fields of the order of 10^4 Gauss, great care must be taken to minimise the areas of magnetic loops. Even so, magnetic field reversal can result in the production of transient signals in the detection circuitry which may easily paralyse the detection equipment.

6.4 Relevant Previous Measurements

Hall's original description of the Hall effect in metals[106] was first extended to semiconductors in 1909 by Baedecker[107], and Hall measurements rapidly became adopted as a valuable tool in the study of transport properties. The first description of Hall measurement equipment using an a.c. electric field was made by Smith[108] in 1912. Early measurements were, however, generally restricted to the examination of 'conventional' semiconductors, characterised by high values of mobility and conductivity. The study of materials relevant to the present project can be considered to have commenced fairly recently. In 1950, Russell and Wahlig[109] described equipment utilising an a.c. electric field and an alternating magnetic field, capable of measuring mobilities down to 1 $cm^2V^{-1}sec^{-1}$ in materials of resistivity higher than 10^4 ohm cm. In the following year, Donoghue and Eatherly[110] described a system, also using an a.c. electric field, which was capable of detecting Hall signals as low as 0.01 μV, but limited to the study of relatively conducting specimens. In 1952, Pell and Sproull[111] reported

apparatus capable of measuring mobilities of 10^{-2} $cm^2V^{-1}sec^{-1}$ in materials of very high resistivity (10^{11} ohm cm). A novel feature of this equipment was the use of an Amplidyne control system for extremely rapid reversal of the polarity of the magnetic field. The Amplidyne equipment automatically reversed the field polarity every six seconds, and the detected Hall output was of a 'square wave' form. The equipment once again employed an a.c. electric field, and an electrometer Hall voltage pre-amplifier. In 1953, Levy[112,113] attempted the extremely difficult task of measuring the ionic Hall effect in sodium chloride crystals. The examination, although unsuccessful, resulted in the development of an extremely sophisticated 'double a.c.' apparatus, which was estimated as being capable of detecting mobilities as low as 10^{-3} $cm^2V^{-1}sec^{-1}$ in the highly resistive crystals. With an improvement in equipment, Read and Katz[114,115] succeeded in measuring the ionic mobility in NaCl; their system being closely based upon that of Levy. In 1960, Kolomiets and Nazarova[25] performed the first measurements on vitreous semiconductors, the system $Tl_2Se{\cdot}As_2(Se_3,Te_3)$ being examined. Hall mobilities of about 5×10^{-2} $cm^2V^{-1}sec^{-1}$ were reported, and it was found that, whilst the thermoelectric power indicated p-type conduction, the Hall effect had an n-type sign. Uphoff and Healy[26] reported a similar anomaly for glasses in the system As_2Se_3-As_2Te_3, with Hall mobilities of the order of 10^{-1} $cm^2V^{-1}sec^{-1}$. The anomaly has also been observed by Peck and Dewald[24] for glasses in the systems As-Te-I and As-Te-Br (mobilities of about 10^{-1} $cm^2V^{-1}sec^{-1}$), by Male[22] in As-Se-Te and As-Se-Te-Tl glasses (mobilities again of the order of $10^{-1}cm^2V^{-1}sec^{-1}$), and in several examinations of liquid semiconductors (e.g., see Mott[4],

and Donally and Cutler[116]. Dresner[23] has measured the photo-Hall effect (i.e. the Hall effect in a specimen in which the carrier concentration has been increased by the application of an intense light beam) in an evaporated film of selenium. His results indicated a negative Hall coefficient, corresponding to an electron mobility of 0.32 $cm^2V^{-1}sec^{-1}$ at room temperature. The hole mobility was estimated as 10^{-1} $cm^2V^{-1}sec^{-1}$. Thus, the hole results are consistent with drift mobility data, but the electron Hall mobility is much higher than the drift value of approximately 6×10^{-3} $cm^2V^{-1}sec^{-1}$, (see Chapter Four).

Where the temperature dependence of the Hall mobility in vitreous or amorphous semiconductors has been examined in the above studies, the mobility has been found to be essentially unactivated, changing very little with temperature.

In terms of experimental equipment, Kolomiets and Nazarova used a double a.c. system, capable of operation with materials of resistivity up to 10^5 ohm cm, whilst Peck and Dewals employed a d.c. technique in conjunction with a 10^5 Gauss electromagnet. Male's equipment utilised an a.c. magnetic field and a d.c. electric field. The magnetic field was provided by a 4.5 kilowatt solenoid, developing 4.5×10^3 Gauss r.m.s. Dresner's measurements were made in a d.c. system, which utilised twin vibrating-reed electrometers in the differential Hall output circuit.

An investigation, important in the present context by virtue of its experimental arrangement, has been reported by Ryan[117]. In this system, an alternating magnetic field was

simulated by rotating the specimen in a static field. A very powerful magnetic field could thus be employed without encountering the problems of power dissipation associated with an a.c. magnet. Ryan's use of the system was limited to the examination of high mobility materials, but the technique has been applied to materials of low mobility and high resistivity by Hermann and Ham [118]. In such materials, the combination of high impedance and low signal level in the Hall output is such that the noise level of the slip-ring commutator system (used to extract the Hall signal from the rotating specimen holder) can become a problem. Hermann and Ham reduced this effect by the introduction of an impedance transforming amplifier in the shaft of the rotating section. Their system also utilised an a.c. electric field, and was capable of the measurement of mobilities down to 10^{-1} $cm^2V^{-1}sec^{-1}$ in materials with resistivities greater than 10^7 ohm cm.

An interesting approach to the utilisation of photo-conductive properties in the study of the Hall mobility in highly resistive materials has been described by Redfield[119]. The method involves the use of an unconventional electrode arrangement, in which a thin specimen is mounted upon a conducting glass substrate. The passage of an electric current down this substrate serves to develop an electric field along the specimen layer. Charge carriers are then produced in the specimen by intense light pulses. With the specimen situated in a magnetic field, the deflection of the (transient) photocarriers is detected by means of a second conducting glass electrode on the opposite specimen surface. Strictly speaking, therefore, the technique is a combination of Hall and drift mobility

examinations, and some care is necessary in the interpretation of the results. Redfield used the system to study the carrier mobility in diamond and alkali halide crystals, and it has subsequently been employed by Kobayashi and Brown[120] for examining silver chloride, and by Nakazawa and Kanzaki[121] to study transport in potassium chloride at low temperatures.

Chapter Seven

Hall Mobility - The Present Examination

7.1 Experimental Technique and Equipment

After examining the various possible systems for measuring the Hall mobility, it was decided that a technique employing an a.c. electric field would be most suitable for the present study. Since it was hoped to examine the frequency dependence of the Hall mobility, the possible use of an alternating magnetic field was discarded, to avoid the limitation of the measurements to low frequencies. However, since it was anticipated that drift in the measurement equipment could well be problematic in the examination of resistive specimens, it was apparent that rapid reversal of the polarity of the magnetic field would be advantageous. To avoid the necessity for the use of a complex system for this purpose, it was decided to periodically reverse the specimen orientation in a steady magnetic field. A rotating specimen holder, incorporating an impedance transforming pre-amplifier, was thus designed. The completed system possessed the advantage that it could be readily converted to 'double a.c.' operation. The equipment is shown in the photograph of figure 59a, while figure 59b shows the specimen holder. For convenience, the design and construction of the specimen holder, of the magnet system, and of the remainder of the measurement equipment, will be separately described below.

a) The Specimen Holder

The construction of this equipment, incorporating a pre-amplifier of high input impedance and low output impedance, is shown in figure 60. The preparation of the specimens themselves (in the

(a) Hall Mobility Measurement Assembly

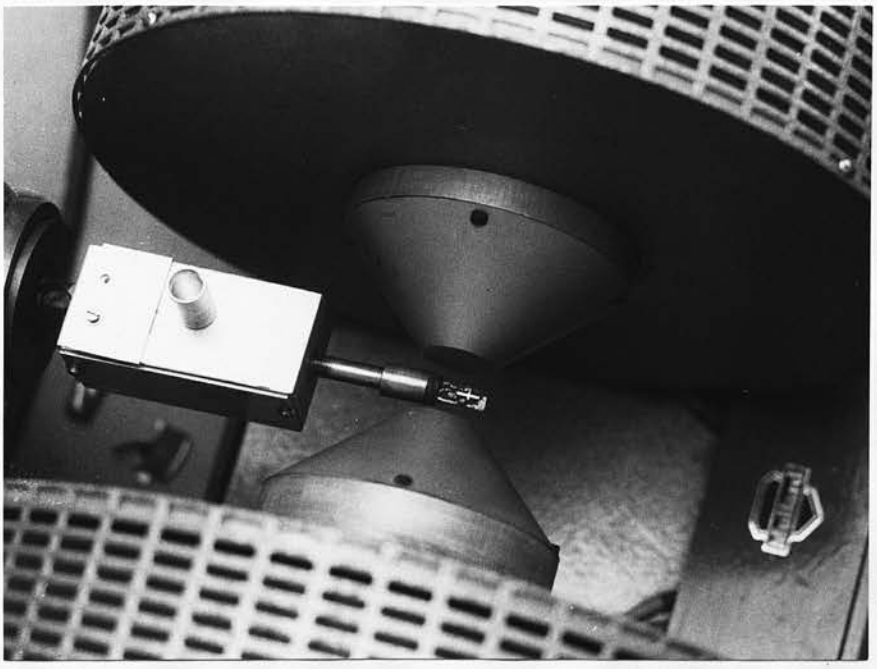

(b) Hall Mobility Specimen Holder

Fig.59

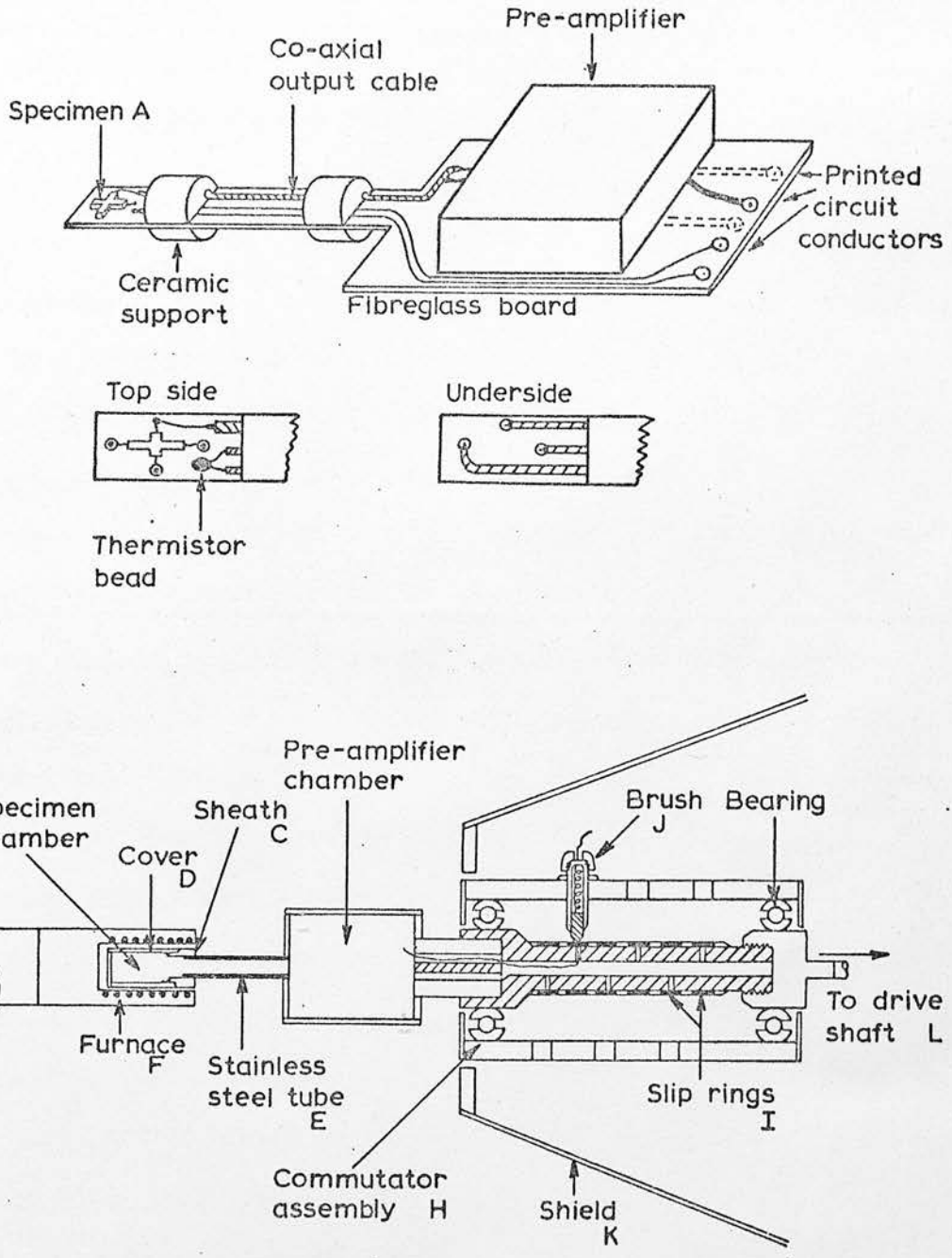

Fig. 60 Specimen Holder for Hall Effect Measurements

'Maltese cross' configuration) has been described in Chapter Three. A shaped section of double sided, fibreglass, printed circuit board was treated by photolithographic techniques to form the specimen mounting assembly. Printed circuit conductors served as leads for the specimen input voltage, and for the earthed side of the Hall output. The non-earthed output lead was taken from the specimen to the pre-amplifier via a miniature co-axial cable, the outer shield of which was soldered to a printed conductor on the board. Printed circuit conductors also served as leads for a sub-miniature thermistor element (for temperature measurement) situated close to the specimen. The specimen itself was connected to the copper leads by means of fine platinum wires, fused into the sample as described in Chapter Three. Shaped ceramic sections were cemented to the board as shown, and served to support it in the remainder of the specimen holder. The assembly was thoroughly degreased after preparation to minimise the possibility of leakage resistances in the high impedance output.

The fibreglass board, complete with specimen and pre-amplifier, fitted into the holder shown in figures 59b and 60. The specimen itself was enclosed in a brass sheath, C, and brass cover, D. A thin walled stainless steel tube, E, served to minimise heat exchange between the specimen enclosure and the bulk of the equipment. This tube lead to a chamber in which the pre-amplifier was positioned. The electrical arrangement of this amplifier will be dealt with below in the general description of the electrical equipment. The amplifier output, together with the specimen input, thermistor, and amplifier power supply leads, were connected to the static sections of the equipment via a commutator, H. The slip rings, I, were formed

from coin silver tubing, and the brushes, J, were of silver impregnated graphite, thus ensuring good electrical contact and minimum commutator noise. Three brushes were used for each slip ring to further improve the electrical contact. To reduce pick-up, the commutator section was enclosed in an earthed shield, K. Rotary drive to the system was provided via a flexible drive shaft, L, leading to a control on the instrument panel.

Heating of the specimen was accomplished by means of a small furnace, F, formed of non-inductively wound nichrome wire on an asbestos tube and enclosed in a copper sheath. The furnace fitted closely over the specimen assembly. A check was made to ensure that the presence of the furnace did not modify the value of the magnetic field experienced by the specimen.

b) The Magnet Assembly

A Mullard 4" electromagnet (EM 684), fitted with tapered 1" pole pieces, was used to provide the magnetic field. This unit required 15 amps d.c, and was powered from four heavy duty 12 volt accumulators in a series-parallel array. The accumulator assembly was capable of supplying 15 amps (24 volts) for over 100 amp. hrs. Control of the magnet current was achieved by a system of switched-out fixed resistors, and by a final heavy duty rheostat. Using this system, a complete reversal of the magnetic field could be accomplished in approximately 10 seconds, which may be compared with the figure of less than $\frac{1}{2}$ second required to reverse the specimen orientation. The field/current characteristic of the magnet was determined prior to Hall measurements, with the specimen holder removed. A Hall probe magnetometer (Newport Instruments Type H) was used to measure the magnetic field in this determination.

With the specimen holder and furnace in place, the minimum magnet pole gap was of the order of one inch, allowing magnetic fields of up to 2×10^4 Gauss to be employed in the Hall measurements.

c) The Electrical Measurement System.

Figure 61 shows a schematic diagram of the electrical system chosen in the present study for Hall effect measurements. The arrangement utilises the following components;

(A) The Signal Generator. This was a Muirhead K205A a.c. generator capable of providing a 3 volt output level in the range 1 Hz to 1 MHz. It served to provide the specimen input voltage, plus signals to the detector and 'balancing' sections.

(B) The Isolation Transformer. For the purpose of isolating the Hall input circuit to allow one of the output probes to be set at earth potential, a Gardners wide band A.F. transformer, type MU.7525 was selected. This component had a frequency range (± 0.5 dB) from 30 Hz to 20 KHz and was connected so as to give a voltage gain of 1:1.4. The transformer possessed electrostatic screening and was cased in Mu-metal to reduce spurious pick-up, a hum reduction of -50dB being quoted.

(C) The Hall Output Pre-amplifier. As previously stated, the requirements of this instrument involved the provision of an extremely high input impedance and an output impedance sufficiently low as to be compatible with the rest of the detection circuitry. Several designs of amplifier were examined in the course of the study, including electrometer and field-effect transistor systems, but none proved completely satisfactory. Finally, a commercial MOS FET amplifier, the Keithley model 302 was employed. This device, utilising a MOS FET input stage, was capable of very high input

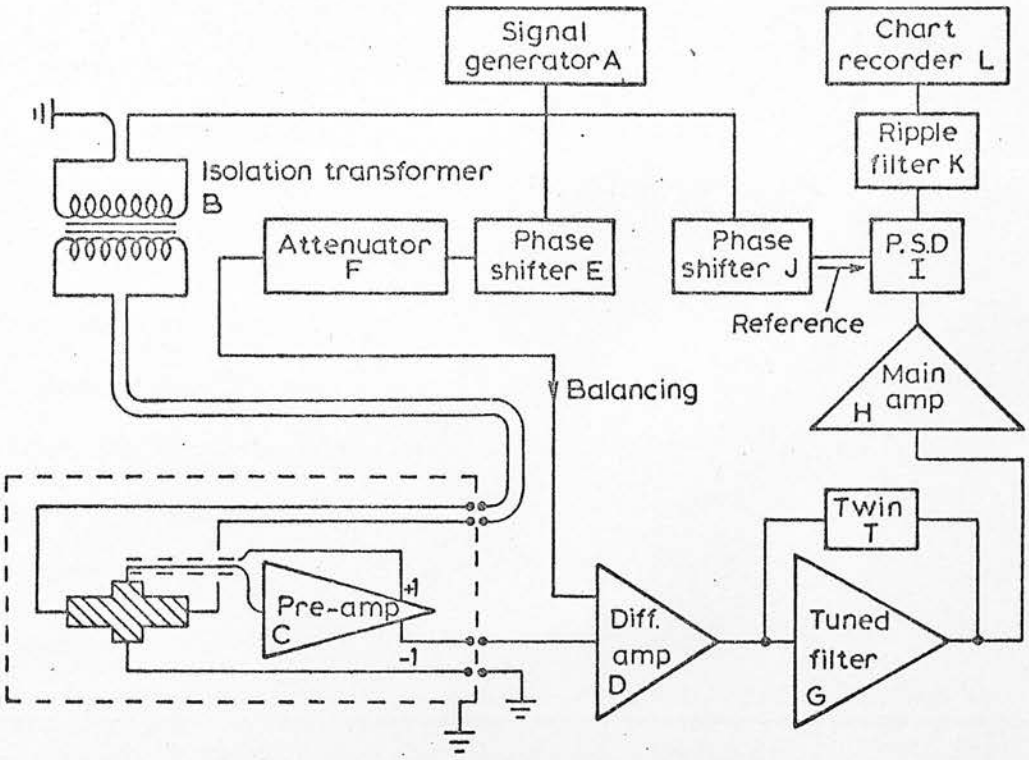

Fig. 61 Electrical System for Hall Effect Measurements

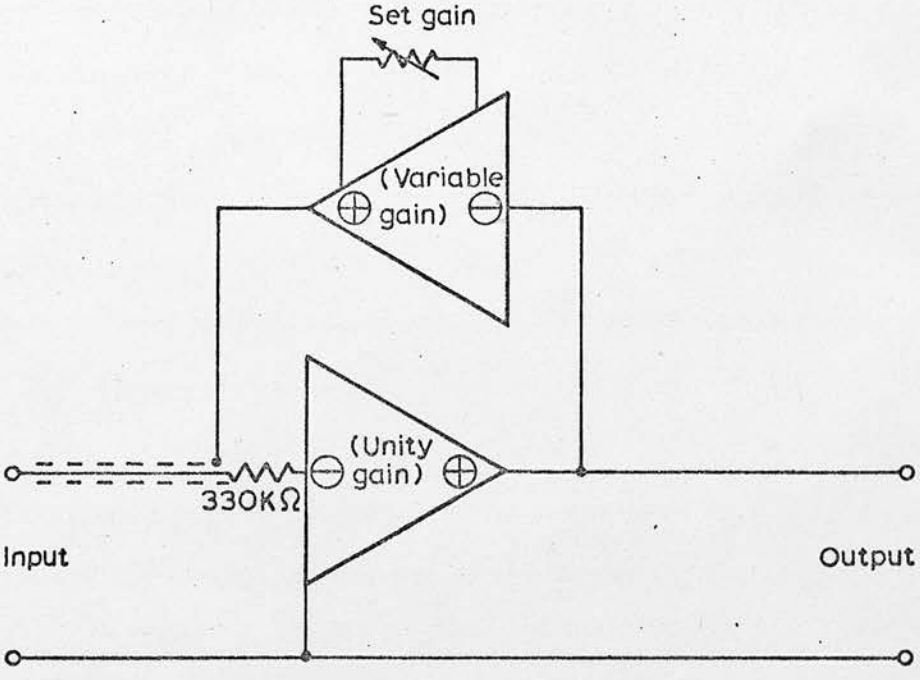

Fig. 62 Pre-amplifier Arrangement

impedance (10^{12} ohms) with a high degree of input protection (± 400 volts overload, in the configuration chosen). The input offset current was very low (10^{-14} amps.) reducing the tendency for polarisation of high impedance specimens. In the adopted arrangement, shown in figure 62, the amplifier was operated in a unity-gain inverting mode. A simple variable gain transistor inverter was fed from the amplifier output and used to drive a shield around the input lead between the specimen and the pre-amplifier, so as to minimise capacitative losses in the input circuit. By this means, it was possible to achieve an input impedance for the complete arrangement of better than 10^{12} ohms at frequencies up to 10 kHz, the upper limit being set by the tendency for the system to break into oscillation if the feedback to the input shield was excessive. The system gain was found to be constant (at unity) over the frequency range 10 Hz to 10 kHz.

(D) The Balancing Section. Situated close to the output of the commutator section of the specimen holder, this system served to eliminate the bulk of the spurious pick-up at the operating frequency of the equipment. The arrangement consisted of an R.C.A. 3008 Operational Amplifier, operating in a differential input mode at low gain (∿ 20x). The non-inverting input was driven from the pre-amplifier output, whilst the inverting input was driven by the 'balancing' signal. This latter was derived from the signal generator via a 0 to 360° phase changing amplifier, E, fitted with a ten-turn helical potentiometer for fine adjustment of the output level (modified version of the Brookdeal FP 317). A stepped attenuator, F, served to reduce the output of the phase shifter to

a level comparable with that of the pick-up signal to be eliminated.

(G) The Tuned Amplifier. Situated on the same circuit board as the 'balancing' amplifier was a second R.C.A 3008 amplifier employing selective feedback in order to filter unwanted frequencies from the signal at this stage. A series of double R C 'T' section feedback elements, mounted on plug-in boards, were constructed to cover the frequency range 20 Hz to 10 kHz. In the case of removal of the feedback element, the system functioned as a non-selective amplifier and the total gain of the balance and 'filter' amplifiers was set to 400 x. With the feedback elements in place, very high rejection of unwanted frequencies was possible (e.g., for a centre frequency of 236 Hz, and with the amplifier operating at very high gain, a 'Q' of 60 could be obtained, giving a band pass of 4 Hz and 43 dB of rejection at 50 Hz). However, such high selectivity had undesirable side effects, since small drifts of the signal frequency produced large variations in the phase and magnitude of the amplified signal. In practice, therefore, the Q was reduced so as to provide acceptable performance, whilst still maintaining a satisfactory rejection of 50 Hz pick-up.

(H) The Main Amplifier. A Brookdeal Model LA 635 amplifier, capable of 75 dB of gain in its main section, and an extra 20 dB of gain in an incorporated pre-amplifier, was used for the purpose of amplifying the tuned filter output to an easily detectable level.

(I) The Detector. Detection and rectification of the output signal was accomplished by means of a Brookdeal PD 629 phase-sensitive detector (P.S.D.) Such an instrument provides an output proportional to $V_o \cos \phi$, where V_o is the magnitude of the input signal at

frequency f_o (the operating frequency), and ϕ is the phase angle between the input signal and a reference signal at frequency f_o. The reference signal was provided from the signal generator via a variable phase shift amplifier (Brookdeal FP317). By virtue of its operating mechanism, a phase-sensitive detector acts as a filter to frequencies other than the reference frequency, the filter bandwidth being approximately equal to reciprocal of the time constant of the detection equipment driven by the P.S.D output. In the present system, the P.S.D was followed by an R-C ladder smoothing filter, K, to eliminate f_o ripple which was present on the output, and the resulting d.c. signal could be capacitatively integrated. Final detection was performed using a Toa Model EPR-2TD pen recorder, L, capable of 1 mV/cm sensitivity, and having a full scale deflection time constant of the order of 0.3 sec. Thus, with no capacitative integration, the P.S.D bandwidth was of the order of 3 Hz, whilst integration provided a further decrease in this bandwidth. In the development of the system, an Astrodata direct reading nanovoltmeter, type 121Z, was used in place of the pen recorder, but examination quickly revealed the enormous advantage of a recording instrument in terms of the capability for subsequent examination and analysis of the output data.

To obtain optimum performance from the equipment described above, it was necessary to make a thorough examination of the possibility of spurious pick up within the measurement system. In particular, it was necessary to eliminate all possible earth loops in the equipment. For instance, in the arrangement shown in figure 61, a potential loop existed in the earthed outer conductors

of the cables connecting the component route A-E-F-D-G-H-I-J-A. This loop was eliminated by disconnecting the outer conductor of cable A-J at J. Other, less evident loops were detected and similarly broken, and a further improvement was made by considering the problems inherent in attaching all the instruments to a common frame. Where necessary, instruments were detached from the frame to eliminate loops. In addition, all the instruments were connected to the 50 Hz power mains earth at a single point, rather than separately. Finally, having minimised pick-up due to earth loops, it was necessary to ensure that all cables were rigidly attached to the framework so as to prevent vibrational interference.

Operation of the Measurement System

In view of the complexity of the measurement system, the alignment of the components and calibration of the system was of a somewhat detailed nature. The procedure adopted was as follows:

(i) A low level signal was applied to the Hall specimen via the transformer.

(ii) With no 'balancing' input, the signal at the output of the tuned filter, G, was monitored on an oscilloscope.

(iii) The oscillator frequency was tuned to give maximum signal level for the particular 'twin T' in use with the tuned filter, thus setting the measurement frequency.

(iv) The system was reconnected and the output of the main amplifier, H, was applied to the oscilloscope 'y' plates. Since the bulk of the signal at this stage could be expected to be due to probe misalignment, and thus to be approximately in phase with the Hall signal, it was possible to effect a preliminary alignment of the

reference signal. This latter was applied to the oscilloscope 'x' plates, and the phase shifter, J, was adjusted until the elliptical Lissajous' figure displayed on the oscilloscope was reduced to a straight line.

(v) Returning the oscilloscope to its internal time base, a 'balancing' signal was applied to the differential amplifier, and its amplitude and phase were varied by means of the phase shifter, E, to minimise the amplifier output. The specimen signal generator output level was then progressively increased with periodic small adjustments to the balance controls to maintain minimum output amplitude.

(vi) The reference signal level was adjusted to provide a suitable signal for the P.S.D. The main amplifier gain was similarly adjusted to give the maximum output amplitude consistent with distortionless operation of the P.S.D.

(vii) The pen recorder was set to a suitable range, and its subsidiary d.c. bias control adjusted to give an on-scale reading.

(viii) The electromagnet was energised, and its current set to give a previously calibrated magnetic field strength.

(ix) The system was allowed to stabilise with periodic adjustments to the 'balancing' signal to maintain the output balance.

(x) After stabilisation was complete, the specimen holder was periodically rotated through 180° to reverse the specimen polarity in the magnetic field; a deflection approximately equal to twice the amplified Hall voltage being observed on the pen recorder. Slight adjustments to the reference signal phase were made to optimise these deflections. By periodically reversing the polarity

of the electromagnet current (and field), it was possible to ascertain that the deflections observed upon specimen reversal were, in fact, caused by the Hall signal rather than by pick-up variations. A number of specimen reversals were performed for both polarities of the electromagnet field to measure the Hall voltage.

(xi) Calibration of the gain of the system was performed in the following manner: since the gain of the pre-amplifier, C, was known to be -1 (to better than 1%), it was possible to calibrate the gain of the rest of the system by application of a known signal to the 'balancing' input of the differential amplifier, which had known gains for both of its input channels (see Appendix II). With no specimen output present, such a signal was applied, and the phase of the P.S.D reference signal was adjusted to give a maximum deflection upon phase reversal of the signal fed to the balance input. The system gain could thus be determined. The validity of this technique had been checked by measuring the deflection produced by applying a known signal to the pre-amplifier input through a high impedance, and observing the measured gain as compared to that determined by applying a signal to the balance input. Calibration of gain was performed both before and after Hall measurements at each frequency of measurement. The sign of the Hall signal was determined by a consideration of the relationship between the polarity of the magnetic field, phase reversals in the amplification system, and the direction of recorder deflection compared to the change in orientation of the Hall specimen. The identification of sign was further checked by observations on a germanium specimen which had previously been characterised by a conventional d.c. Hall measurement system.

7.2 Measurement Errors

The Hall mobility was determined from the experimental readings by application of equation 6.1.8, i.e.

$$\mu_H = \frac{V_y}{V_x} \cdot \frac{\ell}{w} \cdot \frac{10^8}{B_z}$$

The specimen input voltage, V_y, was measured by means of an output voltmeter on the signal generator; a correction for the gain of the input isolation transformer being necessary. The accuracy of the measurement was estimated as ± 2%.

The specimen length, ℓ, was determined by the length of the abrasion mask used in sample preparation. A correction was necessary to allow for the (small) reduction in length produced by fusing the contact wires into the bulk of the specimen. The accuracy of the measured length was estimated as ± 2%.

The width, w, was again determined by the dimensions of the abrasion mask. No correction was necessary to allow for the 'fusing in' of the electrodes, since this took place in the side arms of the specimen. However, the width was relatively small (0.1 cm), and the abrasion technique tended to produce a slight variation of width so that the specimen cross section was not perfectly rectangular in shape. Thus, the error in the width was relatively large, being of the order of ± 10%.

The magnetic field strength, B, was measured using a Hall probe magnetometer, with an accuracy of the order of ± 2%. The measuring equipment was not of sufficiently small dimensions to permit any investigation of the possible variation of magnetic field strength with position in the magnet pole gap but it was indicated that such

variations, if present, did not constitute more than an extra 2% error in the assumed value of the field across the specimen. A total error in B of ± 4% is thus considered to be a reasonable estimate.

The accuracy of the measured Hall voltage was of a composite nature, consisting of the error in the measurement equipment gain, and the statistical error in the actual measurements. The former, including any error in the setting of the phase relationship between the Hall signal and the P.S.D. reference signal, was estimated as ± 5%. In the measurements on the system $As_2Te_3Tl_2Se$, between 20 and 30 deflection readings were averaged to obtain the Hall voltage during each individual measurement. Statistical analysis of the readings indicated an r.m.s. error in the average value which varied from 5% to 25%. The average r.m.s. error in all the measurements was approximately 15%, with almost all the individual errors being close to this value.

Accumulating the above errors, the total accuracy of the Hall measurements on the system $As_2Te_3Tl_2Se$ was found to be ± 38%. Since the major interest of the investigation was in the examination of the dependence of the Hall mobility on temperature and frequency, it is relevant to divide this error into terms which could be expected to vary during the experiment, and terms which would be fixed. Thus, for instance, the inaccuracies in the measurements of the length and width of the specimen would affect each measurement in an identical manner, whilst statistical errors in the values of V_y would vary from measurement to measurement. Dividing the total error in this way, it has been estimated that the error in the points plotted

in figures 64 and 65, relative to each other, is of the order of ± 20%.

7.3 Experimental Results

a) The vitreous 'alloy' $As_2Te_3Tl_2Se$.

A specimen of this material was prepared as previously described, and was found to have a d.c. impedance between the Hall probes of the order of 10^3 ohms at room temperature. During the Hall measurements, the apparatus was found to perform very satisfactorily, with an easily identifiable Hall signal being observed. Figure 63 shows a typical recorder trace of the Hall signal, and it will be noted

(1) that the overall stability of the system with respect to drift was relatively good,

(2) that the observed deflections can be positively associated with a Hall signal, rather than a change in 'pick-up' as the specimen was rotated, since reversal of the polarity of the magnetic field caused the directions of the individual deflections to be reversed.

The Hall mobility was measured as a function of frequency over the range 60 Hz to 10 kHz (at room temperature), and as a function of temperature over the range 20°C to 80°C (at a frequency of 520 Hz). Figures 64 and 65 show the results of these measurements. In all cases, the Hall mobility was found to have a sign characteristic of predominantly n-type transport.

b) Arsenic Triselenide.

In a specimen of this material, the d.c. impedance between the Hall probes was found to be 3×10^9 ohms at 100°C, and 2×10^7 ohms at 170°C. Since the input impedance of the pre-amplifier was of the order of 10^{12} ohms, it was apparent that no 'shorting out' of

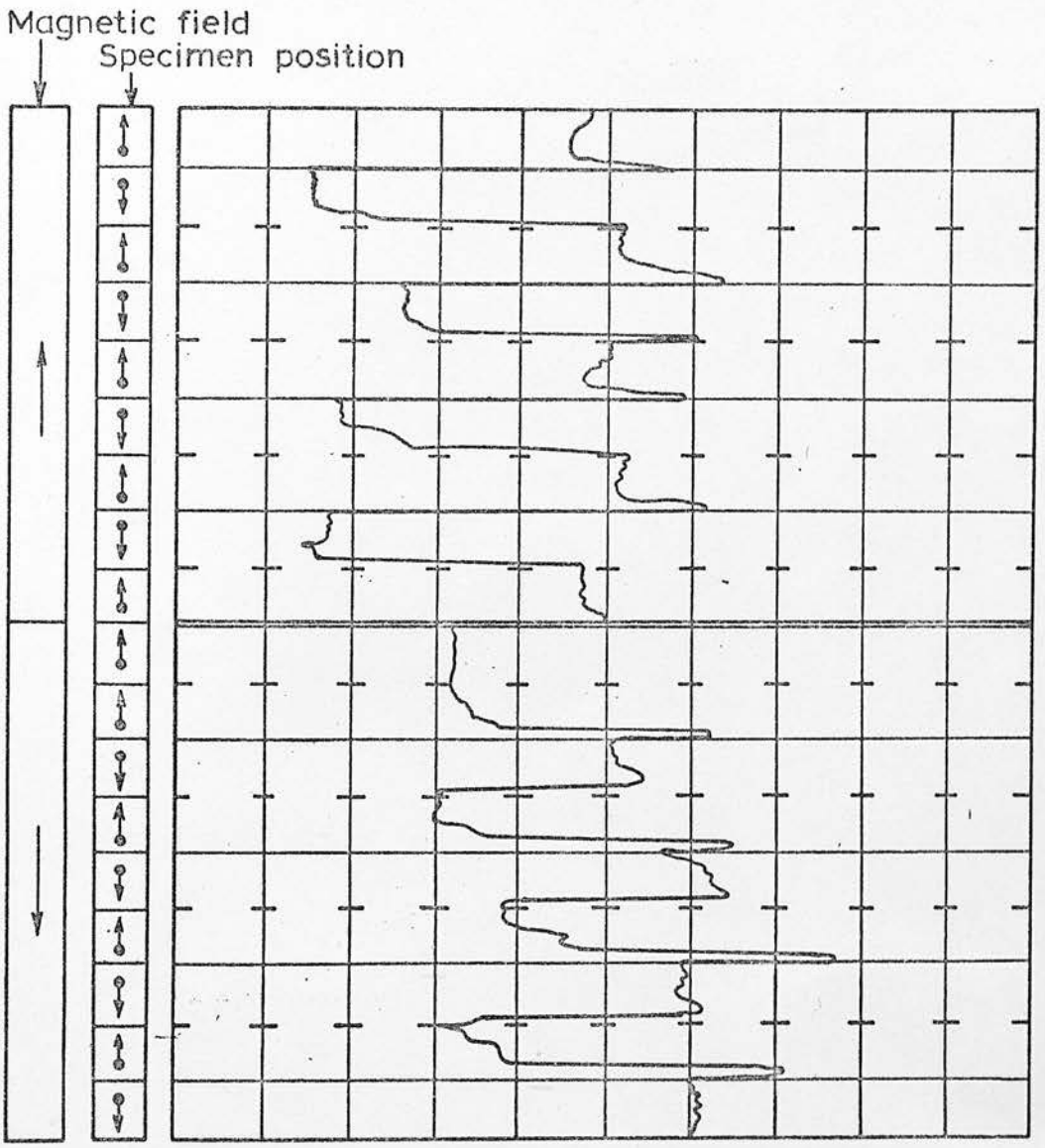

Fig. 63 Output Trace: Hall Signal in $As_2Te_3Tl_2Se$

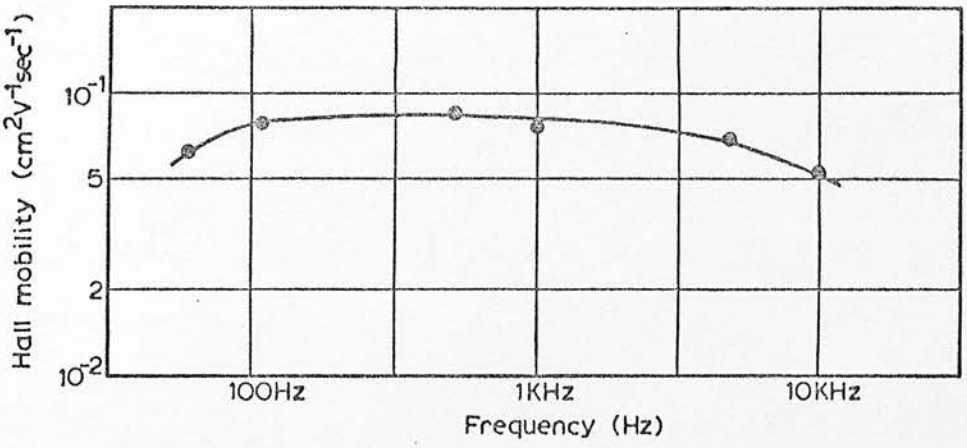

Fig. 64 Variation of Hall Mobility with Frequency at Room Temperature: $As_2Te_3Tl_2Se$

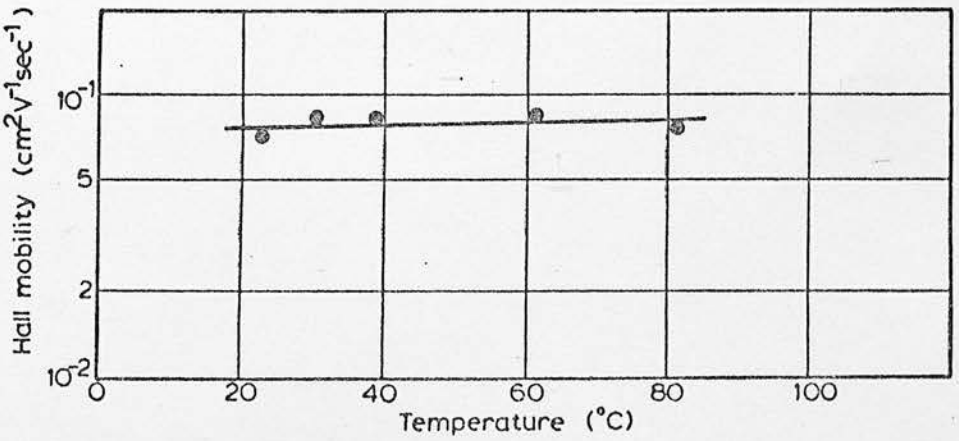

Fig. 65 Variation of Hall Mobility with Temperature at a Frequency of 520Hz: $As_2Te_3Tl_2Se$

the Hall signal should occur due to the measurement equipment. However, the use of a specimen of such high impedance was found to greatly increase the noise level and drift rate of the output signal. In a series of examinations utilising measurement frequencies from 60 Hz to 1 kHz, and temperatures from 20°C to 170°C, no Hall signal was detectable. The resolution and stability of the equipment was such that a Hall signal of 1 μV would have been detected fairly readily, so that it was evident that the Hall mobility was very low. An upper limit for the mobility may be estimated by substituting the system parameters in equation 6.1.8. Thus, taking

input voltage, V_y, = 2V

length/width ratio, ℓ/w, = 8

magnetic field strength, B_z, = 17 kiloGauss

Hall voltage V_x, $\leq$ 1 μV.

then,

$$\mu_H \leq \frac{10^{-6}}{2} \cdot 8 \cdot \frac{10^{8}}{1.7 \times 10^{4}}$$

$$\leq 2 \times 10^{-2} \text{ cm}^2\text{V}^{-1}\text{sec}^{-1}$$

Attempts were made to improve the stability of the equipment by achieving a more stable control of the specimen temperature, since temperature variations appeared to constitute the major source of the drift which limited the stability. However, positive results were not achieved and the experiment was terminated to allow concentration on the drift mobility examination.

7.4 Discussion and Analysis

a) General Performance of the Equipment

The equipment employed during this study had the advantage

of relatively simple construction, since no sophisticated components such as a high power a.c. solenoid or an Amplidyne control for magnetic field reversal were required. In fact, almost all the components were of a standard design. The performance was found to be fairly satisfactory, and the system allowed the measurement of mobilities of less than 10^{-1} $cm^2V^{-1}sec^{-1}$. As previously indicated, the stability of the specimen temperature control proved to be the limiting factor in the examination of materials of very high resistivity. It is considered likely that, with refinements to this control, the sensitivity could be extended to allow the measurement of mobilities of well below 10^{-2} $cm^2V^{-1}sec^{-1}$ in materials of resistivity at least up to 10^9 ohm cm.

b) $As_2Te_3Tl_2Se$.

The magnitude and negative sign of the Hall mobility in this material are in agreement with the data published by Kolomiets and Nazarova[25] on the system $Tl_2Se.As_2(Se_3,Te_3)$. These authors also reported a positive sign for the thermoelectric power, so that an anomaly between the Hall and thermoelectric data was evident. The thermopower was not examined in the present study, so that the anomaly is not positively re-affirmed, but the negative sign of the Hall mobility is considered to reinforce the likelihood of its occurrence.

The lack of any appreciable temperature dependence of the Hall mobility also appears to be a general characteristic of vitreous semiconductors[22-26]. In the present study, allowing for an accuracy of ± 20% in the points in figure 65, an activation energy of less than 0.06 eV is indicated, and it is likely that the

activation energy is less than 0.02 eV. As mentioned previously, the low magnitude, temperature insensitivity, and anomalous sign of the Hall mobility in vitreous semiconductors have not been completely explained in terms of current theories of conduction in such materials. An interpretation in terms of hopping transport seems to provide the best approach to the situation, but the theoretical conditions to be expected in such a case have not been completely resolved at present.

The frequency dependence of the Hall mobility in vitreous semiconductors does not appear to have been previously examined. The results of the present study indicate the mobility to be almost unaffected by frequency changes within the range 60 Hz to 10 kHz. The slight reductions in the value of the measured mobility at the extremes of the frequency range, as shown in figure 64, are possibly due to the response limits of the equipment, although it is equally possible that the effect is erroneous, bearing in mind the estimated accuracy of ± 20% in the experimental points. Theoretical examination of the frequency dependence of the Hall mobility in the hopping region appears to be limited to the study by Holstein[100] of impurity hopping in crystalline semiconductors at low temperatures. Holstein finds that both the hopping probability and the hopping distance are frequency dependent, but it has not been possible to make a quantitative application of his analysis to the situation in vitreous semiconductors. More qualitatively, it may be argued that the lack of any significant frequency dependence of the Hall mobility in $As_2Te_3Tl_2Se$ indicates Holstein's analysis to be inapplicable. Even so, this does not rule out the possibility of hopping conduction in the material, since it is not known whether other forms of hopping would be frequency dependent.

c) Arsenic Triselenide

In the absence of a positive measurement of the Hall mobility in this material, it is impossible to make any quantitative assertions. However, the fact that the mobility was almost certainly less than 10^{-2} $cm^2V^{-1}sec^{-1}$ at temperatures up to 170°C, and for a range of measurement frequencies, deserves some discussion. The observations would seem to be particularly in contradiction to an 'island' structural model, since the high (> 100 $cm^2V^{-1}sec^{-1}$) zone mobility would be expected to produce a signal indicating a mobility of substantially over 10^{-2} $cm^2V^{-1}sec^{-1}$ in an a.c. measurement. If, alternatively, a hopping mechanism is suggested, further problems arise when the results of the present drift mobility examination are considered. It will be recalled that, in Chapter Five, it was estimated that the pre-exponential factor in the expression for the drift mobility was too high to be consistent with hopping motion. In fact, assuming a relationship of the form

$$\mu_d = \frac{A}{T} \exp(-\varepsilon/kT)$$

the constant A was found to be of the order of 10^4 $cm^2V^{-1}sec^{-1}$ °K, giving a pre-exponential 'mobility' of about 30 $cm^2V^{-1}sec^{-1}$ at room temperature, whilst hopping motion would not be expected to give a pre-exponential factor of more than 10^{-1} $cm^2V^{-1}sec^{-1}$. It was concluded in the drift mobility examination that the results were best interpreted in terms of diffusive motion within the band states, and the analysis gave a realistic value of the diffusion distance, a. The behaviour of the Hall mobility in the diffusive region has received no extensive theoretical examination, although Mott[4] has noted the possibility that the sign of the Hall mobility may be

anomalous. From the present examination, it is certainly evident that the magnitude of the Hall mobility is anomalously low if diffusive motion is assumed. Mott[4] indicates that a Hall mobility greater than 10 $cm^2V^{-1}sec^{-1}$ is to be expected, and in the present case the Hall mobility would be expected to be of the order of 30 $cm^2V^{-1}sec^{-1}$ (i.e. the pre-exponential 'mobility' obtained from the drift mobility measurements). In the absence of a rigorous theoretical examination of the nature of the Hall mobility in the diffusive region, the situation must remain unresolved.

d) Conclusions

It is evident that a great deal of study, both of a theoretical and of a practical nature, is required with respect to the form of the Hall mobility in non-crystalline materials. It is felt that practical examinations on thin-film specimens, utilising experimental arrangements such as that described by Redfield[119] may well be of value, especially in that such techniques might allow an examination of material in the 'on' switching state. However caution will be required in the interpretation of such measurements, which normally rely on the photo-excitation of carriers and are often virtually a combination of Hall and drift mobility techniques.

Chapter Eight

Bistable Switching

8.1 Introduction

The phenomenon of switching in non-crystalline semiconductors has recently received a great deal of attention[41-43,73,122-126]. Two forms of switching, termed threshold and memory mechanisms, have been observed. The former concerns the occurrence of a voltage/current relationship of the form shown in figure 66a. The characteristic exhibits a range of differential negative resistance which may be as high as 10^6 ohms. The latter is fundamentally similar in this respect, but an additional 'memory' property is exhibited, as shown in figure 66b. Here, the 'off' (high resistance) state and the 'on' (low resistance) state may differ in resistance by a factor of over eight orders of magnitude. Switching from the off state occurs at a critical value of the applied field, and the device transfers to the on state, in which it remains even when the applied field is reduced to zero. Switching in the reverse direction is accomplished by the passage of a relatively large current pulse through the specimen. Overall agreement upon the nature of the switching process has not been reached, nor is it certain that the process is identical in different materials. Proposed mechanisms have included phase transitions, double carrier injection effects, field controlled dipole phenomena, filament formation within a localised (molten) region, and other processes. Since the observations to be described below are essentially of a superficial nature, it is not proposed to examine such suggestions in any further detail in this account.

The present report concerns the observation of bistable

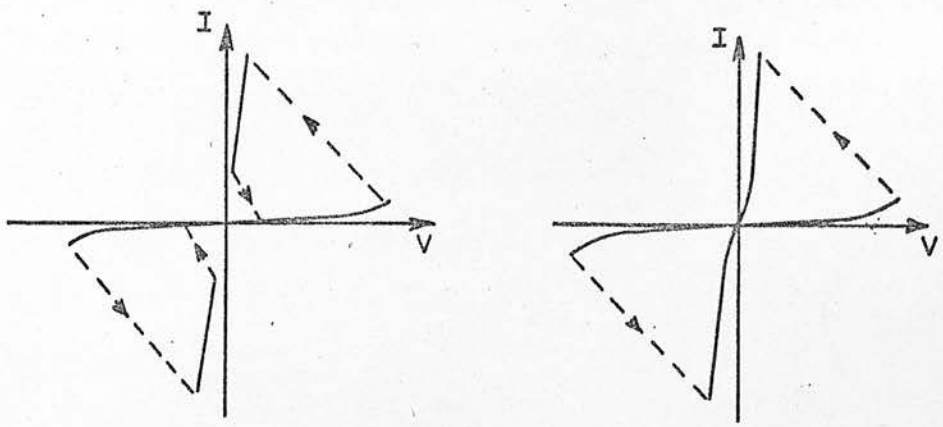

(a) Threshold switch

(b) Bistable (memory) switch

Fig. 66 Switching Characteristics of Amorphous Semiconductors

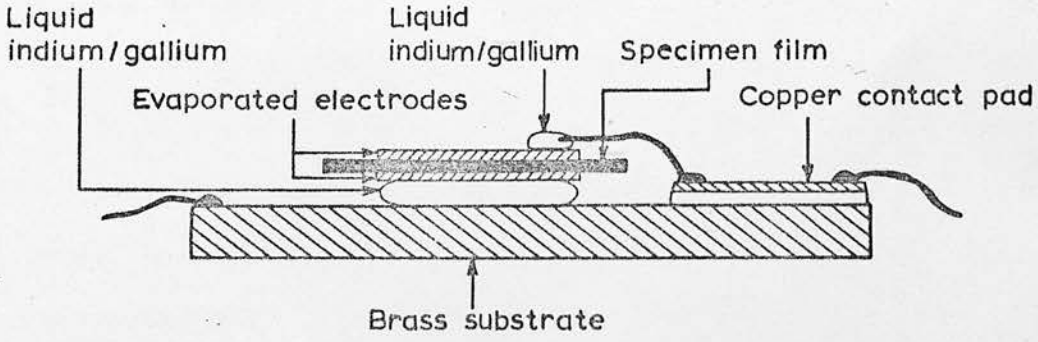

Fig. 67 Specimen Configuration, as used to Examine Switching Properties

(memory) switching in the thin films of arsenic triselenide which were prepared during the drift mobility examination. It is relevant to note that almost all of the switching effects reported in the literature have involved materials of complex composition. The present results are thus of interest in that they describe switching in a material of simple composition, of which the electrical properties have received a relatively high degree of previous examination.

8.2 Experimental Results

The examination utilised thin film specimens, the preparation of which is described in Chapter Three. Film thicknesses were typically from 1 to 5 microns, and aluminium evaporated electrodes were normally employed. In order to allow the dissipation of relatively high power levels due to ohmic heating in the on state, the specimen mounting configuration was modified from that used in drift mobility experiments. The modified arrangement is shown in figure 67. Specimens were mounted on a thick brass substrate measuring approximately 2 x 2 cm in area. Thermal and electrical contact between the specimen and the substrate was achieved by means of a liquid indium/gallium alloy. A further spot of this alloy on the upper surface of the specimen served to provide electrical contact between the upper electrode and a copper wire via which connection to the measurement circuitry was made. The electrical characteristics of the films were determined using an electrometer ohm-meter for low field resistance measurements in the off state, and a Tektronix Type 575 transistor curve tracer for the switching measurements. Specimens in the off state were characterised by a low field resistivity of about

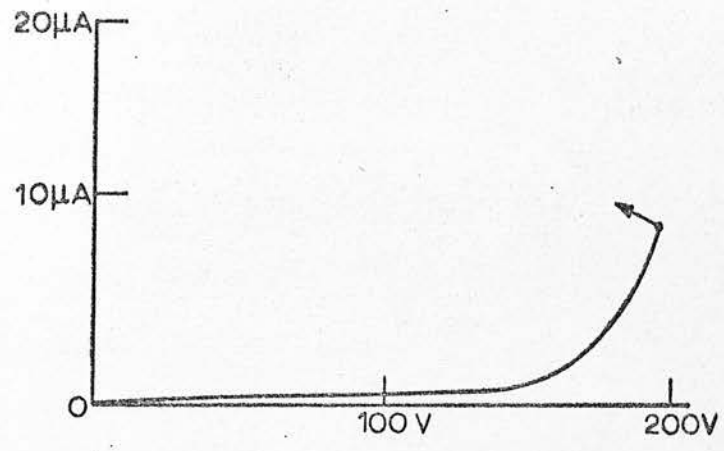

(a) Off state

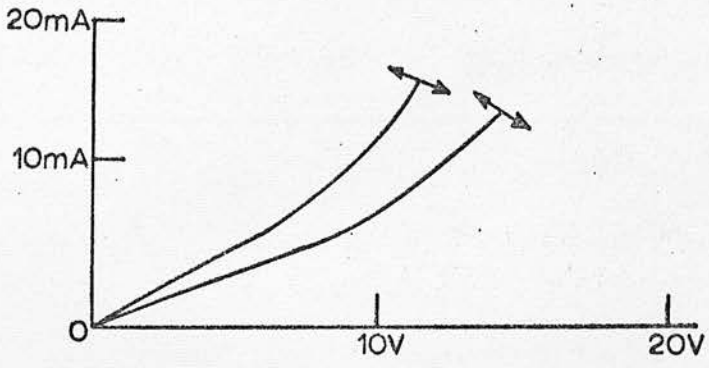

(b) Intermediate state

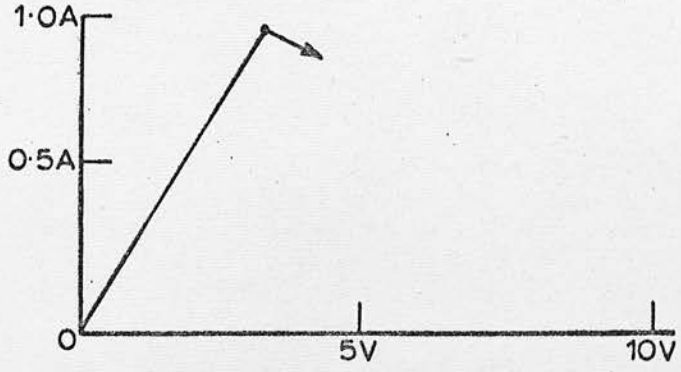

(c) On state

Fig. 68 Bistable Switching Phenomenon: As_2Se_3

10^{11}ohm cm, and shielding of the samples from light was necessary to avoid photoconductive effects in the measurement. The dynamic characteristics of the specimens are illustrated in figure 68. The off state is shown in 68a. In this state, the specimens exhibited a field-dependent resistivity, but the high value of the resistance and hysteresis effects in the measurement system did not allow accurate examination of this state using the curve tracer. Switching occurred at a field value of between 5×10^5 and 10^6 $V.cm^{-1}$., the critical field value being constant to within 10 to 20% for repeated switching of individual specimens. To prevent destructive ohmic heating upon switching, a 10^5 ohm resistor was connected in series with the specimen when voltages were applied in the off state. Upon application of fields greater than the critical value, specimens switched to one of a set of intermediate states as shown in figure 68b. These states were characterised by resistivities in the range 10^5 to 10^6 ohm cm and were intrinsically unstable, being defined by the specimen current level as controlled by circuit series resistors etc. Removal of the 'holding current' from a specimen in an intermediate state caused it to revert to the off state, whilst increase of the current caused further switching into the on state, as shown in figure 68c. This was characterised by a resistivity of approximately 100 ohm cm and was virtually ohmic in nature. A specimen in this state remained there upon the removal of the applied field. With the specimen dimensions adopted, 'on' resistances were in the range 1 to 10 ohms, and currents in excess of 1 amp could be passed without any sign of degradation of properties. Switching to the off state was accomplished by the application of a current pulse, usually supplied

by connecting a 24 volt battery directly across the specimen. The indications were that a great many switching operations could be performed on a single specimen.

The switching phenomenon was also investigated in specimens with gold and silver evaporated electrodes. It was found that the critical voltage was markedly greater in specimens with gold electrodes, whilst those with silver electrodes exhibited a substantially lower 'off resistance' and did not produce reliable switching devices. It is considered likely that the former effect was due to differences in the carrier injection characteristics of gold and aluminium, whilst the latter effect was due to a bulk conductivity reduction following silver diffusion.

A notable factor in the examination was that several specimens were found to be in the on state immediately after preparation, and before the application of any large electric field. Whilst it is possible that electrostatic charging of the films during the evaporation and mounting procedures might have generated the required switching field across such specimens, it is considered to be more likely that the specimens were, in fact, prepared in the on state. If this were so, it would seem to add weight to the theories proposing that the switching phenomenon involves structural reorganisations in the bulk of the specimen, rather than to theories concerning field-induced injection or polarisation effects. It should be mentioned that specimens found to be in the on state upon initial examination behaved in a normal manner during subsequent switching operations. Presumably, the failure to observe the spontaneous occurrence of the on state in thicker specimens would

be a consequence of the statistical processes involved in the production of the state, greatly favouring observations in very thin films.

8.3 Discussion

An interesting speculation which arises from the results of the present study is the possible relationship between the switching phenomenon and the dependence of the carrier drift mobility on the value of the electric field. Thus, for instance, one theory of the switching process envisages the localised heating of a small area of the device, with such heating reducing the conductivity and so increasing the local current. The increase in current then further accelerates the heating, and the process 'avalanches' until a molten filament is produced across the specimen. A great deal of controversy has arisen as to whether the localised heating can be of sufficient magnitude as to be consistent with the very fast switching speed[123,124], and the change of the conductivity with temperature (i.e. the activation energy) becomes the central criterion in evaluating the validity of the model. No serious consideration of the possibility that the mobility of the carriers might increase rapidly with electric field, for fields of the order of the switching value, appears to have been made. However, it would appear that such an increase would rapidly accelerate the switching process, and it will now be demonstrated that sizeable mobility increases may well occur in the switching region.

First, it is necessary to review the results of the examination of the drift mobility in arsenic triselenide, as presented in Chapter Five. It will be recalled that the hole drift mobility

was found to be very low, and that both the magnitude and activation energy of the mobility were found to be field dependent. It was concluded that the experimental data could best be interpreted in terms of trap-controlled band motion, with transport within the band states being envisaged as a diffusive process. The dependence of the mobility on temperature and electric field could then be expressed by an equation of the form

$$\mu_d = \frac{A}{T} \exp(-\varepsilon/kT) \exp(\beta E^{\frac{1}{2}}/kT) \qquad (8.3.1)$$

with $A \simeq 10^4$ $cm^2V^{-1}sec^{-1}$ ^oK, $\varepsilon \simeq 0.46$ eV, and $\beta \simeq 4.3 \times 10^{-4}$ $eV/V^{\frac{1}{2}}cm^{-\frac{1}{2}}$. It is evident from this expression that the activation energy would be reduced to zero at an applied field of approximately 10^6 V/cm, at which point the shallow (mobility controlling) traps would be completely delocalised. The mobility would then be equal to $A/T \simeq 30$ $cm^2V^{-1}sec^{-1}$ at room temperature. Comparing this figure with the value of approximately 3×10^{-7} $cm^2V^{-1}sec^{-1}$ which is estimated at zero field, it is evident that the mobility variation is by no means insignificant. In addition, the mere fact of the delocalisation of the trapping centres may serve to further increase the mobility. In this situation, it is possible that the carriers may move further into the band states, so that 'conventional' band motion, characterised by a mobility in excess of 100 $cm^2V^{-1}sec^{-1}$, will occur.

In a situation where the carrier transport occurs by a hopping process, as suggested for hole carriers in selenium at low temperatures (see Chapter Five), field modification of the mobility may produce even more drastic effects. Thus, considering the low temperature data in figure 30, it appears that the slope of the mobility/temperature curve will be reduced to zero at a field of the

order of 10^6 V/cm, at which point the mobility should be of the order of 10^{-1} $cm^2V^{-1}sec^{-1}$. It is difficult to envisage a situation in which the hopping mobility could increase appreciably with decreasing temperature, and it is considered possible that, for higher values of applied field, the carriers might be transferred to the band states. If this were so, the mobility would be expected to exceed 100 $cm^2V^{-1}sec^{-1}$, and a rapid increase in mobility would thus occur for fields of the order of 10^6 V/cm.

It is realised that the above argument is of a speculative nature, and that switching has not been observed in selenium, possibly because no examination at sufficiently high values of applied field has been performed. Furthermore, the increase in mobility at high fields does not, in itself, lead to a 'memory type' behaviour, so that it is still necessary to assume some mechanism such as local fusion to account for such an effect. Even so, it has been indicated that the behaviour of the mobility during the switching operation should not be neglected in performing theoretical calculations.

Appendix I. Experimental Readings

Summary of Results

Material	Drift Mobility	Hall Mobility
Se	Holes: $\mu_d = 0{\cdot}133\,cm^2V^{-1}sec^{-1}$ at $300^\circ K$ Field effect at low T. $\mu_d = 25\exp(\frac{-0{\cdot}135}{kT}) + \frac{20}{T}\exp(\frac{-0{\cdot}05}{kT})$ Electrons: $\mu_d \sim 2\times10^{-2}\,cm^2V^{-1}sec^{-1}$ at $300^\circ K$	Not examined. See p.131 for Dresner's examination.
Se+1%Ge	Holes: $\mu_d = 0{\cdot}147\,cmV\,sec$ at $300^\circ K$ Field effect at low T. $\mu_d = 11\exp(\frac{-0{\cdot}111}{kT}) + \frac{7{\cdot}2}{T}\exp(\frac{-0{\cdot}0305}{kT})$ Electrons: $\mu_d \sim 5{-}10\times10^{-4}\,cm^2V^{-1}sec^{-1}$ at $300^\circ K$	Not examined.
Se+3%Ge	Holes: Deep trapping. Electrons: $\mu_d \sim 10^{-4}\,cm^2V^{-1}sec^{-1}$ at $300^\circ K$	Not examined.
Se+5%Ge	Holes & Electrons: deep trapping.	Not examined.
Se+7%Ge	Holes: Deep trapping. Electrons: $\mu_d \sim 2{\cdot}5\times10^{-4}\,cm^2V^{-1}sec^{-1}$ at $300^\circ K$	Not examined.
As_2Se_3	Holes: Strong field effect At zero field, $\mu_d \sim 10^{-6}$ at $300^\circ K$ " " " $\varepsilon_{act} \sim 0{\cdot}45\,eV$ Electrons: Deep trapping	$\mu_H \lesssim 10^{-3}\,cm^2V^{-1}sec^{-1}$
As_2Se_2Te	Holes: $3\times10^{-3} \lesssim \mu_d \lesssim 10^{-2}\,cm^2V^{-1}sec^{-1}$ Electrons: Deep trapping	Not examined. See p.112 for comments on Male's examination.
$As_2Te_3I_2Se$	Not examined ('high' conductivity).	$\mu_H \sim 8\times10^{-2}\,cm^2V^{-1}sec^{-1}$. Essentially unactivated.

Ia. Room Temperature Hole Drift Mobility for Various Specimens of Selenium. (for Page 85)

Specimen	Electrodes Top	Bottom	Thickness (microns)	Field (V/cm)	Transit Time (μsec)	Mobility ($cm^2V^{-1}sec^{-1}$)
A	Au	Au	32.0	3.12×10^4	0.90	1.14×10^{-1}
M	Al	Al	37.5	2.67×10^4	1.03	1.37×10^{-1}
M	Al	Al	37.5	8.01×10^4	0.355	1.32×10^{-1}
R	Al	Al	44.0	2.27×10^4	1.21	1.60×10^{-1}
S	Au	Au	37.5	4.00×10^4	0.84	1.12×10^{-1}
V	Au	Al	41.0	2.44×10^4	1.15	1.46×10^{-1}
W	Au	Al	37.0	2.70×10^4	1.10	1.25×10^{-1}
Y	Al	Al	37.0	2.78×10^4	0.97	1.37×10^{-1}
Y	Al	Al	37.0	5.56×10^4	0.50	1.33×10^{-1}

Ib. Variation of Hole Drift Mobility with Temperature and Field.

Pure Selenium (Specimen M) (for Figures 30 and 41)

Temperature T °K	Field (V/cm)	Transit Time (μsec)	Mobility ($cm^2V^{-1}sec^{-1}$)
289	2.67×10^4	1.14	1.24×10^{-1}
289	5.34×10^4	0.57	1.24×10^{-1}
289	8.01×10^4	0.37	1.27×10^{-1}
254	2.67×10^4	2.08	6.78×10^{-2}
254	5.34×10^4	0.97	7.23×10^{-2}
254	8.01×10^4	0.635	7.41×10^{-2}
219	2.67×10^4	4.75	2.95×10^{-2}
218	5.34×10^4	2.10	3.36×10^{-2}
218	8.01×10^4	1.24	3.79×10^{-2}
217	10.68×10^4	0.91	3.89×10^{-2}
195	2.67×10^4	9.60	1.47×10^{-2}
195	5.34×10^4	4.40	1.60×10^{-2}
194	8.01×10^4	2.47	1.90×10^{-2}
194	10.68×10^4	1.70	2.07×10^{-2}
165	2.67×10^4	22.0	6.40×10^{-3}
165	5.34×10^4	9.60	7.35×10^{-3}
165	8.01×10^4	5.13	9.16×10^{-3}
166	10.68×10^4	3.22	1.09×10^{-2}
148	2.67×10^4	35.2	4.01×10^{-3}
147	5.34×10^4	15.4	4.59×10^{-3}
146	8.01×10^4	8.30	5.67×10^{-3}
145	10.68×10^4	5.32	6.62×10^{-3}
120	2.67×10^4	83.0	1.70×10^{-3}
120	5.34×10^4	30.7	2.30×10^{-3}
121	8.01×10^4	16.2	2.90×10^{-3}
121	10.68×10^4	9.80	3.60×10^{-3}
108	2.67×10^4	121	1.17×10^{-3}
108	5.34×10^4	40.0	1.76×10^{-3}
108	8.01×10^4	21.6	2.18×10^{-3}
108	10.68×10^4	13.5	2.61×10^{-3}

Ic. Variation of Electron Drift Mobility with Temperature; Pure Selenium (Specimen M, Applied Field = 9.35×10^4 V/cm)

Temperature T ^{o}K	Transit Time (μsec)	Mobility ($cm^2V^{-1}sec^{-1}$)
295	2.5	1.6×10^{-2}
312.5	1.85	2.2×10^{-2}
319.5	1.6	2.5×10^{-2}
322.5	1.6	2.5×10^{-2}
337.5	1.2	3.4×10^{-2}

Id. Room Temperature Hole Drift Mobility for Various Specimens of Selenium + 1% Germanium (for page 87)

Specimen	Electrodes Top	Bottom	Thickness (microns)	Field (V/cm)	Transit time (μsec)	Mobility ($cm^2V^{-1}sec^{-1}$)
C	Al	Al	42.5	2.35×10^4	1.29	1.40×10^{-1}
F	Al	Au	49	2.06×10^4	1.65	1.44×10^{-1}
H	Al	Al	36	2.78×10^4	0.93	1.39×10^{-1}
X	Al	Al	42.5	2.36×10^4	1.09	1.65×10^{-1}

1e. Variation of Hole Drift Mobility with Temperature and Field.

Selenium + 1% Germanium (Specimen H) (for Figures 32 & 46).

Temperature T °K	Field (V/cm)	Transit Time (μsec)	Mobility ($cm^2V^{-1}sec^{-1}$)
293	$2.78x10^4$	0.94	$1.38x10^{-1}$
231.5	$5.56x10^4$	1.03	$6.26x10^{-2}$
214	$3.89x10^4$	2.24	$3.86x10^{-2}$
197	$5.56x10^4$	2.12	$3.06x10^{-2}$
194	$2.78x10^4$	5.60	$2.32x10^{-2}$
193	$5.56x10^4$	2.66	$2.44x10^{-2}$
193	$8.35x10^4$	1.71	$2.53x10^{-2}$
192	$11.12x10^4$	1.04	$3.12x10^{-2}$
184	$6.95x10^4$	1.98	$2.61x10^{-2}$
170	$6.95x10^4$	2.52	$2.06x10^{-2}$
162	$2.78x10^4$	11.1	$1.17x10^{-2}$
162	$5.56x10^4$	4.77	$1.37x10^{-2}$
163	$8.35x10^4$	2.59	$1.67x10^{-2}$
163	$11.12x10^4$	1.64	$1.98x10^{-2}$
145	$9.75x10^4$	2.59	$1.43x10^{-2}$
139	$2.78x10^4$	20.9	$6.22x10^{-3}$
140	$5.56x10^4$	7.3	$8.91x10^{-3}$
141	$8.35x10^4$	4.0	$1.09x10^{-2}$
142	$11.12x10^4$	2.41	$1.35x10^{-2}$
133	$8.35x10^4$	4.2	$1.03x10^{-2}$
123.5	$8.35x10^4$	4.43	$9.77x10^{-3}$
106.5	$2.78x10^4$	29.1	$4.46x10^{-3}$
106.5	$5.56x10^4$	11.9	$5.44x10^{-3}$
106.5	$8.35x10^4$	6.57	$6.62x10^{-3}$
106.5	$11.12x10^4$	3.53	$9.18x10^{-3}$

If. Electron Transit in Selenium + 1% Germanium (Specimen H)

(for page 87)

Temperature T °K	Field (V/cm)	Transit Time (μsec)	Mobility ($cm^2V^{-1}sec^{-1}$)
297.5	$6.67x10^4$	9.5	$5.7x10^{-3}$
297.5	$6.67x10^4$	6.5	$8.3x10^{-3}$
297.5	$9.34x10^4$	7.25	$5.3x10^{-3}$

Comments.

Pulse completely rounded and of relatively small amplitude. It is possible that a trapping time, rather than a transit time, was being measured. Deep trapping effects caused a rapid disappearance of the pulse.

Ig. Variation of Electron Drift Mobility with Temperature; Selenium + 3% Germanium (Specimen thickness = 35μm, field = $1.43x10^5$V/cm)(for figure 33)

Temperature T °K	Transit Time (μsec)	Mobility ($cm^2V^{-1}sec^{-1}$)
214	750	$3.26x10^{-5}$
221.5	935	$2.62x10^{-5}$
235	850	$2.87x10^{-5}$
248	780	$3.14x10^{-5}$
257.5	725	$3.37x10^{-5}$
266	670	$3.66x10^{-5}$
273	417	$5.88x10^{-5}$
275	500	$4.88x10^{-5}$
278	400	$6.12x10^{-5}$
283	420	$5.82x10^{-5}$
286	272	$8.98x10^{-5}$
293	170	$1.44x10^{-4}$
295	250	$9.75x10^{-5}$
305.5	140	$1.75x10^{-4}$
311.5	185	$1.32x10^{-4}$
322	150	$1.63x10^{-4}$

Comments.

Pulse height much larger than in Se or Se + 1% Ge. Pulse height decreasing for temperatures less than 270°K. Some evidence of slow build up of space charge with time.

Ih. Variation of Electron Drift Mobility with Applied Field. Selenium + 3% Germanium. (Specimen thickness = 35μm. Temperature = 295°K) (for Figure 33).

Field (V/cm)	Transit Time (μsec)	Mobility ($cm^2V^{-1}sec^{-1}$)
$7.15x10^4$	885	$5.55x10^{-5}$
$1.00x10^5$	390	$8.97x10^{-5}$
$1.43x10^5$	250	$9.75x10^{-5}$

Ii. Electron Drift Mobility in Selenium + 7% Germanium. (Specimen Thickness = 45.5μm. Temperature = 299°K) (for page 88)

Field (V/cm)	Transit Time (μsec)	Mobility ($cm^2V^{-1}sec^{-1}$)	Comments
$1.1x10^5$	230	$1.8x10^{-4}$	Situation similar to Se + 3% Ge,
$1.1x10^5$	130	$3.2x10^{-4}$	but pulse height somewhat less. Rapid accumulation of space charge.

Ij. Variation of Hole Drift Mobility with Applied Field. Arsenic Triselenide. (Temperature = 295°K) (for Figure 34)

Specimen	Thickness (microns)	Field (V/cm)	Transit Time (μsec)	Mobility ($cm^2V^{-1}sec^{-1}$)
1	1.275	$9.42x10^4$	105	$1.29x10^{-5}$
1	1.275	$9.42x10^4$	106	$1.27x10^{-5}$
1	1.275	$1.88x10^5$	13.5	$5.02x10^{-5}$
1	1.275	$2.83x10^5$	3.2	$1.41x10^{-4}$
2	2.90	$6.9\ x10^4$	510	$8.25x10^{-6}$
2	2.90	$1.04x10^5$	240	$1.17x10^{-5}$
2	2.90	$1.38x10^5$	86	$2.44x10^{-5}$
2	2.90	$1.38x10^5$	80	$2.63x10^{-5}$
2	2.90	$1.73x10^5$	41.3	$4.07x10^{-5}$
2	2.90	$2.07x10^5$	30	$4.68x10^{-5}$
2	2.90	$2.42x10^5$	17.8	$6.75x10^{-5}$
2	2.90	$2.77x10^5$	10	$1.05x10^{-4}$
2	2.90	$3.23x10^5$	6.3	$1.48x10^{-4}$
2	2.90	$3.47x10^5$	3.6	$2.33x10^{-4}$
5	0.95	$1.05x10^5$	63.3	$1.44x10^{-5}$
5	0.95	$2.11x10^5$	11.5	$3.91x10^{-5}$
5	0.95	$3.16x10^5$	2.65	$1.13x10^{-4}$

Ik. Variation of d.c. Conductivity with Applied Field. Arsenic Triselenide. (Specimen 1; Thickness = 2.9μm, Area = 0.06 cm^2)(Temperature = 295°K) (for Figure 35)

	Field (V/cm)	Current (nanoAmps)	Conductivity ($Ohm^{-1}cm^{-1}$)
Run 1.	$6.90x10^4$	8.4	$2.03x10^{-12}$
	$1.04x10^5$	14	$2.22x10^{-12}$
	$1.38x10^5$	21	$2.54x10^{-12}$
	$1.73x10^5$	31	$2.99x10^{-12}$
	$2.07x10^5$	46	$3.70x10^{-12}$
	$2.42x10^5$	72	$4.95x10^{-12}$
	$3.10x10^5$	168	$9.05x10^{-12}$
Run 2.	$6.90x10^4$	2.6	$6.30x10^{-13}$
	$1.04x10^5$	6	$9.60x10^{-13}$
	$1.38x10^5$	11	$1.33x10^{-12}$
	$1.73x10^5$	14.4	$1.39x10^{-12}$
	$2.07x10^5$	26	$2.09x10^{-12}$
	$2.42x10^5$	40	$2.75x10^{-12}$
	$2.76x10^5$	60	$3.62x10^{-12}$
	$3.10x10^5$	92	$4.95x10^{-12}$
	$3.45x10^5$	160	$7.75x10^{-12}$
	$3.80x10^5$	240	$1.05x10^{-11}$
	$4.14x10^5$	380	$1.53x10^{-11}$
Run 3. Reproducible	$6.90x10^4$	~ 0.2	$\sim 4.9\ x10^{-14}$
	$1.04x10^5$	1.0	$1.60x10^{-13}$
	$1.38x10^5$	2.4	$2.90x10^{-13}$
	$1.73x10^5$	5.2	$5.02x10^{-13}$
	$2.07x10^5$	8.4	$6.76x10^{-13}$
	$2.42x10^5$	18.	$1.24x10^{-12}$
	$2.76x10^5$	34	$2.06x10^{-12}$
	$3.10x10^5$	56	$3.01x10^{-12}$
	$3.45x10^5$	94	$4.53x10^{-12}$
	$3.80x10^5$	152	$6.67x10^{-12}$
	$4.14x10^5$	260	$1.05x10^{-11}$

11. Variation of Hole Drift Mobility with Temperature and Applied Field

Arsenic Triselenide (for Figures 36 and 39)

	Specimen	Thickness (microns)	Field (V/cm)	Temperature (^{o}K)	Transit Time (μsec)	Mobility ($cm^2V^{-1}sec^{-1}$)
Run 1	1	1.275	$9.42x10^4$	295	105	$1.29x10^{-5}$
	1	1.275	$9.42x10^4$	304	125	$1.08x10^{-5}$
	1.	1.275	$9.42x10^4$	316	56	$2.42x10^{-5}$
	1	1.275	$9.42x10^4$	328	41	$3.31x10^{-5}$
	1	1.275	$9.42x10^4$	342	21	$6.46x10^{-5}$
	1	1.275	$9.42x10^4$	361	13	$1.04x10^{-4}$
	1	1.275	$1.88x10^5$	295	13.5	$5.02x10^{-5}$
	1	1.275	$1.88x10^5$	304	11	$6.15x10^{-5}$
	1	1.275	$1.88x10^5$	316	10.5	$6.45x10^{-5}$
	1	1.275	$1.88x10^5$	328	5.6	$1.21x10^{-4}$
	1	1.275	$1.88x10^5$	342	4	$1.69x10^{-4}$
	1	1.275	$1.88x10^5$	361	1.9	$3.57x10^{-4}$
	1	1.275	$2.83x10^5$	295	3.2	$1.41x10^{-4}$
	1	1.275	$2.83x10^5$	304	2.9	$1.56x10^{-4}$
	1	1.275	$2.83x10^5$	316	2.0	$2.26x10^{-4}$
	1	1.275	$2.83x10^5$	328	1.8	$2.51x10^{-4}$
	1	1.275	$2.83x10^5$	343	1.0	$4.52x10^{-4}$
Run 2	1	1.275	$9.42x10^4$	297	106	$1.27x10^{-5}$
	1	1.275	$9.42x10^4$	310	61	$2.22x10^{-5}$
	1	1.275	$9.42x10^4$	338	24	$5.65x10^{-5}$
	1	1.275	$9.42x10^4$	355.5	15.2	$8.92x10^{-5}$
	1	1.275	$9.42x10^4$	366	10.25	$1.32x10^{-4}$
	1	1.275	$9.42x10^4$	386.5	4.6	$2.95x10^{-4}$
	1	1.275	$9.42x10^4$	400	1.7	$7.98x10^{-4}$
	1	1.275	$9.42x10^4$	371	6	$2.26x10^{-4}$
	1	1.275	$9.42x10^4$	354	6	$2.26x10^{-4}$
	1	1.275	$9.42x10^4$	336.5	6.8	$2.00x10^{-4}$
	1	1.275	$9.42x10^4$	312	14	$9.70x10^{-5}$
	1	1.275	$9.46x10^4$	283	28	$4.84x10^{-5}$
	5	0.95	$3.16x10^5$	296	2.65	$1.13x10^{-4}$
	5	0.95	$3.16x10^5$	279	4.5	$6.67x10^{-5}$
	5	0.95	$3.16x10^5$	262	6.2	$4.84x10^{-5}$
	5	0.95	$3.16x10^5$	246	12	$2.50x10^{-5}$

Im. Variation of Specimen Current with Temperature; Arsenic Triselenide. (Specimen 3, Thickness unknown, Applied Voltage = 65.5V)

(for Figure 37)

T °K	385.5	379	376	374	371.5	366.5	363	360	356.5	
I μA	33	24	16	13	12	8.7	7.0	5.2	3.9	
T °K	353.5	353	349.5	342	338	333	326	320	315.5	
I μA	2.6	3.1	1.6	1.1	0.85	0.46	0.2	0.13	0.11	
T °K	313	311	308	304	299.5	296.5	293	289.5	286	283
I μA	0.098	0.082	0.07	0.06	0.048	0.037	0.032	0.028	0.024	0.02

In. Variation of Transit Pulse Height with Reciprocal Transit Time

Arsenic Triselenide (Specimen 4) (for Figure 38)

Temperature (T °K)	Applied Voltage (Volts)	Transit Time (τ μsec)	$\frac{10^{-4}}{\tau}$	Pulse Height (mV)
289.5	115	340	0.30	19.5
298.5	115	320	0.31	16
303	65	450	0.22	4
309.5	65	420	0.24	12.5
315	65	340	0.29	27
319.5	65	240	0.42	35
324.5	65	165	0.61	27
328.5	65	95	1.10	34
335	65	70	1.4	50
339	64	48	2.1	66
344	63.5	40	2.5	48
350	63	30	3.3	61
355	62.5	24	4.2	61
356.5	62	20	5.0	52
361	61	18.5	5.2	62
366.5	59	15.5	6.2	52
371	57.5	16.5	6.1	60
376	55.5	14	7.2	70
382	54	12.5	8.0	65

Io. Electron Transit in Arsenic Triselenide (Specimen 2, thickness = 2.9 μm) (for page 90)

Temperature T °K	Field (V/cm)	Pulse Response Time (mSec)	Comments
345.5	2.07×10^5	2.7	Pulse amplitude very small, but increasing rapidly with temperature. Results indicate a trapping time of about 2.6 mSec, and a mobility of less than 5×10^{-7} $cm^2 V^{-1} sec^{-1}$.
355.5	2.07×10^5	2.8	
377	2.07×10^5	2.5	

Ip. Examination of Hole Transit in As_2Se_2Te; Specimen 1. (thickness = 76 μm ± 2 μm) (for page 91)

Temperature T °K	Field (V/cm)	Pulse Response Time (μsec)	Comments
293	1.3×10^3	20	Hole drift mobility $<< 10^{-1}$ $cm^2 V^{-1} sec^{-1}$. Trapping time ∿ 20 μSec.
293	1.3×10^3	18	
293	2.0×10^3	22	
253	2.4×10^3	44	Hole drift mobility ≤ 10^{-2} $cm^2 V^{-1} sec^{-1}$. Trapping time ∿ 50 μSec.
252	3.7×10^3	60	
252	3.7×10^3	55	

Iq. Dependence of Pulse Height (Holes) on Applied Field; As_2Se_2Te. (Specimen 2, thickness = 25 μm ± 2 μm) (Temperature = 294°K)

Field (V/cm)	Pulse Height (mV)	Comments
0	∿ 0.1	Small pulse observed at zero applied field is due to the charge induced by the excitation pulse. The rise time of the observed pulses was approximately 15 μSec, indicating a trapping time of this order.
2.8×10^3	0.3	
3.2×10^3	0.35	
3.6×10^3	0.4	
4.0×10^3	0.6	
4.8×10^3	1.2	
5.2×10^3	1.4	
5.6×10^3	1.6	

Ir. Variation of Hall Mobility with Frequency; $As_2Te_3Tl_2Se$.
(Temperature = 295°K, Magnetic Field = 17 kGauss, l/w=7.5)
(for Figure 64)

Frequency (Hz)	Input Voltage (volts)	Recorder Defln. (mV)	Gain	Hall Voltage (μV)	Mobility ($cm^2V^{-1}sec^{-1}$)
60	4.08	0.24	20.6	5.83	6.5×10^{-2}
108	4.08	0.31	21.2	7.32	8×10^{-2}
520	4.11	0.33	20.7	7.98	8.5×10^{-2}
1000	4.13	0.31	21.3	7.29	8×10^{-2}
5000	4.08	0.28	21.3	6.57	7×10^{-2}
10000	4.08	0.37	37.5	4.93	5.5×10^{-2}

Is. Variation of Hall Mobility with Temperature; $As_2Te_3Tl_2Se$.
(Frequency = 520 Hz, Magnetic Field = 18.5 kGauss, l/w = 7.5)
(for Figure 65)

Temperature (T °C)	Input Voltage (volts)	Recorder Defln. (mV)	Gain	Hall Voltage (μV)	Mobility ($cm^2V^{-1}sec^{-1}$)
21.5	3.60	0.56	43.2	6.48	7.25×10^{-2}
30.5	3.60	0.65	43.2	7.52	8.5×10^{-2}
39.5	3.60	0.61	43.2	7.06	8×10^{-2}
60.5	3.60	0.66	43.2	7.63	8.5×10^{-2}
81	3.60	0.62	43.2	7.18	8×10^{-2}

Appendix II. Additional Circuitry Details

The construction of the great majority of the equipment used in this study has been described in the text. Exceptions have occurred mainly where integrated circuit modules have been employed, in which case the modules have usually been represented in block form. It is the purpose of this appendix to provide sufficient additional information on such circuits to allow for their construction.

(a) Logic Circuits of the Drift Mobility Control Equipment.

This unit, which has been illustrated in figure 24, was constructed making extensive use of logic microcircuits from the SGS-Fairchild μL range. The individual units in the system were of a fairly standard design, and were derived from the handbook: 'The Applications of Logic Microcircuits', SGS-Fairchild, London. Additional details of the assembly are given in figure 69. The relays shown in this diagram were Elliot mercury-wetted contact units (618 30/11).

(b) Linear Circuits in the Drift Mobility Control Equipment.

A Linear Operational Amplifier module (R.C.A type CA3008) was used as a combined pulse integrator and differentiator, although this unit was not, in fact, employed in the measurements for reasons given previously. The design was again standard, being derived from RCA applications data (see also 'The Applications of Linear Microcircuits', SGS-Fairchild, London, 1967). For convenience, the unit is shown in figure 70 as separate integrator and differentiator modules. These may be combined to provide both functions from a single amplifier by switching in and out the appropriate resistance and capacitance elements.

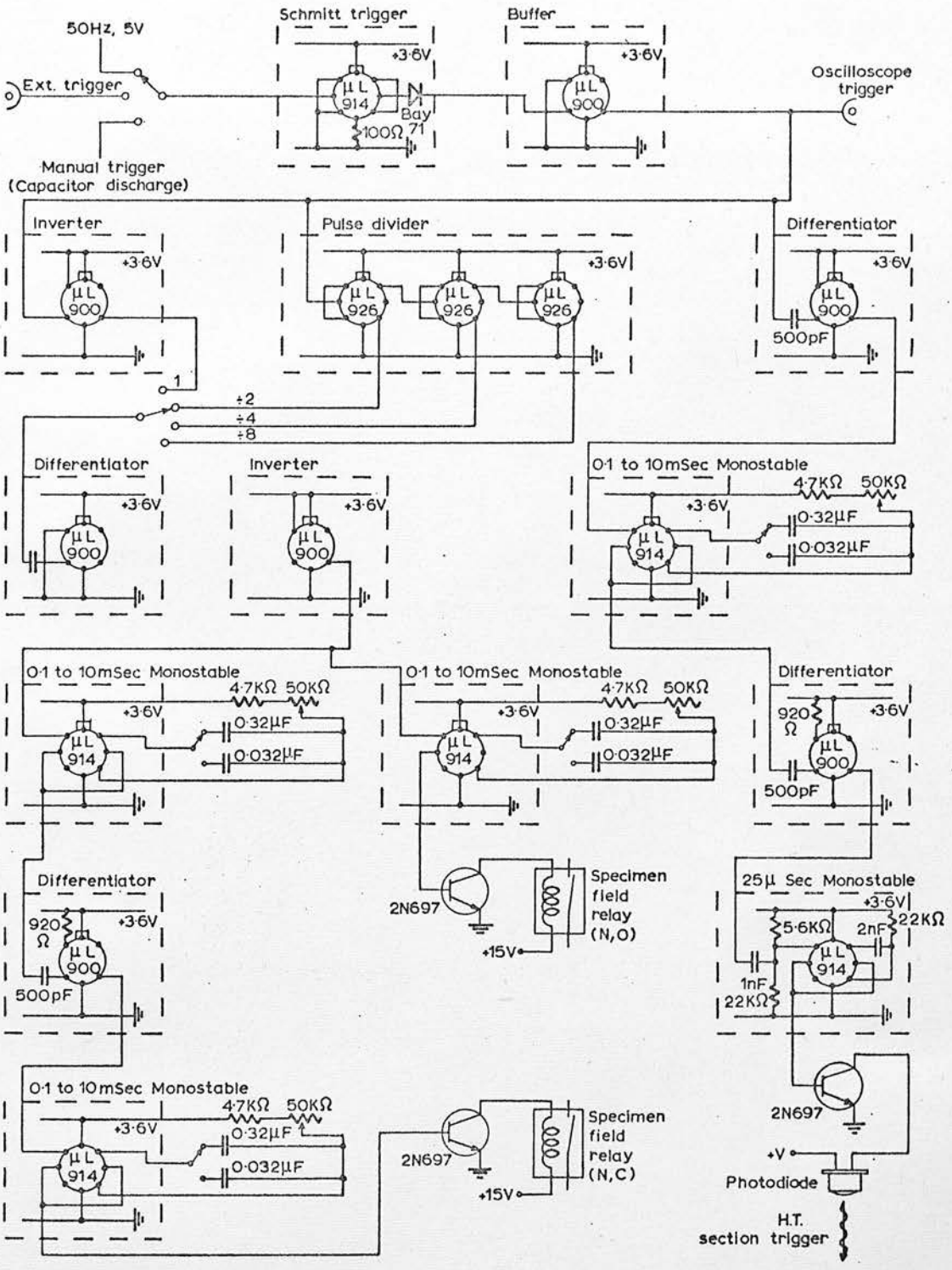

Fig. 69 Drift Mobility Equipment, Logic Control Circuit

(C) Pre-Amplifier Unit in the Hall Mobility Measurement Assembly.

The arrangement used to operate the Keithley 302 amplifier in a unity gain impedance transforming mode is shown in figure 71. Also included is the variable gain amplifier used to drive the shield around the input lead to the Keithley 302. Any low power npn transistor would be suitable for this application.

(d) Balance and Frequency Selective Amplifiers in the Hall Mobility Assembly.

Figure 72 shows the arrangement used to provide the balance and tuned filter functions. The circuits are again standard, and additional information is provided in the SGS-Fairchild Linear Microcircuit handbook, and in the appropriate R.C.A. application reports.

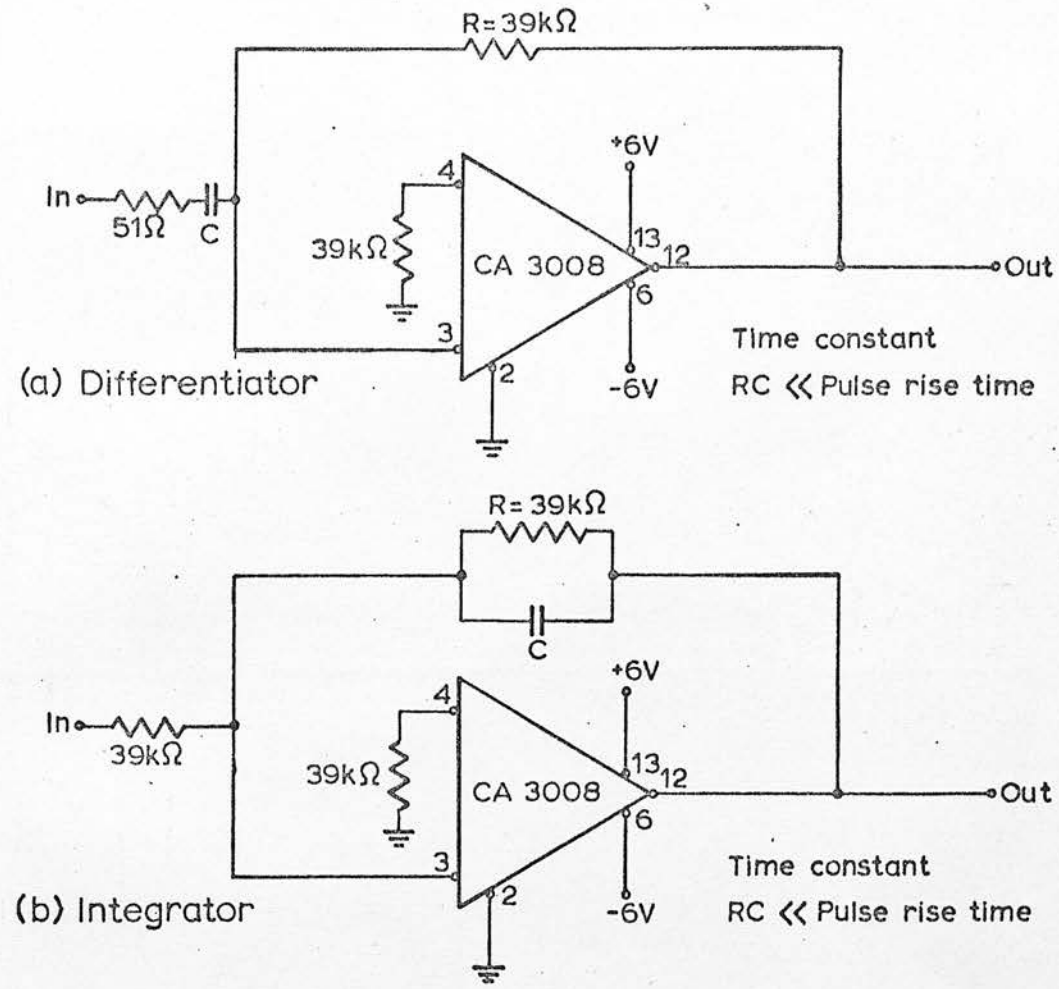

Fig. 70 Differentiator and Integrator Modules in the Drift Mobility Apparatus

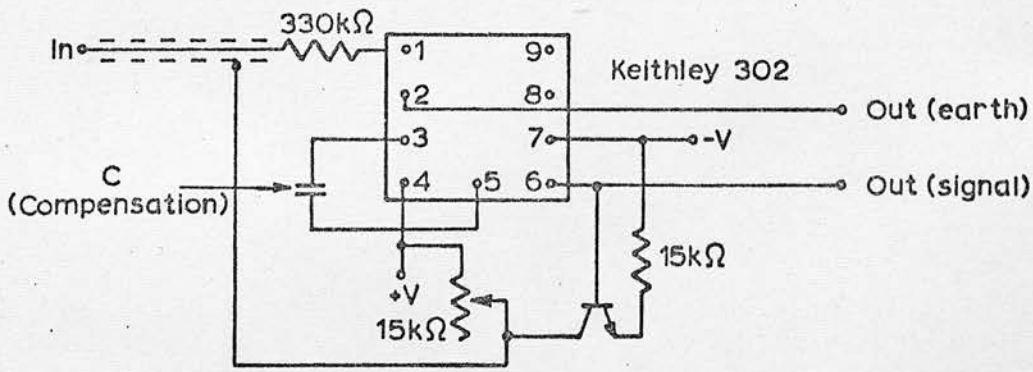

Fig. 71 Impedance Transforming Pre-amplifier Hall Mobility Apparatus

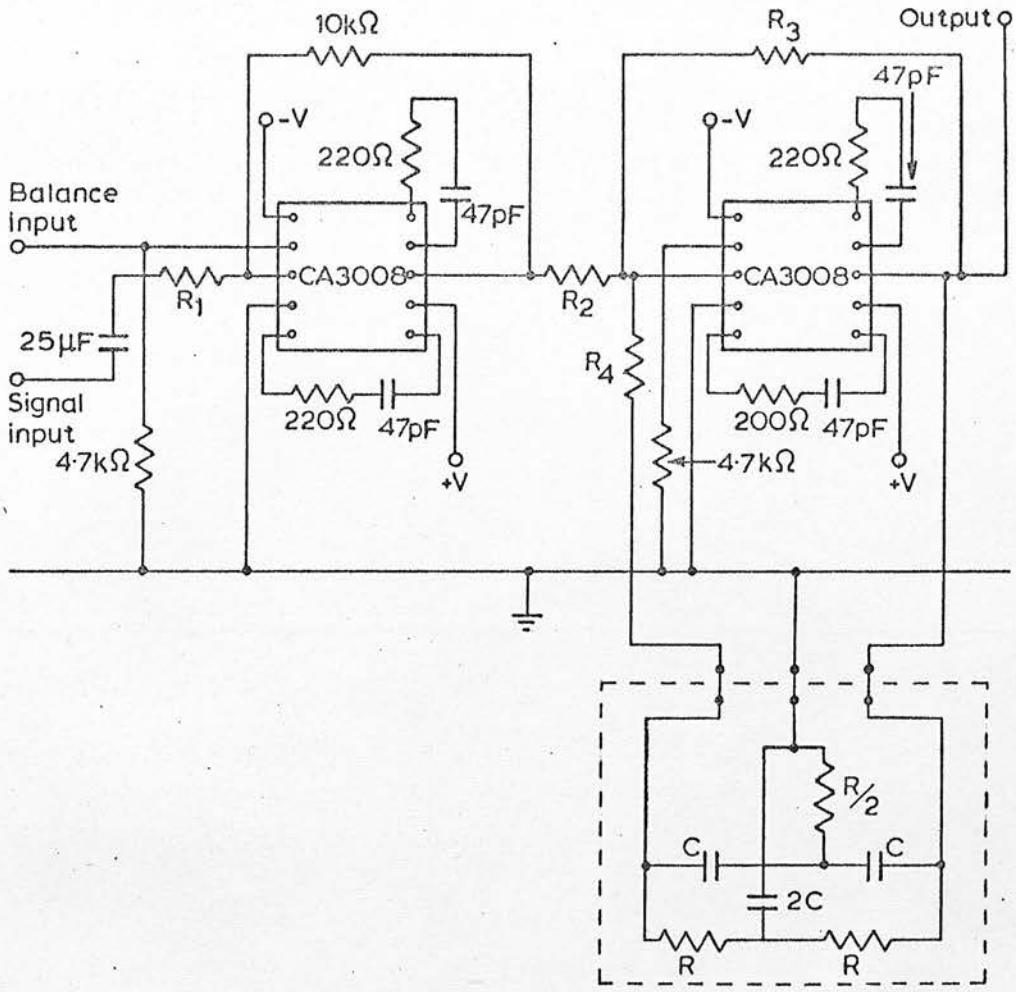

Balance amplifier

Signal gain = $\frac{10^4}{R_1}$

Balance gain = $\frac{R_1+10^4}{R_1}$

Frequency selective amplifier

Centre frequency = $\frac{1}{2\pi RC}$

Quality factor, Q = $\frac{AQ+1}{4}$

$AQ = \frac{R_3}{R_4+R/\sqrt{2}}$

Fig. 72 Balance Amplifier/Frequency Selective Amplifier Hall Effect Apparatus

Appendix III

Comments on a Recent Examination of Carrier Transport in Selenium

Since the preparation of the bulk of this thesis, the author's attention has been drawn to an examination of the transport properties of amorphous selenium by E.L.Rossiter and G. Warfield. An account of this study is contained in:

'An Investigation of the Bulk Conduction Properties of Amorphous Selenium Thin Films.'
E.L. Rossiter and G. Warfield.
University of Princetown (USA),
Dept. of Electrical Engineering,
Device Physics Laboratory,
Technical Report No.10.
October, 1967.

This work does not appear to have been reported elsewhere in the literature, but contains material of direct relevance to the present report, so that a short review of some of the contents is deemed to be valuable, and is provided below.

(1) Hole and electron mobilities have been measured by a 'time of flight' technique (as used in the present study), and by a study of the transient space-charge limited conductivity. Data from the two sources shows general agreement.

(2) Of particular interest here, the hole mobility has been examined as a function of temperature and applied field over the temperature range $2.5 < 10^3/T < 13.5$. The mobility has been found to be field dependent, with the influence of the field increasing with decreasing temperature. Unfortunately, details of the field dependence are not provided in a readily accessible form, but the data (page 73 of the report) indicates that the field has only a minor

effect at room temperature (zero field mobility ~ 0.1 $cm^2V^{-1}sec^{-1}$; measured mobilities ~ 0.12 $cm^2V^{-1}sec^{-1}$). At a temperature of 77^oK, the field modification is much more pronounced (zero field mobility $\sim 9x10^{-4}$ $cm^2V^{-1}sec^{-1}$, measured mobilities $\sim 3.5x10^{-3}$ $cm^2V^{-1}sec^{-1}$). The values of field at which the mobilities were measured are not quoted in the data, but it is stated that the results have been interpreted in terms of the Poole-Frenkel effect, which leads to calculated values of the dielectric constant which are much too high (i.e. in the range 30 to 300, as compared to the accepted figure of 6).

(3) The data on the hole mobility (presumable after correction for field effects by assuming a Poole-Frenkel dependence) is plotted to show log μ as a function of $10^3/T$. In the range $2.5 < 10^3/T < 6$, the results show a linear dependence, with an activation energy of 0.095 eV. A sharp discontinuity of slope occurs at $10^3/T = 6.5$, and the activation energy at lower temperatures is estimated as 0.0093 eV (the 'spread' of experimental points is relatively large at low temperatures, so that it is possible that this figure could be inaccurate, or that different specimens could exhibit different low temperature activation energies).

(4) The electron drift mobility has been studied over a much smaller range of temperature ($3.3 < 10^3/T < 3.9$), but a field dependence, again with unrealistically high values of calculated dielectric constant, has again been reported. It is stated that the calculated values of dielectric constant for electrons and holes are in agreement. Over the measured temperature range, the results (again presumably after correction for field effects) indicate a single value of activation energy; this being 0.27 eV.

Discussion

The major relevance of the above results to the present study is in the examination of the hole mobility at much lower temperatures than have been reported elsewhere in the literature, and in the examination of the field dependence of the mobility over this range. The report of a significant dependence of the magnitude of the mobility on the applied field is in agreement with the present observations, as is the magnitude of the dependence. The decrease of the mobility activation energy at low temperatures is also consistent with the present observations, but it will be recalled that a gradual decrease in activation energy with decreasing temperature was reported in Chapters Four and Five, whilst Rossiter and Warfield's data indicates a much sharper discontinuity of slope. It has not been possible to ascertain whether this disagreement is caused by structural differences between the vitreous films used in the present study and the evaporated specimens used by Rossiter and Warfield, or whether the treatment of the results in the two cases is sufficiently different as to cause the disagreement.

Bibliography

1. Mott,N.F. & Twose, W.D., Advances in Physics, 10, 107, (1961).

2. Bube, R.H., Photoconductivity of Solids (1960)(Wiley).

3. Ioffe, A. & Regel, A., Progress in Semiconductors, Vol.4. (1960) (Heyworth).

4. Mott, N.F., Phil. Mag., 19,835,(1969).

5. Glazov, V.M. et al, Liquid Semiconductors (1969)(Plenum Press).

6. Mooser, E. & Pearson, W.C., Jnl. Phys. Chem. Solids 7, 65, (1958).

7. Henkels, H.W., Jnl. Appl. Physics 22, 1265,(1951).

8. Kozyrev, P.T., Zh. Tekhn. Fiz., 27,35, (1957).

9. Stuke, J., Phys. Stat. Solidi, 6,441,(1964).

10. Lange, V.N. & Regel, A.R., Sov. Phys.-Solid State 1, 507,(1959).

11. Krebs, H., Z. Anorg. Allgem. Chem. 265, 156, (1951).

12. Lukovsky, G. et al., Solid State Comm. 5, 113, (1967).

13. Ward, A.R. & Myers, M.B., Jnl Phys. Chem. 73, 1374, (1969).

14. Eisenberg, A. & Tobolsky, A., Jnl. Polymer Science 46, 19, (1960).

15. Abdullaev, G.B. et al. Sov. Phys.-Solid State 6,786, (1964).

16. Meilikhov, E.Z., Sov. Phys.-Solid State 7, 1407, (1965).

17. Massen, C. et al, Trans. Faraday Soc. 60, 317, (1964).

18. Urazovskii, C.C. & Lyuft, B.D., Zh. Fiz. Khim. 22, 409, (1948).

19. Edmond, J.T., Jnl. Non-Cryst. Solids 1, 39, (1968).

20. Edmond, J.T., Brit. Jnl. Appl. Phys. 17, 979, (1966).

21. Stuke, J. Festkorperprobleme 9, 46, (1969).

22. Male, J.C., Brit. Jnl. Appl. Phys. 18, 1543, (1967).

23. Dresner, J., Jnl. Phys. Chem. Solids 28, 505, (1964).

24. Peck, W.F. & Dewald, J.F., Jnl. Electrochem. Soc. 111, 561, (1960).

25. Kolomiets, B.T. & Nazarova, T.F., Sov. Phys.-Solid State 2, 369,(1960)

26. Uphoff, H.L. & Healy, J.H., ASTIA Report AD 206, 780 (1961).

27. Spear, W.E., Proc. Phys. Soc. (London) B70, 669, (1957).

28. Spear, W.E., Proc. Phys. Soc. (London) 76, 826, (1960).

29. Grunwald, H.P. & Blakney, R.M., Phys. Rev., 165, 1007, (1968).

30. Schottmiller, J. et al., 3rd Internat. Conf. on Liquid and Amorphous Semiconductors (Cambridge, 1969). To be published in Jnl. Non-Crystalline Solids.

31. Tabak, M.D. & Warter, P.J., Phys. Rev. 173, 899, (1968).

32. Tabak, M.D., Proc. 3rd Internat. Photoconductivity Conf. To be published in Jnl. Phys. Chem. Solids.

33. Hartke, J.L., Phys. Rev. 125, 1177, (1962).

34. Kolomiets, B.T. & Lebedev, E.A., Sov. Phys.-Solid State 8, 905, (1966).

35. Kolomiets, B.T. & Lebedev, E.A., Sov. Phys.-Semiconductors 1, 244, (1967).

36. Kolomiets, B.T., Phys. Stat. Solidi 7, 359 & 715, (1964).

37. Owen, A.E., Contemporary Physics, To be published.

38. Ovshinsky, S.R., Phys. Rev. Letters 21, 1450, (1968).

39. Mott, N.F., Contemporary Physics 10, 125, (1969).

40. Stocker, H.J., Appl. Phys. Letters 15, 55, (1969).

41. Walsh, P.J. et al., Phys. Rev. 178, 1274, (1969).

42. Tauc, J., Science 158, 1543, (1967).

43. Mott, N.F., Advances in Physics 16, 49, (1967).

44. Volger, J., Phys. Rev. 79, 1023, (1950).

45. Bube, R.H., Appl. Phys. Letters 13, 136, (1968).

46. Main, C. & Owen, A.E., Physica Status Solidi (a) 1, 297, (1970).

47. Mott, N.F., Festkorperprobleme 9, 22, (1969).

48. Cohen, M.L., Gordon Conference (1968), see Mott[4].

49. Miller, A. & Abrahams, E., Phys. Rev. 120, 745, (1960).

50. Kuper, C.G. & Whitfield, G.D. (Eds.) Polarons and Excitons (1962) (Oliver & Boyd).

51. Klinger, M.I., Repts. on Prog. in Physics 31(pt 1), 225, (1968).

52. Austin, I.G. & Mott, N.F., Advances in Physics 18, 41, (1969).

53. Gubanov, A.I., Quantum Electron Theory of Amorphous Semiconductors, (1965) (Consultants Bureau, N.Y.).

54. Adams, A.R. & Spear, W.E., Jnl. Phys. Chem. Solids 25, 1113, (1964)

55. Gibbons, D.J. & Spear, W.E., Jnl. Phys. Chem. Solids 27, 1917,(1966).

56. Killias, H.R., Physics Letters 20, 5, (1966).

57. Hartke, J.L., Jnl. Appl. Phys. 39, 4871, (1968).

58. Simmons, J.G., Phys. Rev. 155, 657, (1967).

59. Jonscher, A.K., Thin Solid Films 1, 213, (1967).

60. Lamb, D.R., Electrical Conduction Mechanisms in Thin Insulating Films (1967) (Methuen Monographs).

61. Freeman, L.A. et al., Thin Solid Films 3, 367, (1969).

62. Ansbacher, F. & Ehrenberg, W., Proc. Phys. Soc. (London) A64, 362, (1951).

63. Ehrenberg, W. & King, D.E.N., Proc. Phys. Soc. (London) 81, 751, (1963).

64. Spear, W.E., Proc. Phys. Soc. (London) B68, 991, (1955).

65. Shockley, W., Electrons and Holes in Semiconductors (1950) (Van Nostrand).

66. Haynes, J.R. & Shockley, W., Phys. Rev. 82, 935, (1951)

67. Pohl, R.W., Proc. Phys. Soc. (London) 49, 3, (1937).

68. Spear, W.E. et al., Jnl. Sci. Inst. 39, 81, (1962).

69. Bardeen, J. & Shockley, W., Phys. Rev., 80, 72, (1950).

70. Fan, H.Y., Solid State Physics (Eds. Seitz & Turnbull) 1, 283, (1955) (Academic Press, N.Y.)

71. Karpushin, A.A., Sov. Phys.-Solid State 10, 2793, (1969).

72. Pollak, M., Phys. Rev. 138, A1822, (1965).

73. Drake, C.R. et al., Physica Status Solidi 32, 193, (1969).

74. Tefft, W.E., Jnl. Appl. Phys. 38, 5265, (1967).

75. Keating, P.N. & Papadakis, A.C., Proc. of 7th Internat. Conf. on the Physics of Semiconductors, Paris,(1964), Academic Press.

76. Papadakis, A.C., Jnl. Phys. Chem. Sol. 28, 641, (1967).

77. Gibbons, D.J. & Papadakis, A.C., Jnl. Phys. Chem. Sol. 29, 115, (1968).

78. Many, A. & Rakavy, G., Phys. Rev. 126, 1980, (1962).

79 Hecht, K., Z. Physik 77, 235, (1932).

80. Brown, F.C., Phys. Rev. 97, 355, (1955).

81. Spear, W.E., Jnl. Phys. Chem. Sol. 21, 110, (1961).

82. Caywood, J.M. & Mead, C.A., Jnl. Phys. Chem. Sol. To be published.

83. Hirsch, J., Jnl. Phys. Chem. Sol. 27, 1385, (1966).

84. Spear, W.E., Jnl. Non-Crystalline Solids 1, 197, (1969).

85. Owen, A.E., Private Communication.

86. Schnakenberg, J., S. Physik, 185, 123, (1965).

87. Frank, S., Thesis, University of Sheffield (1967).

88. Owen, A.E., Glass Industry 48, 637 & 695, (1967).

89. Putley, E.H., The Hall Effect and Related Phenomena (1960) (Butterworths).

90. Friedman, L. & Holstein, T., Ann. Phys. 21, 494, (1963).

91. Kurosawa, T., Prog. Theor. Physics, Osaka, 29, 159, (1963).

92. Firsov, Yu A., Sov. Phys.-Solid State 5, 1566, (1964).

93. Klinger, M.I., Physica Status Solidi 11, 499, (1965).

94. Klinger, M.I., Physica Status Solidi 12, 745, (1965).

95. Schnakenberg, J., Physica Status Solidi 28, K135, (1968).

96. Holstein, T. & Friedman, L., Phys. Rev., 165, 1019, (1968).

97. Kubo, R., Jnl. Phys. Soc. Japan 12, 570, (1957).

98. Kubo, R. et al., Jnl. Phys. Soc. Japan 14, 56, (1959).

99. Emin, D. & Holstein, T., Ann. Phys. 53, 439, (1969)

100. Holstein, T., Phys. Rev., 124, 1329, (1961).

101. Wood, L.A., Phys. Rev. 41, 231, (1932).

102. Austin, I.G. et al., Proc. Phys. Soc. 90, 157, (1967).

103. Van der Pauw, L.J., Philips Research Reports 13, 1, (1958).

104. McKenzie, H.L. & Tannhauser, D.S., Jnl. Appl. Phys. 40, 4954,(1969).

105. Suchannek, R.G., Rev. Sci. Inst. 37, 589, (1966).

106. Hall, E.H., Amer. Jnl. Math. 2, 287, (1879).

107. Baedecker, K., Ann. Phys. 29, 566, (1909).

108. Smith, A.W., Phys. Rev. 35, 81, (1912).

109. Russell, B.R. & Wahlig, C., Rev. Sci. Inst. 21, 1028, (1950).

110. Donoghue, J.J. & Eatherly, W.P., Rev. Sci. Inst. 22, 513, (1951)

111. Pell, E.M. & Sproull, R.L., Rev. Sci. Inst. 23, 548, (1952).

112. Levy, J.L., Thesis, University of Michigan (1953), Publication 5065, University Microfilms Ann Arbor, Michigan.

113. Levy, J.L., Phys. Rev., 92, 215, (1953).

114. Read, P.L. & Katz, E., ASTIA Report AD 247, 465 (1960).

115. Read, P.L. & Katz, E., Phys. Rev. Letters 5, 466, (1960).

116. Donally, J.M. & Cutler, M., Phys. Rev. 176, 1003, (1969).

117. Ryan, F.M., Rev. Sci. Inst. 33, 76, (1962).

118. Hermann, A.M. & Ham, J.S., Rev. Sci. Inst. 36, 1553, (1965).

119. Redfield, A.G., Phys. Rev. 94, 526, (1954).

120. Kobayashi, K. & Brown, F.C., Phys. Rev. 113, 507, (1959).

121. Nakazawa, F. & Kanzaki, H., Jnl. Phys. Soc. Japan 27, 1184, (1969).

122. Pearson, A.D., I.B.M. Jnl. Research & Development 13, 510 (1969).

123. Fritzsche, H., I.B.M. Jnl. Research & Development 13, 515, (1969).

124. Dewald, J.F. et al, Jnl. Electrochem. Soc. 109, 243C, (1962).

125. Tanaka, K. et al, Solid State Communications 8, 75, (1970).

126. Simmons, J.G., Contemporary Physics 11, 21, (1970).